

ILLUMINATING BIOLOGY WITH MEMBRANE PENETRATING SULFONATE
DELIVERY SCAFFOLDS AND NEAR-INFRARED AZASILINE FLUOROPHORES

A Dissertation Presented
By

Adam Choi

Submitted to the Faculty of the
University of Massachusetts Graduate School of Biomedical Sciences, Worcester in
partial fulfillment of the requirements for the degree of

DOCTOR OF PHILOSOPHY

September 7, 2018

Biochemistry and Molecular Pharmacology

ILLUMINATING BIOLOGY WITH MEMBRANE PENETRATING SULFONATE
DELIVERY SCAFFOLDS AND NEAR-INFRARED AZASILINE FLUOROPHORES

A Dissertation Presented

By

Adam Choi

This work was undertaken in the Graduate School of Biomedical Sciences
Biochemistry and Molecular Pharmacology

Under the mentorship of

Stephen Miller, Ph.D., Thesis Advisor

Mark Alkema, Ph.D., Member of Committee

Heidi Tissenbaum, Ph.D., Member of Committee

Gang Han, Ph.D., Member of Committee

Sivappa Rasapalli, Ph.D., External Member of Committee

William Kobertz, Ph.D., Chair of Committee

Mary Ellen Lane, Ph.D.,
Dean of the Graduate School of Biomedical Sciences

September, 7, 2018

ACKNOWLEDGEMENTS

Firstly, I would like to acknowledge my thesis advisor, Stephen Miller. I am eternally grateful for the opportunity to train in his lab. Stephen has always been patient with his students, regardless of our mistakes or slow progress. His diligence at securing funding has allowed us to exercise our ideas uninhibited. As all graduate students come to realize, the Ph.D. experience isn't only about the project, but the environment as well. My experience in the Miller lab has been adventurous and enjoyable; I can't think of any other lab that would allow one to scream "Yo Dawg or Yo Maaang" as the morning greeting.

Secondly, I thank my lab mates namely, Steven Pauff, Spencer Adams, and David Mofford, and my support group in UMass namely, Yvonne Chan, Sezin Dagdeviren, Songwook Choi and Ebru Kaymak. Grad school wasn't easy, but we did it, together.

Lastly, I thank all my committee members: William Kobertz, Gang Han, Heidi Tissenbaum and Mark Alkema. Your support and guidance have been invaluable. Mark and Heidi, I truly appreciate your continuous efforts in helping me drive the *C. elegans* project from the very beginning until the end. Although the project didn't pan out, it was a fun journey.

ABSTRACT

Near-infrared (NIR) light, with wavelengths of 650 to 900 nanometers, effectively penetrates tissues. The high signal to noise ratio and low phototoxicity of NIR light makes this wavelength range ideal for deep tissue imaging. However, current NIR fluorophores are generally large hydrophobic molecules that are prone to aggregation. Sulfonation can enhance aqueous solubility, but their anionic nature prevents membrane diffusion, and thus, restricts the applications of sulfonated molecules to *in vitro* or fixed cells.

The repertoire of commercially available sulfonated NIR probes is mostly limited cyanines, which have low photostability. Moreover, larger cyanines require multiple sulfonates to maintain aqueous solubility. For example, Indocyanine Green is only sparingly soluble in PBS, despite having two sulfonates.

My work has focused on the delivery of sulfonated dyes into live cells and the development of a new, ultra-compact NIR dye scaffold. First, to expand the in-cell applications of sulfonated fluorophores, I designed reductively-labile sulfonate protecting groups. Using these scaffolds, I have successfully delivered the fluorophore dansyl sulfonate into live cells, where the cytosolic reducing environment unmasks the anionic sulfonate. Secondly, to create a compact, photostable NIR fluorophore, I pioneered the discovery of azasilines dyes. The two azasiline derivatives, ASiFluor710 and ASiFluor730, fluoresce over 700 nanometers and are among the most compact NIR

fluorophores currently known. ASiFluor730 also retains the high photostability of oxazine dyes, highlighting their potential in long exposure applications. Beyond the immediate applications in fluorescence microscopy and *in vivo* imaging, I envision that my work will serve as a framework for the future design of soluble, membrane permeable, NIR fluorescent probes.

TABLE OF CONTENTS

ACKNOWLEDGEMENTS	iii
ABSTRACT.....	iv
TABLE OF CONTENTS	vi
LIST OF FIGURES	viii
LIST OF SCHEMES	xi
LIST OF TABLES.....	xi
LIST OF THIRD PARTY COPYRIGHTED MATERIAL.....	xii
LIST OF SYMBOLS AND ABBREVIATIONS	xiii
PREFACE.....	xvii
CHAPTER I: Introduction	1
<i>Fluorescence</i>	<i>2</i>
<i>Fluorescence in Biology.....</i>	<i>7</i>
<i>Near Infrared (NIR) Fluorophores</i>	<i>11</i>
<i>Sulfonated Fluorophores.....</i>	<i>18</i>
<i>Red-shifted Rhodamines.....</i>	<i>21</i>
<i>Oxazines and Si-Oxazines (Azasilines)</i>	<i>24</i>
<i>Summary.....</i>	<i>26</i>
CHAPTER II: Reductively-Labile Sulfonate Ester Protecting Groups That Are Rapidly Cleaved By Physiological Glutathione.....	27
<i>Summary.....</i>	<i>28</i>
<i>Introduction.....</i>	<i>28</i>
<i>Results and Discussions</i>	<i>33</i>
<i>Conclusion.....</i>	<i>56</i>
<i>Materials and Methods.....</i>	<i>57</i>
<i>NMR Spectra</i>	<i>81</i>

CHAPTER III: Silicon Substitution in Oxazine Dyes Yields Near-Infrared Azasiline Fluorophores That Absorb and Emit Beyond 700 Nm	124
<i>Summary</i>	125
<i>Introduction</i>	125
<i>Results and Discussion</i>	129
<i>Conclusions</i>	149
<i>Materials and Methods</i>	151
<i>NMR Spectra</i>	180
CHAPTER IV: Discussions and Future Directions	222
APPENDIX.....	238
<i>Conjugation of MeSSTFMP to NIR Fluorophores</i>	239
<i>Identification of Cuticle Permeable Scaffolds in C. elegans</i>	244
<i>Materials and Methods</i>	247
<i>NMR Spectra</i>	264
BIBLIOGRAPHY	292

LIST OF FIGURES

Figure 1.1: Jablonski diagram	4
Figure 1.2: Optical properties of fluorescein.....	6
Figure 1.3: Examples of chemical sensors	8
Figure 1.4: Fixed and live cell fluorescent staining.....	10
Figure 1.5: Autofluorescence and absorption of endogenous chromophores	12
Figure 1.6: Structures of popular classes of NIR fluorophores	13
Figure 1.7: Structure of Indocyanine Green (ICG)	14
Figure 1.8: Excitation and emission of different cyanines	15
Figure 1.9: General synthesis of squaraine fluorophores.....	16
Figure 1.10: Commercially available sulfonated fluorophores.....	19
Figure 1.11: Protection of Calcein AM	20
Figure 1.12: O to Si substitution causes large bathochromic shifts in Pyronin Y	21
Figure 1.13: Structures of rhodamines and substituted rhodamines and their optical properties	22
Figure 1.14: Structural similarities between rhodamines and oxazines	24
Figure 1.15: Potential spectral properties of azasilines.....	25
Figure 2.1: EMS alkylation of guanine into O6-ethylguanine	29
Figure 2.2: Design and proposed release mechanism of the esterase-labile AcOTFMB	31
Figure 2.3: Design and proposed release mechanism of reductively-labile sulfonate protecting groups.....	32
Figure 2.4: Accessing thiophenols using Newman-Kwart rearrangement	33
Figure 2.5: Excitation and emission wavelengths of dansyl-sulfonate and AcOTFMB-Dan	35

Figure 2.6: Structures of simple, reductively-labile MeSSTFMP and non-cleavable TFMB dansylates.....	36
Figure 2.7: Potential sulfonate release from simple dansylates via nucleophilic activity of GSH	36
Figure 2.8: TFMB-Dan does not release sulfonates under reducing conditions	38
Figure 2.9: MeO-Dan does not efficiently release sulfonates under reducing conditions.....	39
Figure 2.10: EtO-Dan does not release sulfonates under reduction conditions	40
Figure 2.11: MeSSTFMB-Dan can release sulfonates under reducing conditions	41
Figure 2.12: Substitution of benzene with pyridine as the core scaffold of RLPG	42
Figure 2.13: Accessing aryl thiophenols using thiol surrogates.....	43
Figure 2.14: MeSSTFMP-Dan rapidly releases sulfonates under reducing conditions.....	45
Figure 2.15: Generation of <i>p</i>-thioquinone methide during MeSSTFMP-Dan reduction	46
Figure 2.16: Mass of products detected during MeSSTFMP-Dan reduction.....	47
Figure 2.17: Purposed structures of byproducts detected with LCMS during MeSSTFMP-Dan reduction	48
Figure 2.18: Reduction of disulfide 2.16 yields the byproduct observed during MeSSTFMP-Dan reduction	49
Figure 2.19: Photodiode array spectra are identical between the isolated disulfide and the byproduct observed during MeSSTFMP-Dan reduction	50
Figure 2.20: Real-time fluorescence monitoring of sulfonate release from MeSSTFMB-Dan and MeSSTFMP-Dan	51
Figure 2.21: Cytotoxicity of different dansylates	52
Figure 2.22: Delivery of dansyl sulfonate into live HeLa cells with RLPGs.....	54
Figure 2.23: Live images of HeLa cells treated with different dansylates	55

Figure 3.1: Expansion of π-conjugation red-shifts the fluorescence of cyanines	127
Figure 3.2: Excitation and emission wavelengths of SiR720 are red-shifted by ~170 nm compared to TMR.....	128
Figure 3.3: Possible approaches for accessing azasilines	130
Figure 3.4: Excitation and emission of azasilines in ethanol.....	135
Figure 3.5: Measurement of quantum yields and molar extinction coefficients of ASiFluors.....	136
Figure 3.6: HPLC analysis of AsiFluor710 degradation	137
Figure 3.7: LCMS analysis of AsiFluor710 degradation.....	138
Figure 3.8: Proposed degradation mechanism of ASiFluor710.....	140
Figure 3.9: Excitation and emission of ASiFluor730 in various solvents.....	142
Figure 3.10: ASiFluor730 is stable in PBS.....	143
Figure 3.11: Azasilines retain the high photostability of oxazines	144
Figure 3.12: Cytotoxicity of ASiFluor730 in HeLa cell	146
Figure 3.13: HeLa cells stained with ASiFluor730	147
Figure 3.13: ASiFluor730 and MitoTracker Green co-localized in the mitochondria	148
Figure 4.1: Thioester AcOTFMB (<i>S</i>-AcOTFMB) could be less cytotoxic	225
Figure 4.2: Protection of sulfo-Cy5 with MeSSTFMP typically yields the monoester as the major product.....	226
Figure 4.3: Accessing RLPG protected sulfo-Cy5 via a Bunte salt intermediate.....	228
Figure 4.4: Different ways to access thiosulfonates intermediates	229
Figure 4.5: Possible initiation step of ASiFluor710 degradation.....	231
Figure 4.6: Optical properties of oxazine derivatives.....	232
Figure 4.7: Modifying azasilines via aryl-halide intermediates.....	233

Figure 4.8: Potential R-group attachments on silicon of ASiFluors	234
Figure 4.9: Azasilines can accommodate multiple modifications simultaneously	236
Figure A1: Sporadic worm distribution lowers the Z'.	246

LIST OF SCHEMES

Scheme 2.1: Synthesis of MeSSTFMB-Dan.....	34
Scheme 2.2: Synthesis of MeSSTFMP-Dan	44
Scheme 3.1: Modeling azasiline synthesis after oxazines	129
Scheme 3.2: Attempted synthesis of an azetidenyl-azasiline.....	132
Scheme 3.3: Synthesis of a difluoro-azasiline (ASiFluor710).....	134
Scheme 3.4: Synthesis of a dimethyl-azasiline (ASiFluor730)	141
Scheme 4.1: Purposed sulfonation method for ASiFluors	235
Scheme A1: MeSSTFMP is labile to iodide	239
Scheme A2: MeSSTFMP ester forms adduct with methoxy tetrahydroquinoline	240
Scheme A3: Synthesis of MeSSTFMP protected oxazine via sulfonyl fluorides	242
Scheme A4: Synthesis of MeSSTFMP-protected sulfo-Cy5.....	243

LIST OF TABLES

Table 3.1: Size comparison of fluorophores	145
---	------------

LIST OF THIRD PARTY COPYRIGHTED MATERIAL

<u>Figure</u>	<u>Copyright holder</u>	<u>License number</u>
Figure 1.5b	Nature Publishing Group	4410370815520

The following figures were reproduced from journals: No permission required

Figure 1.4a	Nikon
Figure 1.5a	PNAS
Chapter II artwork	Royal Society of Chemistry
Chapter III artwork	American Society of Chemistry

LIST OF SYMBOLS AND ABBREVIATIONS

α	alpha
A	adenine
ACN	acetonitrile
AM	acetoxymethyl
AcOH	acetic acid
AcOTFMB	<i>p</i> -Acetoxytrifluoromethylbenzyl
Aq	aqueous
AU	absorbance unit
BINAP	2,2'-Bis(diphenylphosphino)-1,1'-binaphthyl
BME	β -Mercaptoethanol
BODIPY	Boron-dipyrromethene
$^{\circ}\text{C}$	degrees Celsius
c	speed of light
C	cytosine
Cu	copper
CF_3	trifluoromethyl
CHO	Chinese hamster ovary
cm	centimeters
CPS	counts per second
Cy	Cyanine
d^*	d antibonding orbitals
DABCO	1,4-diazabicyclo[2.2.2]octane
DAD	diode array detector
Dan	Dansylate
DAPI	4',6-Diamidino-2-phenylindole
DCM	dichloromethane
DFT	Density fFunctional Theory
DIC	Differential Interference Contrast
DMEM	Dulbecco's Modified Eagle's Medium
DMF	N,N'-Dimethylformamide
DMPU	N,N'-Dimethylpropyleneurea
DMSO	dimethyl sulfoxide
DTT	dithiothreitol
ϵ	molar extinction coefficient
E	energy
EG	ethylene glycol
ELISA	enzyme-linked immunosorbant assay
Em	peak emission
EMS	Ethyl methanesulfonate
ER	endoplasmic reticulum

ESI-HRMS	Electrospray Ionization-High Resolution Mass Spectrometry
Et ₂ O	diethyl ether
EtO	ethoxy
EtOH	ethanol
<i>Ev</i>	electron volts
Ex	peak excitation
FBS	fetal bovine serum
FDA	Food and Drug Administration
G	guanine
Ge	Germanium
GeR	Germanium substituted rhodamine
GFP	Green Fluorescent Protein
GSH	glutathione
<i>h</i>	Planck's constant
hr	hour
H ⁺	proton
HBSS	Hank's balanced salt solution
HCl	hydrochloric acid
HOMO	highest occupied molecular orbital
HPLC	high performance liquid chromatography
<i>i</i>	initial
I ₀	initial intensity
I ₂	Iodine
ICG	Indocyanine Green
λ	wavelength
λ_{ex}	peak absorption/ excitation wavelength
λ_{em}	peak emission wavelength
LCMS	liquid chromatography mass spectrometry
LD ₅₀	lethal dose, 50%
LUMO	highest occupied molecular orbital
μM	micromolar
M	molar
<i>m</i>	<i>meta</i>
MeO	methoxy
MeOH	methanol
Me ₃ SiCF ₃	Trifluoromethyltrimethylsilane (Ruppert's reagent)
MeSS	methyl disulfide
MeSSO ₂ Me	Methyl methanethiosulfonate
MH ⁺	mass of parent + proton
mM	millimolar
mmol	millimole
mw	molecular weight

m/z	mass over charge ratio
<i>n</i>	refractive index
N ₂ PhNO ₂	4-Nitrobenzenediazonium tetrafluoroborate
NaBH ₄	sodium borohydride
NADPH	reduced Nicotinamide adenine dinucleotide phosphate
NaH	Sodium hydride
NaOtBu	Sodium <i>tert</i> -butoxide
NaN ₃	Sodium azide
NaI	Sodium iodide
NBS	<i>N</i> -Bromosuccinimide
<i>n</i> -BuLi	<i>n</i> -Butyllithium solution
NIR	near-infrared
nm	nanometers
NMR	Nuclear Magnetic Resonance
NR	no reaction
OLED	organic light-emitting diode
Ox	oxazine
Φ _{Fl}	fluorescence quantum yield
π	pi
π*	pi antibonding orbital
<i>p</i>	<i>para</i>
PBS	phosphate buffered saline
Pd[0]	palladium 0
Pd ₂ (dba) ₃	Tris(dibenzylideneacetone)dipalladium(0)
PDT	photodynamic therapy
pK _a	acid dissociation constant
PMB-Cl	<i>p</i> -Methoxybenzyl chloride
PR	phosphorus substituted rhodamine
ROS	Reactive Oxygen Species
RT	room temperature
σ*	sigma antibonding orbital
S ₀	ground singlet state
S _{n>0}	excited singlet state
Si	Silicon
SiMe ₂ Cl ₂	Dichlorodimethylsilane
SiP	Silylated Pyronin Y
SiR	Silylated rhodamine
SiTMR	Silylated tetramethylrhodamine
Sn	Tin
S _N 2	bimolecular nucleophilic substitution
SnR	Tin substituted rhodamine
SO ₃ -	sulfonate molecular formula
SO ₂ R	Sulfone substituted rhodamine

Sulfo-Cy	Sulfonated cyanine
RLPG	reductively-labile protecting group
τ_{Fl}	fluorescence lifetime
T	thymine
$T_{\text{n}} \neq 0$	excited triplet state
TBAF	Tetra-n-butylammonium fluoride
TBS	<i>tert</i> -Butyldimethylsilyl
TCEP	Tris(2-carboxyethyl)phosphine
TFA	Trifluoroacetic acid
TFMB	α -Trifluoromethylbenzyl
TFMP	α - Trifluoromethylpyridyl
TFMT	α -Trifluoromethyltolyl
THF	tetrahydrofuran
TLC	Thin Layer Chromatography
TMR	tetramethylrhodamine
TMS	trimethylsilyl
ν	wave frequency
v	volume
Xantphos	4,5-Bis(Dfaiphenylphosphino)-9,9-dimethylxanthene

PREFACE

Publications derived from work contained within this thesis:

CHAPTER II:

Choi, A.; Miller, S. C. Reductively-Labile Sulfonate Ester Protecting Groups That Are Rapidly Cleaved by Physiological Glutathione. *Org. Biomol. Chem.* **2017**, *15* (6), 1346–1349.

CHAPTER III:

Choi, A.; Miller, S. C. Silicon Substitution in Oxazine Dyes Yields Near-Infrared Azasiline Fluorophores That Absorb and Emit Beyond 700 Nm. *Org. Lett.* **2018**, *20* (15), 4482–4485.

Cell images and toxicity data in CHAPTER III were derived from unpublished data.

I thank Dr. Sangram Parelkar (Umass Small Molecule Screening Facility) and Dr. Yvonne Chan (Matthews lab) for their tireless efforts to optimize the screening conditions described in the Appendix. I thank Dr. Ebru Kaymak (Ryder lab) for her guidance in *C. elegans* culture techniques. I thank the entire Ryder, Kelch, and McCollum lab for the use of their equipment.

CHAPTER I:

Introduction

Fluorescence

Fluorescence is the optical phenomenon whereby a molecule becomes excited via photon absorption and relaxes via photon emission. Generally, the energy of the photon absorbed is higher than the one released.¹ However, a fluorescent molecule can also become excited when it absorbs two lower energy photons, a process known as two-photon absorption, where each photon is roughly half the energy needed to excite the molecule. The energy of the photon can be calculated with the Planck-Einstein relation (**Eq. 1.1**). According to the equation, wave frequency (ν) is proportional to energy (E) and inversely proportional to the wavelength (λ) of the photon, where h and c are Planck's constant and the speed of light, respectively. That is, the longer the wavelength, the lower the energy. For example, fluorescein has a peak absorption (a.k.a. excitation, λ_{ex}) wavelength of 491 nm (2.5 eV) and a peak emission (λ_{em}) wavelength of 515 nm (2.4 eV).²

$$E = h\nu = \frac{hc}{\lambda} \quad [\text{Eq. 1.1}]$$

The main steps of fluorescence can be illustrated using a Jablonski diagram (**Figure 1.1**). When a fluorophore becomes excited, an electron is promoted from the ground state (S_0) to an excited state (S_1 , S_2 , S_3 , etc). Once excited, the electron equilibrates to the lowest vibrational energy level of S_1 . An electron already in the S_1 state can simply relax to the lowest S_1 vibrational level via vibrational relaxation. An

electron in a higher excited state such as S_2 must first relax via vibrational relaxation to an energy level that overlaps with S_1 , and then enter S_1 via internal conversion. From S_1 , the electron finally relaxes back to S_0 by emitting a photon, a process known as radiative relaxation (fluorescence). Energy is dissipated during vibrational relaxation prior to emission, thus the energy of the emitted photon is always lower than the photon absorbed. In the case of two-photon excitation, the energy of the emitted photon is always less than the combined energies of the photons absorbed.

Instead of radiative relaxation, which gives rise to fluorescence, the electron in S_1 can also enter a triplet state (T_1), by a process called intersystem crossing. Like internal conversion, intersystem crossing is possible between S_1 and T_1 states with overlapping energies. However, the rate of intersystem crossing is magnitudes lower than internal conversion because it is spin forbidden and thus, requires spin conversion (flip). An electron in T_1 can relax to S_0 via radiative relaxation (phosphorescence) if another spin conversion occurs. Since two rate-limiting spin conversions are required, the radiative rate of phosphorescence is much lower than fluorescence.

Most molecules are in a singlet state and do not interact with diatomic oxygen (3O_2), which is in a triplet state. However, triplet state molecules can interact with 3O_2 to form singlet state oxygen (1O_2) and other oxygen species (ROS) via energy transfer. The generated ROS can, in turn, interact with and destroy the fluorophore (photobleaching) or induce phototoxicity, a property that has been exploited in photodynamic therapy (PDT).^{1,3-6}

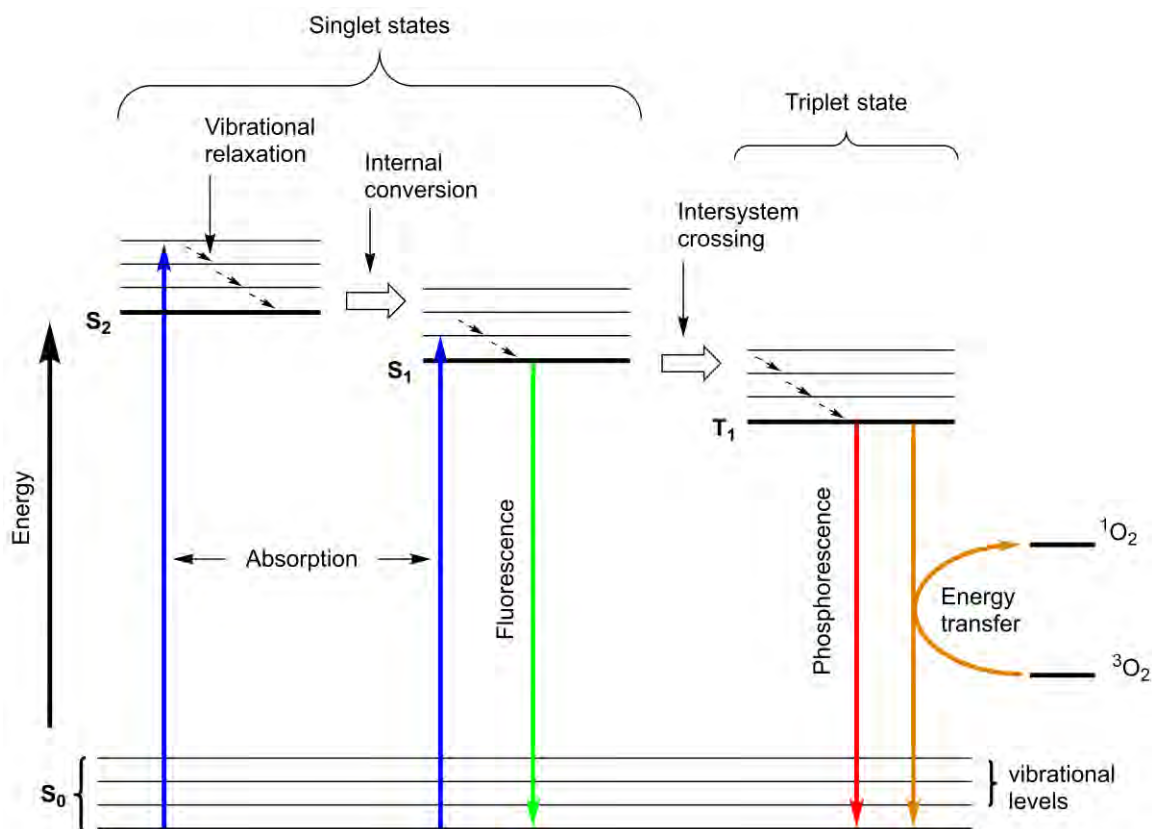


Figure 1.1: Jablonski diagram. Absorption of a photon excites the fluorophore, promoting an electron from S_0 to an excited state (S_x) (blue arrow). An electron from a higher excited state (i.e. S_2) can enter S_1 through internal conversion and then relax to the lowest vibrational level of S_1 via vibrational relaxation (black dashed arrows). From S_1 , the electron can either relax back to S_0 via radiative relaxation (green arrow, fluorescence) or enter the triplet state T_1 via intersystem crossing. In T_1 , the electron either relaxes back to S_0 via radiative relaxation (red arrow, phosphorescence) or undergoes energy transfer with triplet state oxygen (3O_2) to form singlet state oxygen (1O_2).

A fluorophore has several important photophysical characteristics: peak excitation and emission wavelengths, molar extinction coefficient, fluorescent lifetime, and quantum yield. As discussed previously, due to energy losses during vibration relaxation, the energy required for excitation is always higher than the energy of the photon emitted. This energy difference is reflected by the difference between the peak excitation (λ_{ex}) and emission (λ_{em}) wavelengths in nanometers, known as the Stokes' shift ($\lambda_{\text{ex}} - \lambda_{\text{em}}$). For example, the Stokes' shift of fluorescein is 24 nm (515-491) (**Figure 1.2**). The molar extinction coefficient (ϵ) measures how well the fluorophore absorbs photons. Fluorescence lifetime (t_{fl}) describes how long the fluorophore remains in the excited state before photon emission. Lastly, the fluorescence quantum yield (Φ_{fl}) measures how efficiently the fluorophore reemits a photon.

A simple view of the Φ_{fl} is the ratio of photons emitted over photons absorbed (**Eq. 1.2**). For example, if a fluorophore absorbs 100 photons and in turn, reemits 100 photons, then the $\Phi_{\text{fl}} = 1$ or 100% ($100/100 = 1$). Conversely, if a fluorophore absorbs 100 photons and in turn, reemits only 50 photons, then the Φ_{fl} becomes 0.5 ($50/100 = 0.5$). Accordingly, a non-emitting molecule has a Φ_{fl} of 0 ($0/100 = 0$).

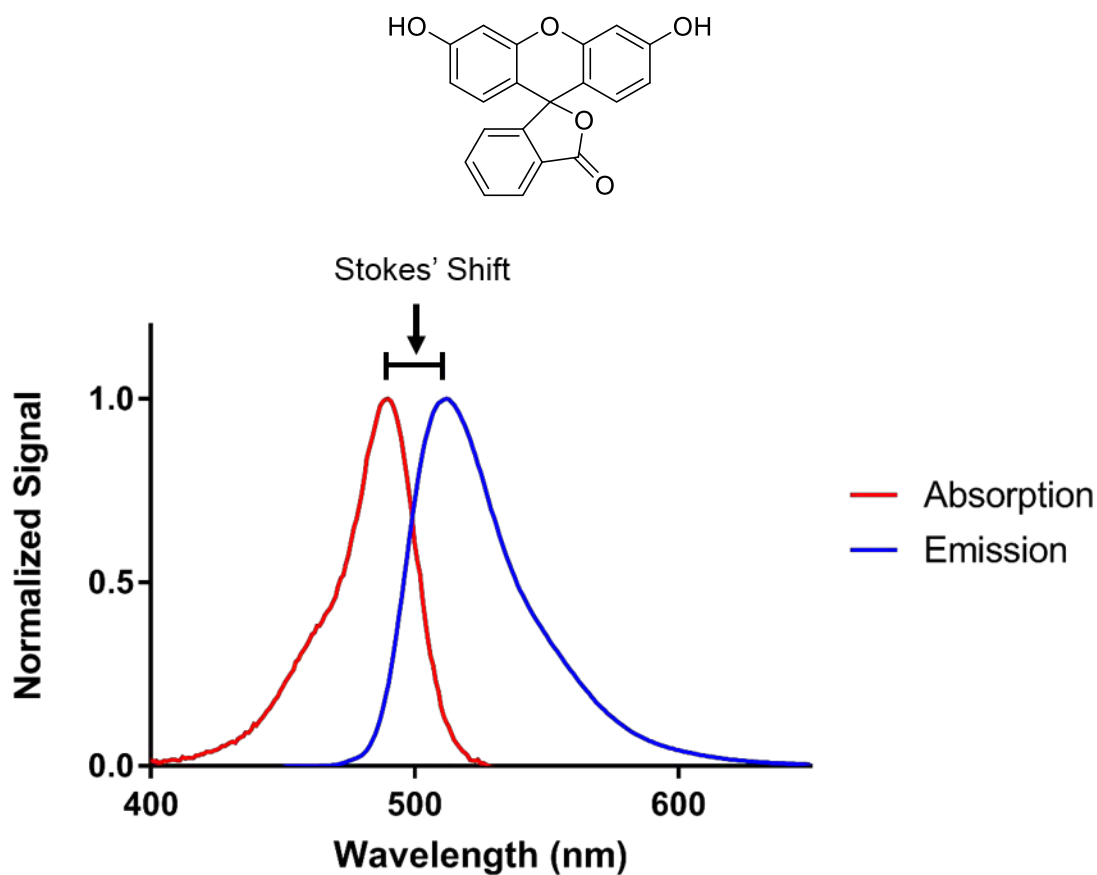


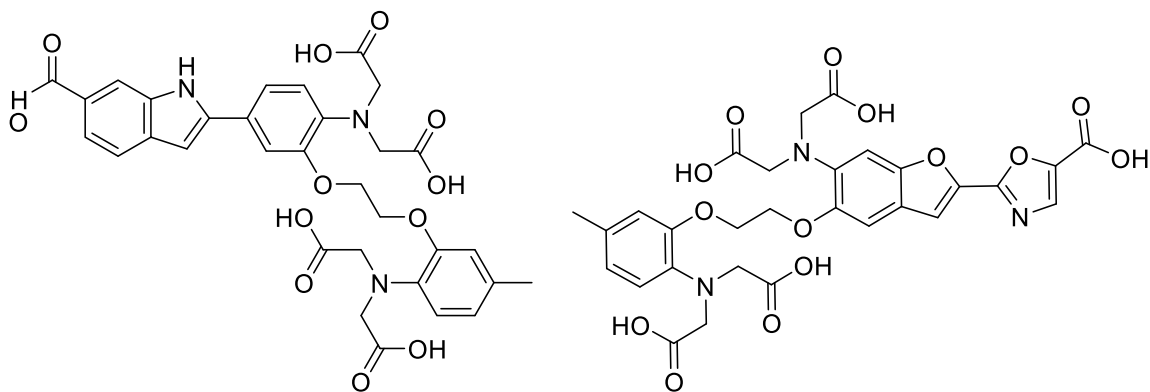
Figure 1.2: Optical properties of fluorescein. Absorption (red), emission (blue), Stokes' shift (black) and structure (top) of fluorescein

$$\Phi_{\text{fl}} = \frac{\text{photons emitted}}{\text{photons absorbed}} \quad [\text{Eq. 1.2}]$$

Fluorescence in Biology

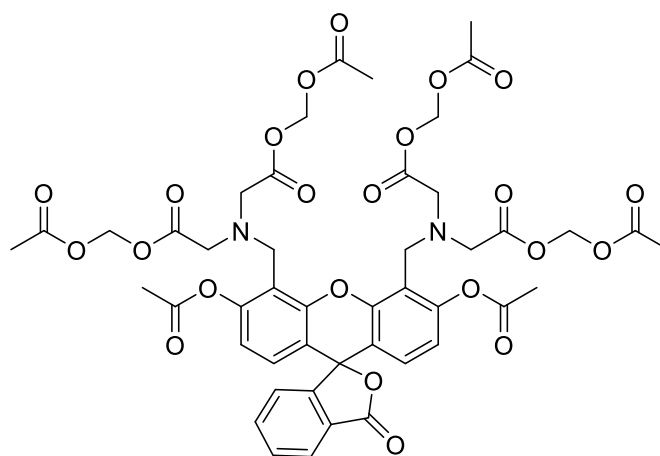
Chemical fluorescent probes or fluorophores are heavily utilized to elucidate key biological processes as well as to visualize structural morphology. These light emitting molecules allow us to noninvasively visualize, locate and identify biological targets with great detail.⁷ They are extremely versatile, having found important roles in both research and clinical settings.^{8,9} Popular examples of fluorescence-based techniques include: ion sensing, enzyme-linked immunosorbent assay (ELISA), and fluorescence microscopy.

Fluorescent-based probes have been widely used as sensors to detect ion flux. Binding of the sensor to its orthogonal target will either lead to activation or inhibition (quenching) of fluorescence.¹⁰⁻¹² For example, Calcein AM, Fura-2, and Indo-1 are three popular calcium sensors (**Figure 1.3**). Although they are all calcium sensors, their underlying mechanisms are different. Calcein AM is a single wavelength sensor, where calcium binding increases the fluorescence. In contrast, Fura-2 and Indo-1 are ratiometric sensors, meaning that calcium-binding changes their spectral profiles. For Fura-2, calcium binding shifts the absorption spectra (from 340 to 380 nm), while maintaining the same peak emission wavelength. Calcium concentration is calculated by the ratio of emission signals from 340 nm and 380 nm excitation. Calcium binding to Indo-1 shifts the peak emission from 340 to 300 nm and the concentration of calcium is calculated by the ratio of two emission signals.¹³



Indo-1

Fura-2



Calcein AM

Figure 1.3: Examples of chemical sensors

ELISA utilizes enzyme-conjugated antibodies to detect proteins of interest. Traditional ELISA was chemiluminescence-based, however, fluorescence-based assays predominate in modern applications. In an ELISA assay, samples are treated with primary antibodies to detect a specific protein of interest, followed by an enzyme linked-secondary antibody that recognizes the primary antibody. The enzyme on the secondary antibody then acts on a fluorophore precursor (*leuco-dye*) to generate the active fluorophore allowing for instrumental detection.

Fluorescence microscopy can be performed on either fixed or live cells (**Figure 1.4**). Fixed cells offer a convenient way to detect specific proteins and selectively image structures of interest using fluorescently labeled antibodies, a technique known as immunofluorescence microscopy.¹⁴ Live cells offer a more realistic image of cellular dynamics and physiology, but this procedure is usually limited to the usage of fluorescent proteins. Antibodies simply cannot diffuse across cellular membranes. Although site-specific antibodies aren't suitable for live cells, there are a plethora of fluorescent markers. These fluorescent markers are specially designed to identify and survey specific subcellular compartments in cells. For example, commercially available ERTracker, MitoTracker, LysoTracker, and DRAQ5 are designed to accumulate in the endoplasmic reticulum (ER), mitochondria, lysosomes, and nucleus, respectively.^{15–19} Moreover, ion sensors such as Calcein AM and others can be used in live-cell imaging to monitor ion flux. Finally, applications of fluorophores are not confined to research settings. For example, fluorescein is used as a beacon to guide rescuers to the site of distress during

sea rescues and to detect physical damage of the cornea. Clearly, fluorescent probes have widespread applications, which will continue to expand.

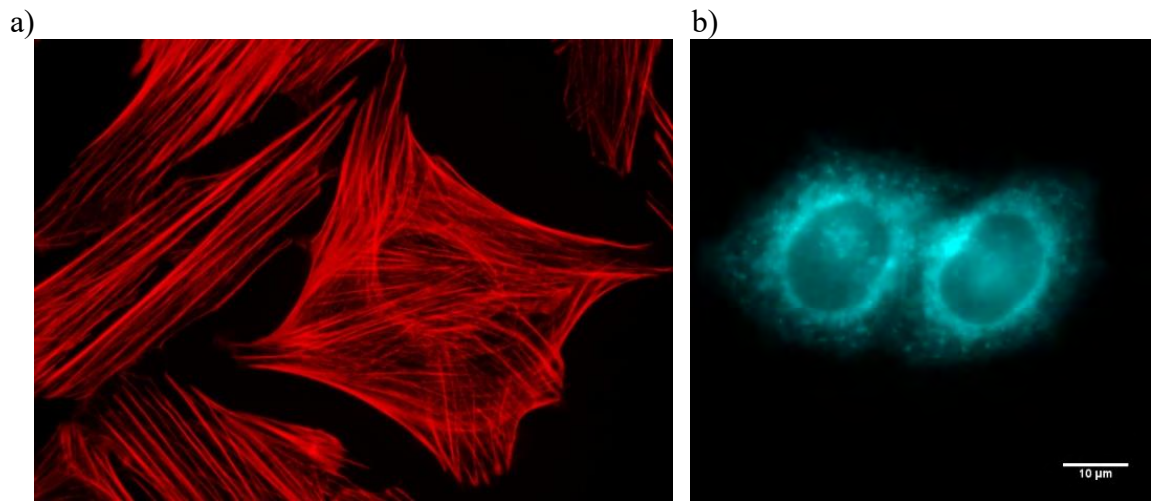


Figure 1.4: Fixed and live cell fluorescent staining. Actin stained with Alexa Fluor 633 conjugated phalloidin in fixed Indian Muntjac deerskin fibroblast cells. Image is adopted from <https://www.microscopyu.com/gallery-images/indian-muntjac-actin-cytoskeleton>. (a) Live Hela cells stained with ER-Tracker (b).

Near Infrared (NIR) Fluorophores

Visible-light fluorophores (400 – 650 nm) are compatible with a wide range of applications as previously mentioned. However, the employment and detection of visible light in biological samples can be problematic. First, endogenous chromophores typically absorb between 240 and 500 nm and emit (autofluorescent) between 280 and 570 nm (**Figure 1.5a**). Other components include chlorophyll, which can absorb and emit at much longer wavelengths, and hemoglobin, which strongly absorbs light up to 700 nm (**Figure 1.5b**)^{4,20–22} Under many experimental conditions, visible-light fluorophores such as fluorescein and rhodamines are bright enough to overcome the background, however, these fluorophores may be inadequate for assays that require low fluorophore loading. Second, short wavelength illumination can excite endogenous chromophores and induce the formation of reactive oxygen species (ROS) leading to cytotoxicity or cell death (phototoxicity).^{23–26} Third, since hemoglobin strongly absorbs light up to 700 nm, *in vivo* deep tissue imaging with visible fluorophore is challenging (**Figure 1.5**).

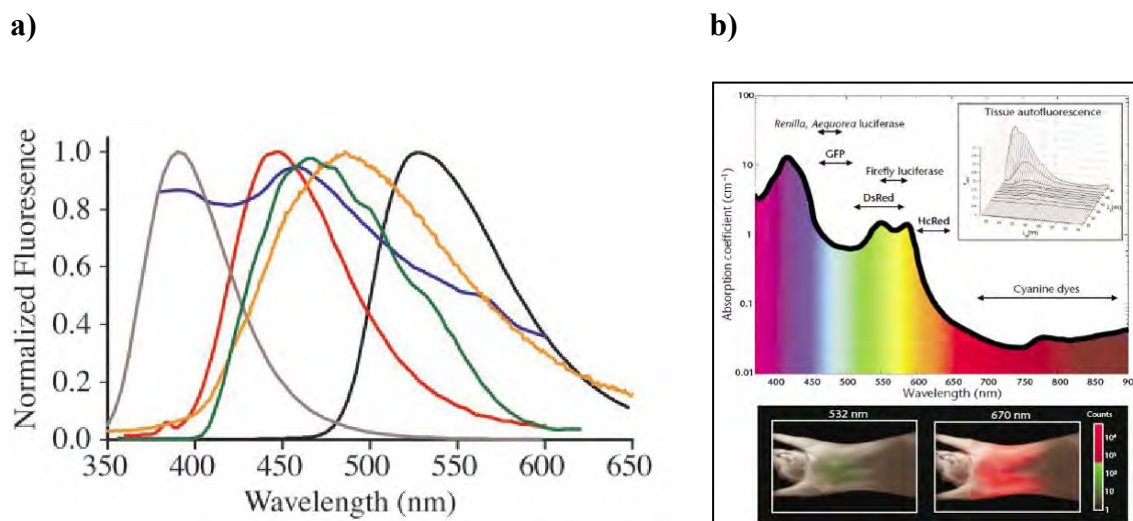


Figure 1.5: Autofluorescence and absorption of endogenous chromophores.

Emission of riboflavin (black), NADH (green), folic acid (red), cholecalciferol (purple), pyridoxine (tan) and retinol (orange) (a). Figure adopted from Zipfel et al.²¹ Hemoglobin strongly absorbs up to 700 nm. NIR light effectively penetrates deep tissues, giving higher fluorescence signal (b) Figure adopted from Weissleder et al.²²

The employment of near-infrared (NIR) fluorophores can circumvent many of the disadvantages of visible-light fluorophores. NIR light (650 - 900 nm) can more effectively penetrate deep tissues and avoid the excitation of most endogenous chromophores.²⁷ Samples imaged with NIR probes are optically clearer compared to their visible-light counterparts and thus, more effective in cell and deep tissue imaging (**Figure 1.5**).²² NIR fluorophores can also complement the wide palette of visible-light fluorescent probes with little or no spectral overlap. However, these major benefits are countered by several major drawbacks to NIR fluorophores. First, most NIR fluorophores have hyperextended π -conjugation, yielding planar compounds that are prone to self-quenching via hydrophobic stacking and nonspecific binding.²⁸ Second, quantum yields

of NIR fluorophores are typically lower than those of visible-light fluorophores.^{2,29,30} Third, the diversity of NIR scaffolds remains scarce. Currently, the popular NIR fluorophore scaffolds include cyanines, squaraines, and boron-dipyrromethenes (BODIPYs) (**Figure 1.6**).^{31,32}

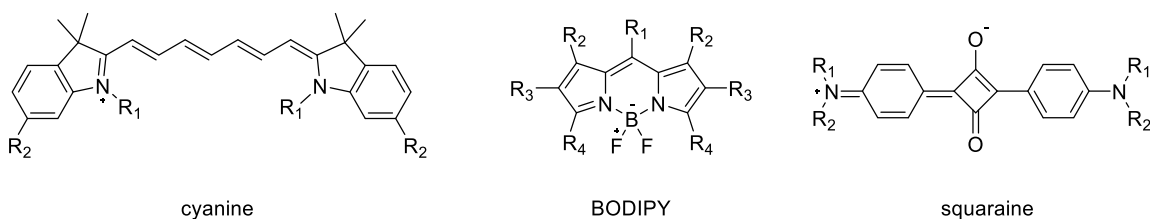


Figure 1.6: Structures of popular classes of NIR fluorophores

Cyanines are by far the most popular class of NIR fluorophores and dominate the commercial markets. The most well-known cyanine derivative is perhaps Indocyanine Green (ICG), one of the three FDA approved imaging probes approved for human use (**Figure 1.7**).^{27,33} The excitation and emission wavelengths of cyanine dyes can be readily fine-tuned through the length of their polymethine chain. Moreover, cyanines have two nitrogens that can be functionalized with labeling moieties (**Figure 1.8**). Cyanines typically require 5 or more carbons within the polymethine chain to achieve NIR excitation/emission wavelengths. However, the polymethine chain is a hydrophobic planar structure that is part of the conjugated aromatic system. Thus, as the chain length increases, aqueous solubility, in turn, decreases.

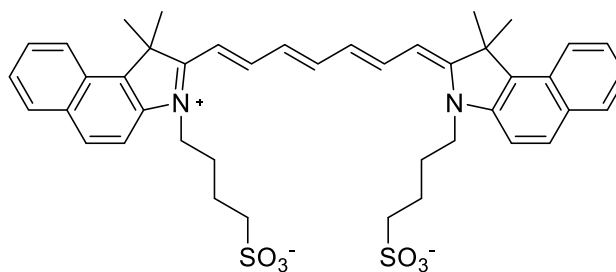


Figure 1.7: Structure of Indocyanine Green (ICG)

Negatively charged functional groups such as sulfonates (SO_3^-) are frequently used to endow aqueous solubility to hydrophobic molecules for reasons that will be discussed in the following section. The introduction of sulfonates greatly enhances the aqueous solubility and quantum yield of cyanines in water.³⁴ However, large cyanines, such as ICG, even bis-sulfonation (two sulfonates) is not enough to grant complete aqueous solubility (**Figure 1.7**). In contrast to unsulfonated cyanines, most sulfonated cyanines cannot diffuse across the membrane of cells. The poor photostability of NIR cyanines also remains a critical weakness. Interestingly, due to their ability to generate singlet oxygen, which is related to the lack of photostability, cyanines are currently being evaluated as potential candidates for PDT.^{35,36}

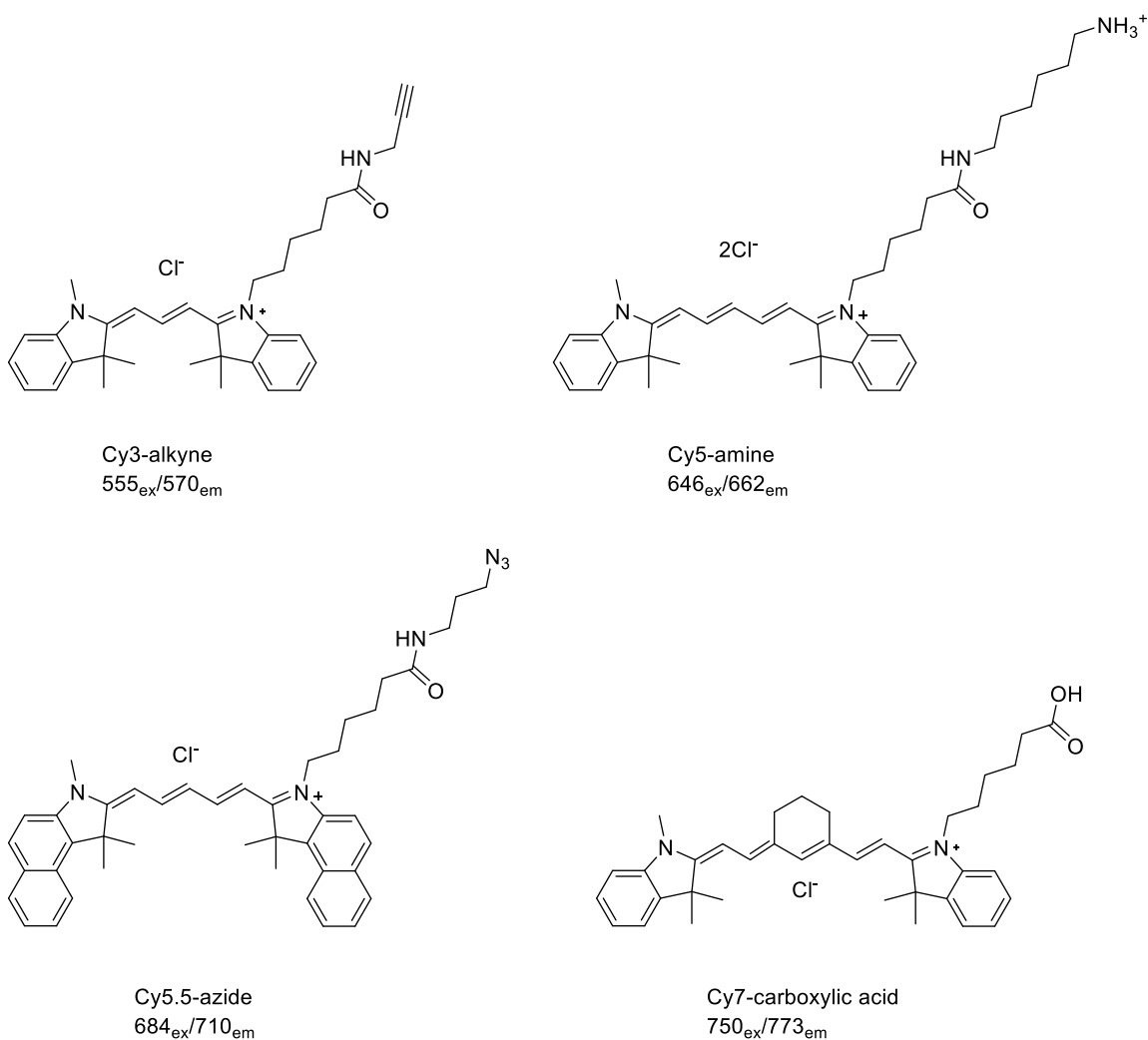


Figure 1.8: Excitation and emission of different cyanines. The length of polymethine chain determines the ex/em wavelengths of cyanines. Nitrogens of the indoline moiety support functionalization with different affinity tags. Structures are compiled from www.lumiprobe.com.

Squaraine fluorophores are excellent NIR fluorophores with high extinction coefficient (ϵ).^{31,32} Squaraines can be synthesized via simple condensation of squaric acid with two equivalence of a secondary aniline (**Figure 1.9**).^{37,38} However their planar structure limits aqueous solubility and renders them susceptible to quenching via aggregation.³¹ Moreover, the oxycyclobutenolate core is electron deficient and susceptible to nucleophilic attacks.^{38,39} Encapsulation of the oxycyclobutenolate moiety with tetralactam macrocycles (rotaxane), as reported by Arunkumar *et al.* dramatically increases aqueous stability, but the aqueous solubility remains suboptimal.⁴⁰ Unfortunately, all squaraine dyes suffer from low quantum yields in aqueous media. Addition of aqueous-soluble sulfonate groups successfully increases solubility but does not improve quantum yields.⁴¹

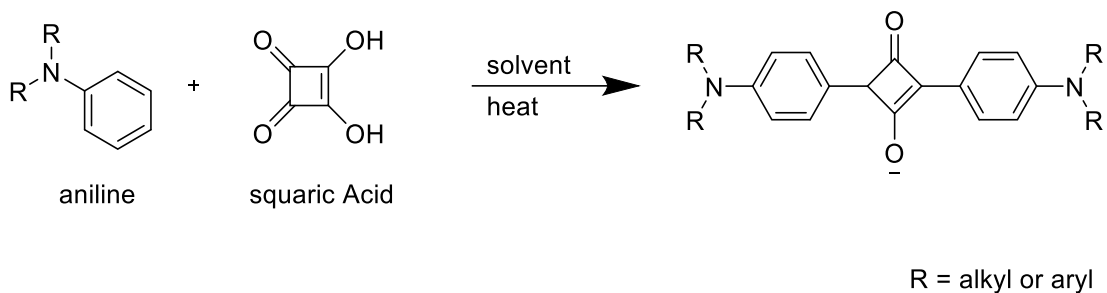


Figure 1.9: General synthesis of squaraine fluorophores. Condensation between squaric acid and two equivalence of aniline forms squaraine fluorophores.

BODIPYs have been heavily investigated for their potential as NIR imaging probes. Since their introduction in the mid-1990s, the BODIPY scaffold has been exhaustively modified to achieve excitation and emission wavelengths beyond 800 nm, with moderate to high quantum yields.³² BODIPYs are highly modular; every aryl position on the molecule can be modified (**Figure 1.6**). Unfortunately, like squaraine and cyanines, their extended π -conjugation limits aqueous solubility. Sulfonated visible-light BODIPYs show increased aqueous solubility^{42–44}, however, sulfonated NIR BODIPYs are unstable.⁴⁵

Sulfonated Fluorophores

Sulfonation is frequently used to enhance the aqueous solubility and brightness of hydrophobic fluorophores in water.^{34,46,47} In fact, most commercially available fluorophores, both visible and NIR, have at least one sulfonate (**Figure 1.10**). Sulfonates are excellent at solubilizing hydrophobic compounds for two reasons. First, their tetrahedral geometry helps prevent stacking of the planar dye. Second, sulfonic acids are strong acids, usually with negative pK_as. Their high acidity ensures ionization across a wide pH range leading to an increase in polarity.⁴⁶ However, the aqueous solubility endowed by sulfonates also prevents cellular membrane diffusion.^{47–49} As a result, sulfonated fluorophores are generally restricted to applications utilizing fixed cells or use *in vitro* assays.

Protection or masking of anionic groups is a common strategy to deliver polar charged compounds into live cells.^{50,51} For example, Calcein AM is a protected fluorophore with its negatively charged carboxylates protected (masked) as neutral esters. Upon cellular entry, Calcein AM is deprotected (unmasked) by intracellular esterases and retained by cells (**Figure 1.11**). Unfortunately, the design of sulfonate-protecting groups is not as straightforward as other polar groups. While esterification of a carboxylic acid yields stable esters, sulfonate esters are generally unstable.⁵² Their alpha-carbon is highly electrophilic, which is prone to nucleophilic attacks that could lead to promiscuous sulfonate deprotection and non-specific alkylation of biomolecules. For example, ethyl

methanesulfonate (EMS) is a common DNA alkylation agent used to induce G:C to A:T mutations.

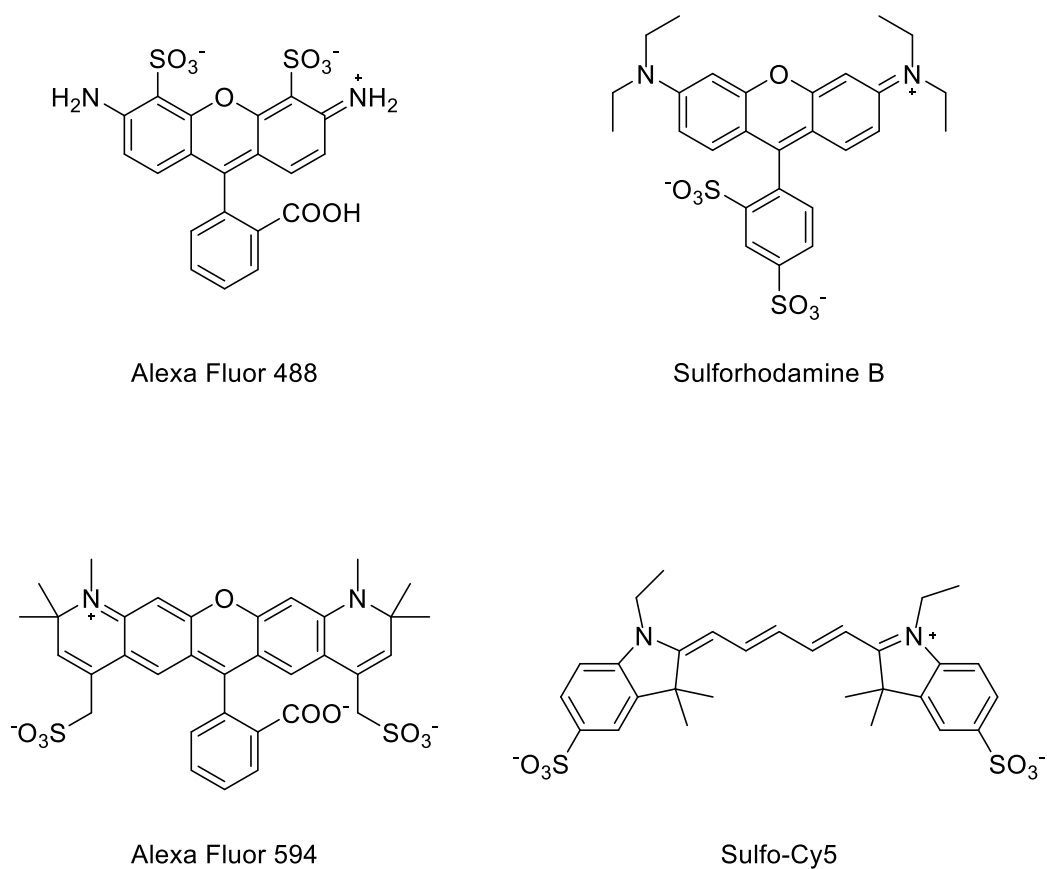


Figure 1.10: Commercially available sulfonated fluorophores. Structures of Alexa Fluors were drawn without linkers and obtained from <https://www.atdbio.com/content/34/Alexa-dyes>.

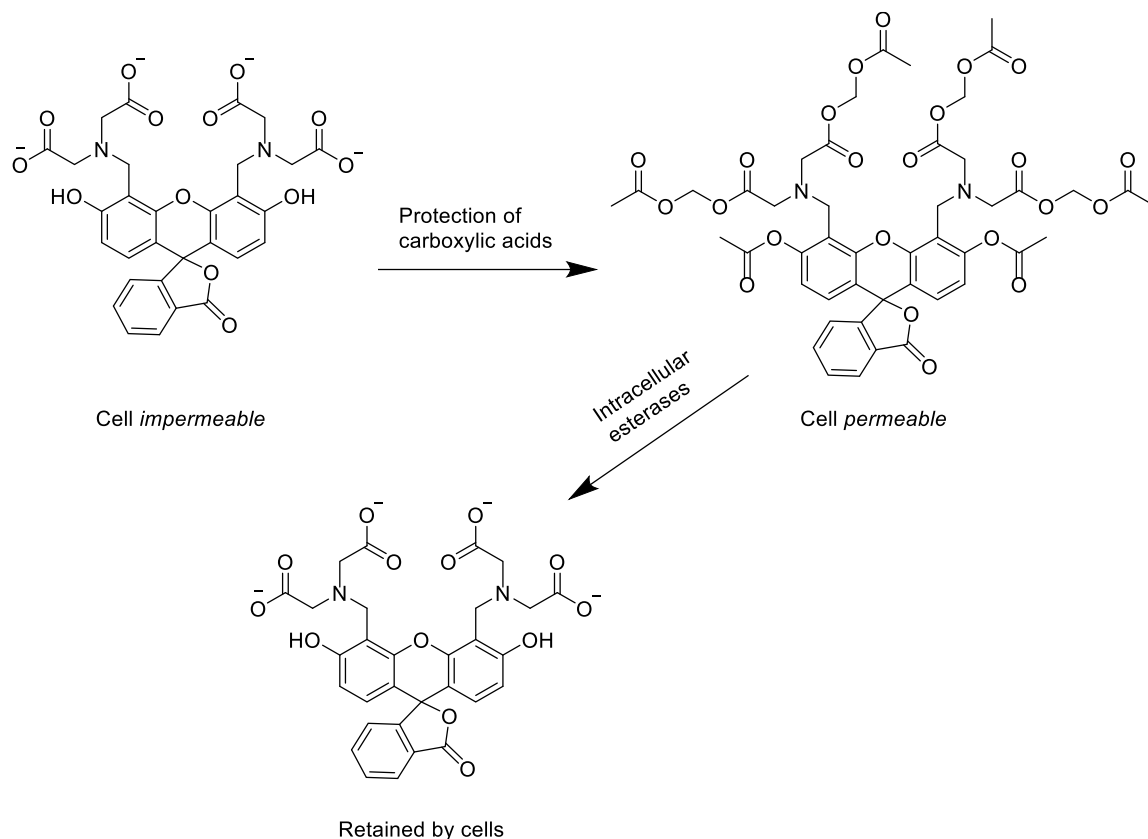


Figure 1.11: Protection of Calcein AM. Polar carboxylic acids are masked with neutral esters, which grants cell permeability. Activity of esterase unmasks the esters to polar carboxylic acids, which are retained by cells.

In 2011, Rusha and Miller successfully formulated an esterase-labile stable protecting group for sulfonates. Using this group, they delivered a sulfonated fluorophore, dansyl sulfonate, into live Chinese Hamster Ovarian (CHO) cells.⁴⁸ Unfortunately, this remains the only example of protecting groups designed to deliver sulfonated molecules into live cells.

Red-shifted Rhodamines

In 2008, Fu et al. revolutionized fluorescent probe design when they replaced the oxygen in a xanthene fluorophore called Pyronin Y with silicon (**Figure 1.12**). This single substitution red-shifted both the excitation and emission wavelengths by about 90 nm, from 552_{ex}/569_{em} to 641_{ex}/659_{em}.⁵³ Since the introduction of Si-Pyronin Y (SiP), a wave of novel Si-rhodamines (SiR) have subsequently emerged (**Figure 1.13**).^{39,54–57}

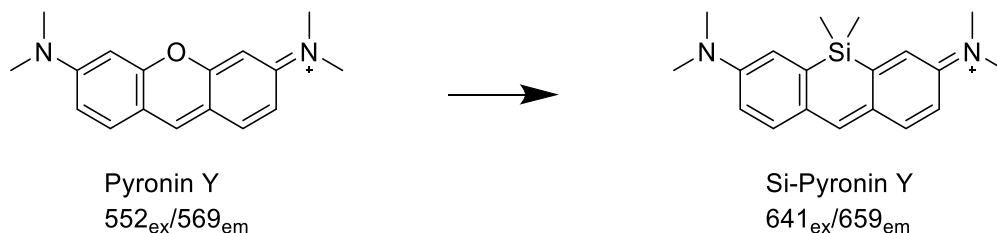


Figure 1.12: O to Si substitution causes large bathochromic shifts in Pyronin Y

Rhodamines are within the xanthene family and like Si-Pyronin Y, Si-rhodamines (SiR) exhibit similar bathochromic shifts. For example, the excitation and emission wavelengths of tetramethylrhodamine (TMR) (548_{ex}/572_{em}) are red-shifted by ~90 nm in Si-tetramethylrhodamine (SiTMR) (643_{ex}/662_{em}) (**Figure 1.13**).⁴⁷ Moreover, Si-rhodamines retain the high photostability of rhodamines with quantum yields comparable to near-IR cyanine fluorophores.^{57,58} These advantageous properties of Si-rhodamines have been exploited for live-cell, *in vivo*, and super-resolution microscopic techniques.^{10,55,59–61}

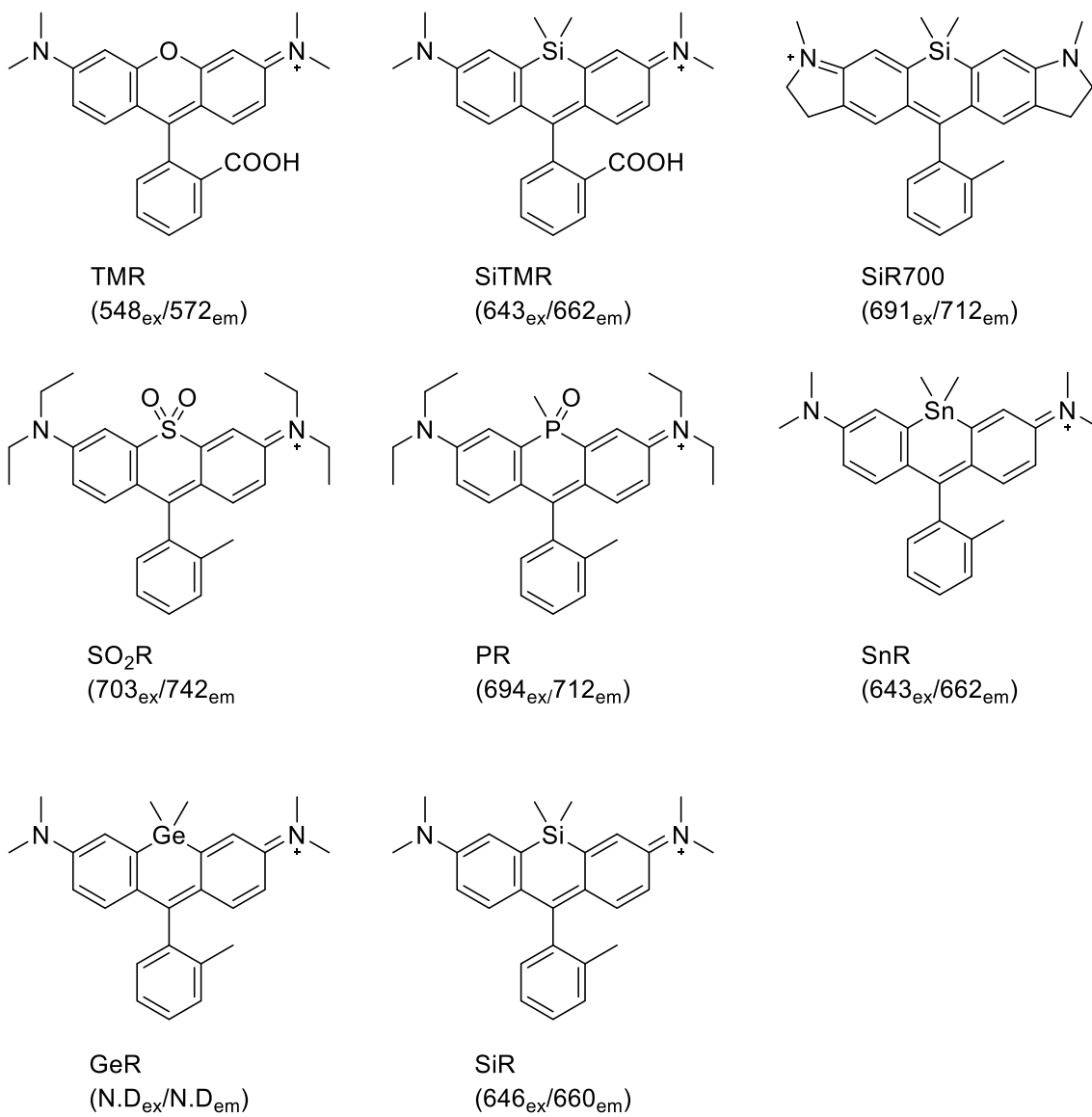


Figure 1.13: Structures of rhodamines and substituted rhodamines and their optical properties

Other group 14 elements such as Tin (Sn) and germanium (Ge) have been installed into rhodamines to yield Sn-rhodamine (SnR) and Ge-rhodamine (GeR), respectively (**Figure 1.13**). GeR has slightly smaller bathochromic shifts compared to SiR. The excitation and emission wavelengths of SnR were not reported but SnR has been shown to have extremely low photostability, even when compared to Cy5.⁶² Phosphorus and sulfones have also been installed into rhodamines to yield P-rhodamines (PR) and SO₂-rhodamines (SO₂R), respectively (**Figure 1.13**). Remarkably, both PR and SO₂R displayed noteworthy bathochromic shifts of ~140 nm in both excitation and emission, although PR suffers from a large drop in quantum yield.^{63,64}

The bathochromic shifts of SiR have been attributed to the narrowing of the HOMO-LUMO energy gap. Cyclic voltammetry analysis of Si-Pyronin Y (SiP) showed increased and decreased HOMO and LUMO energy levels, respectively. Density functional theory (DFT) analyses of SiR produced similar results. However, DFT analyses of phosphorus-rhodamine (PR) and sulfone-rhodamine (SO₂R) also showed decreased HOMO energy levels. Because of the higher HOMO energy levels and lower LUMO energy levels, the HOMO-LUMO energy gap of PR and SO₂R are even smaller than those found in SiR. The HOMO energy levels are thought to be affected inductively through the σ -bonds of the bridging atom and the adjacent carbons, where higher inductivity yields higher HOMO levels. On the other hand, the lowered LUMO energy levels are projected to be the result of overlapping p orbitals of the aromatic carbon atoms adjacent to the bridging atom with s orbitals of the methyl groups ($\sigma^*-\pi^*$ conjugation) and/or d orbitals of the bridging atom ($d^*-\pi^*$ conjugation).^{53,62-64}

Oxazines and Si-Oxazines (Azasilines)

Oxazines are one of the most compact classes of NIR fluorophores. They are structurally related to rhodamines, but with a nitrogen substitution in position 9 (**Figure 1.14**). Unlike other larger NIR fluorophores such as ICG, sulfonation readily confers water-solubility to oxazines.⁴⁹ The typical excitation and emission wavelengths of oxazines are 640 and 660 nm, respectively, which are 90 nm longer than rhodamines.

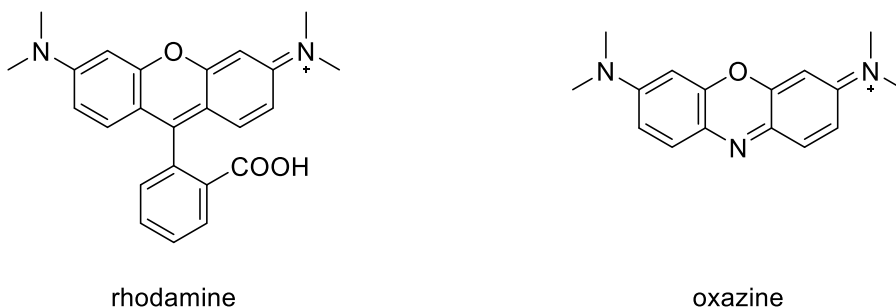


Figure 1.14: Structural similarities between rhodamines and oxazines

Substitution of the oxygen atom (silylation) with the goal of bathochromic shifts in both excitation and emission has been exclusively investigated in the rhodamine scaffold. Given the structural similarities between oxazines and rhodamines, oxygen to silicon in oxazines should also result in similar bathochromic shifts. Both Si-rhodamines and oxazines absorb and emit at wavelengths ~90 nm longer than rhodamines. Thus, the combination of the two modifications could potentially yield “Si-oxazines” (azasilines) with excitation and emission wavelengths over 700 nm (**Figure 1.15**).

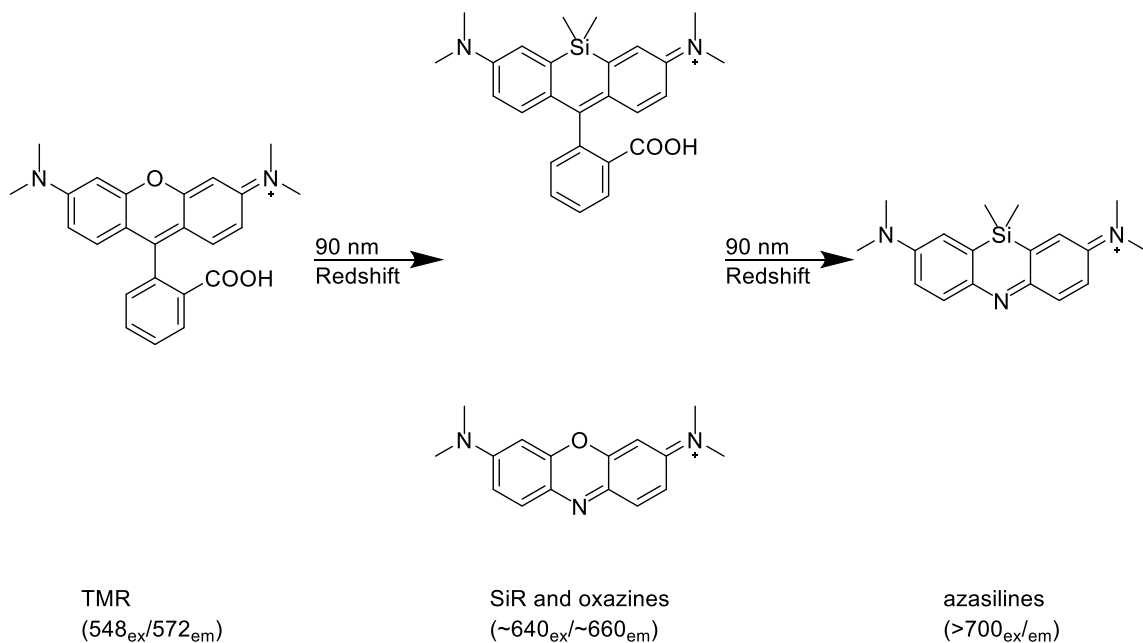


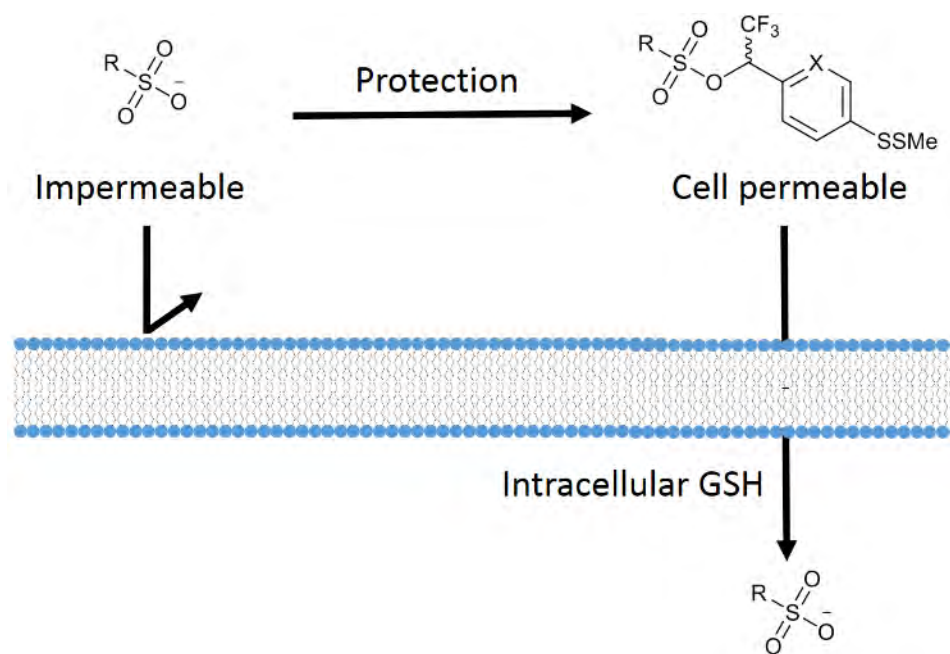
Figure 1.15: Potential spectral properties of azasilines. TMR is red-shifted by 90 nm via O to Si substitution. SiR and oxazines have similar excitation/emission wavelengths. Exchanging O for Si in oxazines (azasilines) could potentially yield an additional red-shift of 90 nm.

Summary

NIR fluorophores are highly desirable for two important reasons. First, there is minimal spectral overlap between NIR fluorophores, endogenous chromophores and visible-light fluorophores (chemical or protein). Since the light source used to excite NIR fluorophores do not excite endogenous chromophores, autofluorescence and phototoxicity are minimal. Moreover, NIR fluorophores are compatible with visible-light fluorophores in multicolored fluorescence assays. Second, NIR light is poorly absorbed by endogenous chromophores, it can penetrate deeper into and out of tissues, with a lower loss of the fluorescence signal, allowing for deep tissue *in vivo* imaging. Unfortunately, most NIR fluorophores are large hydrophobic molecules that suffer from poor photostability and/ or low aqueous solubility. Large hydrophobic surface areas can cause nonspecific binding, which decreases the signal to noise ratio in both *in vitro* and *in vivo*.⁶⁵ Sulfonation increases aqueous solubility, but prevents membrane diffusion and thus, limits the applications of sulfonated fluorophores to *in vitro* or fixed-cell assays. Moreover, molecular size can override the effects of sulfonates, as in the case of ICG, highlighting the difficulty in solubilizing larger organic molecules. Taken together, new classes of more compact, photostable NIR fluorophores, especially ones that absorb and emit over 700 nm, coupled with strategies to deliver sulfonated fluorophores across the cellular membrane are necessary to expand the utility of fluorescent probes.

CHAPTER II:

Reductively-Labile Sulfonate Ester Protecting Groups That Are Rapidly Cleaved By Physiological Glutathione



Adopted from Choi and Miller⁶⁶

Summary

Sulfonates are frequently used to endow aqueous solubility on hydrophobic molecules. However, most sulfonated molecules cannot diffuse across the cellular membrane, which limits their applications in live cells. Only few sulfonate protecting groups exist and their cleavage often requires harsh chemical conditions. Here, I describe the first sulfonate esters that are cleaved by mild reductants such as glutathione, and their application to deliver a sulfonated dye into live mammalian cells.

Introduction

Sulfonation can dramatically increase the aqueous solubility of NIR fluorophores. In fact, many commercially available fluorophores are sulfonated (**Figure 1.10**). Although sulfonated fluorophores are more soluble, they are generally membrane impermeable.^{47–49} A common strategy to deliver polar species into cells is through protection, where the polar group is chemically converted (masked) into a neutral one.^{50,51} For example, the carboxylic acids on calcium sensor Calcein are converted to acetoxymethyl (AM) to yield the cell permeable Calcein AM (**Figure 1.11**). However, unlike carboxylates, sulfonates cannot be protected via simple esterification because the resulting sulfonate esters are generally highly electrophilic.⁵² Alkylation by EMS highlights the instability of sulfonate esters (**Figure 2.1**).

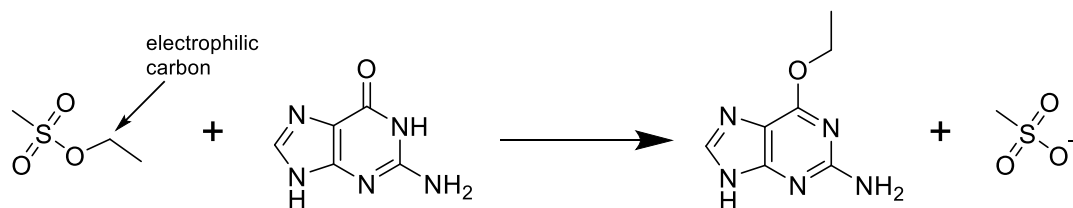


Figure 2.1: EMS alkylation of guanine into O6-ethylguanine.

Protecting groups may either carry a chemical or enzymatic trigger. However, enzymes are known to hold a certain degree of specificity towards their substrates. Further modifications of the protecting group motif may decrease or abolish enzyme recognition and/or activity completely.⁶⁷ Payload release efficiency is dependent on enzyme concentration and thus, could vary between cell types.⁶⁸ In contrast, chemical deprotection does not require enzyme recognition, which confers higher modularity by design. Potentially, longer, bulkier targeting moieties could be accommodated without losing efficiency.

There are a few examples of sulfonate protecting groups that cleave under chemical conditions; unfortunately, none were specifically designed for use in biological settings.^{52,69,70} Reported protecting groups often require harsh chemicals for deprotection, such as overnight treatment with sodium hydroxide or refluxing in ammonia.^{52,69}

The only examples of sulfonate protecting groups applicable for *in cellulo* use were reported by Rusha and Miller in 2011.⁴⁸ While several protecting groups were explored, the acetoxy trifluoromethyl benzyl (AcOTFMB) group was most efficient at sulfonate

release. AcOTFMB is based on the α -trifluoromethyl benzyl (TFMB) scaffold, which is comprised of three essential parts. First, a benzene group acts as the core scaffold, connecting the release trigger and sulfonate payload. Second, a trifluoromethyl group (CF_3) is mounted on the alpha carbon to stabilize it against nucleophilic attacks. The inductive electron-withdrawing properties of the CF_3 group confer stability through the destabilization of the partial positive charge or carbocation formed during nucleophilic substitution reactions (electronic deactivation). Compared to the methylated alpha carbons counterparts, trifluoromethylated alpha carbons were shown to be more resistant to nucleophilic attacks.⁷¹ Third, an esterase-labile acetoxy trigger is installed at the *para* position. **(Figure 2.2).**^{48,52}

Later, Pauff and Miller reported the TFMT, which is an acid-labile TFMB-based sulfonate protecting group..⁷² While TFMT cannot release sulfonates under biological conditions, it underlines the modularity of TFMB. Hence, I hypothesize that TFMB can be modified with biocompatible chemical release triggers.

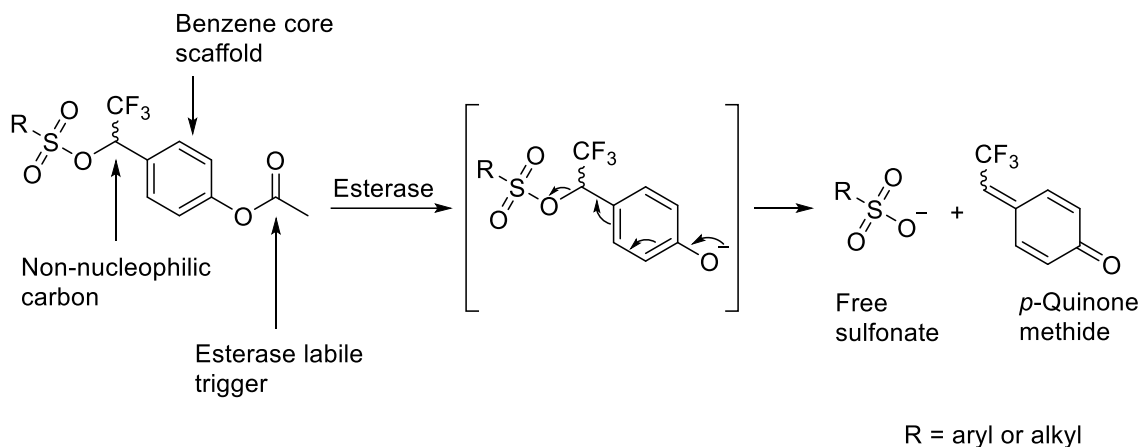


Figure 2.2: Design and proposed release mechanism of the esterase-labile AcOTFMB. Esterase activity instigates 1-6 elimination, releasing the sulfonate and forming a *p*-quinone methide as a byproduct.

The interior and exterior of cells are reducing and oxidizing, respectively.⁷³ The reducing intracellular environment of mammalian cells is largely maintained by the tripeptide glutathione (GSH), which protects the cell against oxidative stress.⁷⁴⁻⁷⁶ Maintenance of a high GSH level, typically 0.5-10 mM, is essential for cell survival. Thus, I proposed to take advantage of the reductive intracellular environment of cells by designing reductively-labile protecting groups (RLPG) for sulfonates. These RLPGs would be stable under oxidizing, extracellular environment, but rapidly release sulfonates after cell entry due to the activity of GSH.

The design of our RLPG is based on AcOTFMB. However, instead of an acetoxymethyl group, a disulfide group is placed in the *para* position of the TFMB scaffold. This disulfide serves as a linker between the TFMB and modular group. Reduction of the disulfide bond (reductive cleavage) should liberate the sulfonate via a 1,6-elimination

mechanism and forms a *p*-thioquinone methide, an poorly studied compound that is rarely if ever isolated (**Figure 2.3**).^{77–79} However, like *p*-quinone methide formed from AcOTFMB, the *p*-thioquinone methide is expected to further react and form adducts with nucleophiles.⁴⁸

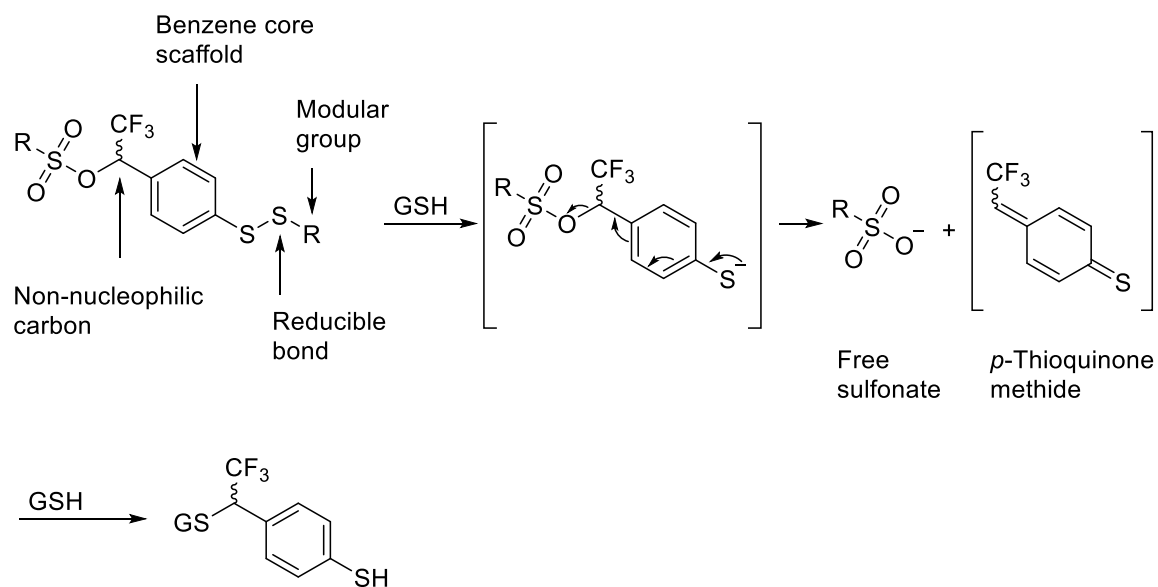


Figure 2.3: Design and proposed release mechanism of reductively-labile sulfonate protecting groups. Reduction of the disulfide bond (labeled as reducible bond) triggers 1-6 elimination, releasing the sulfonate and forming a thioquinone methide intermediate, which further reacts and forms an adduct with GSH.

Results and Discussions

Newman-Kwart rearrangement is a common method access thiophenols via the oxygen to sulfur rearrangement of the dimethyl thiocarbamate, followed by base-mediated hydrolysis (**Figure 2.4**).^{80,81} However, this rearrangement often requires temperatures over 250 °C.^{82,83} Thus, a synthetic route was adopted to access thiophenols.

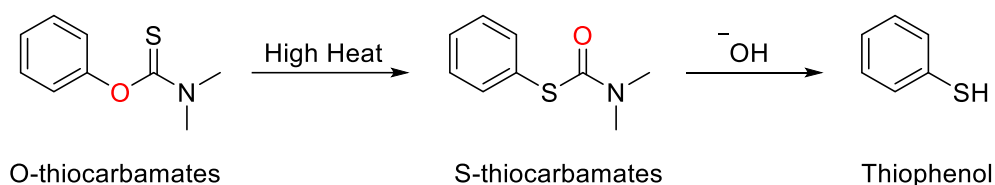
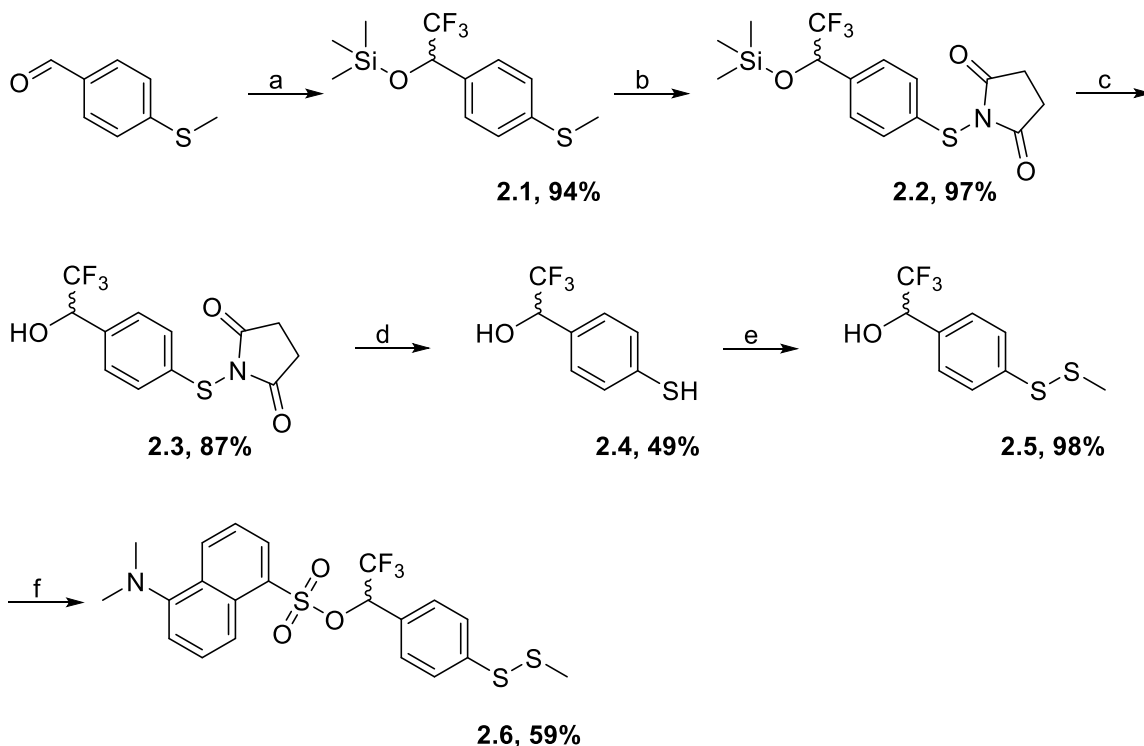


Figure 2.4: Accessing thiophenols using Newman-Kwart rearrangement. O-thiocarbamates rearranges under high heat to form S-thiocarbamates, which are hydrolyzed to yield thiophenols.

First, the Ruppert-Prakash reaction was used to convert commercially available 4-thiomethyl-benzaldehyde into the trimethylsilyl (TMS) protected trifluoromethyl alcohol **2.1**. Treatment of aq. HCl and THF mixture removed the TMS group to yield the free benzyl alcohol **2.2**. NBS treatment converted the thiomethyl group into the N-(thio)succinimide **2.3**. The succinimidyl group was removed with sodium borohydride reduction to afford the free thiophenol **2.4**, which was subsequently reacted with S-methyl methanethiosulfonate to yield the methyl disulfide, MeSSTFMB **2.5**. Finally, the dansyl sulfonate ester (dansylate) MeSSTFMB-Dan **2.6** was formed using DABCO and dansyl chloride (**Scheme 2.1**).



Scheme 2.1: Synthesis of MeSSTFMB-Dan. Reagents and conditions: (a) Me_3SiCF_3 , TBAF, THF, 0 °C to RT; (b) NBS, DCM, RT; (c) 1:1 aq. HCl/THF, RT; (d) NaBH_4 , MeOH, -40 °C to RT; (e) MeSSO_2Me , MeOH, pH 8 buffer, RT; (f) dansyl chloride, DABCO, DCM, RT.

Dansyl sulfonate contains an aromatic sulfonate. Esterification of the sulfonate increases the dipole moment by lowering the electron density of the oxygen atom on the sulfonate, which in turn, elongates both excitation and emission wavelengths. For example, the free dansyl-sulfonate and AcOTFMB-Dan have excitation/emission wavelengths of 332/498 nm and 346/557 nm, respectively (**Figure 2.5**). Further, successful delivery and release of free sulfonates into live cells yields diffusive fluorescence, whereas uncleavable sulfonate esters, such as TFMB, which lacks a trigger

are membrane permeable, but form aggregate puncta in the cell membrane (**Figure 2.6**).⁴⁸ Therefore, dansylates offer a convenient way to determine and evaluate sulfonate release efficiency, both *in vitro* and in live cells.⁴⁸

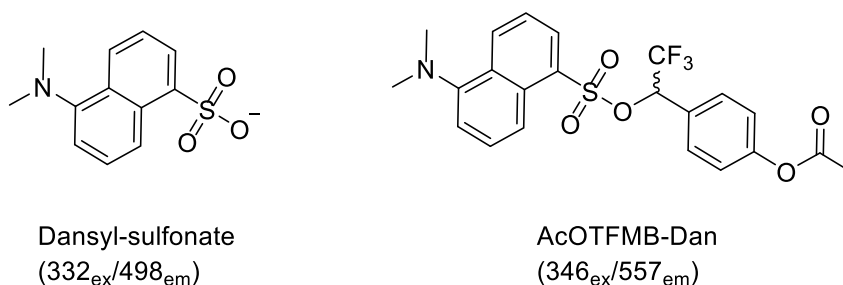


Figure 2.5: Excitation and emission wavelengths of dansyl-sulfonate and AcOTFMB-Dan. Dansyl sulfonate esters have red-shifted fluorescence compared to free sulfonate fluorophore.

Our goal was to design a RLPG that can deliver their entire payload (sulfonates) into live cells within 15 minutes, which is the typical incubation time for commercial fluorescent probes. To evaluate the sulfonate release efficiency, MeSSTFMB-Dan, along with other dansylates were incubated in the presence of reducing agents, either GSH (5 mM) or TCEP (1 mM) (**Figure 2.6**). TFMB-Dan lacks a release trigger and served as the uncleavable, negative control.⁴⁸ Two simple alkyl dansylates (methyl, **2.7** and ethyl, **2.8**) were also included to test whether GSH was capable of releasing sulfonates by acting as a nucleophile (**Figure 2.7**). If GSH can initiate efficient sulfonates release from simple alkyl dansylates, it would imply that enzyme-free sulfonate delivery could be achieved without special sulfonate protecting groups.

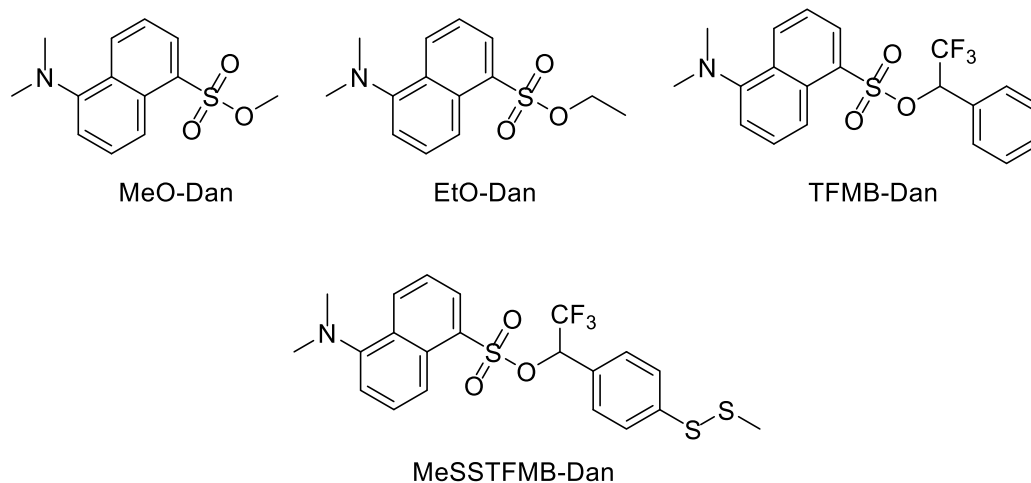


Figure 2.6: Structures of simple, reductively-labile MeSSTFMP and non-cleavable TFMB dansylates. From left to right, methyl dansylate (MeO-Dan), ethyl dansylate (EtO-Dan), TFMB, and MeSSTFMB-Dan.

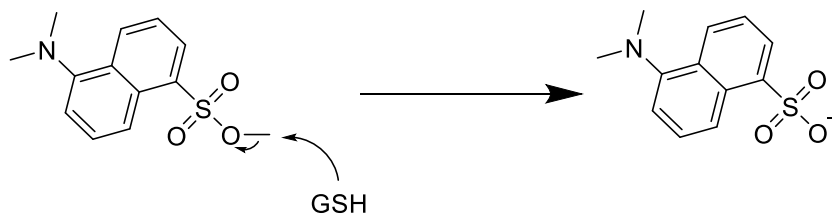


Figure 2.7: Potential sulfonate release from simple dansylates via nucleophilic activity of GSH. Simple dansylates are electrophilic. GSH may act as a nucleophile and trigger sulfonate release via a S_N2 mechanism.

Each sample was incubated with a reducing agent for 15 minutes at room temperature in the dark and then analyzed with high performance liquid chromatography (HPLC) to detect free dansyl sulfonates, unreacted dansylates, and the byproducts formed during reductive cleavage. As expected, TFMB-Dan did not yield free sulfonate under any reducing conditions tested (**Figure 2.8**). Surprisingly, the stability of the simple alkyl dansylates was higher than initially thought; the majority of the alkyl dansylates remained intact after treatment. Only minuscule amounts of free dansyl sulfonates were released by the methyl-dansylate (MeO-Dan) (**Figure 2.9 and 2.10**). In stark contrast, the MeSSTFMB-Dan afforded ~30% and ~90% cleavage from GSH and TCEP treatment, respectively (**Figure 2.11**).

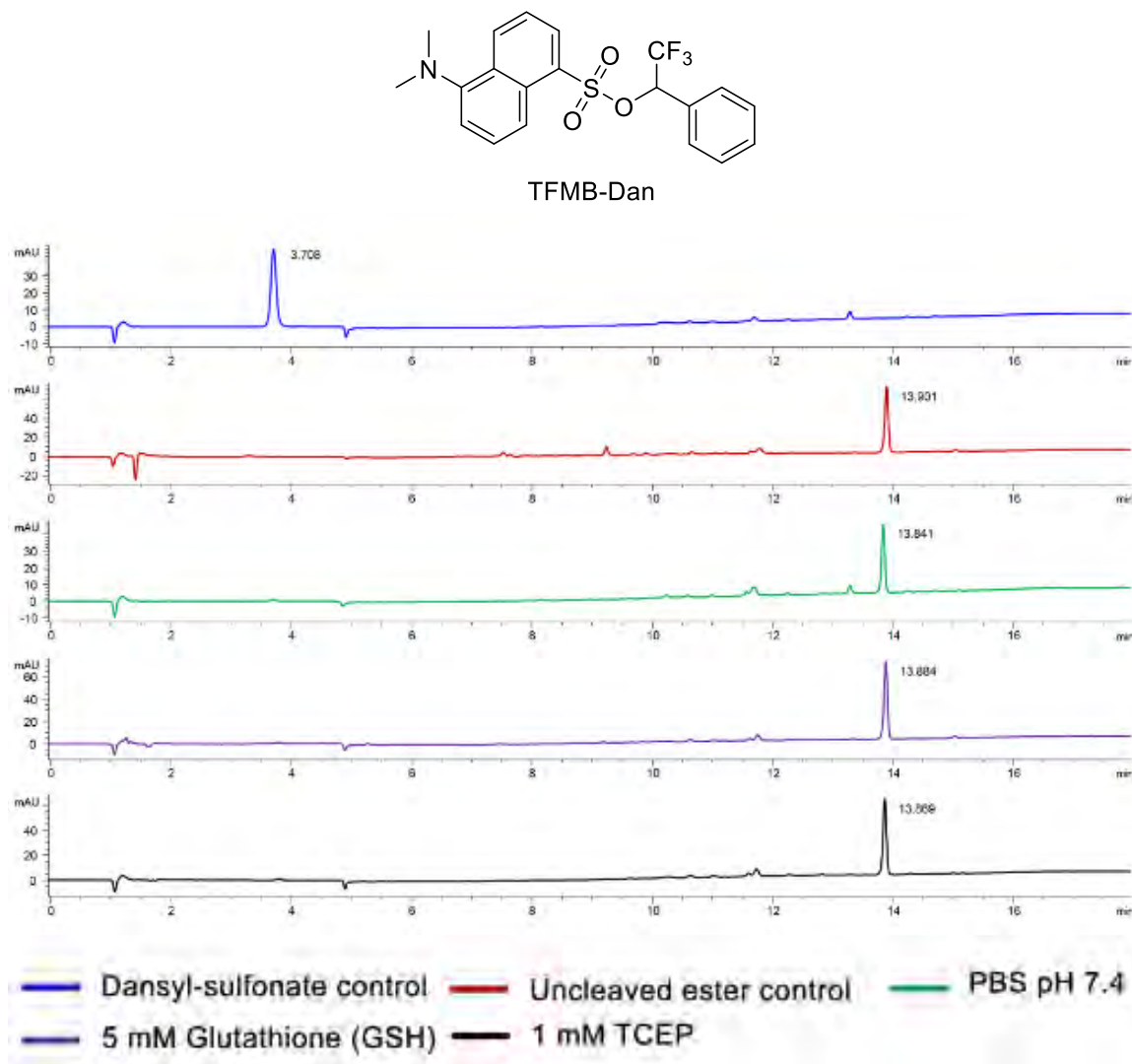


Figure 2.8: TFMB-Dan does not release sulfonates under reducing conditions. HPLC analysis of TFMB-Dan treated under different reducing condition. TFMB-Dan was treated with reducing agents or PBS alone for 15 minutes. Control samples were injected immediately, without prior incubation. Each peak is labeled with its retention time.

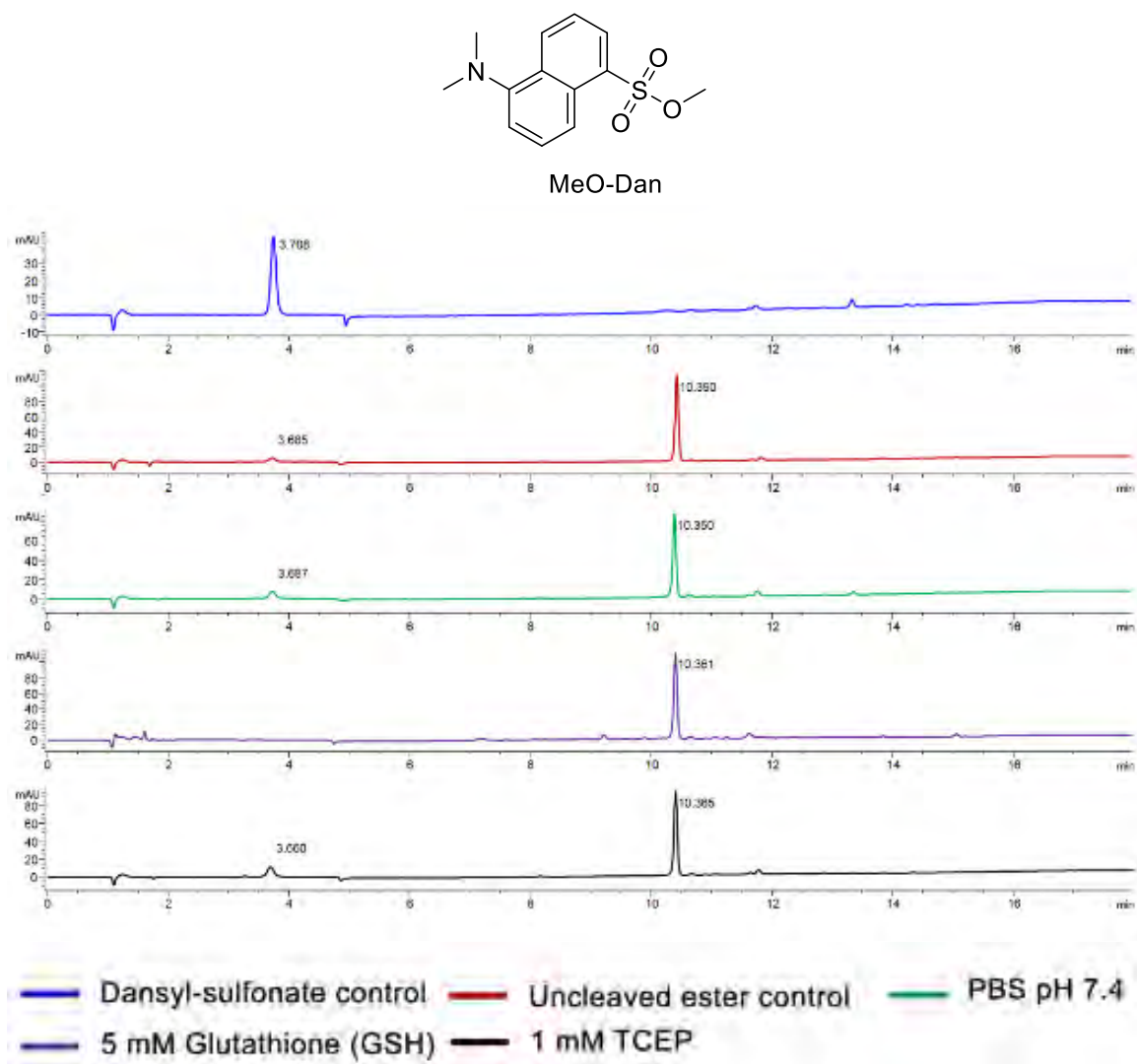


Figure 2.9: MeO-Dan does not efficiently release sulfonates under reducing conditions. HPLC analysis of MeO-Dan treated under different reducing conditions. MeO-Dan was treated with reducing agents or PBS alone for 15 minutes. Control samples were injected immediately, without prior incubation. Each peak is labeled with its retention time.

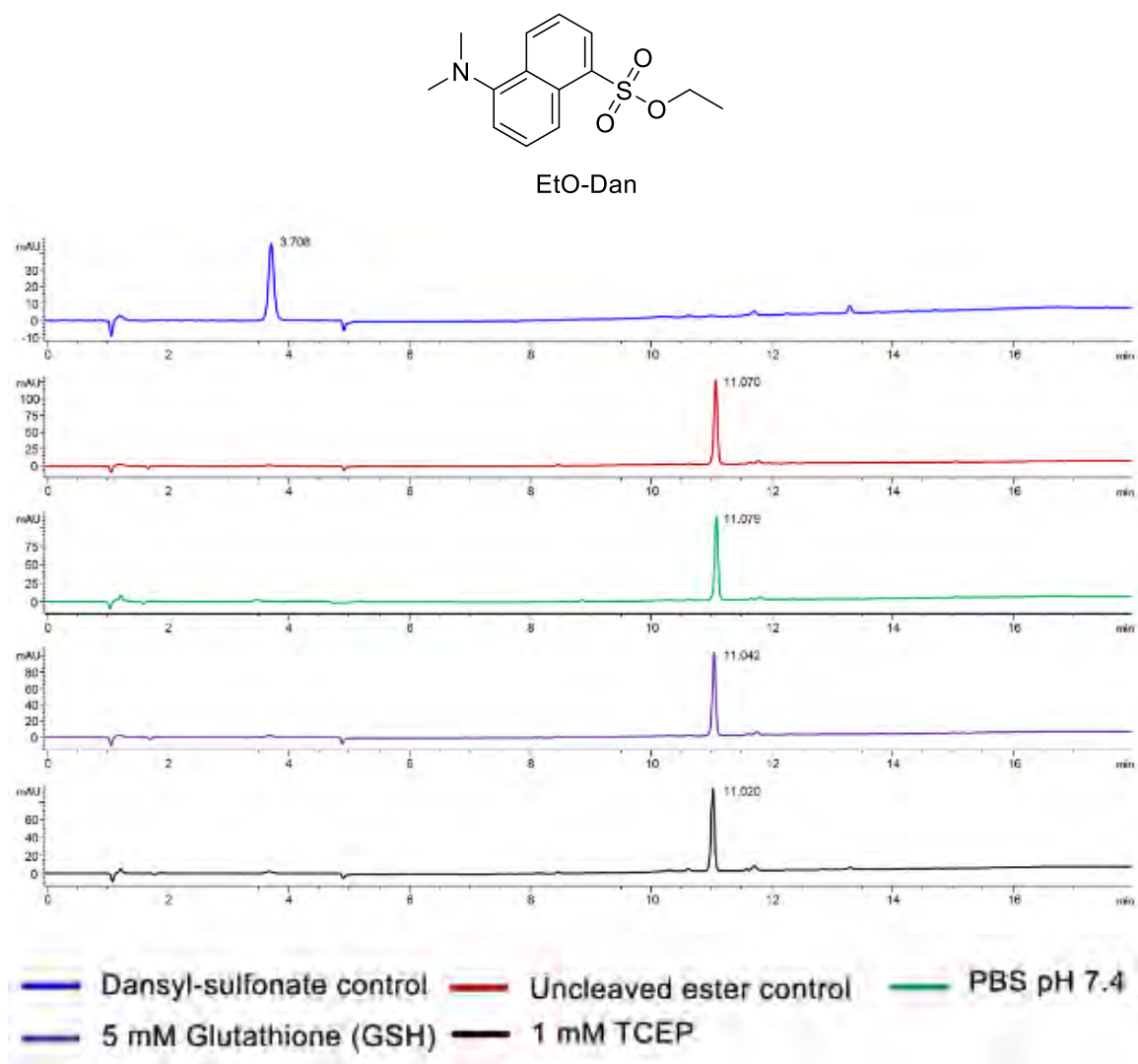


Figure 2.10: EtO-Dan does not release sulfonates under reduction conditions. HPLC analysis of EtO-Dan treated under different reducing conditions. EtO-Dan was treated with reducing agents or PBS alone for 15 minutes. Control samples were injected immediately, without prior incubation. Each peak is labeled with its retention time.

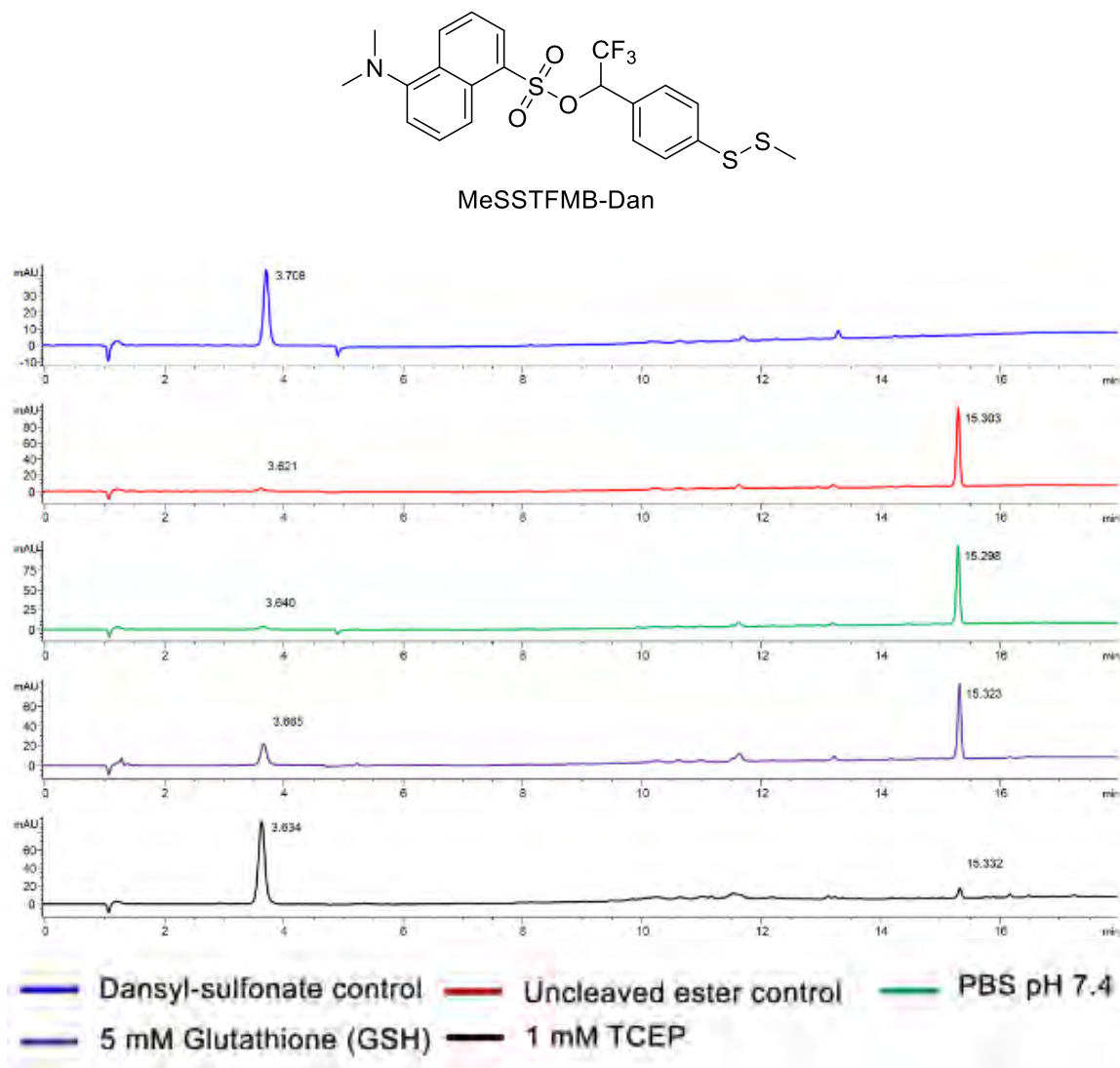


Figure 2.11: MeSSTFMB-Dan can release sulfonates under reducing conditions.

HPLC analysis of MeSSTFMP-Dan treated under different reducing conditions.

MeSSTFMB-Dan was treated with reducing agents or PBS alone for 15 minutes. Control samples were injected immediately, without prior incubation. Each peak is labeled with its retention time.

While MeSSTFMB-Dan displayed enhanced cleavage rates compared to simple alkyl dansylates, sulfonate release under 5 mM GSH treatment was rather slow. The sluggish cleavage rate under GSH treatment *in vitro* suggests that free sulfonate release in cells would be too slow. To increase the rate of sulfonate release, I revisited my design of the MeSSTFMB and postulated that the oxidation potential of the disulfide bond could be increased by replacing benzene with a pyridine ring (**Figure 2.12**). Compared to benzene, pyridine contains an electron withdrawing nitrogen, which lowers the electron density of the disulfide bond, making it more electrophilic.

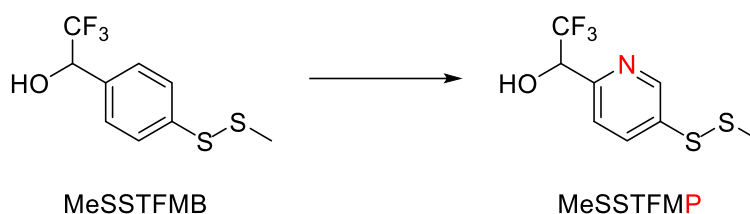


Figure 2.12: Substitution of benzene with pyridine as the core scaffold of RLPG. The disulfide bond becomes more electrophilic due to the electron withdrawing effects of the nitrogen.

The synthetic scheme to access the pyridyl-RLPG or MeSSTFMP (**2.14**) was mostly analogous to that of the MeSSTFMB. However, pyridyl-thiophenols could not be accessed via demethylation with NBS due to the unavailability of commercial S-methyl pyridines. Instead, pyridyl-thiophenols were accessed through thiol surrogates, a strategy reported by Itoh and Mase.^{84,85} In this strategy, aryl halides are coupled to thiols using

palladium-catalyzed coupling chemistry. Later, the aryl sulfides are cleaved to yield the aryl thiols (**Figure 2.13**).

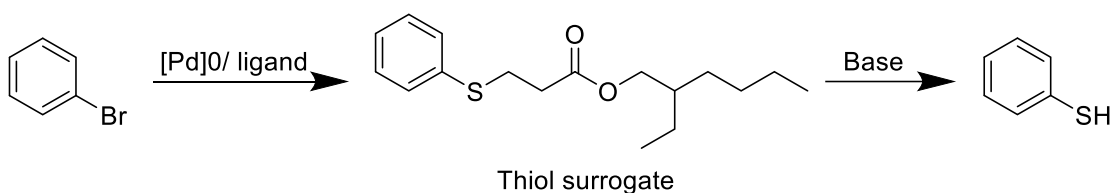
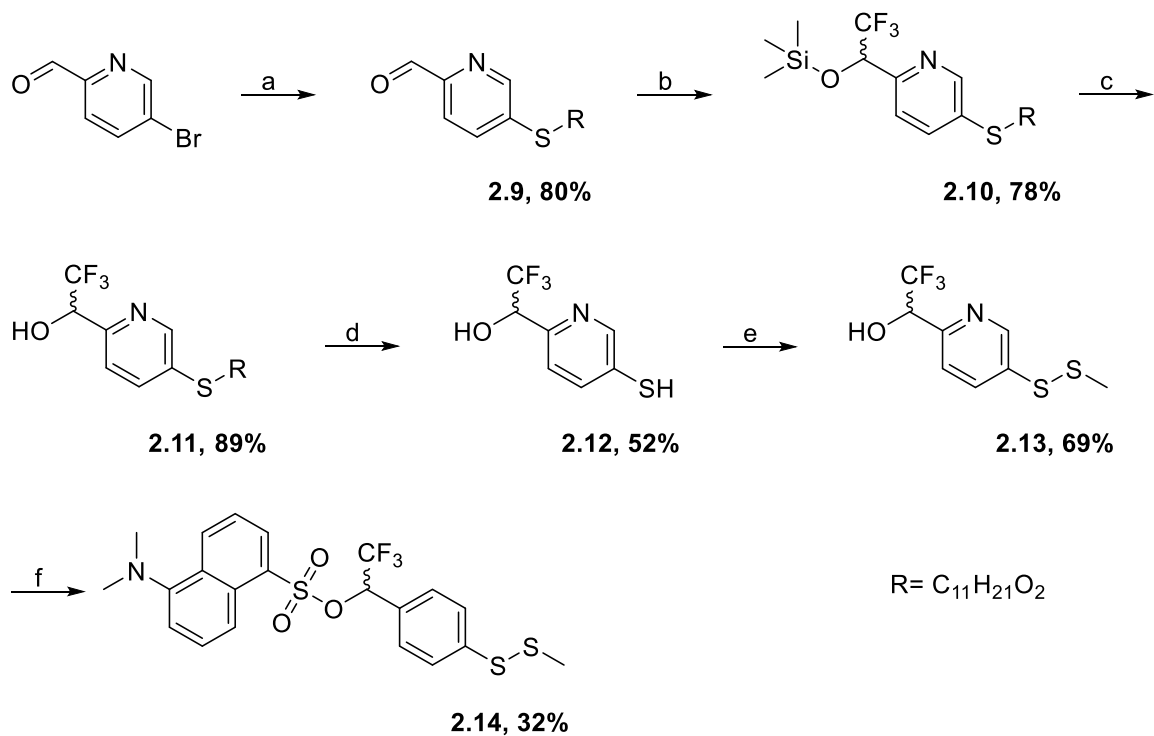


Figure 2.13: Accessing aryl thiophenols using thiol surrogates. A thiol surrogate is added on to the aryl ring using palladium-catalyzed coupling and subsequently cleaved with base to generate the thiophenol.

In our revised route, palladium-catalyzed coupling was performed between commercially available 5-bromo-2-pyridinecarboxaldehyde and 2-ethylhexyl 3-mercaptopropionate to yield the thiol surrogate **2.9**. Ruppert–Prakash reaction and subsequent TMS deprotection with aq. 1M HCl and THF mixture afforded the alcohol **2.11**. The ester was removed via base-mediated elimination with sodium methoxide to yield the thiophenol **2.12**. Subsequent treatment with methyl methanethiosulfonate and dansylation afforded MeSSTFMP **2.13** and the final product MeSSTFMP-Dan **2.14**, respectively (**Scheme 2.2**).

As I hypothesized, MeSSTFMP-Dan displayed improved cleavage rates compared to MeSSTFMB. Complete cleavage occurred within 15 minutes under all conditions tested (**Figure 2.14**). Aside from dansyl-sulfonate with a retention time of 3.7 minutes, another byproduct with a retention time of 9.6 minutes was also detected.



Scheme 2.2: Synthesis of MeSSTFMP-Dan. Reagents and conditions: (a) 2-Ethylhexyl 3-Mercaptopropionate, Pd₂(dba)₃, Xantphos, toluene, reflux; (b) Me₃SiCF₃, TBAF, THF, 0 °C to RT; (c) 1:1 aq. HCl/THF, RT; (d) toluene, 25% NaOMe in MeOH, RT; (e) MeSSO₂Me, MeOH, pH 8 buffer, RT; (f) dansyl chloride, DABCO, DCM, RT.

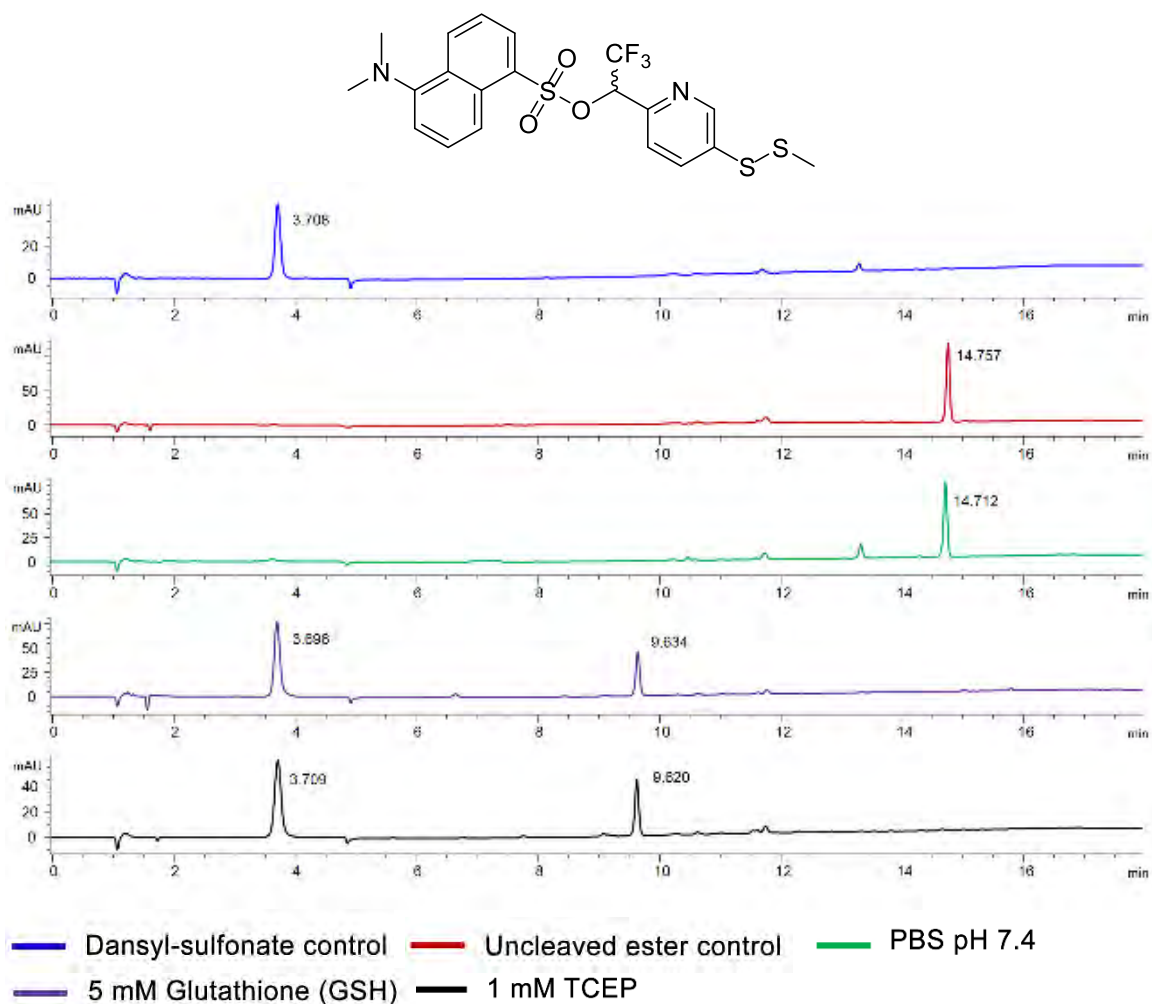


Figure 2.14: MeSSTFMP-Dan rapidly releases sulfonates under reducing conditions. HPLC analysis of MeSSTFMP-Dan treated under different reducing conditions. MeSSTFMP-Dan was treated with reducing agents or PBS alone for 15 minutes. Control samples were injected immediately, without prior incubation. Each peak is labeled with its retention time. The peak at 9.8 minutes is presumed to be derived from the thioquinone methide cleavage product.

To further characterize the byproducts formed during reduction, MeSSTFMP-Dan was incubated with different reducing agents, including GSH (5 mM), BME (1 mM), DTT (1 mM) and TCEP (1 mM). Interestingly, liquid chromatography mass spectrometry (LCMS) revealed a major byproduct with the mass of 194 under all four conditions, suggesting the formation of a two-electron reduction product of the *p*-thioquinone methide intermediate (**Figure 2.15**). Minor byproducts unique to each reduction condition were detected with masses consistent with adducts formed between the *p*-thioquinone methide and reducing agents (**Figure 2.16 and 2.17**). For example, unique to DTT treatment of MeSSTFMP-Dan, a product with a mass of 346 and retention time of 5.1 minutes was detected. Interestingly, a byproduct with the mass of 384 was consistently detected, suggesting a dimer of the two-electron reduction product.

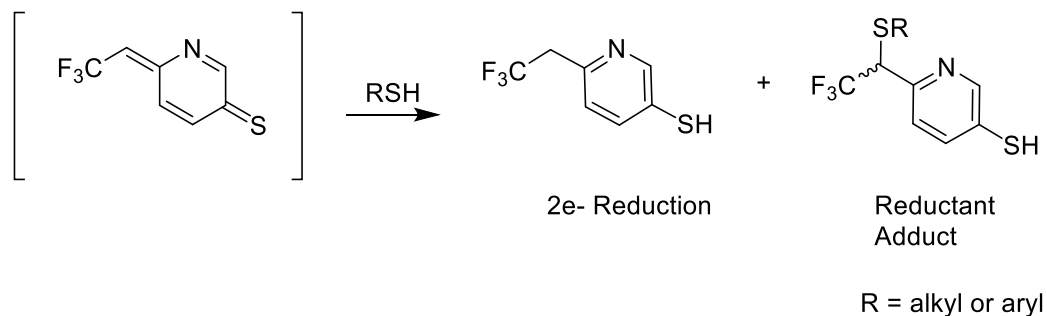


Figure 2.15: Generation of *p*-thioquinone methide during MeSSTFMP-Dan reduction. Thioquinone methide becomes further reduced, forming the two-electron reduction product (major) and reductant adduct (minor).

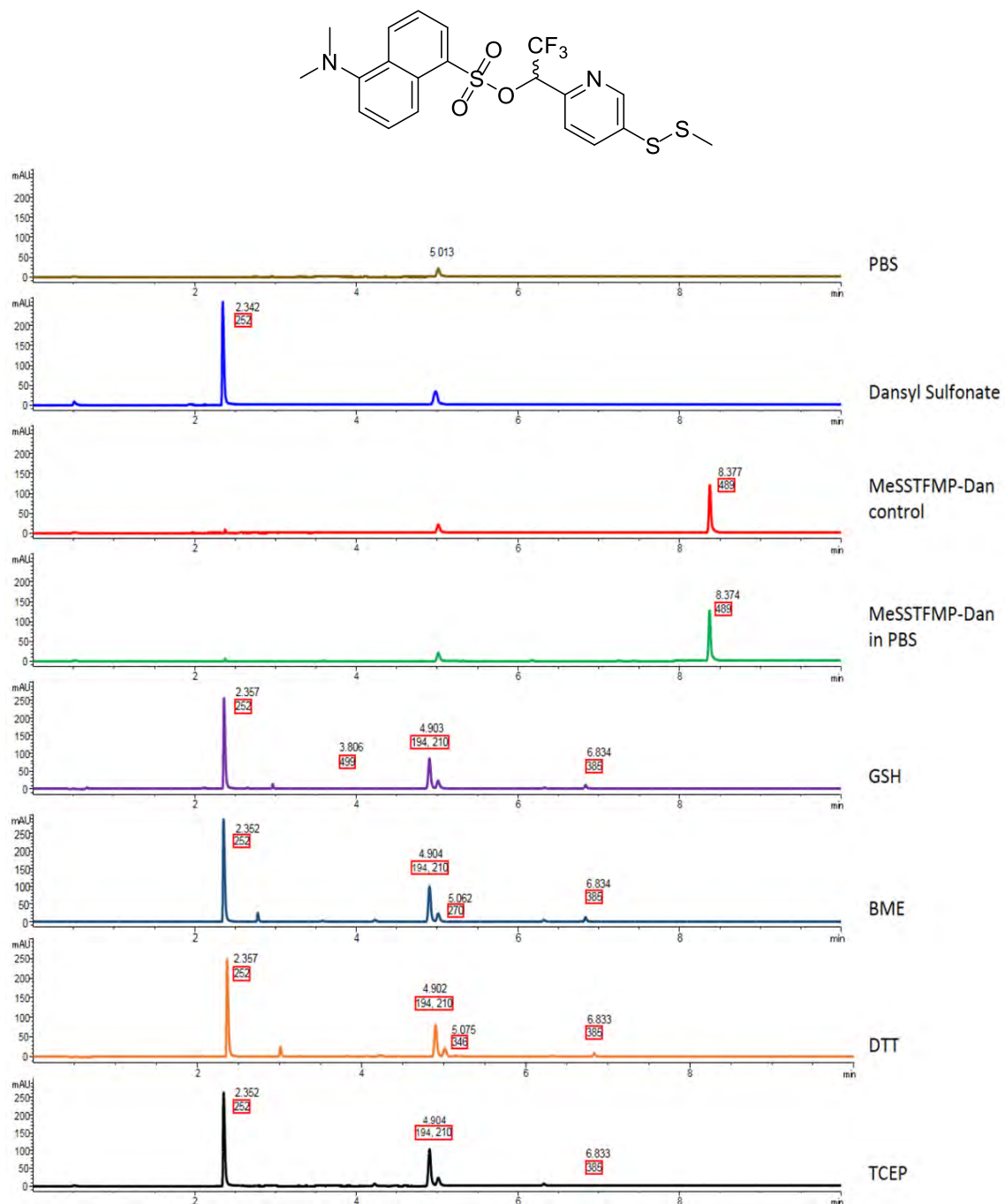


Figure 2.16: Mass of products detected during MeSSTFMP-Dan reduction.

LCMS analysis of MeSSTFMP-Dan after treatment with reducing agents. Background spectrum of PBS alone (gold); purified dansyl sulfonate (blue); and MeSSTFMP-Dan control without pre-incubation (red). Treatment conditions included: PBS alone (green); 5 mM GSH (purple); 1 mM BME (navy blue); 1 mM DTT (orange); or 1 mM TCEP (black). Retention times are labeled with their observed masses (MH+) in red boxes.

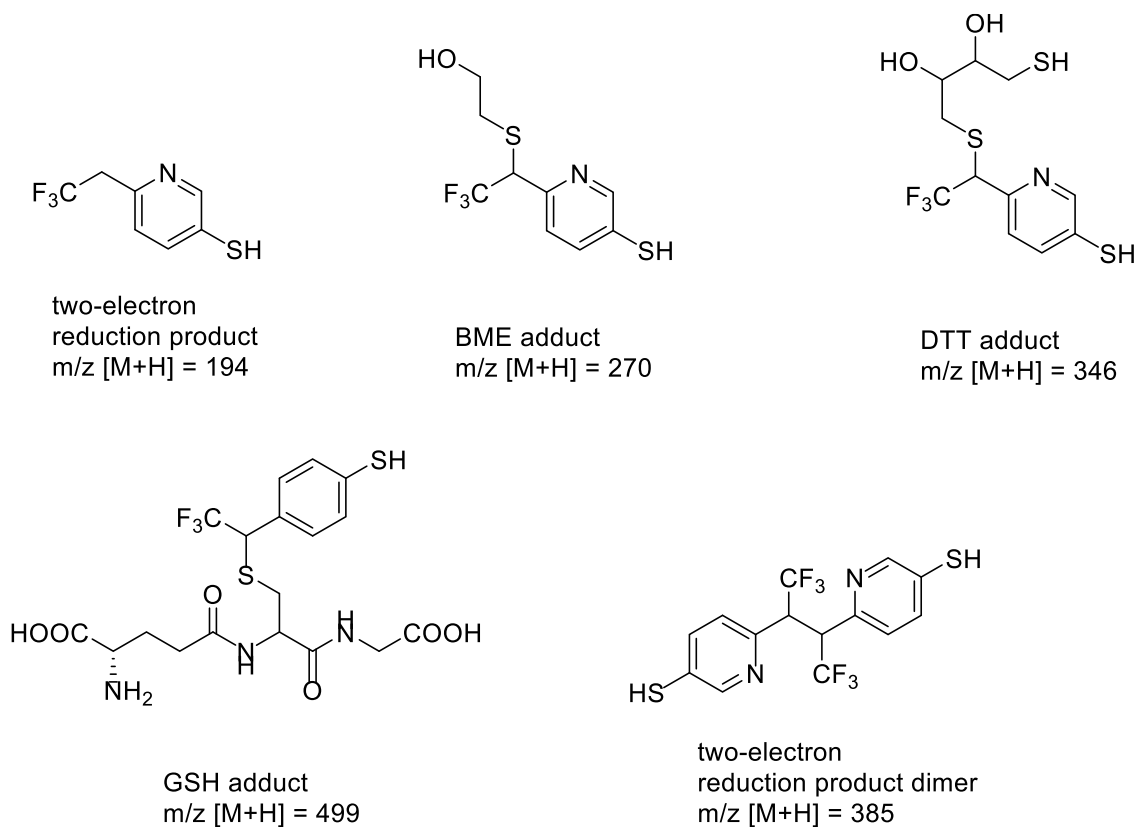


Figure 2.17: Purposed structures of byproducts detected with LCMS during MeSSTFMP-Dan reduction. The mass of each by product is listed beneath the structures.

To isolate and fully characterize the major byproduct, a larger scale reduction of MeSSTFMP-Dan was performed. Only the disulfide form of the two-electron reduction product **2.15** was isolated. HPLC and LCMS analyses of **2.15** pretreated with TCEP showed identical retention time, mass, and photodiode array (PDA) signals as the major byproduct observed from MeSSTFMP-Dan reduction (**Figure 2.18 and 2.19**). Taken together, unlike quinone methides that typically yield nucleophilic addition products, thioquinone methides have a strong preference for a further reduction to form a two-electron reduction product.^{48,86}

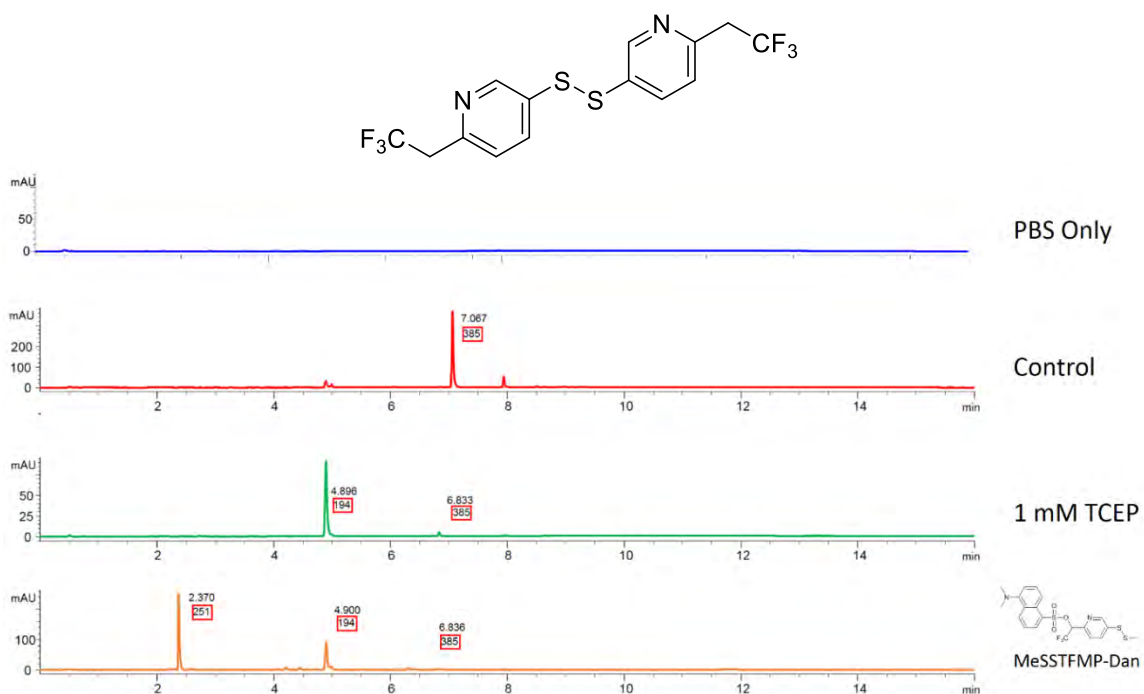


Figure 2.18: Reduction of disulfide 2.16 yields the byproduct observed during MeSSTFMP-Dan reduction. LCMS analysis of disulfide and MeSSTFMP-Dan after TCEP treatment. PBS blank run (blue); Disulfide **2.16** alone in PBS (red); Reduction of with 1 mM TCEP (green) compared to reduction of MeSSTFMP-Dan (orange). Retention times are labeled with their observed masses (MH⁺) in red boxes.

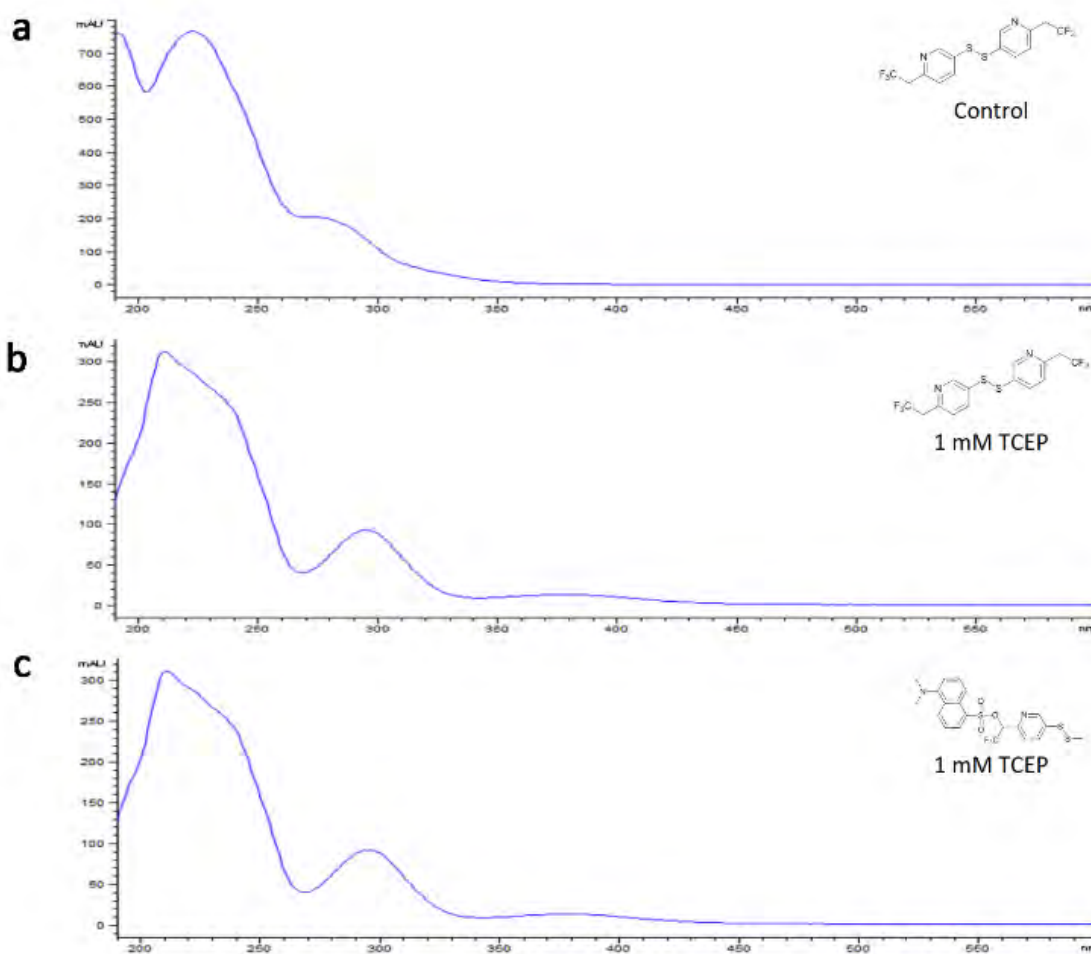


Figure 2.19: Photodiode array spectra are identical between the isolated disulfide and the byproduct observed during MeSSTFMP-Dan reduction. Control was immediately injected (a), Compound 2.15 (b), and MeSSTFMP-Dan (c) were pretreated with 1 mM TCEP for 15 minutes prior to injection.

To directly compare the rate of sulfonate release between MeSSTFMB and MeSSTFMP, I monitored their reductive cleavage in real-time, based on the fluorescence signal from free dansyl sulfonates. Each dansylate was treated with either 1 mM BME, 1 mM DTT, 1 mM TCEP, or 5 mM GSH, and monitored for 15 minutes. Consistent with the HPLC results, MeSSTFMB-Dan did not show significant sulfonate release when treated with BME, DTT, or GSH. Although sulfonate release was substantially faster with TCEP, it did not reach completion. Conversely, complete sulfonate liberation from MeSSTFMP-Dan occurred within 3 minutes under all conditions (Figure 2.20).

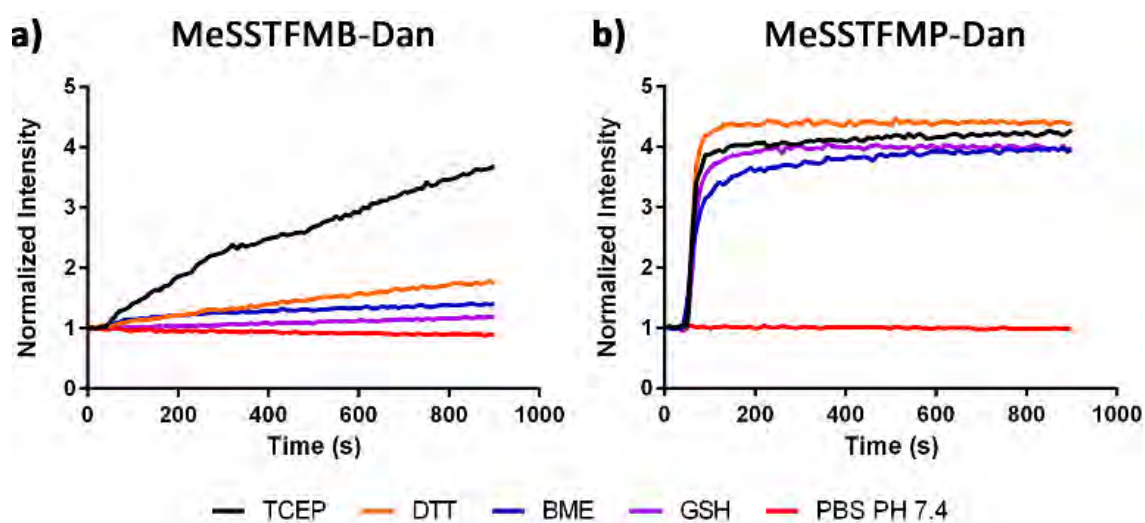


Figure 2.20: Real-time fluorescence monitoring of sulfonate release from MeSSTFMB-Dan and MeSSTFMP-Dan. Reductive cleavage of (a) MeSSTFMB-Dan and (b) MeSSTFMP-Dan under different reducing conditions in PBS. Cleavage was followed by monitoring the fluorescence emission of dansyl sulfonate (498 nm).

Quinone methides are an electrophilic species and potentially cytotoxic.⁸⁷ To evaluate the toxicity of MeSSTFMB and MeSSTFMP, the LD₅₀ was determined in HeLa cells using a standard cell proliferation assay called XTT. HeLa cells were dosed with each dansylate at concentrations up to 30 μ M, the aqueous solubility limit of MeSSTFMB-Dan. TFMB-Dan and MeSSTFMB-Dan showed no signs of toxicity at the tested concentrations. In contrast to MeSSTFMB-Dan, MeSSTFMP-Dan displayed a higher level of toxicity, though only at concentrations above 10 μ M. AcOTFMB-Dan displayed higher toxicity with an LD₅₀ of ~ 8 μ M (**Figure 2.21**). This could imply that quinone methides are inherently more cytotoxic than thioquinone methides.

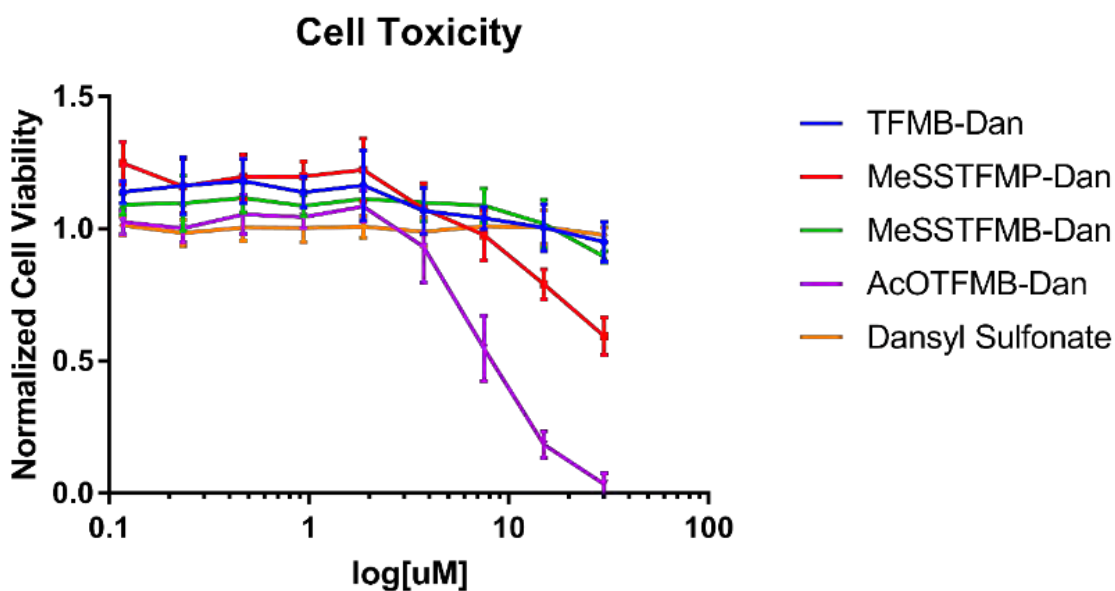


Figure 2.21: Cytotoxicity of different dansylates. Live HeLa cells were treated with different concentrations of each dansylate (30 μ M – 0.11 μ M) for 1 hour. Toxicity was assessed using an XTT cell proliferation assay 48 hours after treatment. Signals were normalized to the DMF vehicle control.

Lastly, sulfonate delivery was evaluated in live cells. HeLa cells were treated with 1 μ M dansylates for 15 minutes and then imaged with fluorescent microscopy. Diffusive blue fluorescence signifies the successful release of dansyl-sulfonate release in the cytoplasm, whereas yellow puncta indicate aggregation within the cellular membrane. Dansyl-sulfonate could not enter cells, while TFMB-Dan was retained in the cell membranes and formed puncta in the cell membrane (**Figure 2.22 and 2.23**). As reported, AcOTFMB-Dan efficiently delivered dansyl-sulfonate into cells (**Figure 2.23**). Both MeSSTFMB-Dan and MeSSTFMP-Dan delivered sulfonates into cells, but MeSSTFMP-Dan did so more rapidly (**Figure 2.22**). However, alkyl dansylates did not deliver any appreciable amounts dansyl-sulfonate into cells (**Figure 2.23**).

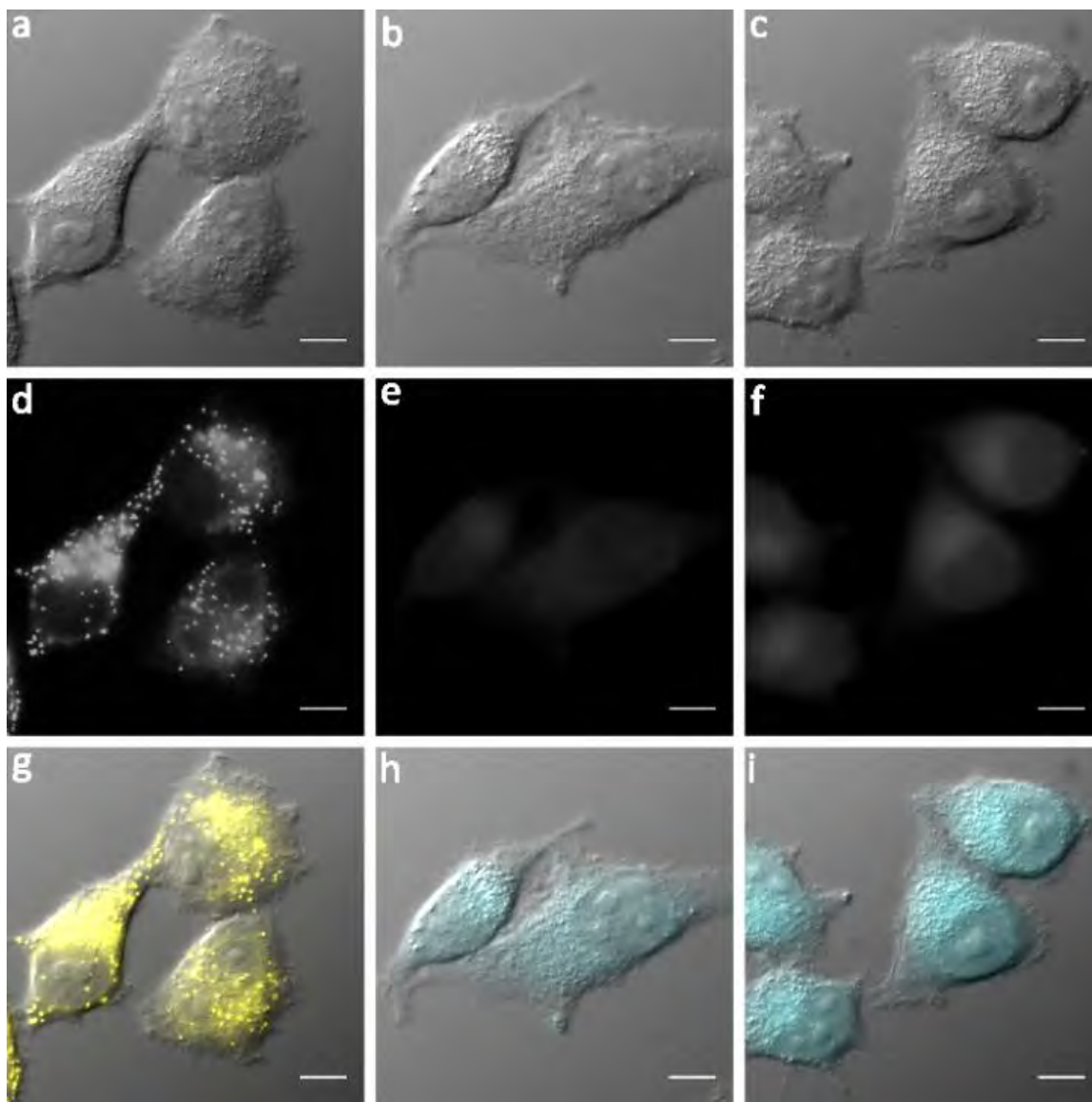


Figure 2.22: Delivery of dansyl sulfonate into live HeLa cells with RLPGs.

Fluorescence (a-c) and differential interference contrast (DIC) images (d-f) of cells treated with TFMB-Dan (a and d); MeSSTFMB-Dan (b and e); or MeSSTFMP-Dan (c and f). Images are shown at 50x magnification. Composite pictures g-i are pseudocolored. Scale bars = 10 μ m.

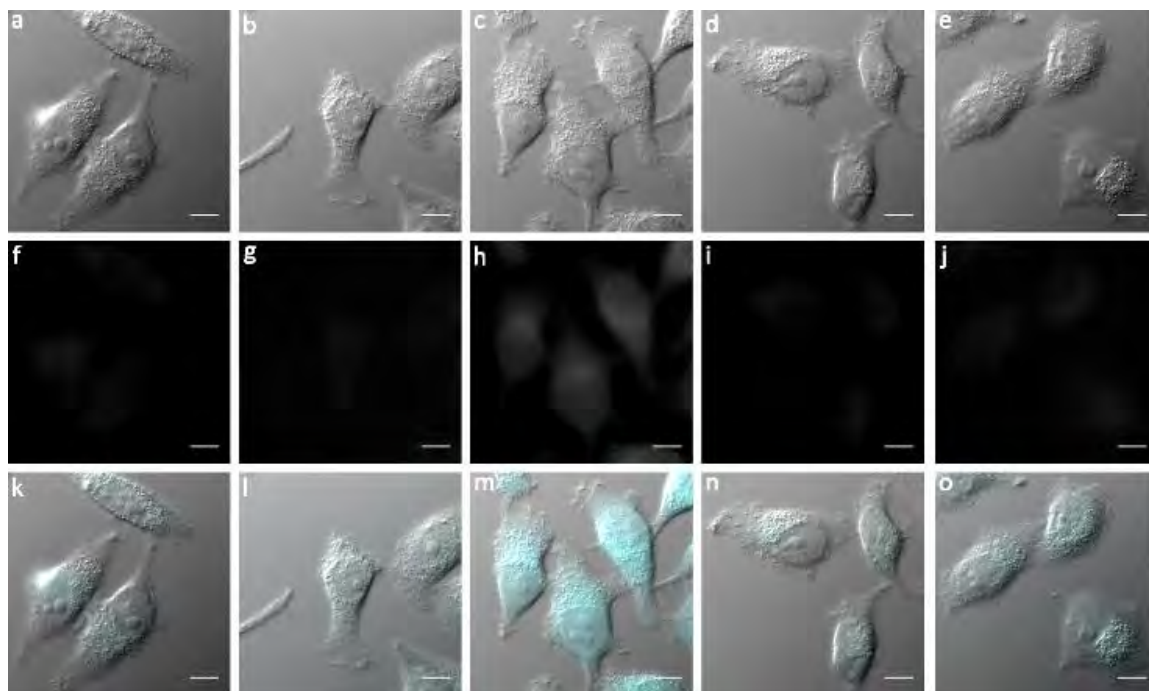


Figure 2.23: Live images of HeLa cells treated with different dansylates. DIC images (a-e), fluorescence images (f-j), and composite images (k-o) of cells treated with DMF vehicle (a, f, k); dansyl sulfonate (b, g, l); AcOTFMB-Dan (c, h, m); MeO-Dan (d, i, n); or EtO-Dan (e, j, o). Composite images are pseudo-colored to match the fluorescence seen through the eyepiece. Scale bar = 10 μ m.

Conclusion

Sulfonation can greatly enhance aqueous solubility at the cost of membrane permeability. In this work, I introduced two reductively labile protecting groups, MeSSTFMB and MeSSTFMP that are capable of intracellular delivery of sulfonates (**Figure 2.23**). The synthetic scheme for obtaining both RPLGs are short and straightforward, consisting of only 5 steps allowing for easy derivation.

MeSSTFMB-Dan was capable of sulfonate release *in vitro*, albeit at a slow rate. Despite the slow release *in vitro*, it delivered an appreciable amount of dansyl-sulfonate into live HeLa cells. Importantly, MeSSTFMB did not show any toxicity in HeLa cells at concentrations up to 30 μ M. In contrast, MeSSTFMP-Dan rapidly released sulfonates, both *in vitro* and in cells. Cytotoxicity was slightly higher, but only at concentrations above 10 μ M. Moreover, the cytotoxicity of both RLPGs was lower than the reported AcOTFMB. These results suggest that cytotoxicity could be correlated with the rate of (thio)quinone methide generation and/ or that thioquinone methides are less toxic than quinone methides.⁸⁷

Finally, the different release rates of MeSSTFMB and MeSSTFMP can be exploited for either sustained or rapid sulfonate release, respectively. Given their many attributes, I envision MeSSTFMB, MeSSTFMP, and other RLPGs to not only find widespread applications as delivery scaffolds for sulfonated molecules, but also encourage the design of novel sulfonated probes and drugs.

Materials and Methods

General:

Commercially available products were used without purification and purchased from Aldrich, Frontier Scientific, Matrix, Oakwood, Chem-Impex, Combi-Blocks, or TCI. Anhydrous solvents were purchased from Acros. Compounds were purified with the CombiFlash Rf+ system or manual silica gel column with HPLC-grade ChromoSolv solvents purchased from Sigma-Aldrich.

NMR spectra (^1H , ^{19}F , and ^{13}C) were obtained on a Varian Mercury 400 or Bruker Ascend 500. Analytical HPLC was performed on an Agilent 1100 equipped with a Zorbex C8 column and a PDA detector (G1315A DAD). LCMS was performed on an Agilent 1260 Infinity equipped with a Zorbex SB-C18 column and a 6130 Quadrupole detector. High resolution mass spectrometry was performed at the UMass Mass Spectrometry core on a Thermo Scientific Orbitrap Velos Pro. Excitation and emission data were obtained on Fluoromax-4. Images were acquired with a Nikon Eclipse E600, equipped with a Hamamatsu Orca-ER and a mercury lamp. Data were graphed and fitted using Graphpad Prism 7. NMR spectra were analyzed with MestReNova. Images were processed with Fiji (ImageJ).

Excitation and Emission Spectra of Dansylates

Compounds at 1 mM stock concentration were diluted 1:500 in PBS pH 7.4 (6 μ L into 3 mL) to a final concentration of 2 μ M. For all acquisitions, the temperature was maintained at 20 °C and slit widths were set to 1 mm (excitation) and 5 mm (emission).

Equipment and Conditions:

System: Horiba Scientific FluoroMax-4

Temperature Controller: Newport Model 350B

Acquisition software: FluorEssence

Temperature: 20 °C

Fluorometric Detection of Dansylate Cleavage

Compounds at 1 mM stock concentration were diluted 1:500 in PBS pH 7.4 (6 μ L into 3 mL) to a final concentration of 2 μ M. The release of dansyl sulfonate was monitored using wavelengths of 324 nm (excitation) and 498 nm (emission). The temperature was maintained at 20°C and slit widths were set to 1 mm (excitation) and 5 mm (emission). Data points were collected every 10 seconds for 15 minutes. To establish fluorescence baseline, reducing agents were added 50 seconds after the initial time point.

Equipment and Conditions:

System: Horiba Scientific FluoroMax-4

Temperature Controller: Newport Model 350B

Acquisition software: FluorEssence

Temperature: 20°C

Concentrations and volumes of reducing agents:

Reducing Agent	Stock Concentration in PBS (mM)	Volume Added (μ L)	Final Concentration (mM)
TCEP	500	6	1
DTT	500	6	1
BME	500	6	1
Glutathione	500	30	5

HPLC Analysis of Dansyl Cleavage

Compounds at 10 mM stock concentration in DMF were diluted 1:1000 in PBS pH 7.4 (1 μ L in 1 mL) with or without reducing agent to a final concentration of 10 μ M. Compound standards were injected into the HPLC immediately after filtration through a 0.45 μ M PTFE syringe filter. In all other conditions, compounds were incubated in the dark at room temperature for 15 minutes prior to filtration and injection. The HPLC column was equilibrated for at least 25 minutes at 1.4 mL/min prior to sample injection. TCEP was used at 1 mM and GSH was used at 5 mM.

Equipment and Conditions:

Injection volume: 200 μ L

HPLC system: Agilent Series 1100

Filter: 13mm 0.45 μ M PTFE

Column: Agilent Zorbax XDB-C8 μ m 4.6 mm x 150 mm

Wavelength monitored: 290 nm / 800 nm (reference)

System: 0.1% TFA H₂O/acetonitrile

Ramp:

Time (m)	% Acetonitrile	Flow rate (mL/ min)
2	0	1.4
15	90	1.4
17	90	1.4
18	0	1.4
Post-run (25 minutes)	0	1.4

LCMS Analysis of Dansyl Cleavage

Sample preparation and concentrations were identical to the HPLC protocol. The LCMS column was equilibrated for 5 minutes at 1.0 mL/min before each injection.

TCEP, DTT and BME were used at 1 mM and GSH was used at 5 mM.

Note: The injection protocol of the LCMS auto-sampler took approximately 2 minutes to complete; total incubation time was therefore about 17 minutes for test samples and 2 minutes for control samples.

Equipment and Conditions:

Injection volume: 100 μ L

LCMS system: Agilent 1260 Infinity with auto-sampler, 6130 Quadrupole LC/MS

Column: PoroShell 120 EC-C18 4.6x150 mm 2.7 μ m

Wavelength monitored: 290 nm / 595 nm (reference)

System: 0.1% aq. formic acid/acetonitrile

Ramp:

Time (m)	% Acetonitrile	Flow rate (mL/ min)
0	0	1.0
8	100	1.0
10	100	1.0
Post-run (5 minutes)	0	1.0

Live Cell Imaging

Cell culture

HeLa cells were cultured with DMEM containing 10% FBS and 1% Pen/Strep at 37 °C. Cells were first cultured in T-75 TC flasks to 70% confluency, then trypsinized and diluted to 50,000 cells/mL. Coverslips (#1.5 18 mm) were seeded in a 10 cm petri dish using 10 mL of cell solution. Cells were allowed to adhere for 20 hours at 37°C.

Staining

Coverslips were washed twice with HBSS and placed in a 35 mm petri plate containing HBSS (2 mL). Dansylates (2 μ l of a 1 mM stock) were added to achieve a final concentration of 1 μ M and then incubated for 15 minutes at 37°C. After incubation, the coverslips were washed twice with HBSS and mounted using a technique adapted from Chazotte.⁸⁸ Instead of using VALAP, Vaseline was used to seal the chamber and 200 μ L of HBSS was used to fill the chamber to prevent the formation air bubbles.

Image processing

Raw 16-bit images were cropped to the desired 2 square inch frames (600 dpi) and normalized to the pixel intensity (min: 350, max: 3500), except for TFMB-Dan (min: 350, max: 6000). Those images were then converted to 8-bit images, and a scale bar was applied (7.85 pixel/ μ m). Composite pictures were prepared using the merge channel function in the FIJI software, and pseudocolored to match the fluorescence seen through the eyepiece (longpass emission filter).

Equipment

Coverslips: Deckgläser No. 1.5, 18 mm round glass

Microscope slides: Fisherfinest Premium Plain

Microscope: Nikon Eclipse E600

Camera: Hamamatsu Orca-ER with controller

Objective: Nikon Plan 50x oil immersion

Filter Set: Nikon UV-2A (330-380 nm bandpass excitation; 420 nm longpass emission)

Light Source: Chiu Technical Corporation 100W Mercury Lamp

Exposure time: 100 ms

Imaging processing software: FIJI

Toxicity Assay

Cell culture

HeLa cells were cultured with DMEM containing 10% FBS and 1% Pen/Strep at 37 °C. Cells were first cultured in T-75 TC flasks to 70% confluency, then trypsinized and diluted to 50,000 cells/mL. 96-well plates were seeded with 5000 cells/well. Cells were allowed to adhere for 24 hours at 37 °C.

XTT Assay

DMEM medium was removed via aspiration and the cells were washed once with HBSS (100 μ L). After washing, the wells were filled with HBSS (50 μ L). Compounds (50 μ L) were added and incubated for 1 hr at 37 °C. After treatment, the compounds were removed via aspiration and the cells were washed once with HBSS (100 μ L). The cells were supplied with fresh DMEM (100 μ L) and allowed to proliferate for 48 hours at 37 °C. Activated XTT reagent (50 μ L) were added and incubated at 37°C for 4 hour. Wells were read at 490 nm and 660 nm.

Compounds at 10 mM stock concentration in DMF were first diluted in HBSS (6 μ L in 1 mL), then serially diluted (1:2) in HBSS. Concentrations ranged from 60 μ M to 1.9 μ M at 2X.

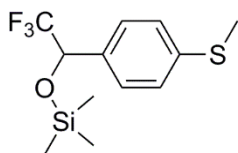
Equipment

Plates: BD 35-3072

Plate Reader: BioRad IMark

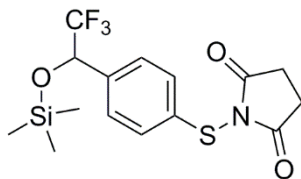
XTT Reagent: ATCC XTT Kit 30-1011K

Synthetic Methods



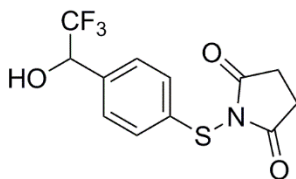
Trimethyl(2,2,2-trifluoro-1-(4-(methylthio)phenyl)ethoxy)silane (2.1)

In a 50 mL round bottom flask, 4-(Methylthio)benzaldehyde (2 g, 13.2 mmol) and trimethyl(trifluoromethyl)silane (3 mL, 20.3 mmol) were dissolved in anhydrous THF (13.5 mL) under argon. The temperature was lowered to 0°C, followed by the dropwise addition of 1 M TBAF in THF (70 μ L, 0.07 mmol). The reaction was raised to room temperature and stirred for 10 minutes. The solvent was removed under reduced pressure and the product was purified by silica gel chromatography (0-7.5% EtOAc/hex) to afford a pale yellow oil (2.1 g, 7.14 mmol, 94%). ^1H NMR (400 MHz, CDCl_3) δ 7.39 (d, J = 8.4 Hz, 2H), 7.26 (m, 2H), 4.91 (q, J = 6.4 Hz, 1H), 2.49 (s, 3H), 0.14 (s, 9H). ^{19}F NMR (376 MHz, CDCl_3) δ -78.53 (d, J = 6.4 Hz). ^{13}C NMR (101 MHz, CDCl_3) δ 139.8, 132.1 – 132.0 (m), 128.1 – 127.9 (m), 125.9, 124.2 (q, J = 283.6 Hz), 72.9 (q, J = 32.3 Hz), 15.3, -0.3. HR-EIMS m/z calculated for $\text{C}_{12}\text{H}_{18}\text{F}_3\text{OSSi}^+$: 295.0794, found: 295.0779



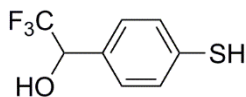
1-((4-(2,2,2-trifluoro-1-((trimethylsilyl)oxy)ethyl)phenyl)thio)pyrrolidine-2,5-dione (2.2)

In a 50 mL round bottom flask, compound **2.1** (860 mg, 2.9 mmol) and NBS (781 mg, 4.4 mmol) were dissolved in anhydrous DCM (6 mL) under argon. The reaction was stirred in the dark at room temperature for 24 hours. The solvent was removed under reduced pressure and the product was purified by silica gel chromatography (neat DCM) to afford a white solid (1.1 g, 2.9 mmol, 97%). ^1H NMR (400 MHz, CDCl_3) δ 7.58 – 7.54 (m, 2H), 7.41 (d, J = 8.0 Hz, 2H), 4.88 (q, J = 6.4 Hz, 1H), 2.84 (s, 4H), 0.09 (s, 9H). ^{19}F NMR (376 MHz, CDCl_3) δ -78.31 (d, J = 6.4 Hz). ^{13}C NMR (101 MHz, CDCl_3) δ 176.4, 137.0, 134.9, 131.3, 128.5 – 128.4 (m), 123.9 (q, J = 283.6 Hz), 72.6 (q, J = 32.4 Hz), 28.6, -0.3. HR-EIMS m/z calculated for $\text{C}_{15}\text{H}_{19}\text{F}_3\text{NO}_3\text{SSi}^+$: 378.0802, found: 378.0808.



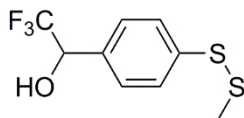
1-((4-(2,2,2-trifluoro-1-hydroxyethyl)phenyl)thio)pyrrolidine-2,5-dione (2.3)

In a 50 mL round bottom flask, compound **2.2** (250 mg, 0.9 mmol) was dissolved in 1:1 1 M aq. HCl/THF (10 mL) and stirred at room temperature for 1.5 hours. THF was first removed under reduced pressure, then the product was extracted with EtOAc (3 x 25 mL). The organic layers were combined and washed with H₂O (3 x 50 mL) and brine (50 mL), then dried over Na₂SO₄. The solvent was removed under reduced pressure and the product was purified by silica gel chromatography (0-70% EtOAc/hex) to afford a white solid (200 mg, 0.65 mmol, 87%). ¹H NMR (400 MHz, CD₃OD) δ 7.47 (s, 4H), 5.04 (q, *J* = 7.2 Hz, 1H), 2.83 (s, 4H). ¹⁹F NMR (376 MHz, CD₃OD) δ -79.61 (d, *J* = 7.1 Hz, 1H). ¹³C NMR (101 MHz, CD₃OD) δ 177.7, 136.3 – 136.2 (m), 135.7, 128.5, 128.4 – 128.2 (m), 124.7 (q, *J* = 282.8 Hz), 71.0 (q, *J* = 31.5 Hz), 28.3. HR-EIMS *m/z* calculated for C₁₂H₁₁F₃NO₃S⁺: 306.0406, found: 306.0412.



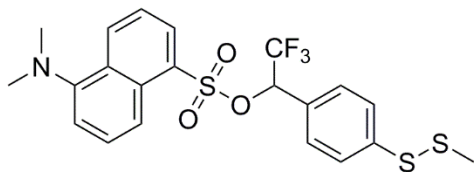
2,2,2-trifluoro-1-(4-mercaptophenyl)ethan-1-ol (2.4)

In a 200 mL round bottom flask, compound **2.3** (300 mg, 0.98 mmol) was dissolved in anhydrous methanol (20 mL) and degassed three times at -40°C . NaBH_4 (400 mg, 11 mmol) was added to the reaction in small proportions. The reaction was raised to room temperature and stirred under argon for 3 hours. The reaction was quenched using glacial acetic acid (20 mL). Toluene (50 mL) was added to the reaction mixture and the solvents were removed under reduced pressure. The crude product was dissolved in EtOAc (50 mL), washed with H_2O (3 x 50 mL) and brine (50 mL), then dried over Na_2SO_4 . The solvent was removed under reduced pressure and the product was purified by silica gel chromatography (0–30% EtOAc/hex) afforded a white solid (100 mg, 0.48 mmol, 49%). ^1H NMR (400 MHz, CDCl_3) δ 7.37 – 7.28 (m, 4H), 4.98 (dq, $J = 6.4, 4.4$ Hz, 1H), 3.51 (s, 1H), 2.48 (d, $J = 4.4$ Hz, 1H). ^{19}F NMR (376 MHz, CDCl_3) δ -78.55 (d, $J = 6.4$ Hz). ^{13}C NMR (101 MHz, CDCl_3) δ 133.1, 131.1 – 131.1 (m), 129.1, 128.2 – 128.1 (m), 124.1 (q, $J = 283.1$ Hz)*, 72.4 (q, $J = 32.2$ Hz). [*Only 3 of the 4 peaks for the quartet at 124.06 are visible.] HR-EIMS m/z calculated for $\text{C}_8\text{H}_6\text{F}_3\text{OS}$ –: 207.0097, found: 207.0091.



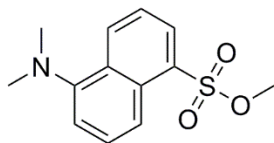
2,2,2-trifluoro-1-(4-(methylthio)phenyl)ethan-1-ol (2.5)

In a 25 mL round bottom flask, compound **2.4** (58 mg, 0.24 mmol) and S-methyl methanethiosulfonate (42 mg, 0.33 mmol) were dissolved in anhydrous MeOH (3 mL) under argon. Degassed 100 mM sodium phosphate pH 8 buffer (4 mL) was added to the reaction. The reaction was stirred at room temperature under argon for 2.5 hours. The reaction mixture was poured into EtOAc (50 mL), washed with H₂O (3 x 25 mL) and brine (25 mL), then dried over Na₂SO₄. The solvent was removed under reduced pressure and the product was purified by silica gel chromatography (0-30% EtOAc/hex) afforded a white solid (70 mg, 0.28 mmol, 98%). ¹H NMR (400 MHz, CDCl₃) δ 7.58 – 7.54 (m, 2H), 7.44 (d, *J* = 8.4 Hz, 2H), 5.04 – 4.97 (m, 1H), 2.78 – 2.73 (m, 1H), 2.45 (s, 3H). ¹⁹F NMR (376 MHz, CDCl₃) δ -78.38 (d, *J* = 6.8 Hz). ¹³C NMR (101 MHz, CDCl₃) δ 138.8, 132.3 – 132.2 (m), 128.2 – 128.0 (m), 127.0, 124.1 (q, *J* = 283.2 Hz), 72.4 (q, *J* = 32.2 Hz), 22.9.



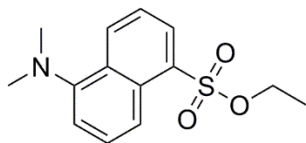
2,2,2-trifluoro-1-(4-(methyldisulfanyl)phenyl)ethyl 5-(dimethylamino)naphthalene-1-sulfonate (2.6)

In a 50 mL round bottom flask, compound **2.5** (18 mg, 0.07 mmol), DABCO (11 mg 0.1 mmol), and dansyl chloride (24 mg, 0.09 mmol) were dissolved in anhydrous DCM (3 mL) under argon. The reaction was stirred at room temperature under argon for 3 hours. The solvent was removed under reduced pressure and the product was purified by silica gel chromatography (0-30% EtOAc/hex) to afford a yellow solid (20 mg, 0.04 mmol, 59%). ^1H NMR (400 MHz, CDCl_3) δ 8.46 (dt, $J = 8.8, 1.2$ Hz, 1H), 8.22 – 8.17 (m, 1H), 8.08 (dd, $J = 7.2, 1.2$ Hz, 1H), 7.56 (dd, $J = 8.4, 7.6$ Hz, 1H), 7.36 (dd, $J = 8.4, 7.2$ Hz, 1H), 7.18 – 7.09 (m, 3H), 7.03 (d, 8.4 Hz), 5.59 (q, $J = 6.4$ Hz, 1H), 2.83 (s, 6H), 2.37 (s, 3H). ^{19}F NMR (376 MHz, CDCl_3) δ -75.86 (d, $J = 6.4$ Hz). ^{13}C NMR (101 MHz, CDCl_3) δ 151.7, 139.7, 132.0, 131.4, 130.3, 129.7, 129.5, 128.9, 128.6, 126.9, 125.7, 122.6, 122.1 (q, $J = 282.3$ Hz), 119.2, 115.5, 78.2 (q, $J = 34.7$ Hz), 45.40, 22.76. HR-EIMS m/z calculated for $\text{C}_{21}\text{H}_{21}\text{F}_3\text{NO}_3\text{S}_3^+$: 488.0630, found: 488.0666.



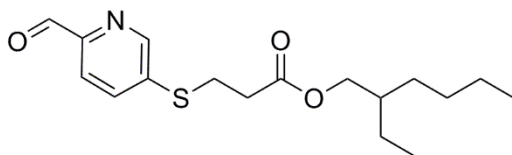
Methyl 5-(dimethylamino)naphthalene-1-sulfonate (2.7)

In a 50 mL round bottom flask, dansyl chloride (100 mg, 0.37 mmol) and DABCO (50 mg, 0.45 mmol) were dissolved in methanol (10 mL). The reaction was stirred for 6 hours at room temperature. The solvent was removed under reduced pressure and the crude mixture was dissolved in EtOAc (50 mL). The organic layer was washed with H₂O (3 x 50 mL) and brine (50 mL), then dried over Na₂SO₄. Removal of solvent under reduced pressure yielded a pure yellow oil (30 mg, 0.11 mmol, 30%). ¹H NMR (400 MHz, CDCl₃) δ 8.61 (dt, *J* = 8.8, 1.2 Hz, 1H), 8.28 (dd, *J* = 7.2, 1.2 Hz, 1H) 8.26 – 8.23 (m, 2H), 7.63 – 7.52 (m, 2H), 7.21 (dd, *J* = 7.6, 0.7 Hz, 1H), 3.72 (s, 3H), 2.89 (s, 6H). ¹³C NMR (101 MHz, CDCl₃) δ 151.8, 131.6, 130.8, 130.4, 129.9, 129.8, 128.8, 123.0, 119.3, 115.6, 56.4, 45.4. HR-EIMS *m/z* calculated for C₁₃H₁₆NO₃S⁺: 266.0845, found: 266.0869



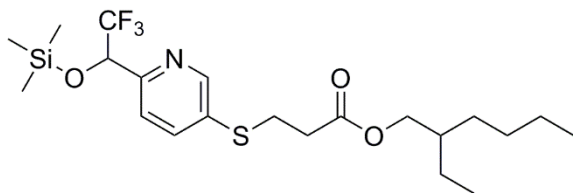
Methyl 5-(dimethylamino)naphthalene-1-sulfonate (2.8)

In a 50 mL round bottom flask, dansyl chloride (100 mg, 0.37 mmol) and DABCO (41 mg, 0.37 mmol) were dissolved in ethanol (5 mL). The reaction was stirred at room temperature for 4 hours. The solvent was removed under reduced pressure and the product was purified by silica gel chromatography (0-20% EtOAc/hex) to afford a yellow oil (100 mg, 0.29 mmol, 80%). ^1H NMR (400 MHz, CDCl_3) δ 8.59 (dt, $J = 8.8, 1.2$ Hz, 1H), 8.27 (dd, $J = 7.6, 1.2$ Hz, 2H), 7.56 (ddd, $J = 18.4, 8.4, 7.6$ Hz, 2H), 7.20 (dd, $J = 7.6, 0.4$ Hz, 1H), 4.07 (q, $J = 6.8$ Hz, 2H), 2.88 (s, 6H), 1.25 (t, $J = 7.2$ Hz, 3H). ^{13}C NMR (101 MHz, CDCl_3) δ 151.7, 131.5, 131.4, 130.4, 129.9, 129.8, 128.6, 123.0, 119.4, 115.5, 67.1, 45.4, 14.7. HR-EIMS m/z calculated for $\text{C}_{14}\text{H}_{18}\text{NO}_3\text{S}^+$: 280.1002, found: 280.1027



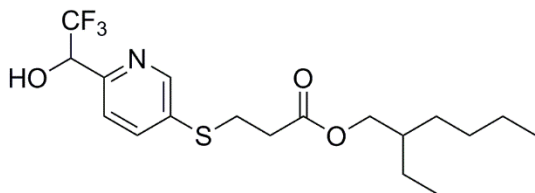
2-ethylhexyl 3-((6-formylpyridin-3-yl)thio)propanoate (2.9)

To a 200 mL round bottom flask equipped with a reflux condenser was added 5-Bromo-2-pyridinecarboxaldehyde (1 g, 5.4 mmol), 2-Ethylhexyl 3-Mercaptopropionate (1.3 g, 5.9 mmol), tris(dibenzylideneacetone)dipalladium(0)-chloroform adduct ($\text{Pd}_2(\text{dba})_3 \cdot \text{CHCl}_3$) (123 mg, 0.12 mmol) and Xantphos (156 mg, 0.27 mmol). The flask was first flushed with argon, then anhydrous toluene (30 mL) and DIPEA (1.4 g, 8 mmol) were added in series. The reaction was refluxed at 130°C under argon for 4.5 hours. The reaction was cooled to room temperature and filtered with Celite. The solvent was removed under reduced pressure and the product was purified by silica gel chromatography (0-30% EtOAc/hex) to afford a golden yellow oil (1.4 g, 4.33 mmol, 80%). ^1H NMR (400 MHz, CDCl_3) δ 9.93 (d, $J = 0.8$ Hz, 1H), 8.56 (dd, $J = 2.4, 0.8$ Hz, 1H), 7.80 (dd, $J = 8.0, 0.4$ Hz, 1H), 7.66 (ddd, $J = 8.4, 2.4, 0.8$ Hz, 1H), 4.01 – 3.90 (m, 2H), 3.26 (t, $J = 7.2$ Hz, 2H), 2.66 (t, $J = 7.2$ Hz, 2H), 1.54 – 1.44 (m, 1H), 1.31 – 1.16 (m, 8H), 0.81 (t, $J = 7.5$ Hz, 6H). ^{13}C NMR (101 MHz, CDCl_3) δ 192.4, 171.1, 149.8, 148.1, 140.2, 134.6, 121.5, 67.4, 38.6, 33.7, 30.3, 28.8, 27.1, 23.7, 22.9, 14.0, 10.9. HR-EIMS m/z calculated for $\text{C}_{17}\text{H}_{26}\text{NO}_3\text{S}^+$: 324.1628, found: 324.1655.



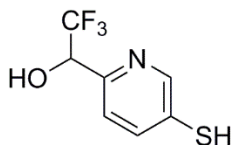
2-ethylhexyl 3-((6-(2,2,2-trifluoro-1-((trimethylsilyl)oxy)ethyl)pyridin-3-yl)thio)propanoate (2.10)

In a 200 mL round bottom flask, compound **2.9** (2.11 g, 6.5 mmol) and trifluoromethyltrimethylsilane (1.08 g, 7.6 mmol) were dissolved in anhydrous THF (50 mL) under argon. The temperature was lowered to 0°C, followed by the dropwise addition of 1 M TBAF in THF (100 μ L, 0.1 mmol). The reaction was then raised to room temperature and stirred for 3 hours. The solvent was removed under reduced pressure and the product was purified by silica gel chromatography (0-20% EtOAc/hex) to afford a clear oil (2 g, 5.08 mmol, 78%). ^1H NMR (400 MHz, CDCl_3) δ 8.50 (dd, J = 2.4, 0.8 Hz, 1H), 7.71 (dd, J = 8.0, 2.4 Hz, 1H), 7.54 (d, J = 8.4 Hz, 1H), 5.04 (q, J = 6.4 Hz, 1H), 4.04 – 3.95 (m, 2H), 3.19 (t, J = 7.2 Hz, 2H), 2.64 (t, J = 7.6 Hz, 2H), 1.59 – 1.50 (m, 1H), 1.37 – 1.20 (m, 8H), 0.86 (t, J = 7.6 Hz, 6H), 0.11 (s, 9H). ^{19}F NMR (376 MHz, CDCl_3) δ -77.69 (d, J = 6.4 Hz). ^{13}C NMR (101 MHz, CDCl_3) δ 171.4, 153.5 – 153.4 (m), 149.1, 137.7, 133.4, 123.8 (q, J = 284.0 Hz), 122.4 – 122.2 (m), 74.3 (q, J = 31.7 Hz), 67.3, 38.7, 34.2, 30.3, 28.9, 28.7, 23.7, 22.9, 14.0, 10.9, -0.4. HR-EIMS m/z calculated for $\text{C}_{21}\text{H}_{35}\text{F}_3\text{NO}_3\text{SSi}^+$: 466.2054, found: 466.2094.



2-ethylhexyl 3-((6-(2,2,2-trifluoro-1-hydroxyethyl)pyridin-3-yl)thio)propanoate (2.11)

In a 200 mL round bottom flask, compound **2.10** (800 mg, 1.7 mmol) was dissolved in 1:1 aq.1M HCl/THF (100 mL) and stirred at room temperature overnight. THF was first removed under reduced pressure, then the product was extracted with EtOAc (3 x 50 mL). The organic extracts were combined, washed with H₂O (3 x 50 mL) and brine (50 mL), then dried over Na₂SO₄. The solvent was removed under reduced pressure and the product was purified by silica gel chromatography (0-30% EtOAc/hex) to afford a pale yellow oil (600 mg, 1.53 mmol, 89%). ¹H NMR (400 MHz, CDCl₃) δ 8.54 (d, *J* = 1.6 Hz, 1H), 7.74 (dd, *J* = 8.4, 2.4 Hz, 1H), 7.35 (d, *J* = 8 Hz, 1H), 5.00 (q, *J* = 6.4 Hz, 1H), 4.08 – 3.91 (m, 2H), 3.21 (t, *J* = 7.2 Hz, 2H), 2.64 (t, *J* = 7.2 Hz, 2H), 1.60 – 1.50 (m, 1H), 1.37 – 1.21 (m, 8H), 0.86 (t, *J* = 7.2 Hz, 6H). ¹⁹F NMR (376 MHz, CDCl₃) δ -78.05 (d, *J* = 6.39 Hz). ¹³C NMR (101 MHz, CDCl₃) δ 171.9, 149.4 - 148.8 (m), 148.6, 138.0, 134.3, 123.9 (q, *J* = 283.9 Hz), 122.62 - 122.53 (m), 70.63 (q, *J* = 31.9 Hz), 67.39, 38.6, 34.1, 30.3, 28.9, 28.8, 23.7, 22.9, 14.0, 10.9. HR-EIMS *m/z* calculated for C₁₈H₂₇F₃NO₃S⁺: 394.1658, found: 394.1694.



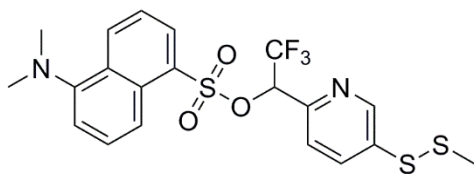
2,2,2-trifluoro-1-(5-mercaptopyridin-2-yl)ethan-1-ol (2.12)

In a 200 mL round bottom flask, compound **2.11** (432 mg, 1.1 mmol) was dissolved in anhydrous toluene (20 mL) and degassed 25% sodium methoxide in methanol (10 mL) under argon. The reaction was stirred at room temperature for 3 hours. The reaction was quenched with glacial acetic acid (10 mL). The solvents were removed under reduced pressure and the crude material was dissolved EtOAc (50 mL). The organic layer was washed with H₂O (3 x 50 mL) and brine (50 mL), then dried over Na₂SO₄. The solvent was removed under reduced pressure and the product was purified by silica gel chromatography (0-50% EtOAc/hex) afforded an off-white solid (120 mg, 0.57 mmol, 52%). ¹H NMR (400 MHz, CDCl₃) δ 8.56 – 8.46 (m, 1H), 7.69 (dd, *J* = 8.2, 2.4 Hz, 1H), 7.30 (d, *J* = 8.0 Hz, 1H), 5.16 (d, *J* = 7.2 Hz, 1H), 5.02 – 4.95 (m, 1H), 3.52 (s, 1H). ¹⁹F NMR (376 MHz, CDCl₃) δ -78.20 (d, *J* = 6.8 Hz, 1H). ¹³C NMR (101 MHz, CDCl₃) δ 148.3 – 148.2 (m), 147.8, 137.6, 130.1, 123.9 (q, *J* = 284.0 Hz), 122.5 (m), 70.6 (q, *J* = 32.0 Hz). HR-EIMS *m/z* calculated for C₇H₇F₃NOS⁺: 210.0195, found: 210.0215.



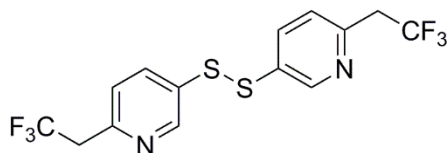
2,2,2-trifluoro-1-(5-(methylthio)pyridin-2-yl)ethan-1-ol (2.13)

In a 50 mL round bottom flask, compound **2.12** (120 mg, 0.57 mmol) and S-methyl methanethiosulfonate (72 mg, 0.57 mmol) were dissolved in anhydrous MeOH (4 mL) under argon. Degassed 100 mM sodium phosphate pH 8 buffer (3 mL) was then added. The reaction was stirred at room temperature under argon for 3 hours. The reaction mixture was poured into EtOAc (50 mL), washed with H₂O (3 x 25 mL) and brine (25 mL), then dried over Na₂SO₄. The solvent was removed under reduced pressure and the product was purified by silica gel chromatography (0-20% EtOAc/hex) to afford an off-white solid (100 mg, 0.39 mmol 69%). ¹H NMR (400 MHz, CDCl₃) δ 8.71 – 8.68 (m, 1H), 7.96 (dd, *J* = 8.4, 2.4 Hz, 1H), 7.40 (d, *J* = 8 Hz, 1H), 5.30 – 5.20 (m, 1H), 5.07 – 4.98 (m, 1H), 2.48 (s, 3H). ¹⁹F NMR (376 MHz, CDCl₃) δ -78.04 (d, *J* = 7.52 Hz). ¹³C NMR (101 MHz, CDCl₃) δ 149.5 (m), 146.9, 136.3, 135.8, 123.9 (q, *J* = 284.0 Hz), 122.7 (m), 70.6 (q, *J* = 32.1 Hz), 22.9. HR-EIMS *m/z* calculated for C₈H₉F₃NOS₂⁺: 256.0072, found: 256.0095.



2,2,2-trifluoro-1-(5-(methyldisulfanyl)pyridin-2-yl)ethyl 5-(dimethylamino)naphthalene-1-sulfonate (2.14)

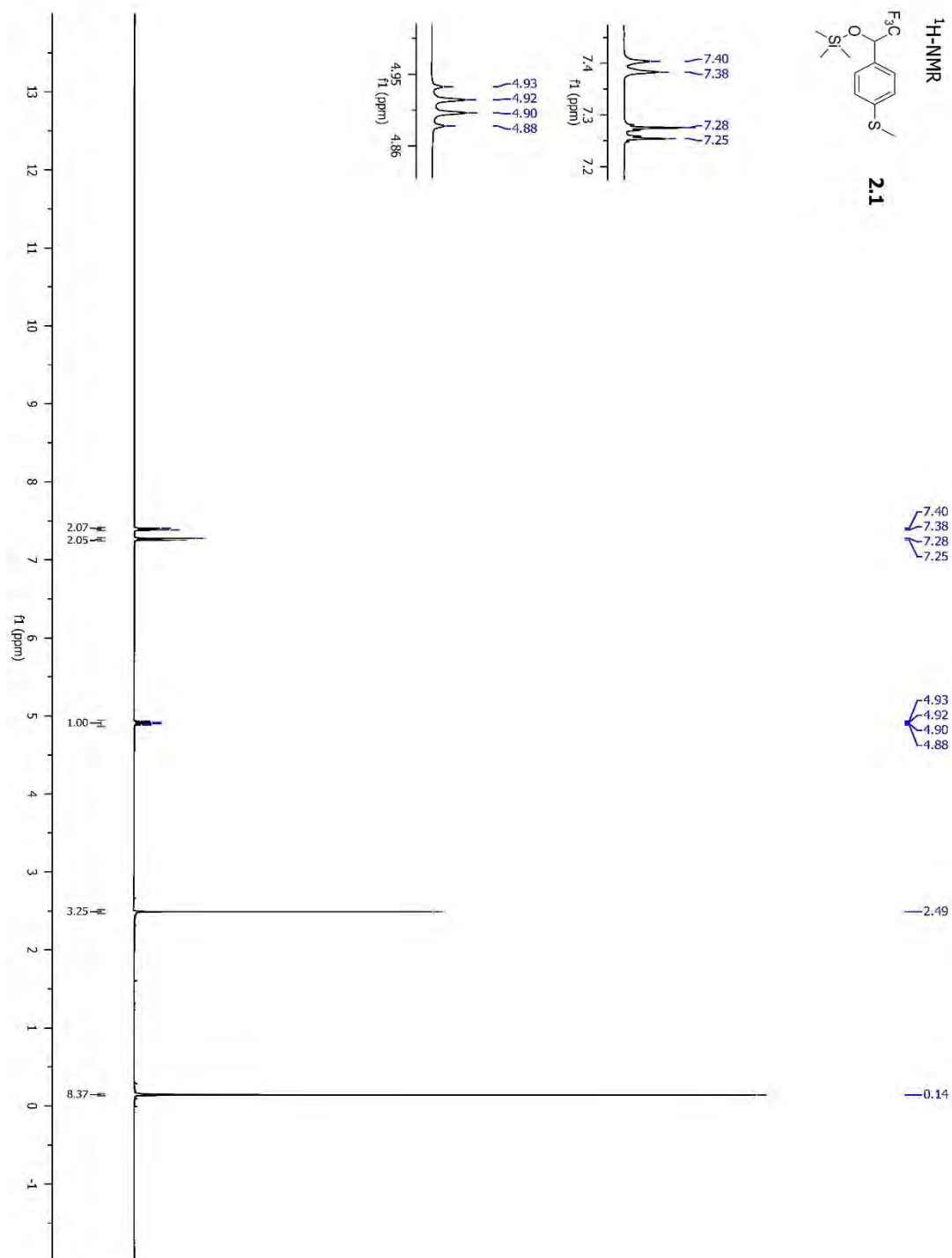
In a 50 mL round bottom flask, compound **2.13** (100 mg, 0.39 mmol), DABCO (44 mg, 0.39 mmol) and dansyl chloride (127 mg, 0.47 mmol) were dissolved in anhydrous DCM (6 mL) under argon. The reaction was stirred at room temperature under argon for 3 hours. The solvent was removed under reduced pressure and the product was purified by silica gel chromatography (0-25% EtOAc/hex) to afford a yellow solid (62 mg, 0.21 mmol, 32%). ^1H NMR (400 MHz, CDCl_3) δ 8.51 (d, $J = 8.4$ Hz, 1H), 8.36 (d, $J = 1.6$ Hz, 1H), 8.22 (d, $J = 8.4$ Hz, 1H), 8.18 (dd, $J = 7.2, 0.8$ Hz, 1H), 7.61 – 7.54 (m, 1H), 7.50 (dd, $J = 8.4, 2.4$ Hz, 1H), 7.44 (dd, $J = 8.0, 7.2$ Hz, 1H), 7.22 (d, $J = 8.4$ Hz, 1H), 7.17 (d, $J = 7.6$ Hz, 2H), 5.71 (q, $J = 6$ Hz, 1H), 2.85 (s, 6H), 2.41 (s, 3H). ^{19}F NMR (376 MHz, CDCl_3) δ -75.34 (d, $J = 6.4$ Hz). ^{13}C NMR (125 MHz, CDCl_3) δ 151.8, 147.5, 146.8, 135.9, 134.5, 132.2, 131.0, 130.8, 129.7, 129.5, 128.9, 122.9, 122.7, 121.9 (q, $J = 280.1$ Hz), 119.2, 115.5, 78.7 (q, $J = 33.9$ Hz), 45.4, 22.9. HR-EIMS m/z calculated for $\text{C}_{20}\text{H}_{20}\text{F}_3\text{N}_2\text{O}_3\text{S}_3^+$: 489.0583, found: 489.0625.

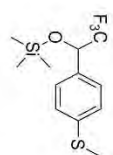


1,2-bis(6-(2,2,2-trifluoroethyl)pyridin-3-yl)disulfane (2.15)

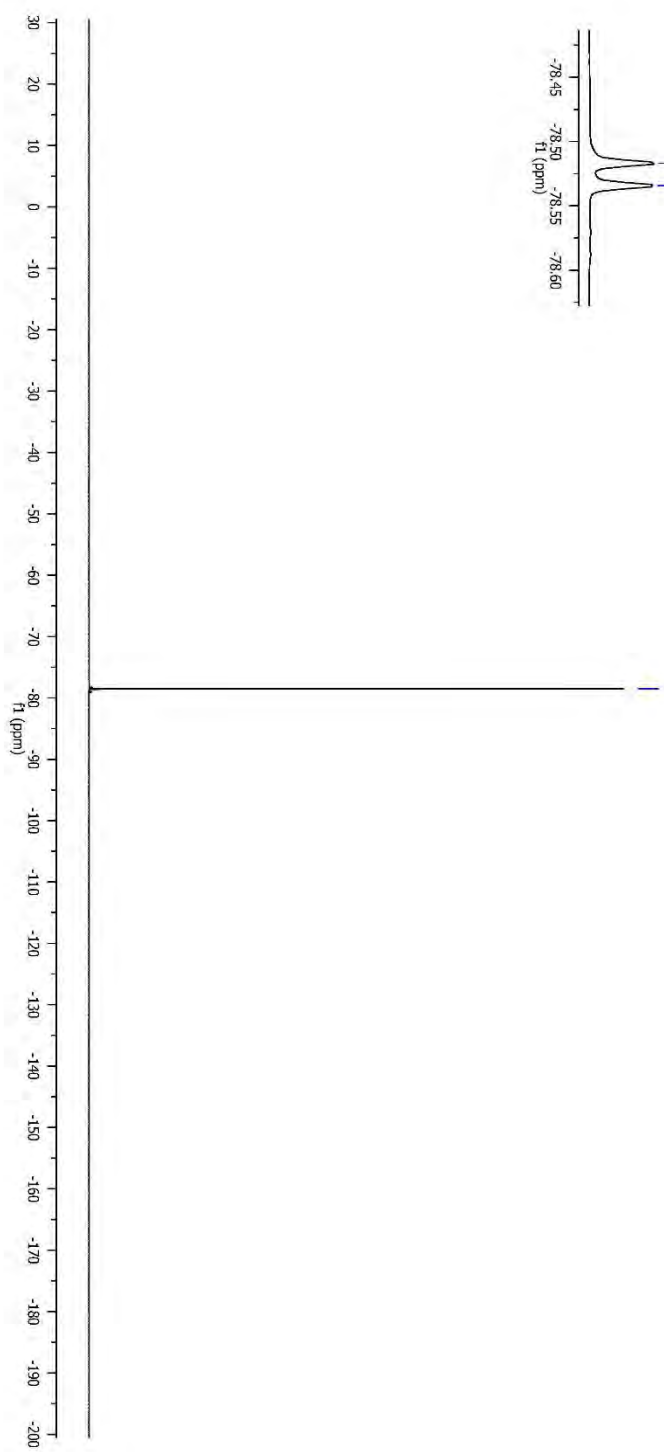
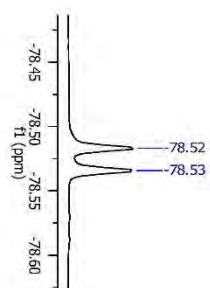
In a 50 mL round bottom flask, **2.14** (50 mg, 0.1 mmol) was dissolved in ACN (9 mL). TCEP hydrochloride (286 mg, 1 mmol) was dissolved separately in H₂O (10 mL) and adjusted to pH 7. The two solutions were combined and stirred at room temperature for 2 hours. The reaction mixture was poured into brine (50 mL) and the product was extracted with diethyl ether (3 x 20 mL). The combined organic layers were washed with brine (50 mL) and dried over Na₂SO₄. The solvent was removed under reduced pressure and the product was purified by silica gel chromatography (0-20% EtOAc/hex) to afford an off-white solid (6 mg, 0.016 mmol, 16%). ¹H NMR (400 MHz, CDCl₃) δ 8.66 (dd, *J* = 2.4, 0.6 Hz, 2H), 7.83 (dd, *J* = 8.2, 2.5 Hz, 2H), 7.31 (d, *J* = 8.2 Hz, 2H), 3.60 (q, *J* = 10.6 Hz, 3H). ¹⁹F NMR (376 MHz, CDCl₃) δ -64.68 (t, *J* = 10.6 Hz). ¹³C NMR (125 MHz, CDCl₃) δ 150.1 - 190.3 (m), 149.2, 137.0, 133.1, 125.2 (q, *J* = 275.6 Hz), 124.8, 42.3 (q, *J* = 29.5 Hz). HR-EIMS *m/z* calculated for C₁₄H₁₁F₆N₂S₂⁺: 285.0262, found: 285.0251.

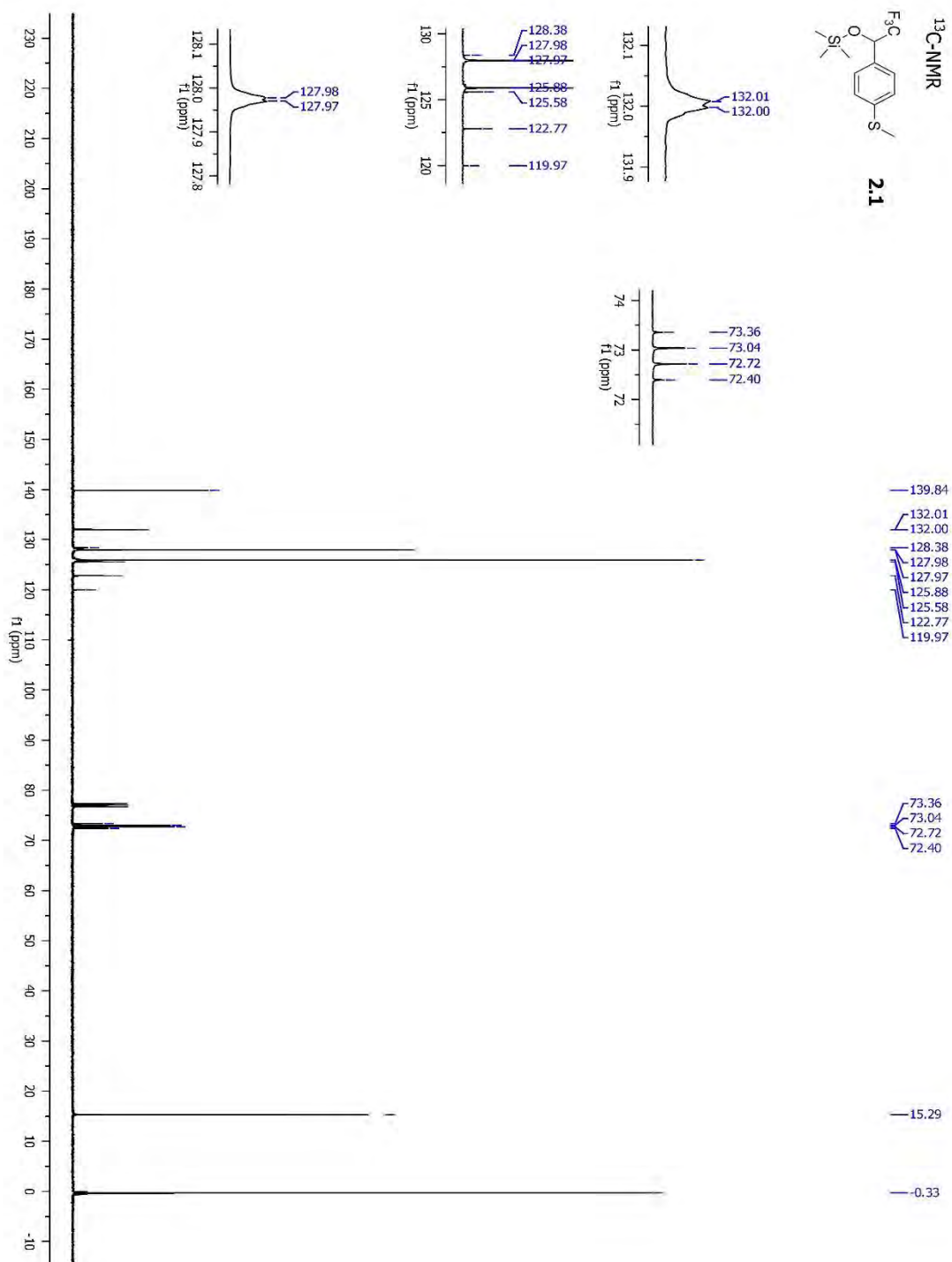
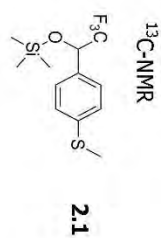
NMR Spectra

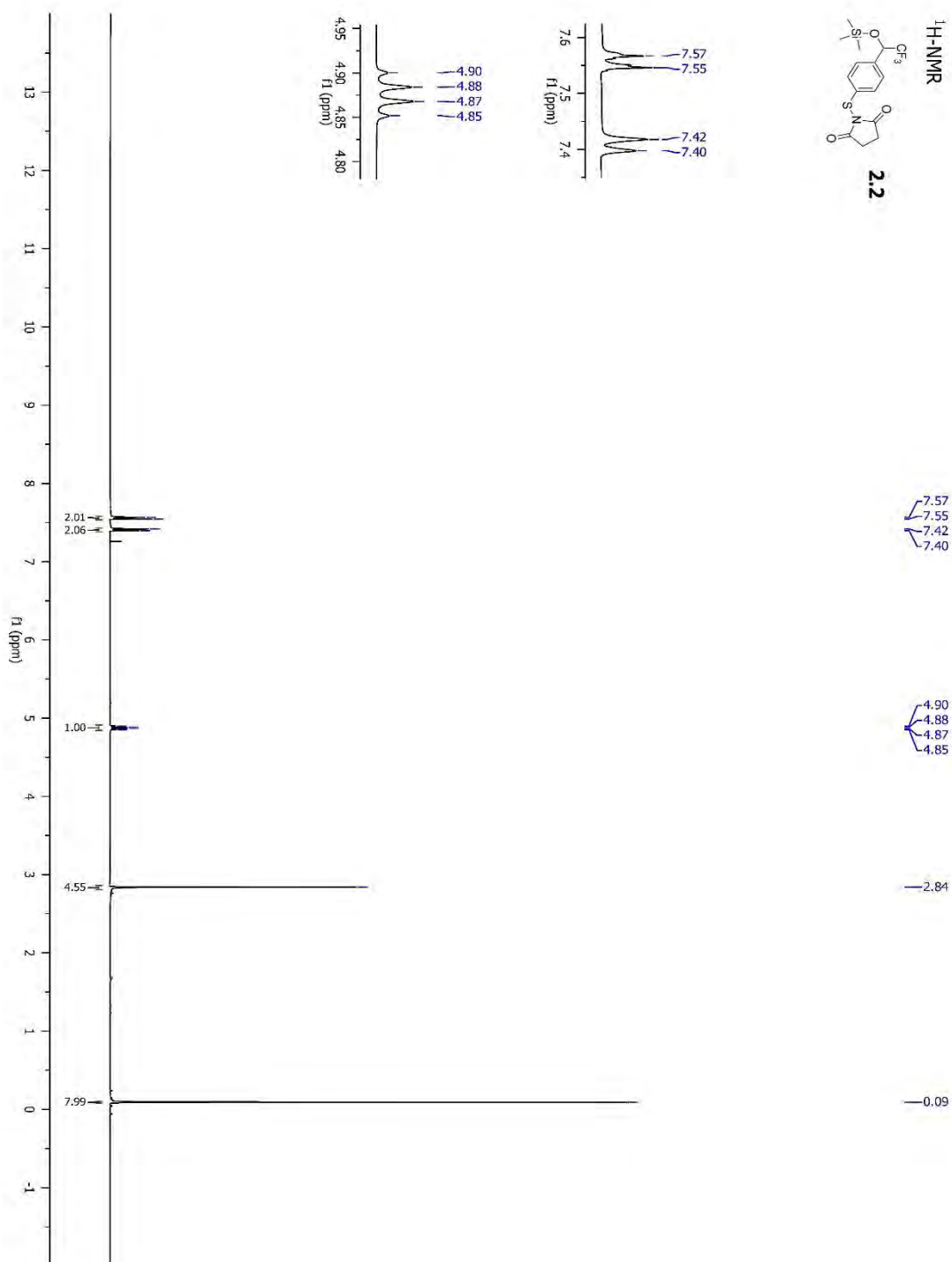
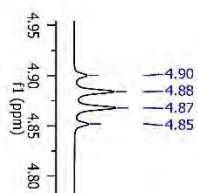
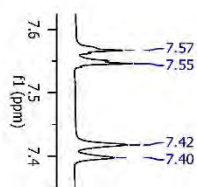
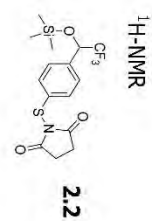


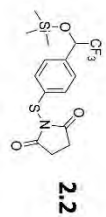
¹⁹F-NMR**2.1**

-78.52
-78.53

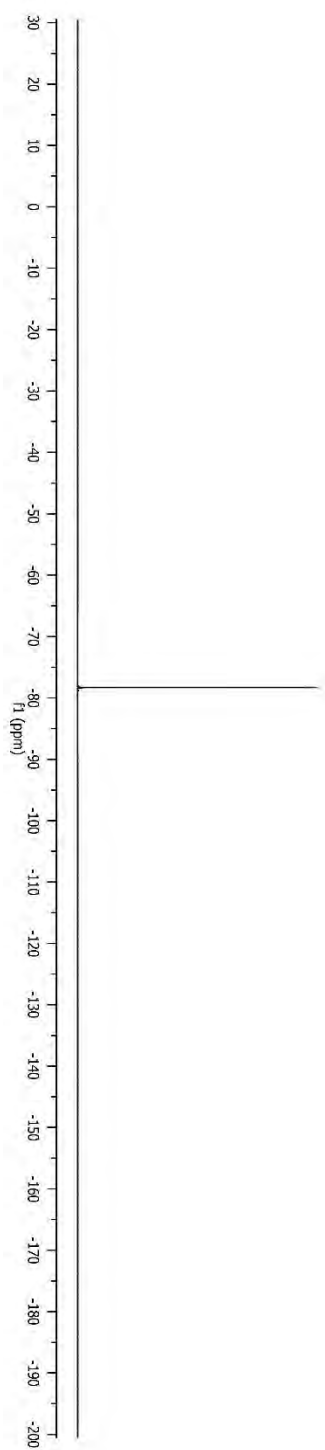
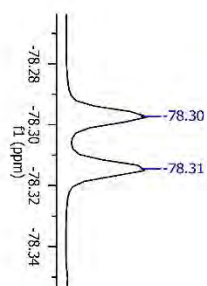


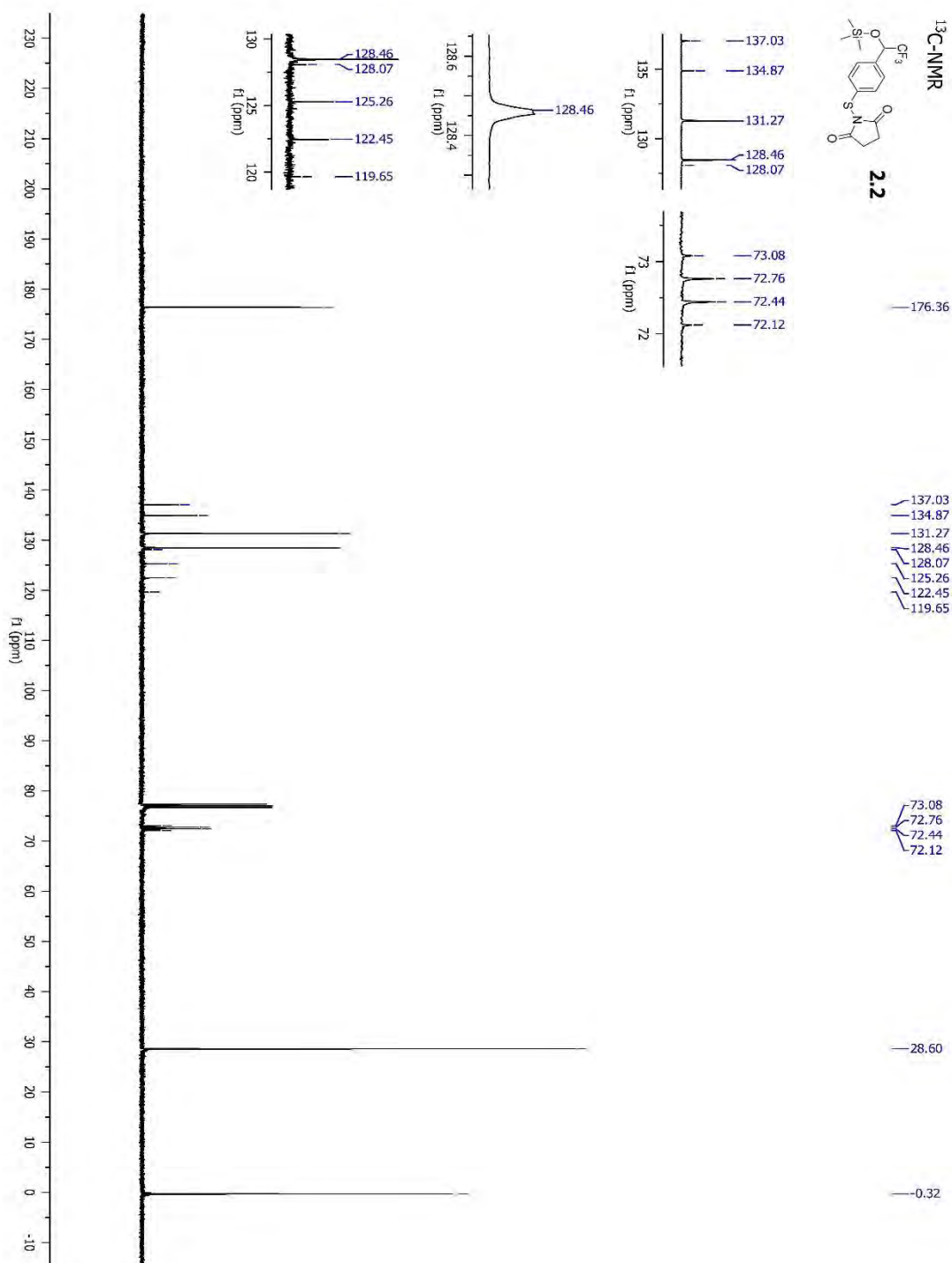
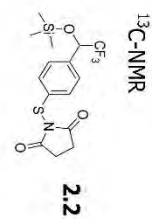


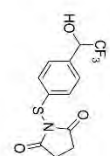


¹⁹F-NMR

-78.30
-78.31



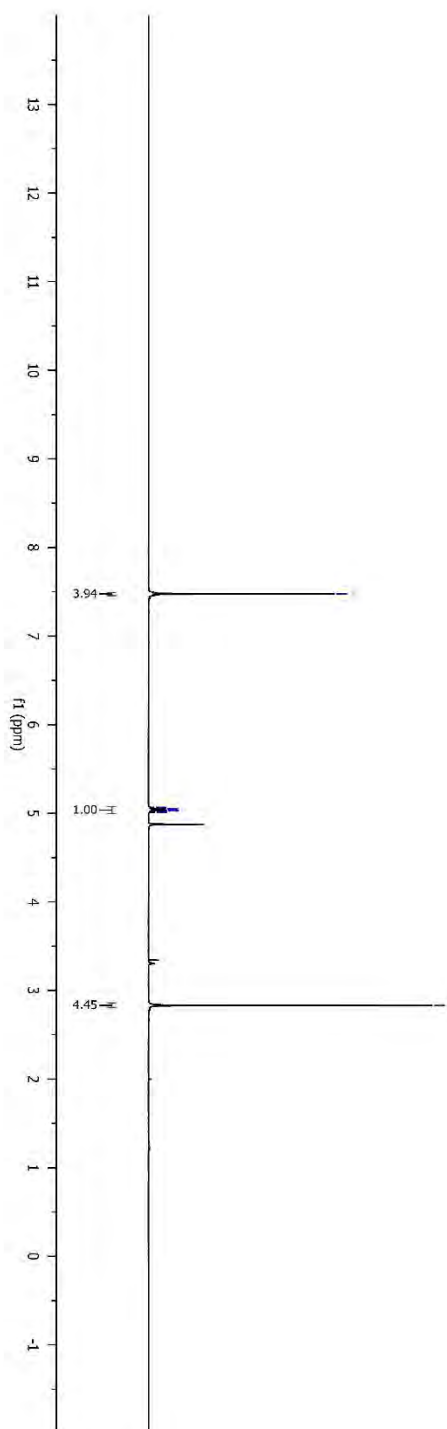
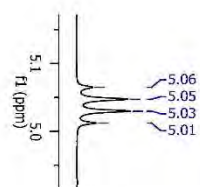


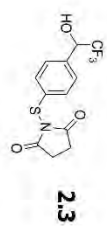
¹H-NMR**2.3**

— 7.47

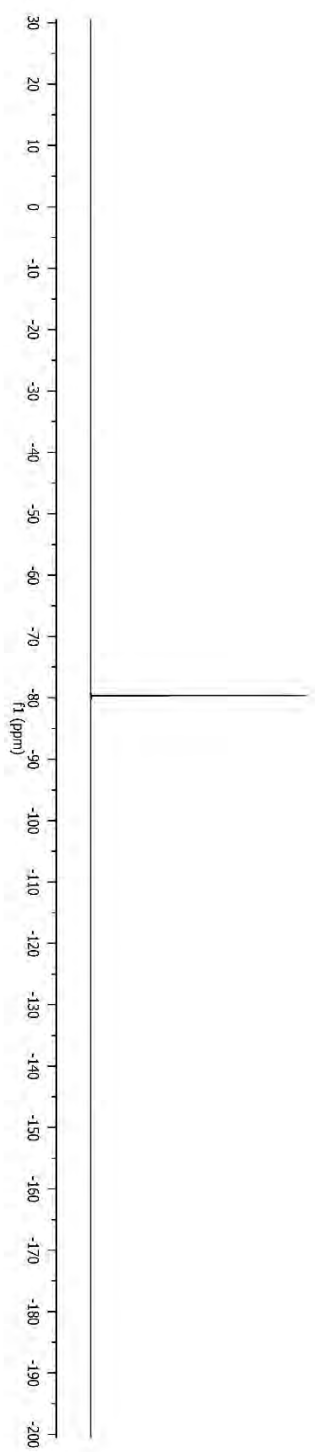
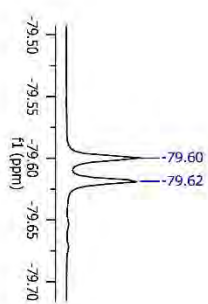
— 5.06
— 5.05
— 5.03
— 5.01

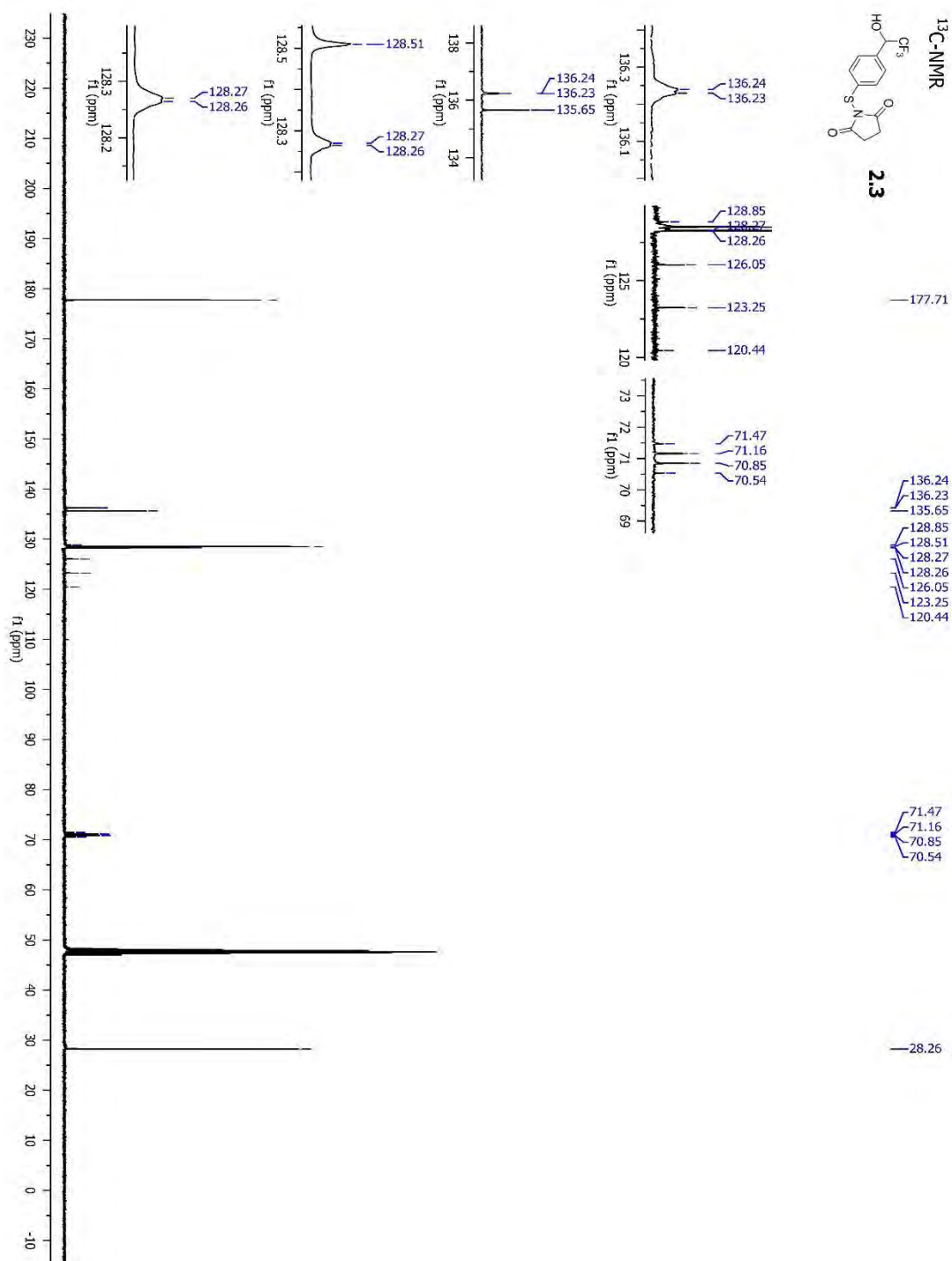
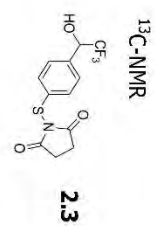
— 2.83

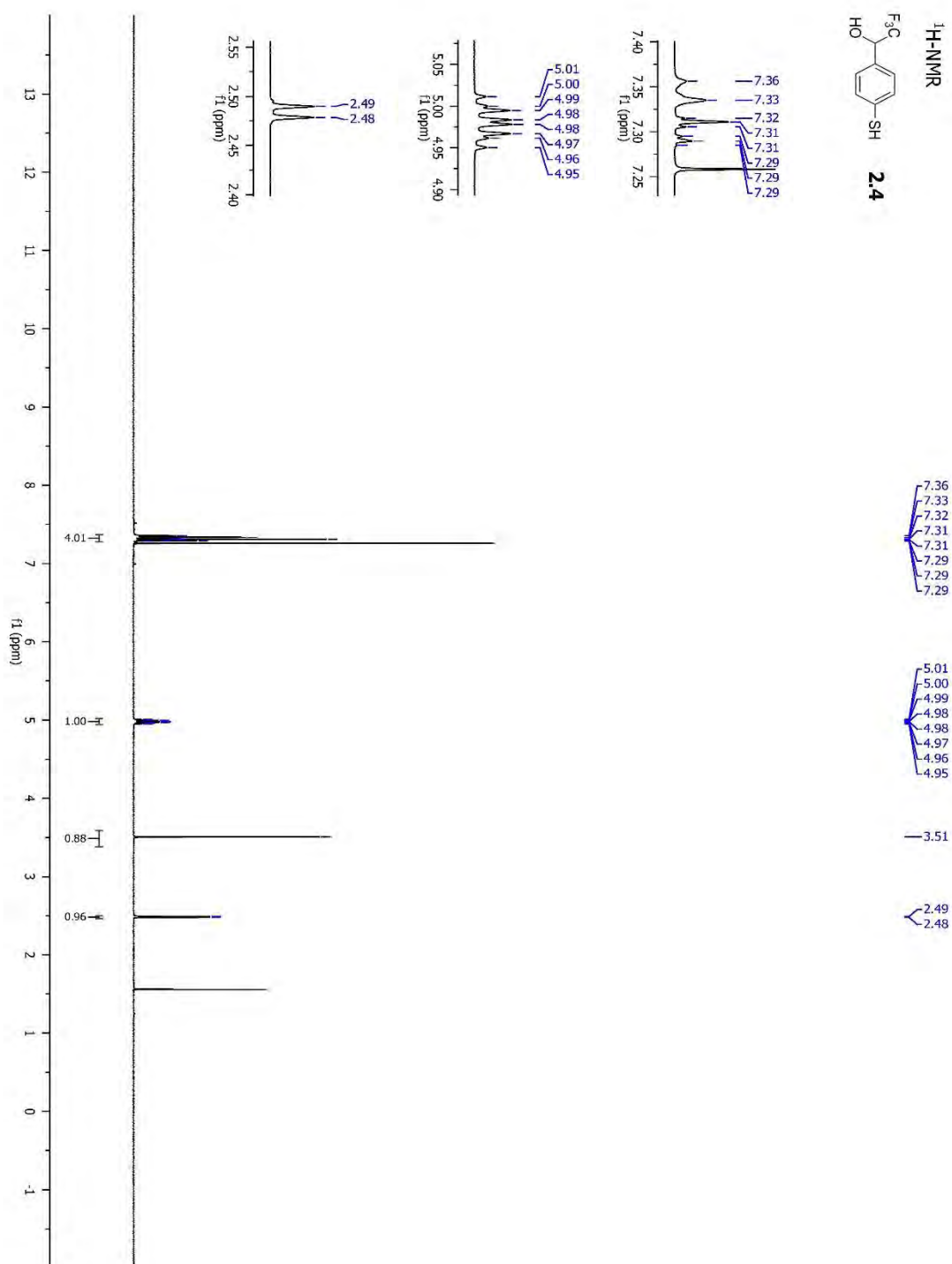
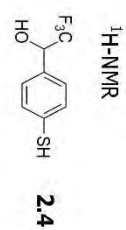


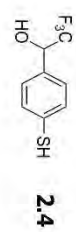
¹⁹F-NMR

-79.60
-79.62

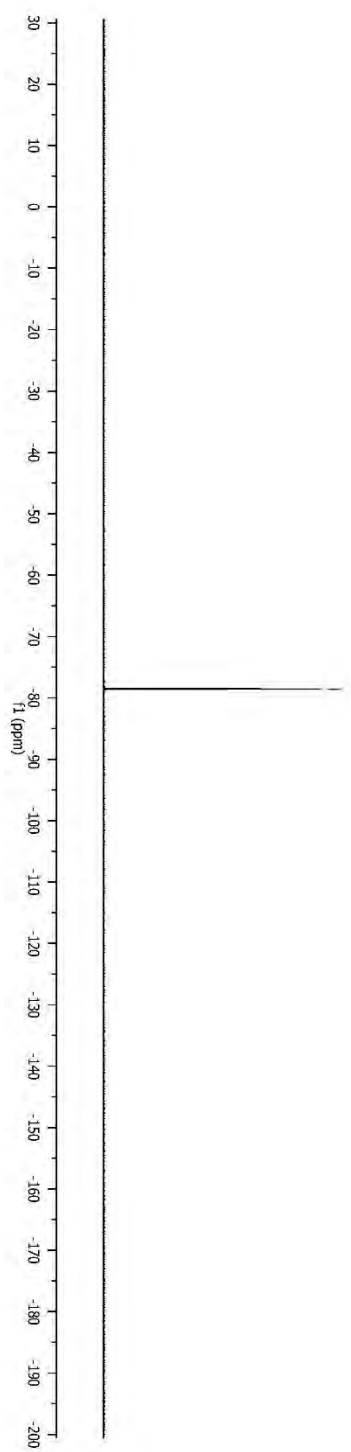
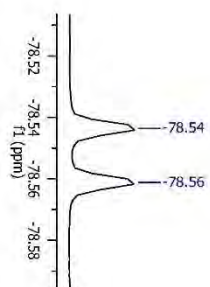


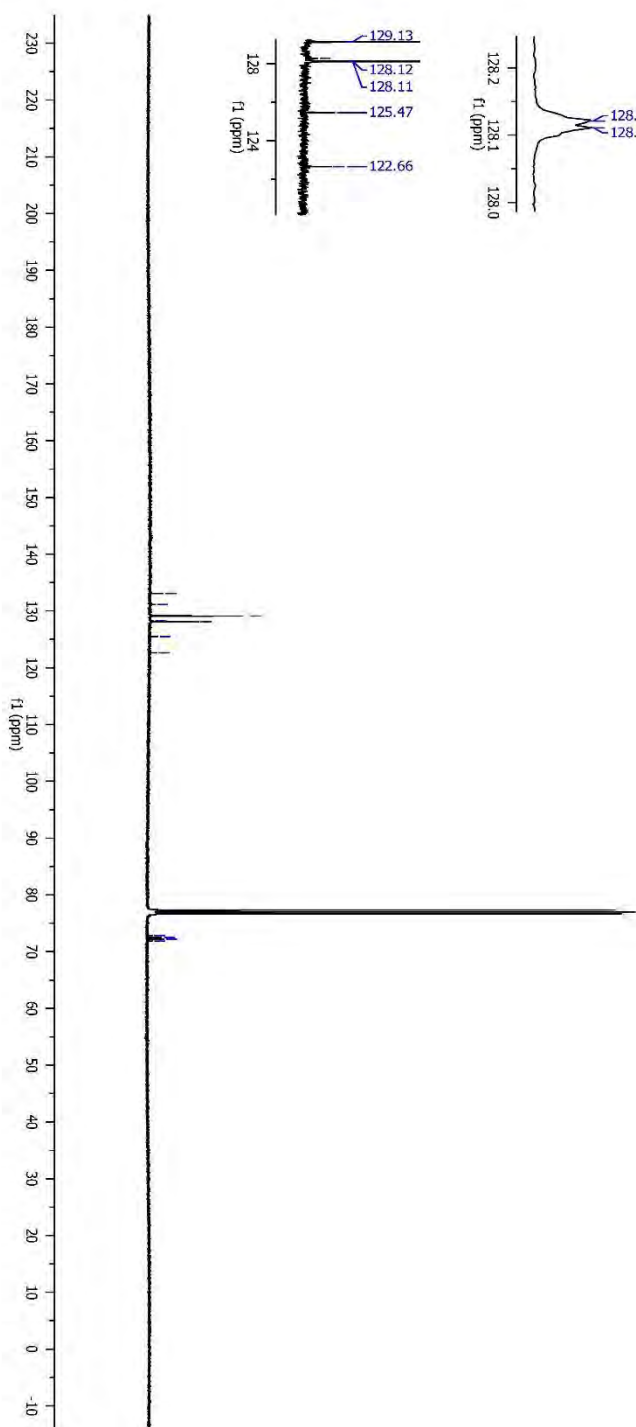
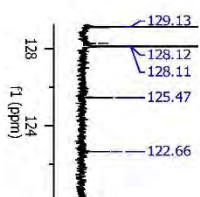
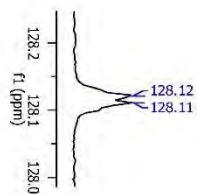
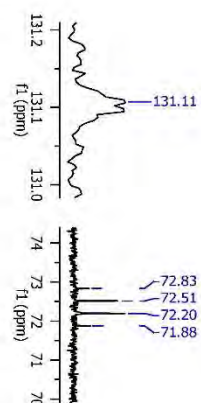
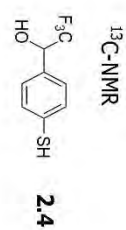


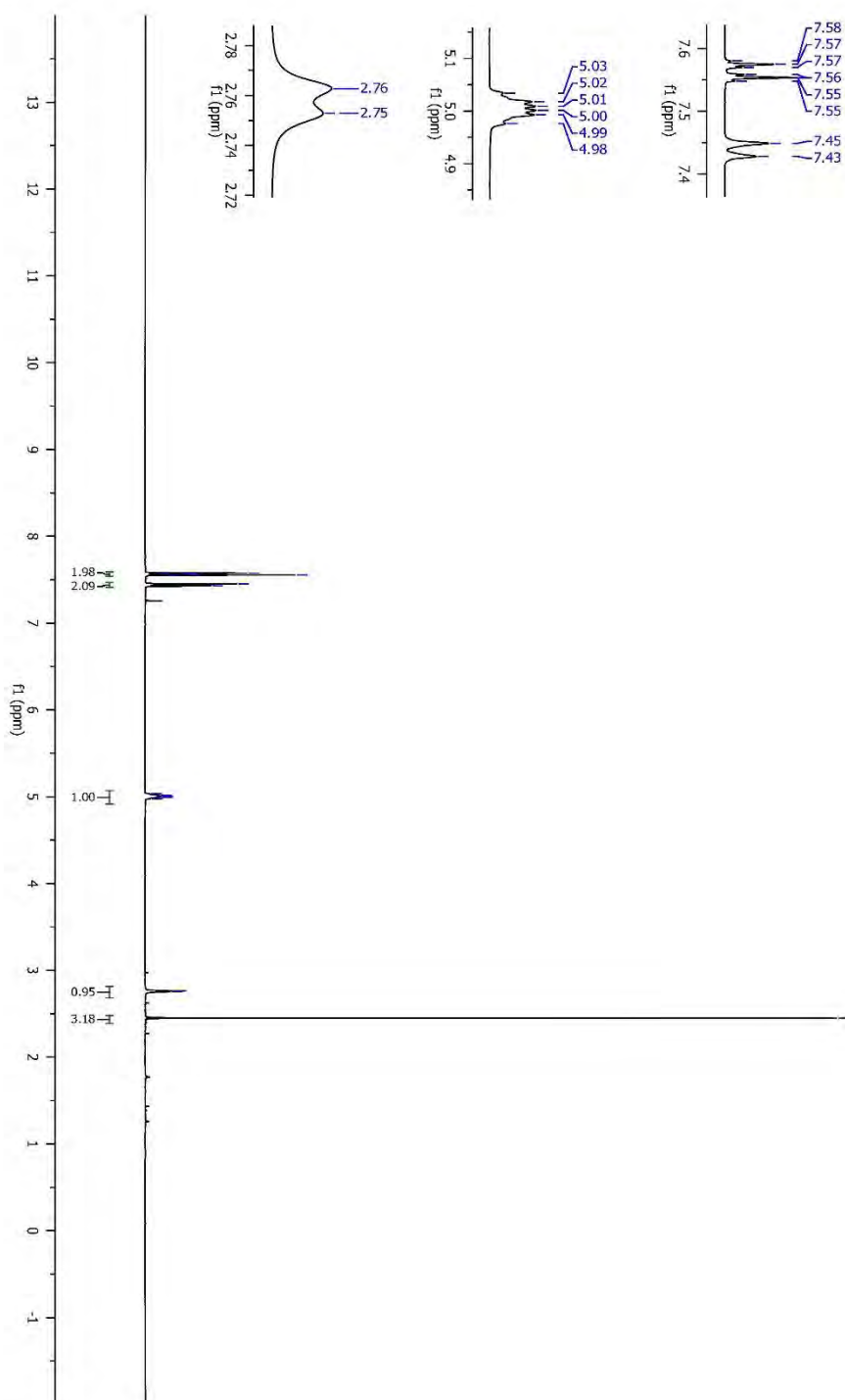
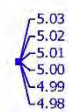
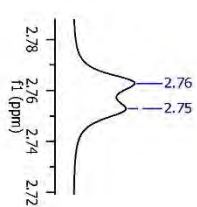
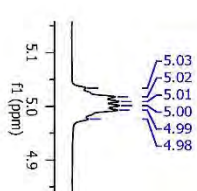
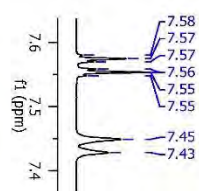
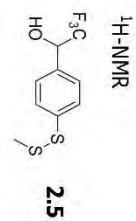


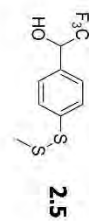
¹⁹F-NMR

-78.54
-78.56

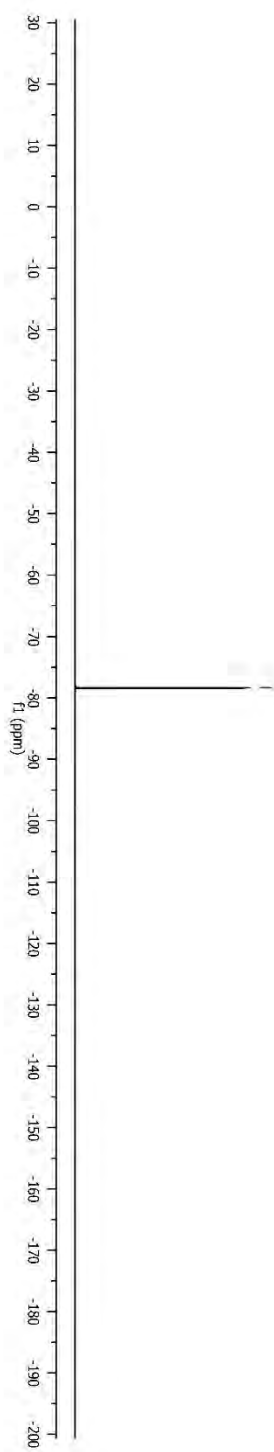
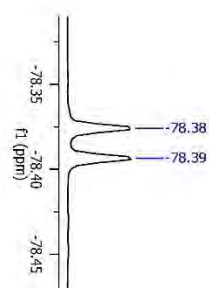


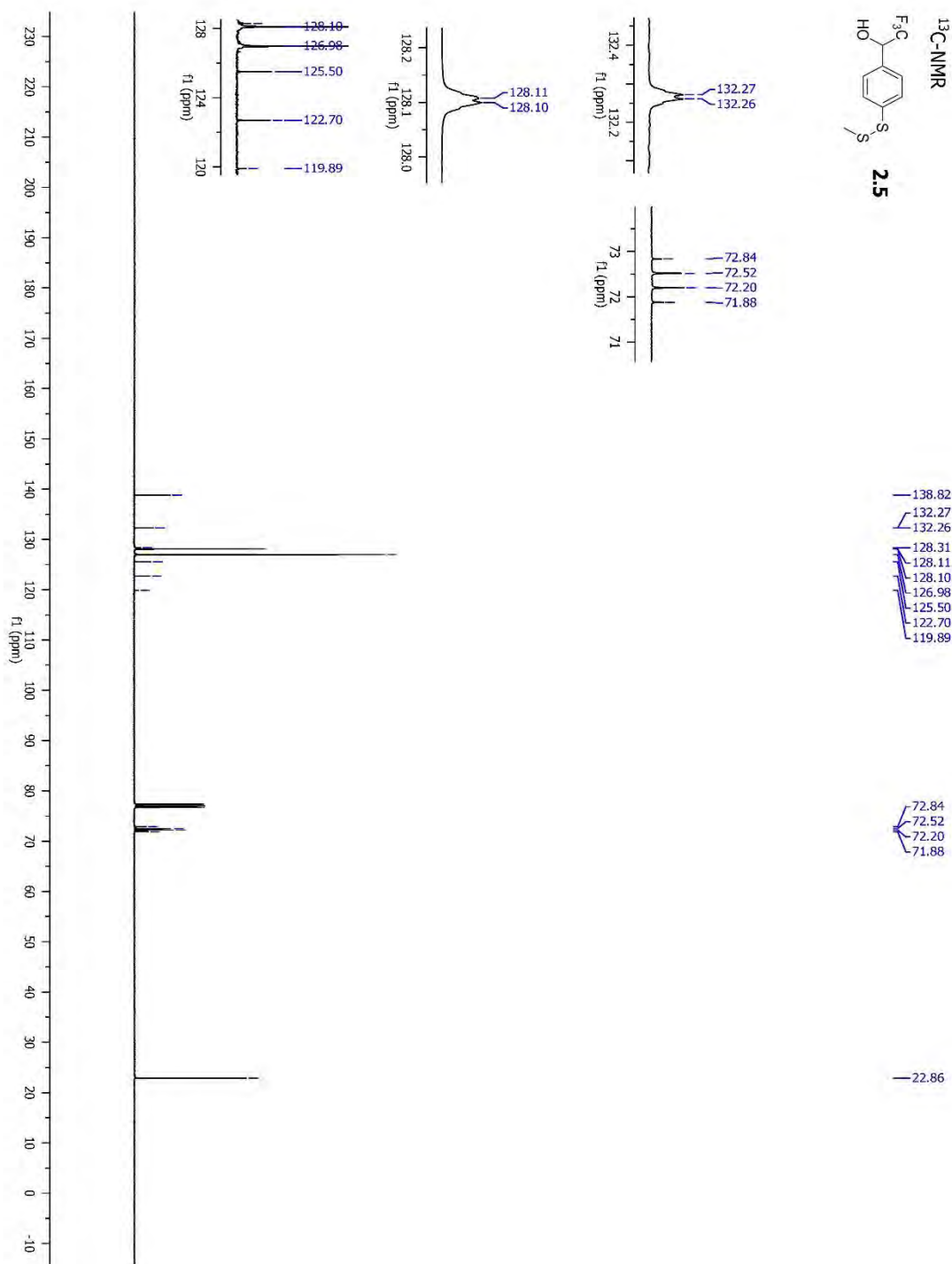
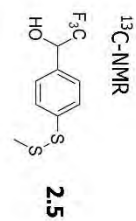


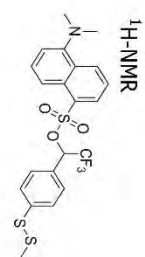
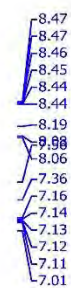


¹⁹F-NMR

78.38
78.39

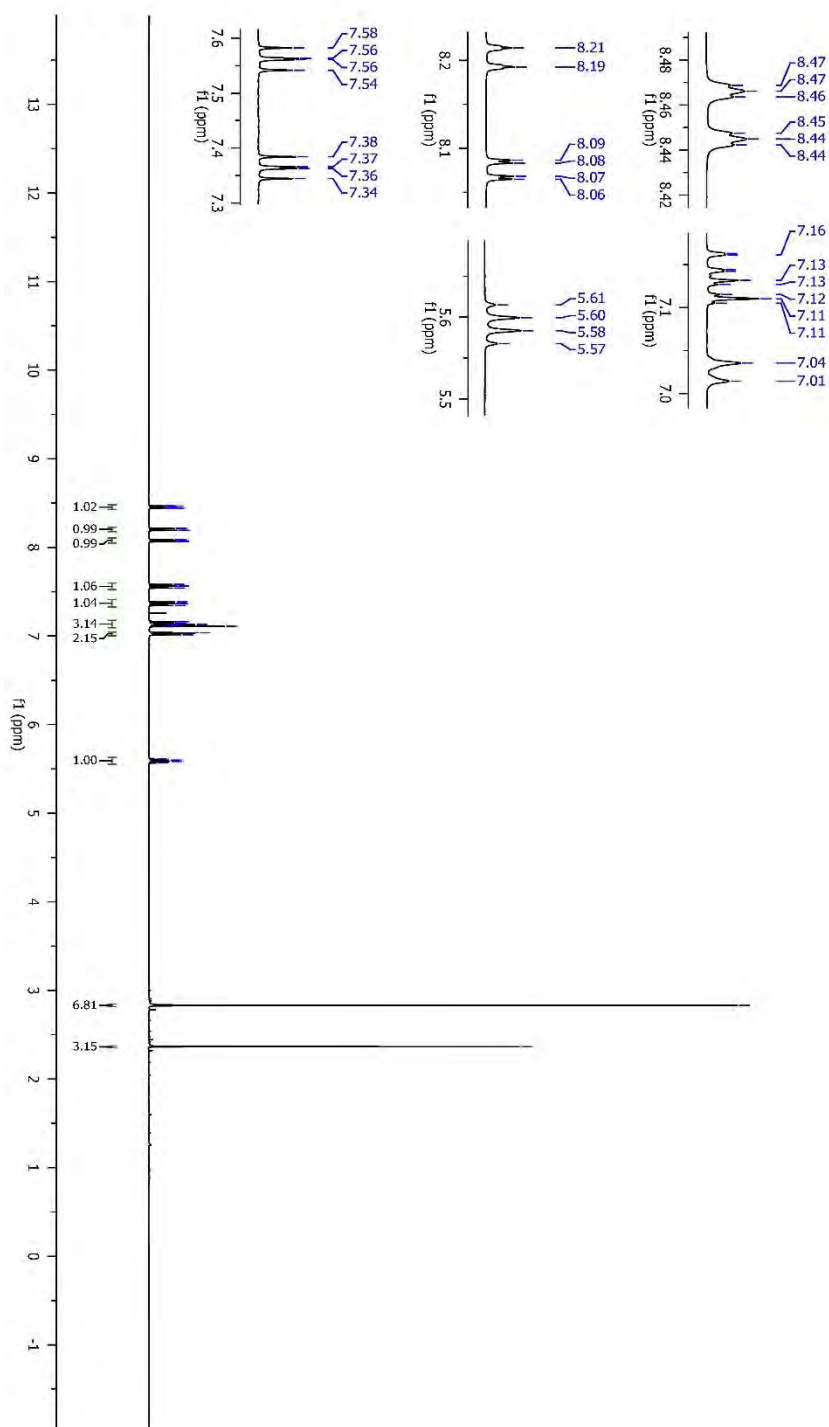


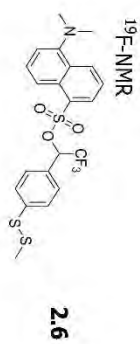


**2.6**

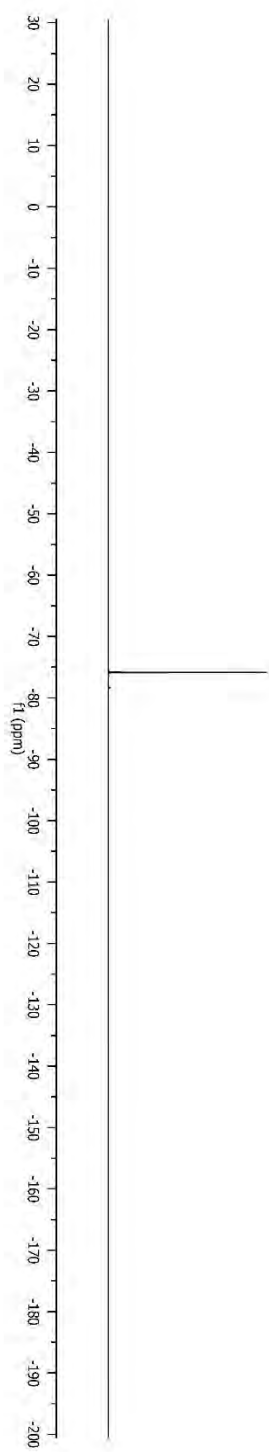
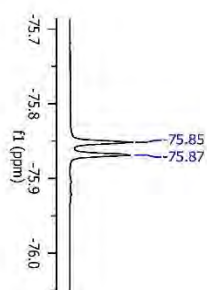
— 2.83

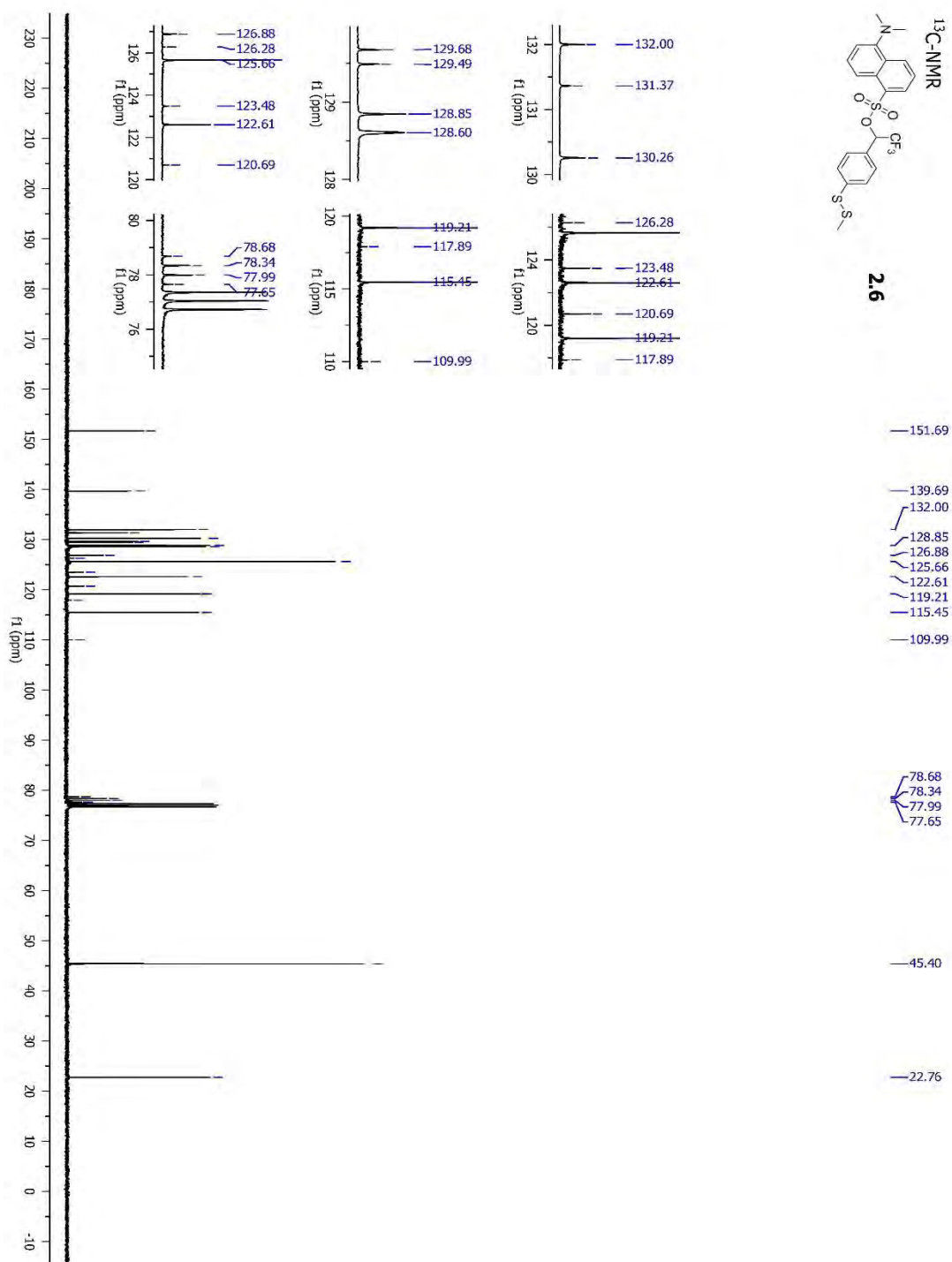
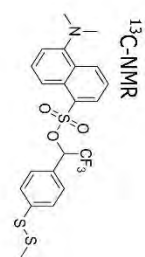
— 2.37

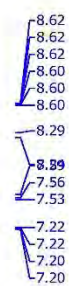
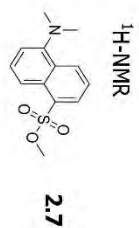




-75.85
-75.87

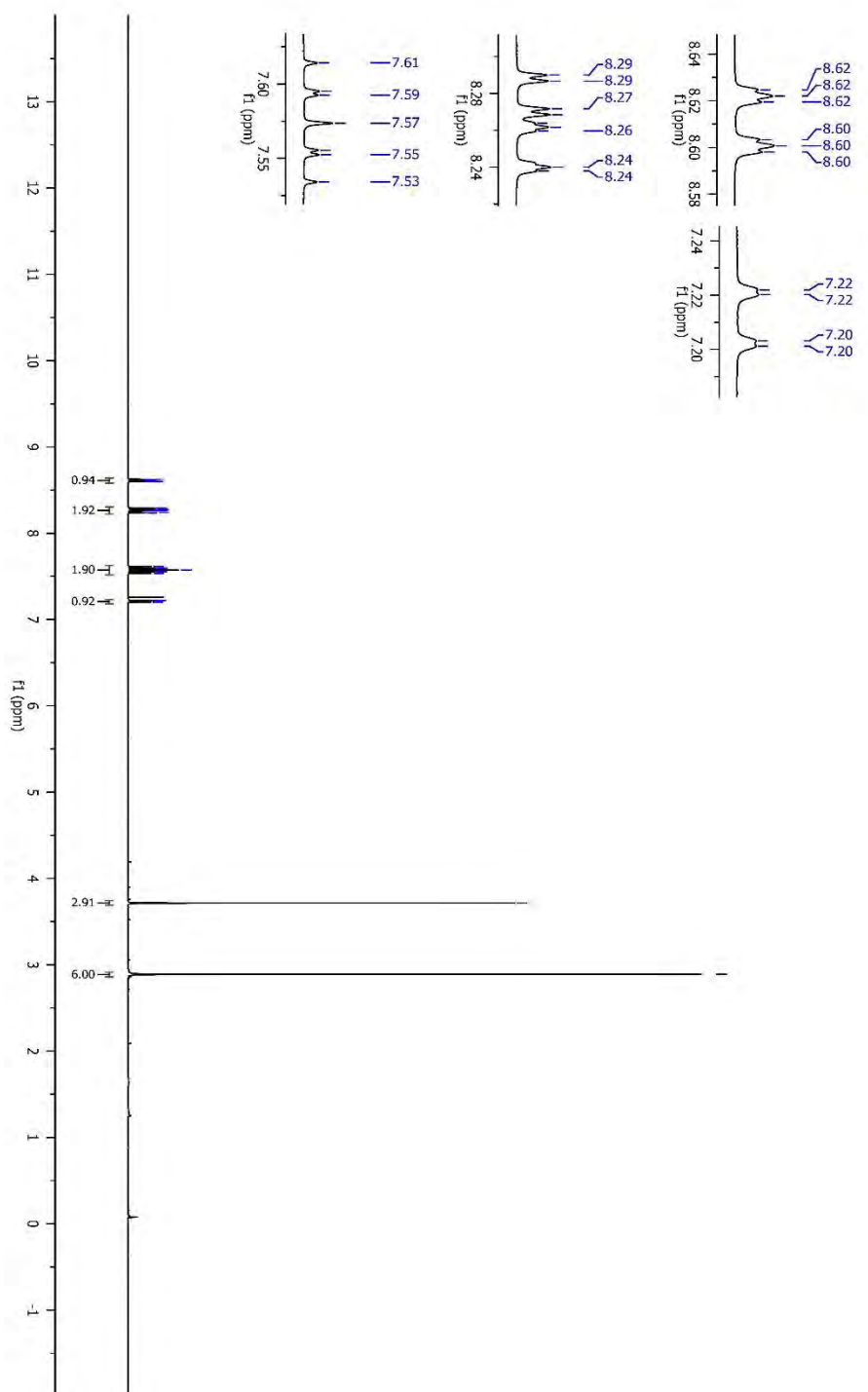


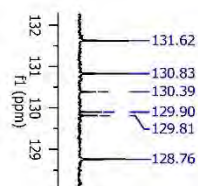
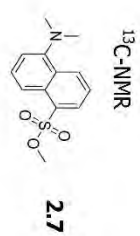




3.72

2.89





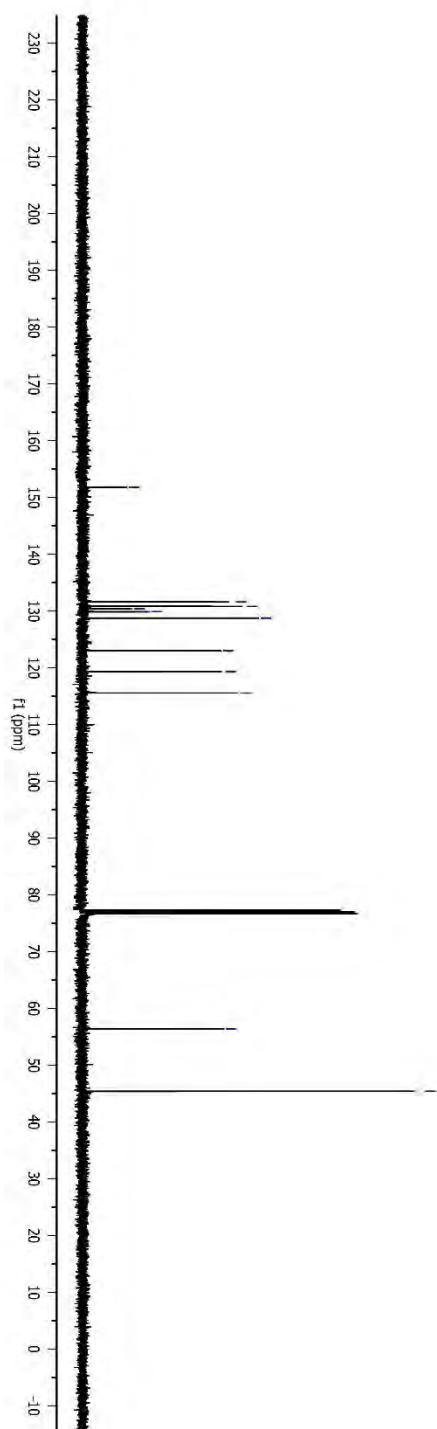
151.78

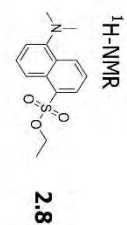
130.83
130.39
129.90
129.81
128.76

123.02
119.32
115.56

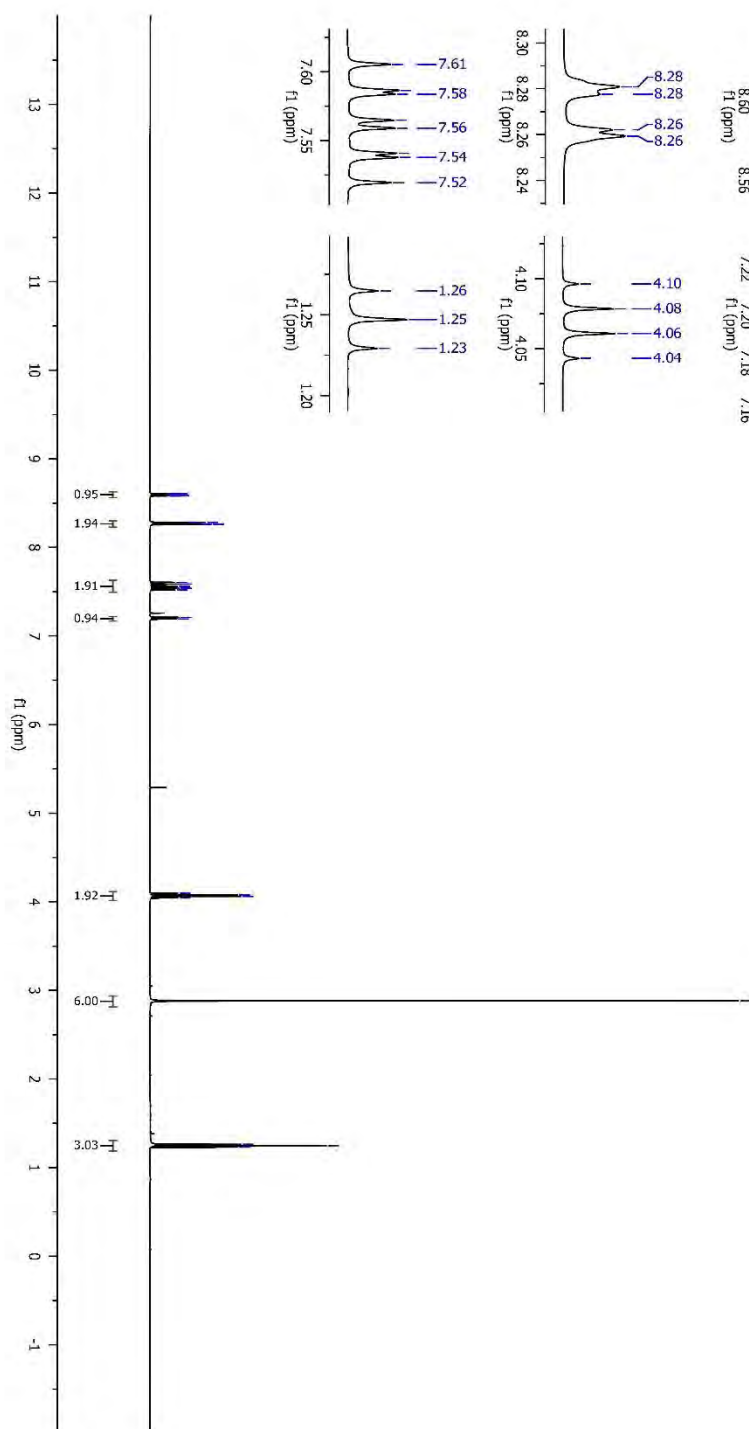
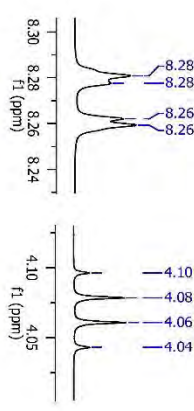
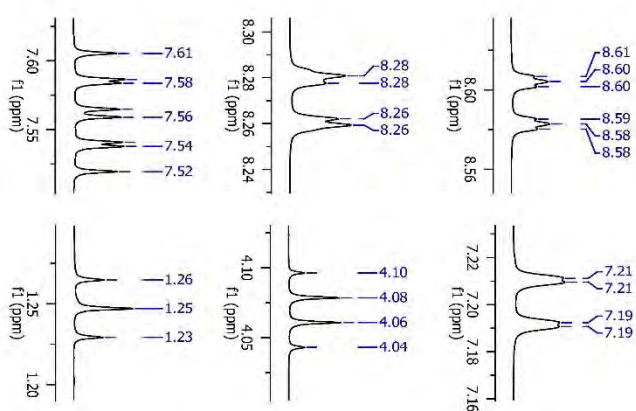
56.40

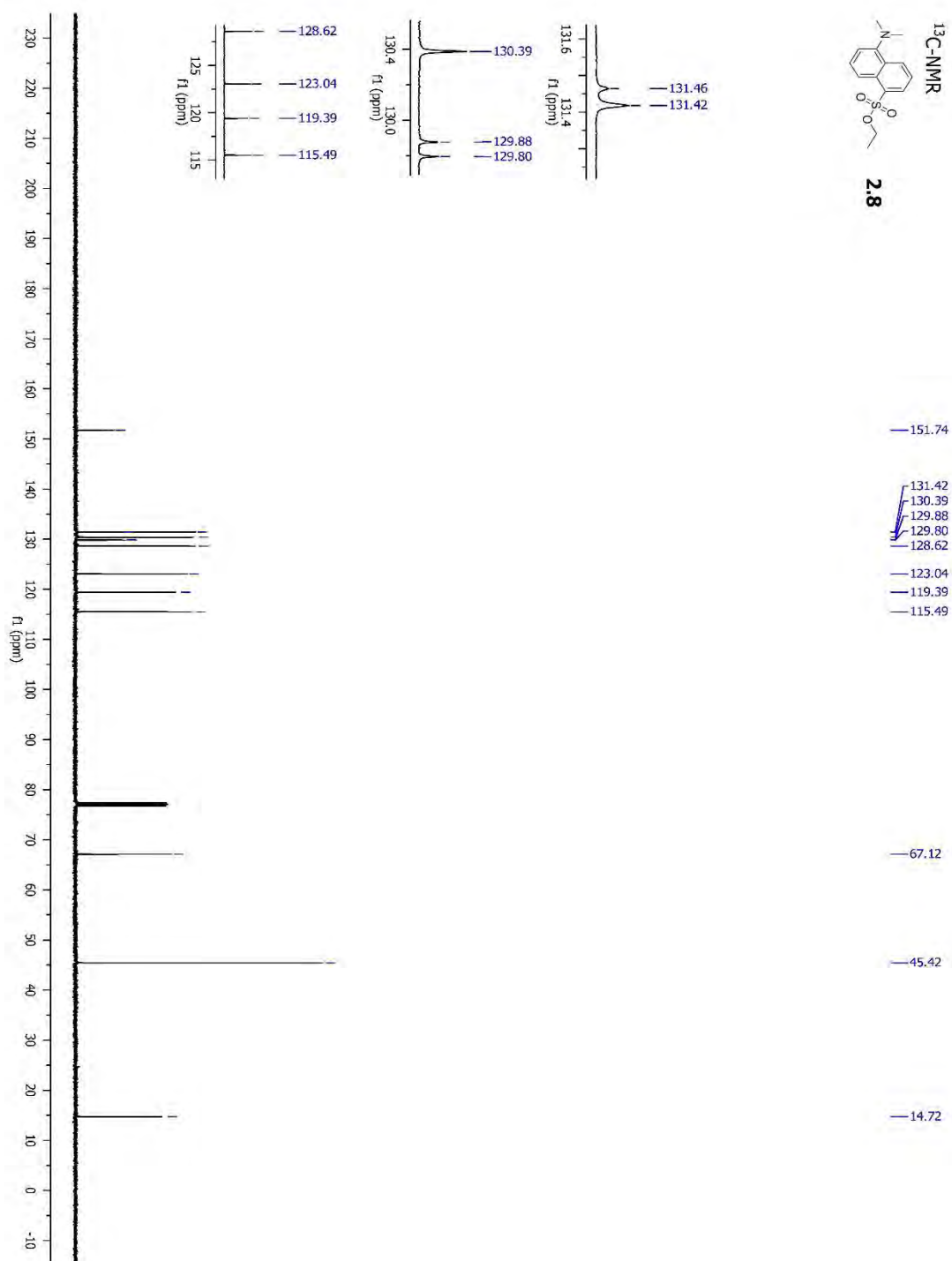
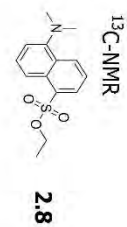
45.42

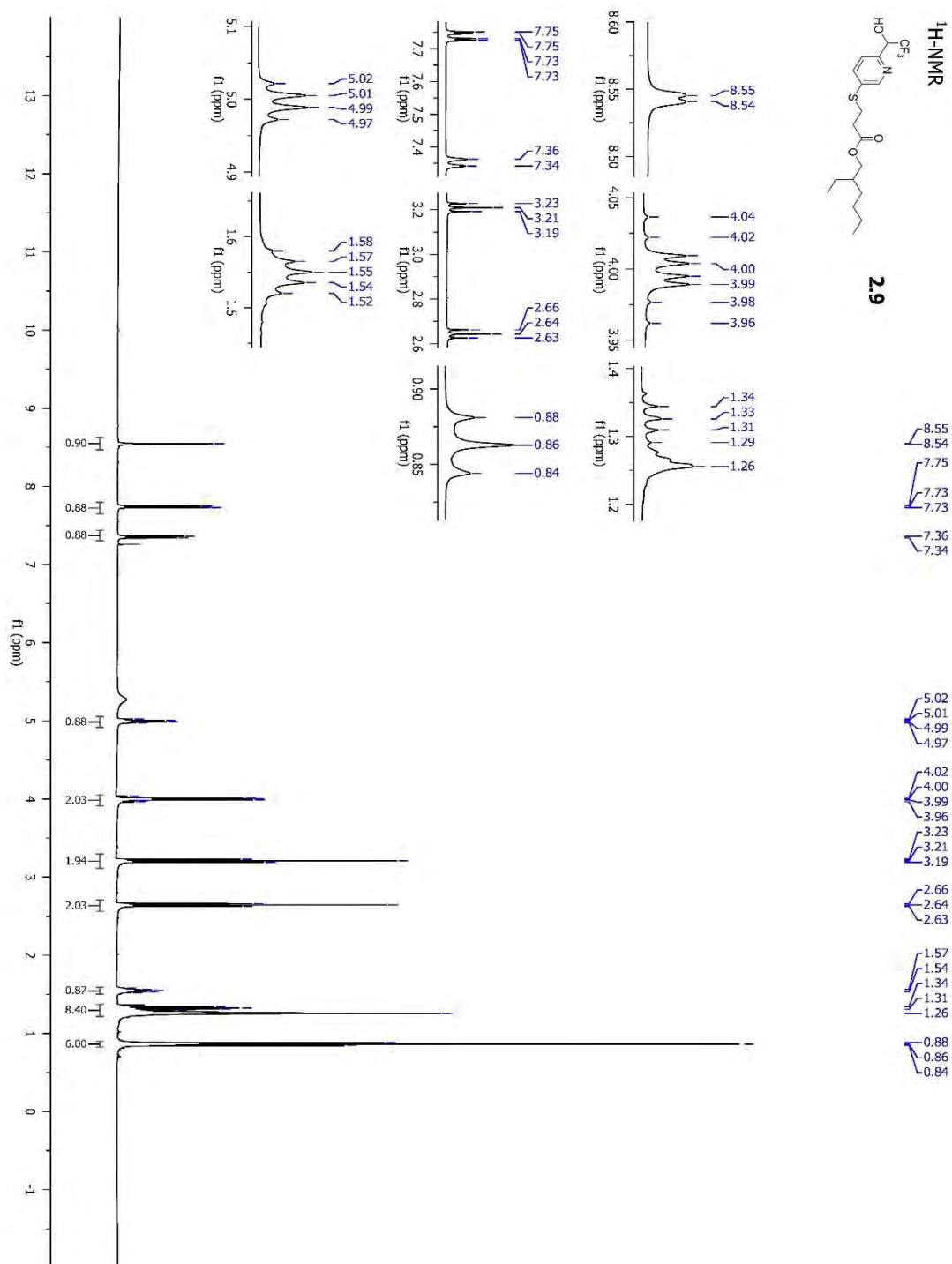


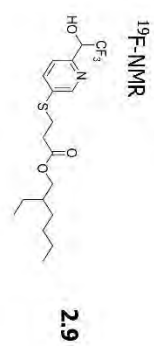


— 2.88

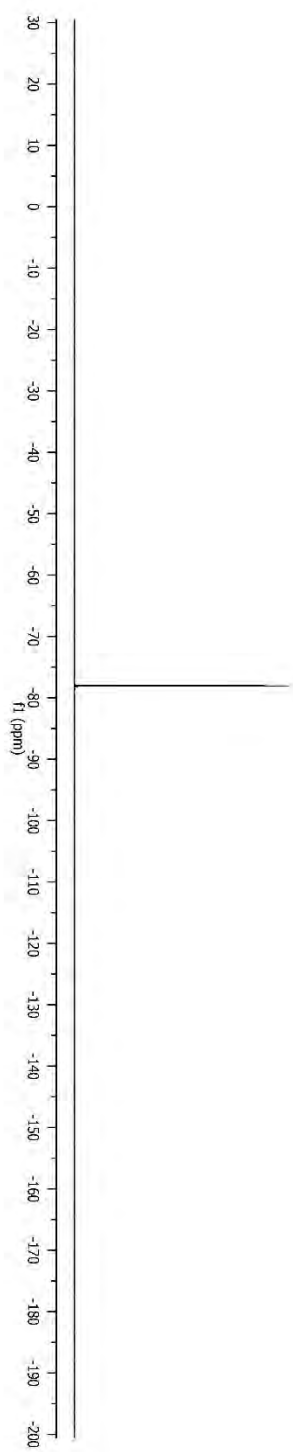
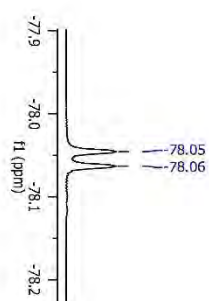


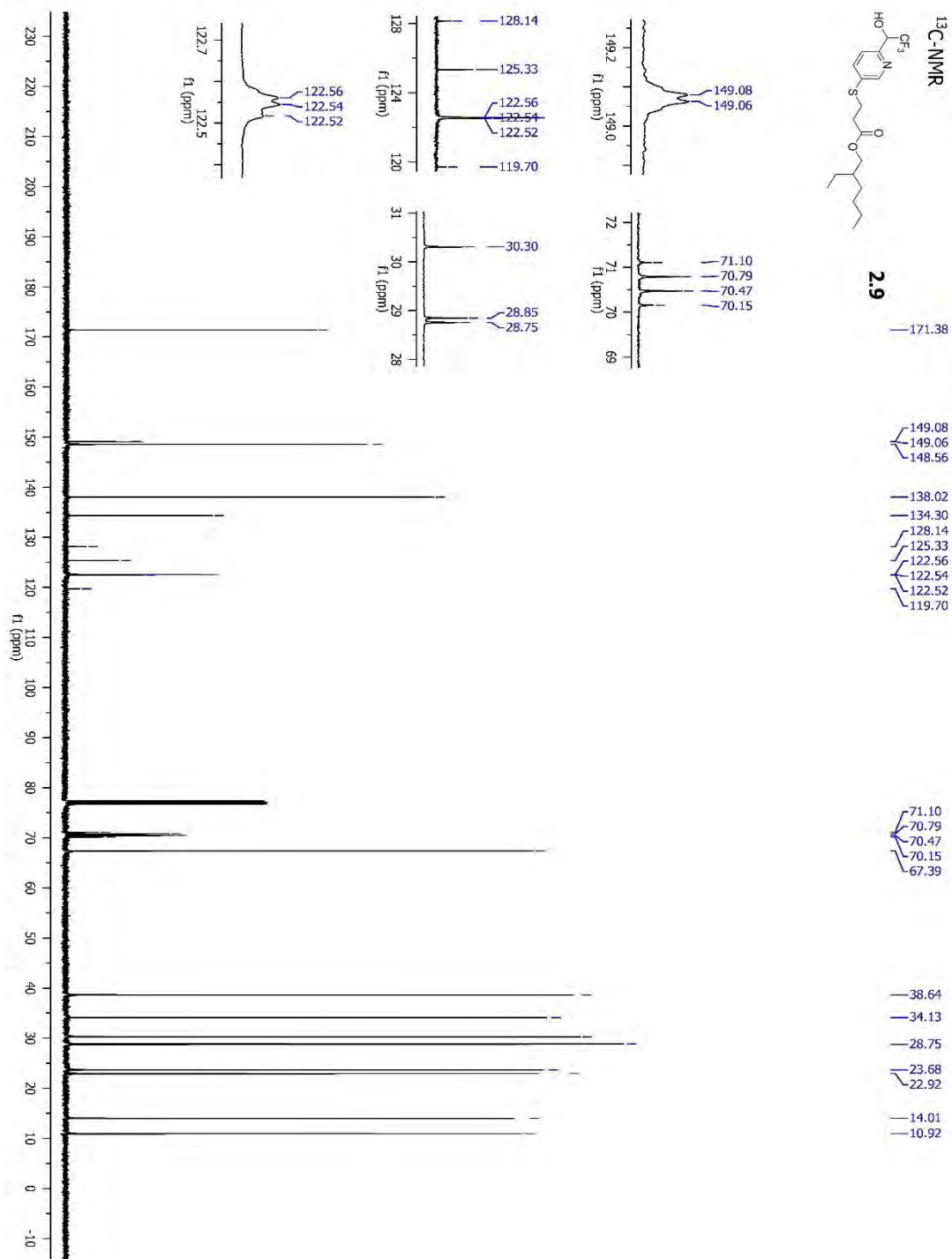
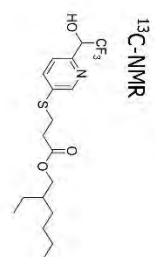


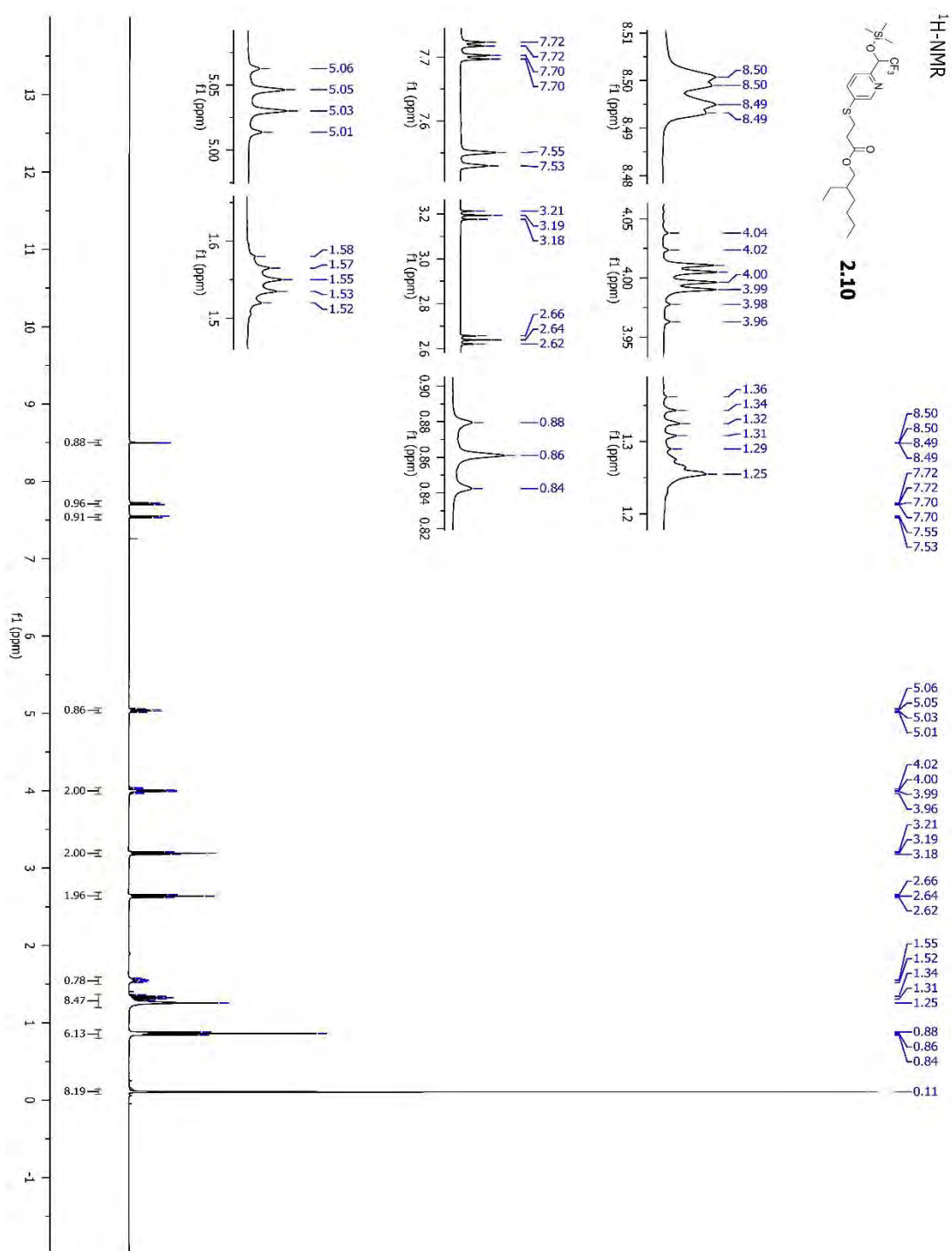


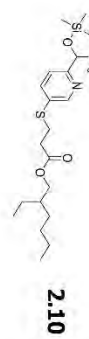


-78.05
-78.06

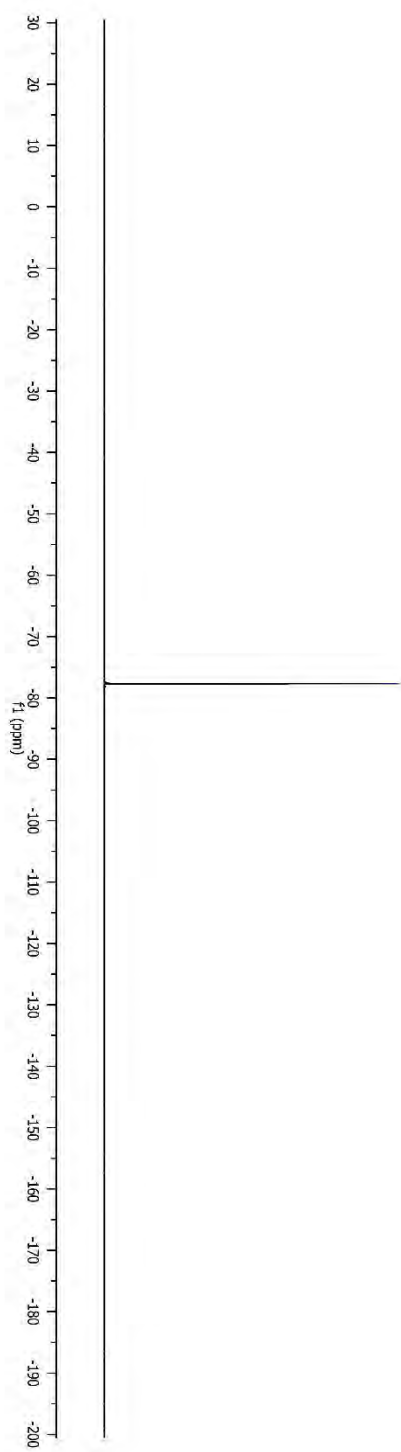
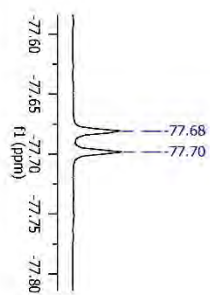


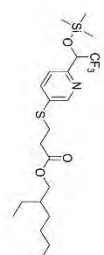




¹⁹F-NMR

-77.68
-77.70



¹³C-NMR**2.10**

— 171.40

 153.46
 153.45
 — 149.05

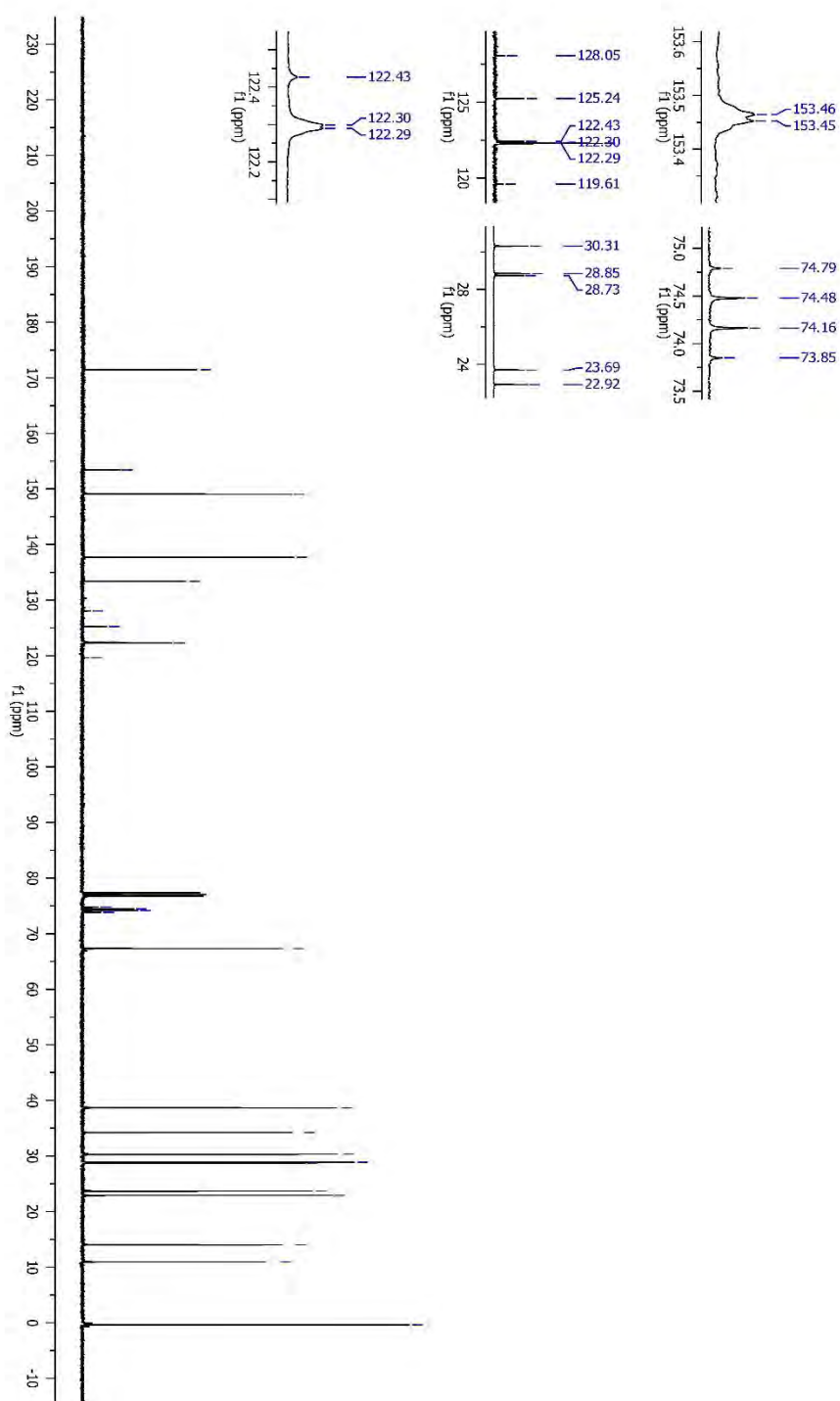
 — 137.68
 — 133.36
 — 128.05
 — 125.24
 — 122.43
 — 122.30
 — 122.29
 — 119.61

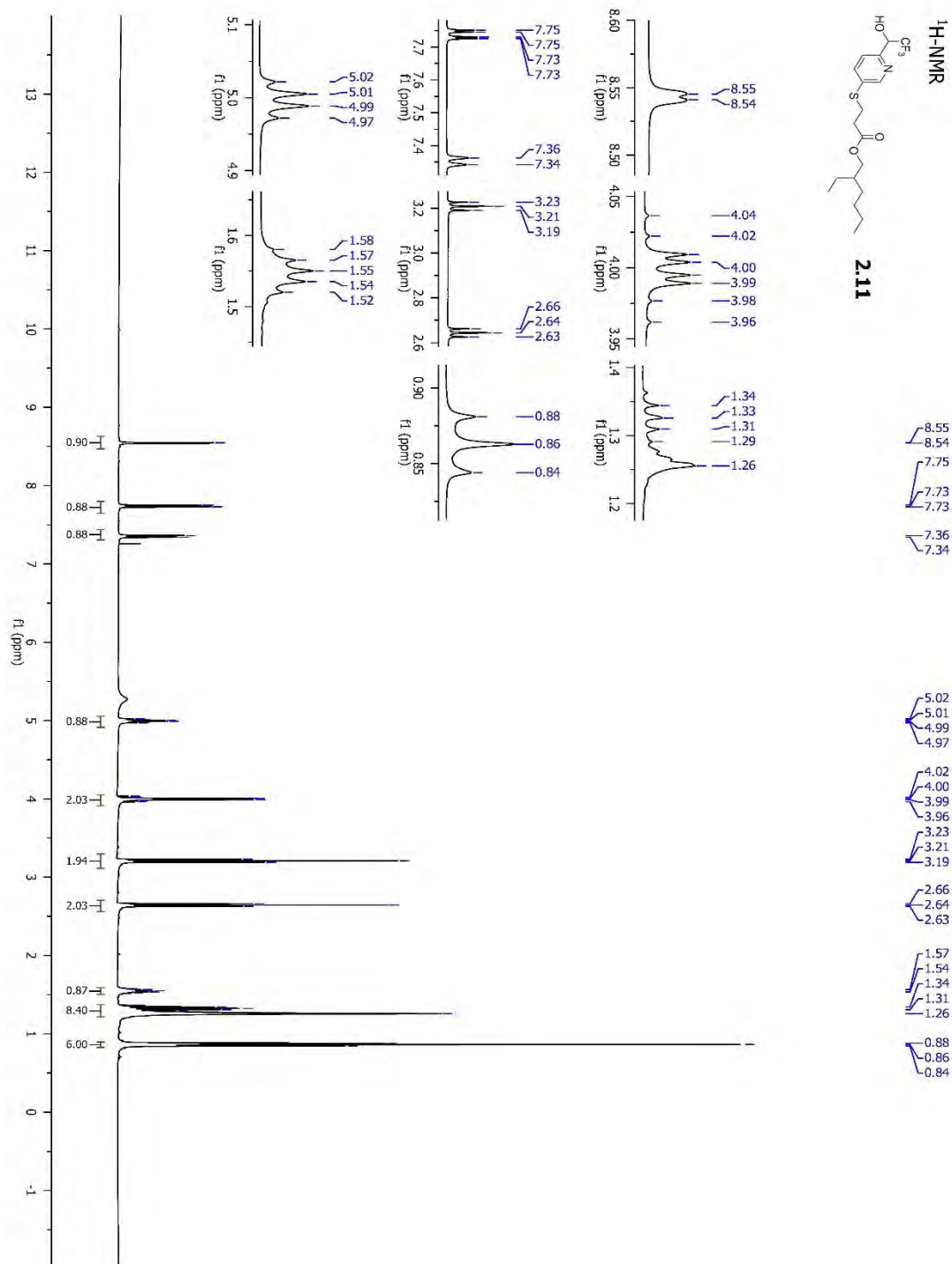
 — 74.79
 — 74.48
 — 74.16
 — 73.85
 — 67.31

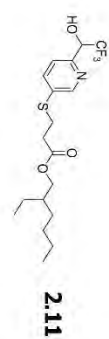
 — 38.65
 — 34.20
 — 28.73
 — 23.69
 — 22.92

 — 14.01
 — 10.93

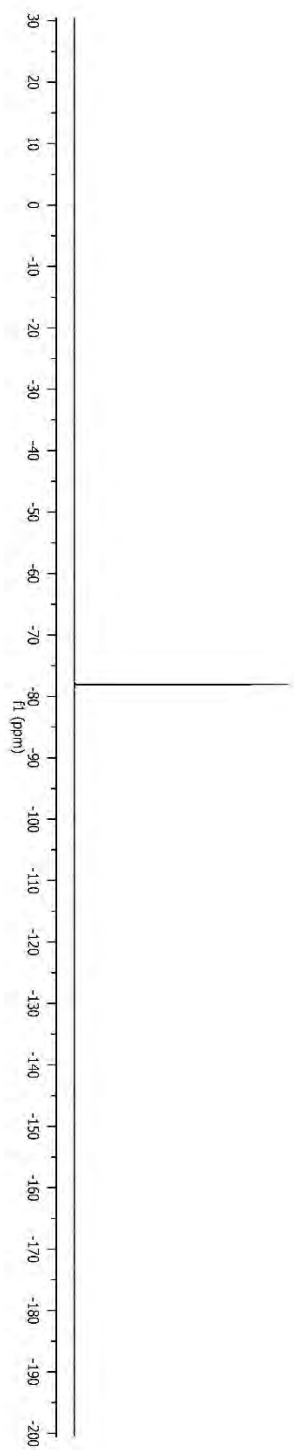
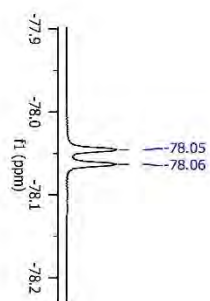
— 0.38

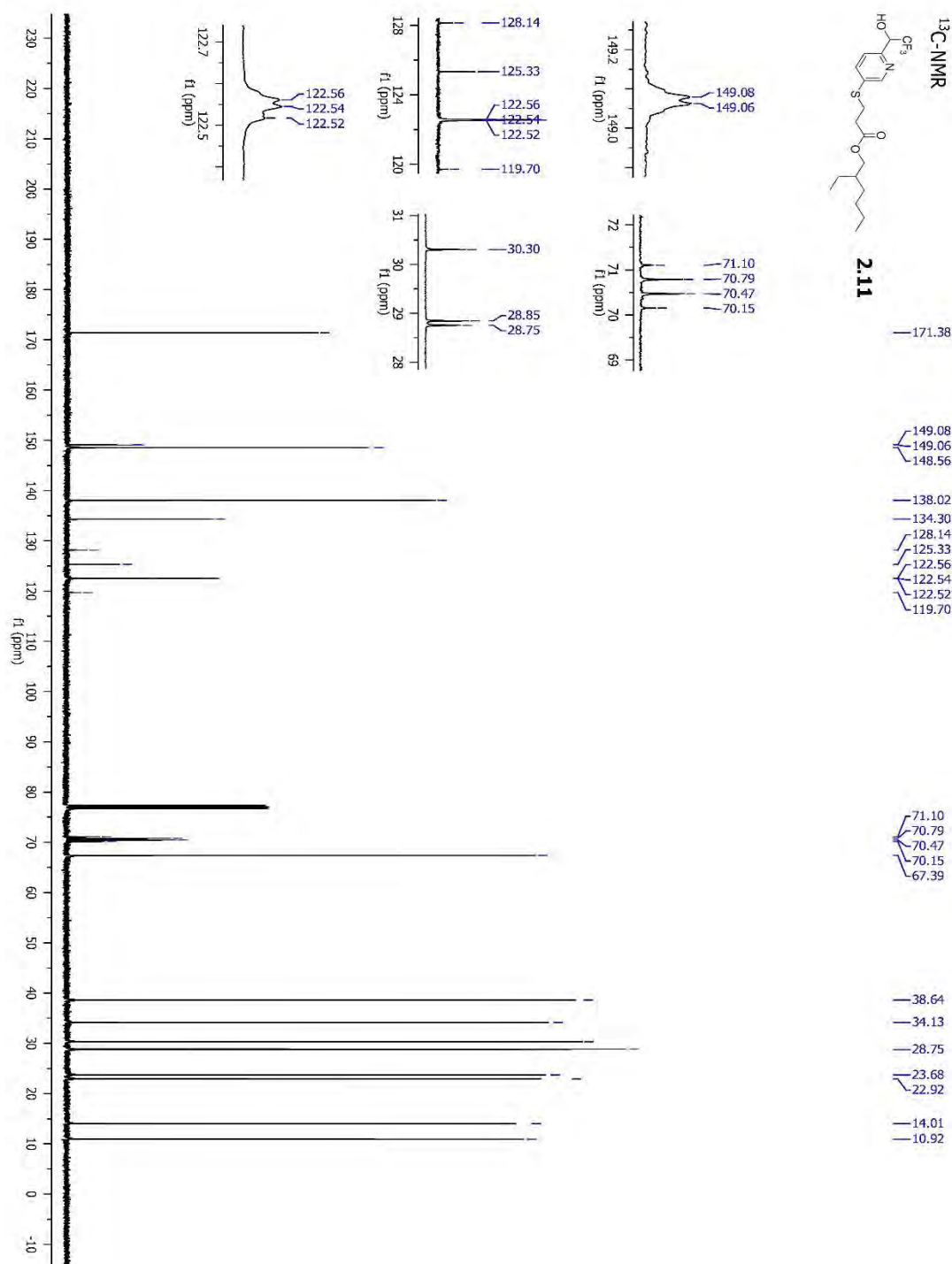
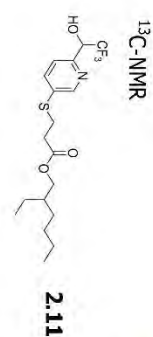


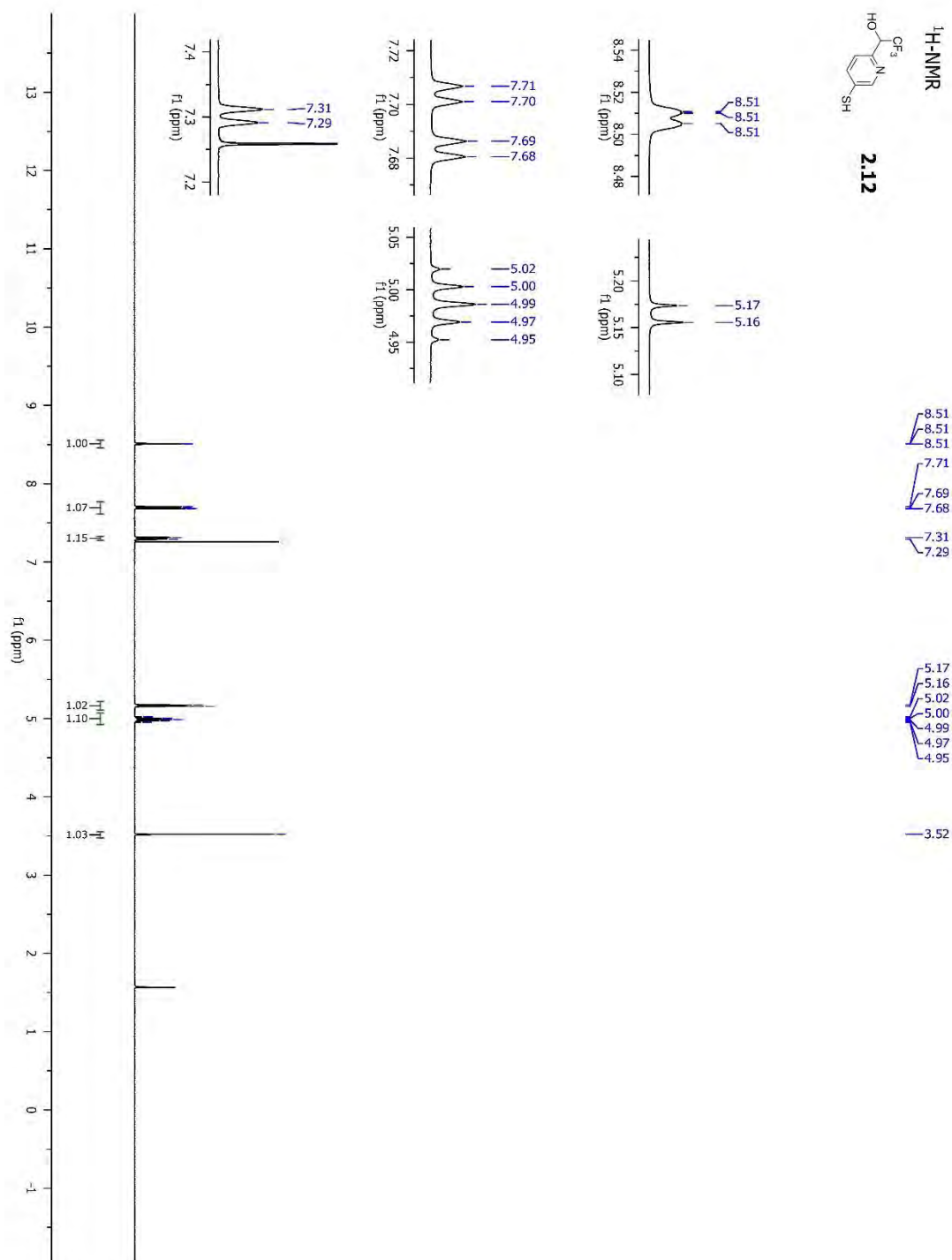
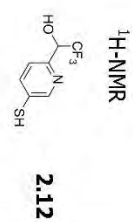


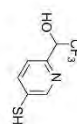
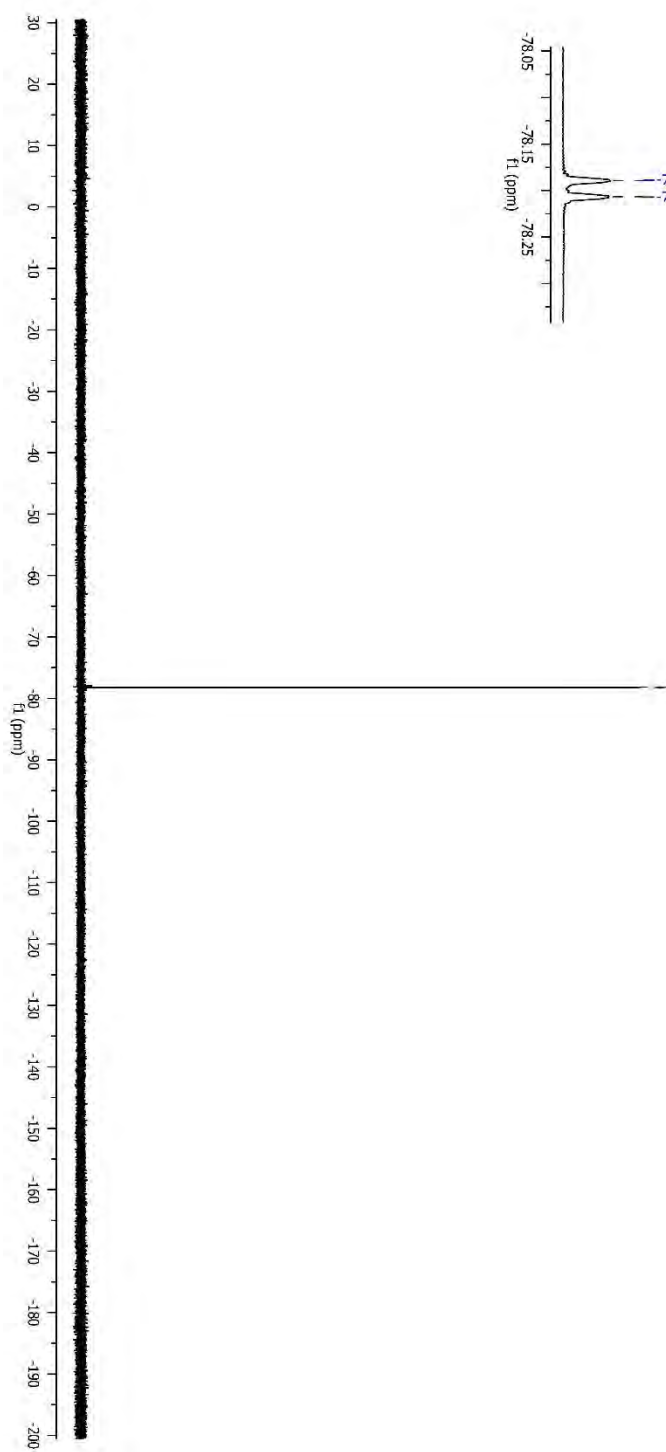
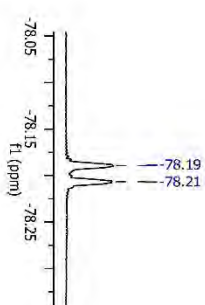
¹⁹F-NMR**2.11**

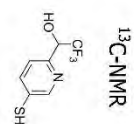
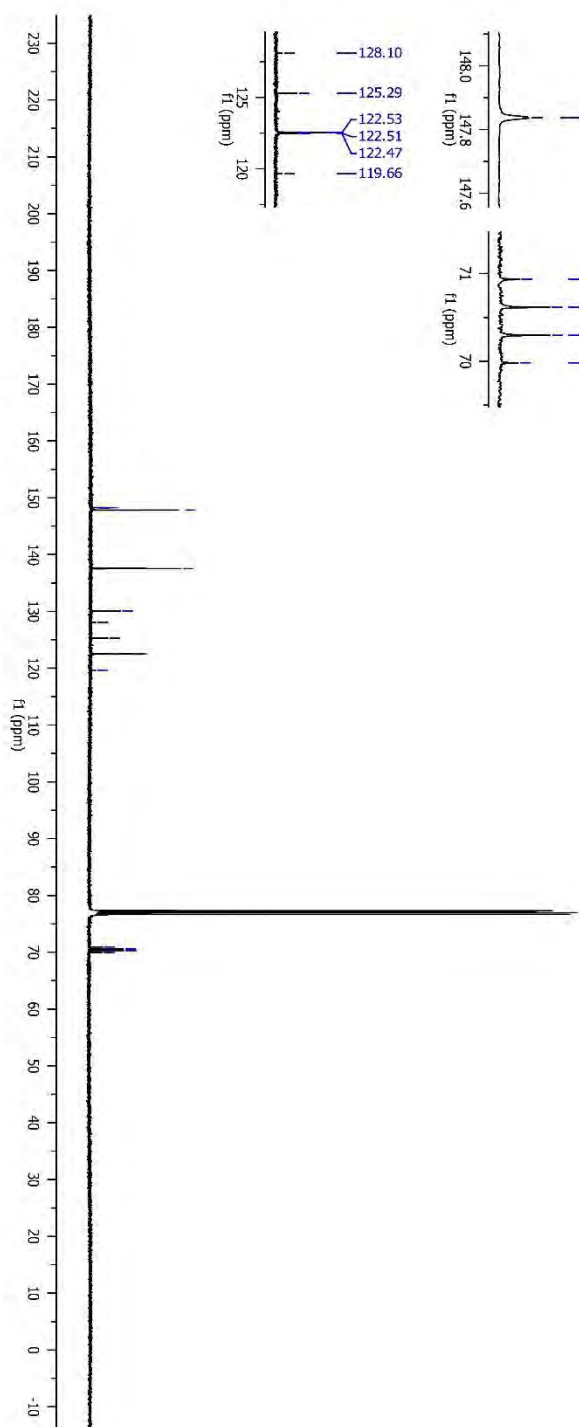
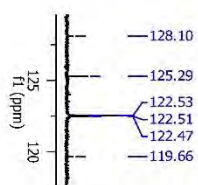
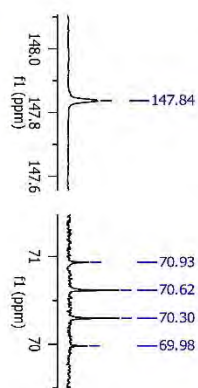
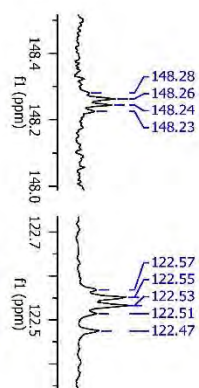
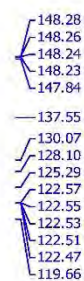

Chemical structure of compound 2.11, showing the trifluoromethyl group (CF₃) and the carboxylic acid group (COOH).

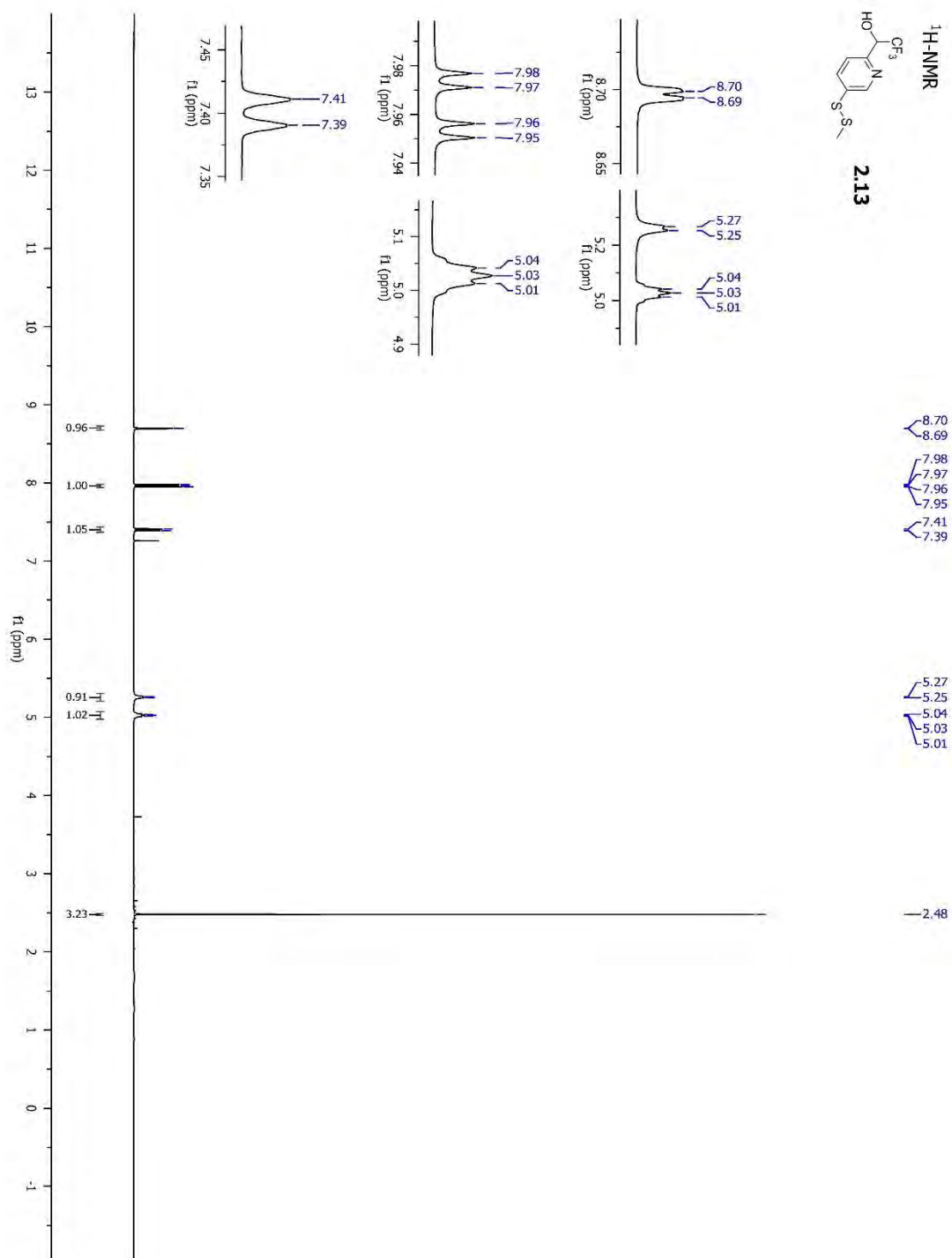
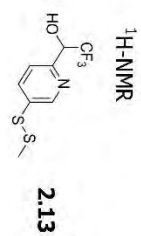


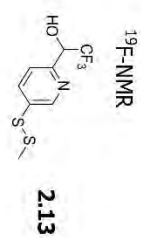




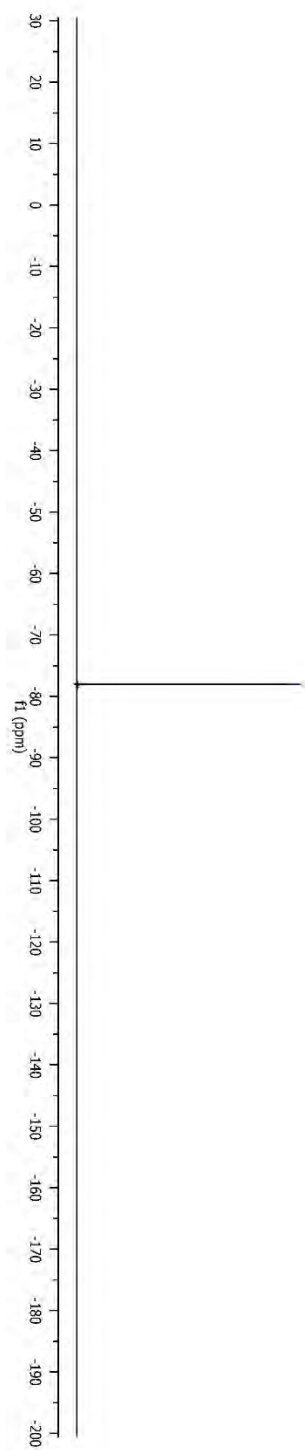
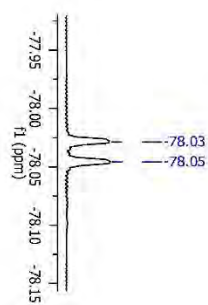
¹⁹F-NMR**2.12**-78.19
-78.21

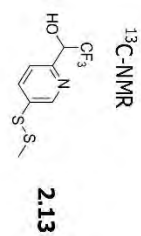
**2.12**





-78.03
-78.05

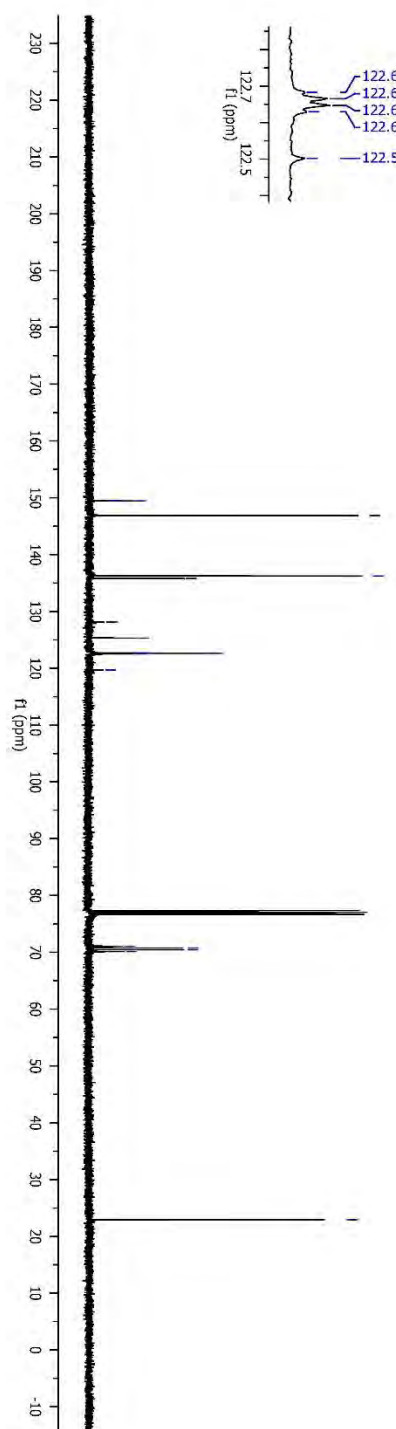
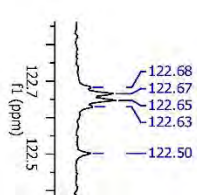
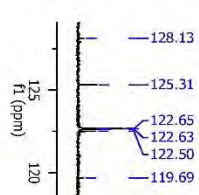
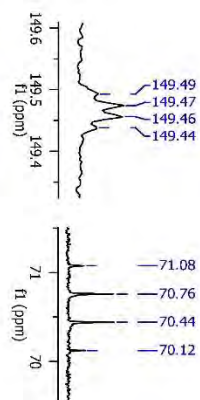


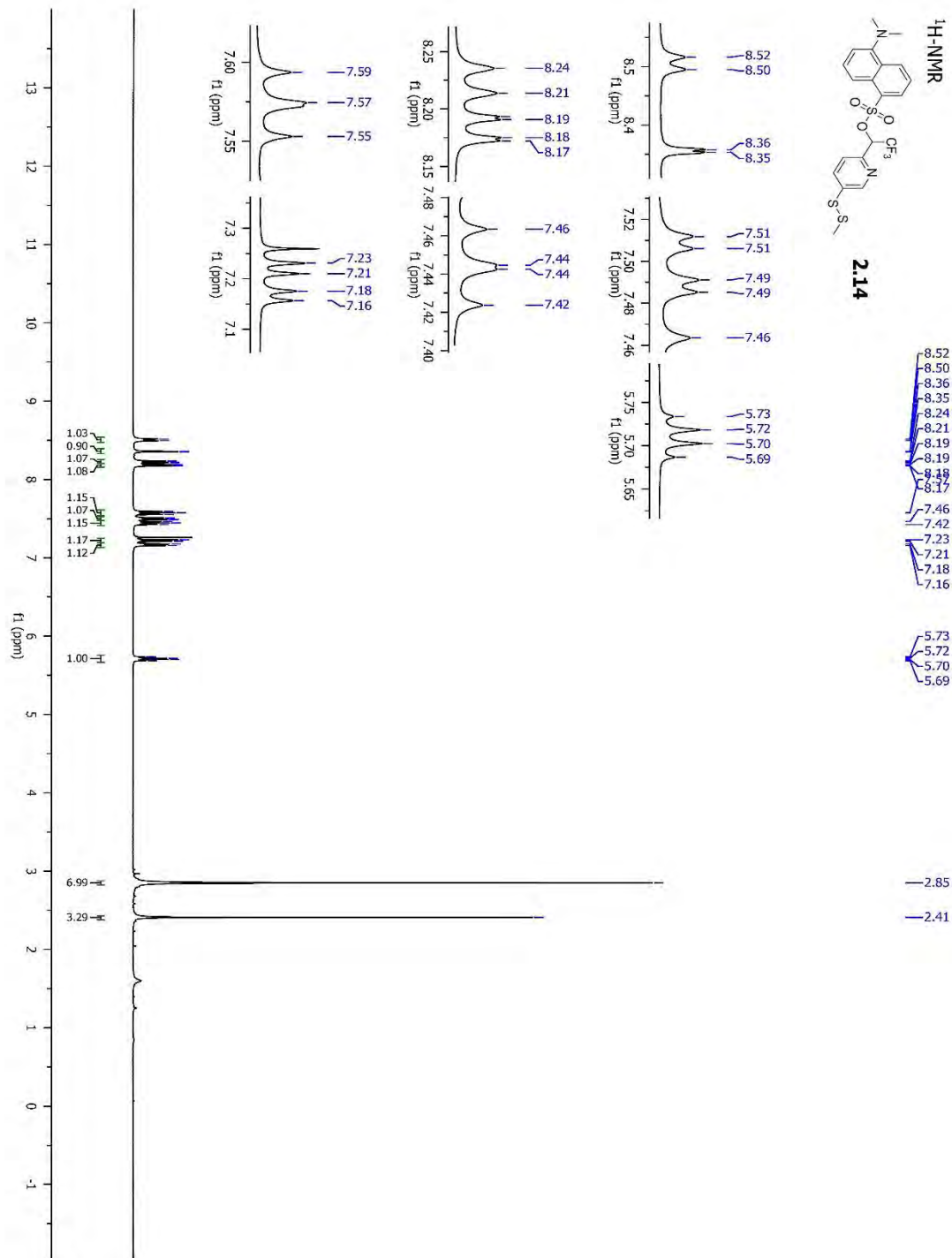


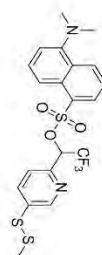
149.49
149.47
149.46
149.44
146.87
136.25
135.80
128.13
125.31
122.68
122.67
122.65
122.63
122.50
119.69

71.08
70.76
70.44
70.12

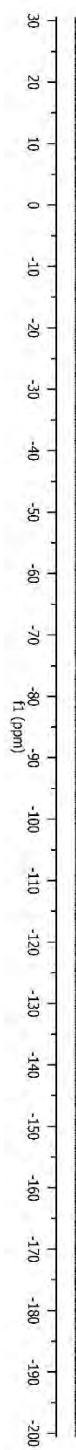
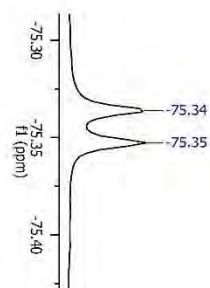
22.91

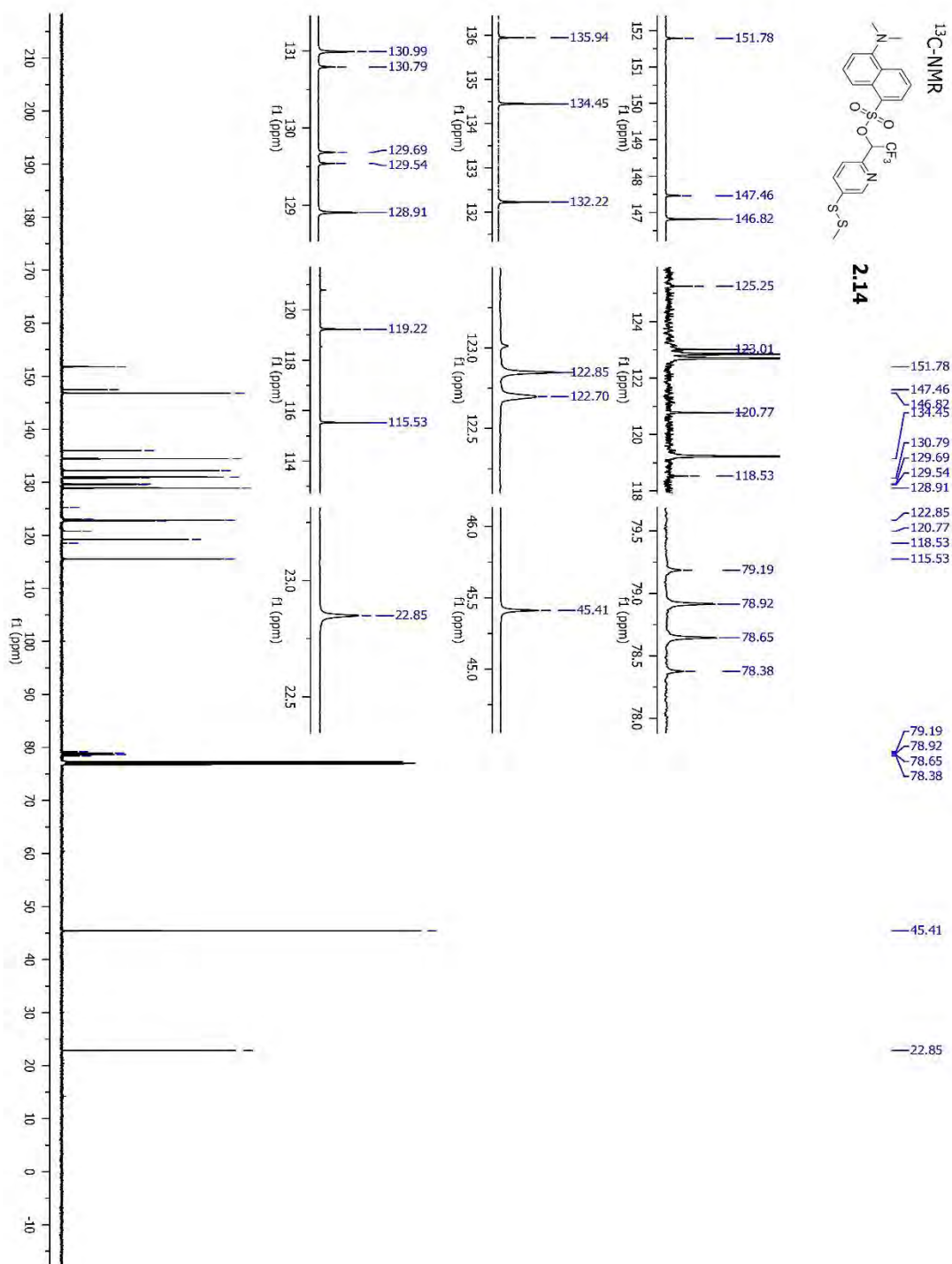
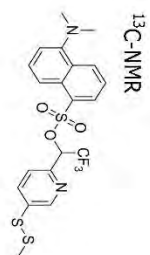


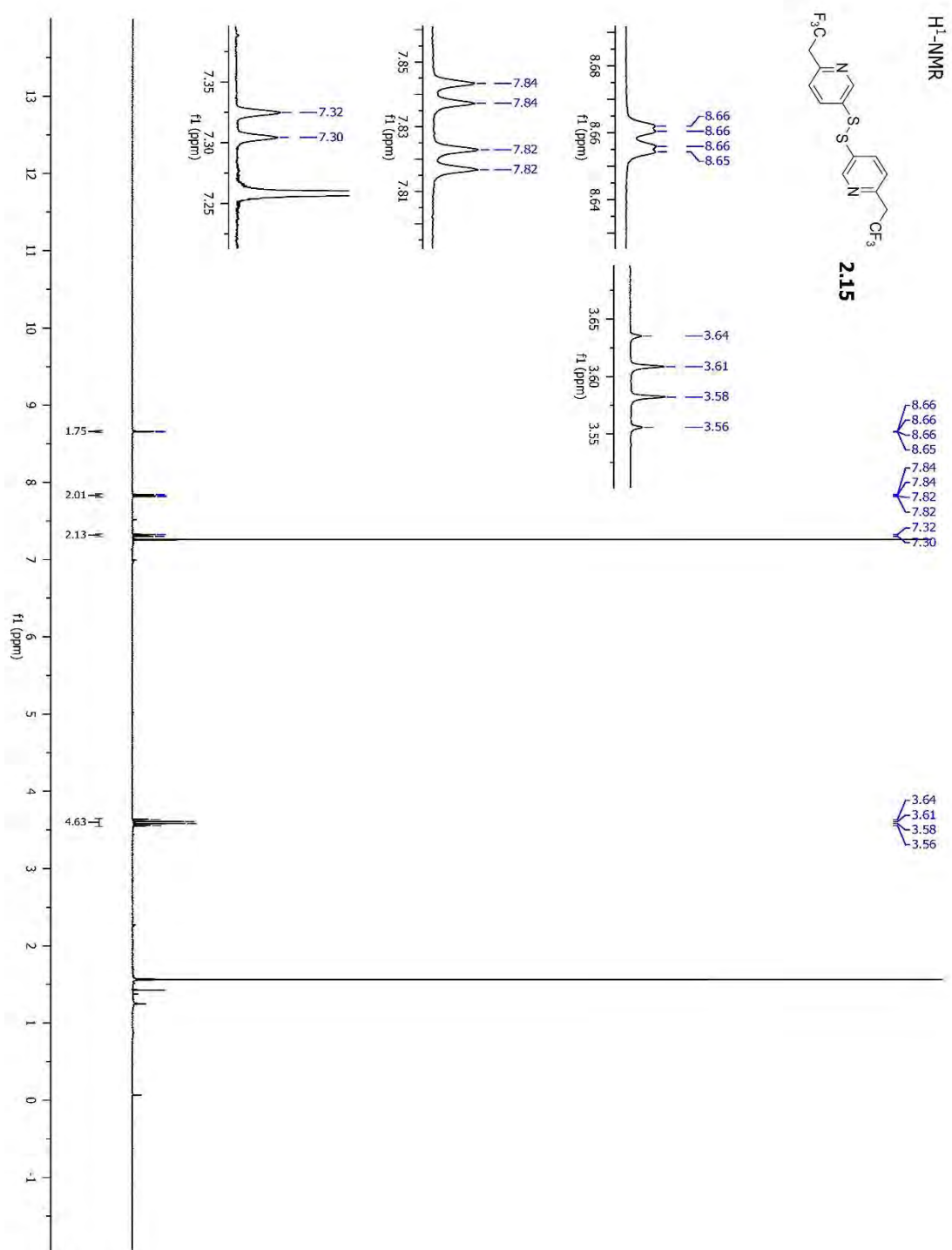


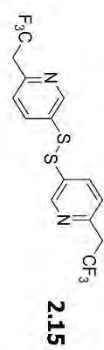
¹⁹F-NMR**2.14**

-75.34
-75.35

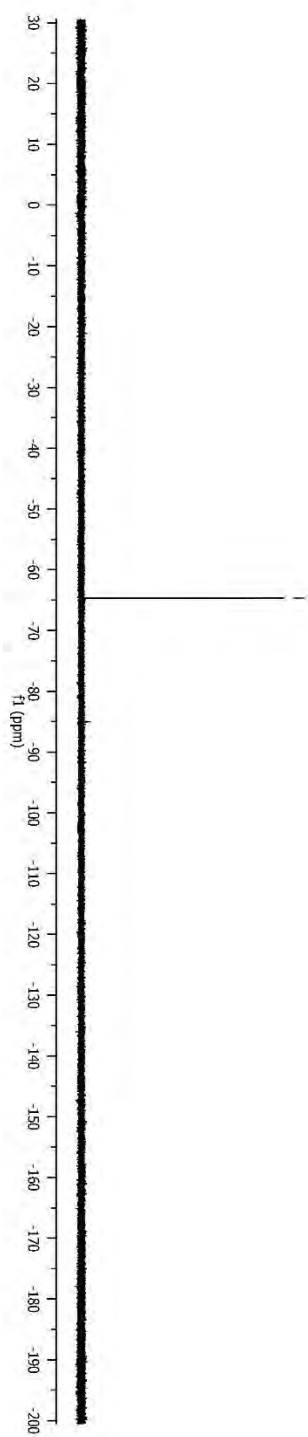
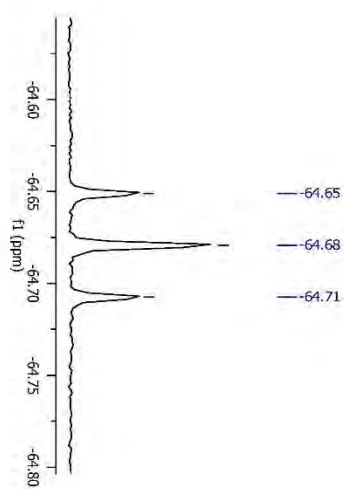


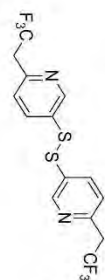
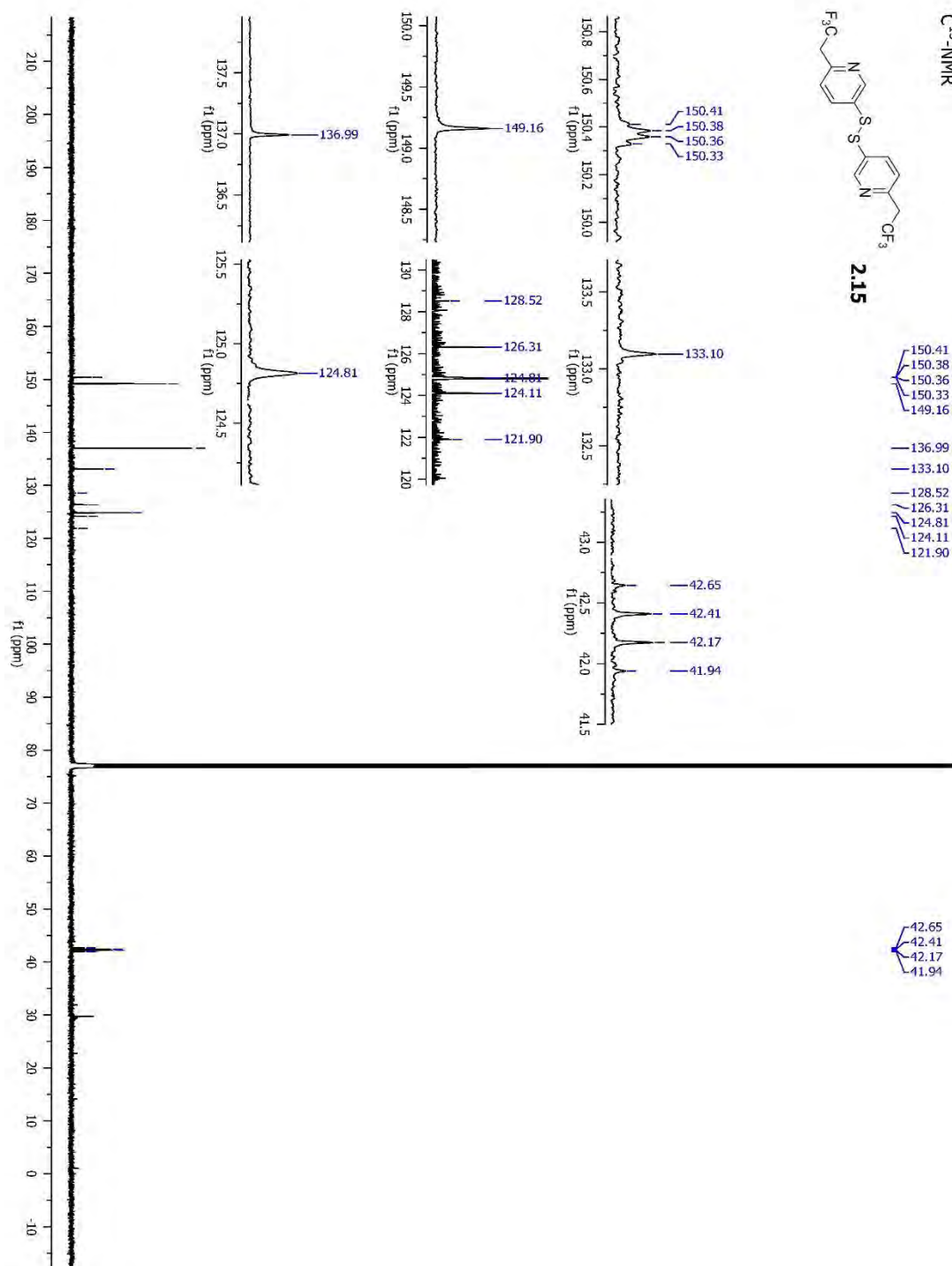




^{19}F -NMR

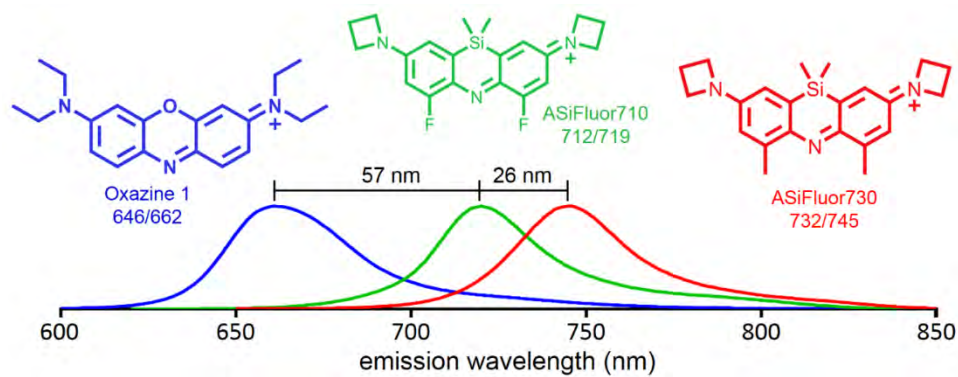
-64.65
-64.68
-64.71



C^{13} -NMR**2.15**

CHAPTER III:

Silicon Substitution in Oxazine Dyes Yields Near-Infrared Azasiline Fluorophores That Absorb and Emit Beyond 700 Nm



Adopted from Choi and Miller⁸⁹

Summary

Near-Infrared (NIR) fluorophores are generally large hydrophobic molecules owing to their extended π -conjugation. Large hydrophobic surfaces decreases aqueous solubility and promote nonspecific binding to proteins. The repertoire of commercial available NIR fluorophore is also largely limited to cyanines, which has low photostability. Thus, smaller and more photostable NIR dyes are desired. Oxygen to silicon substitution (silylation) can dramatically red-shift the excitation and emission wavelengths of rhodamine fluorophores from the orange to the far-red, without significantly increasing the overall size through π -conjugation extension. Here, I describe the design, synthetic approaches, and properties of azasiline fluorophores that resulted from silylation of oxazine dyes.

Introduction

Tissues are most transparent to near-infrared (NIR) light between 650 and 900 nm. Consequently, fluorescent images acquired using NIR imaging probes generally have a higher signal to noise compared to visible-light probes. Moreover, NIR light is poorly absorbed by endogenous chromophores, which minimizes phototoxicity.²⁷ While the benefits of NIR fluorophores have long been recognized, the selection of NIR fluorophores remains limited, especially ones with high aqueous solubility and stability.^{31,32}

Most NIR fluorophores are massive hydrophobic molecules. In fact, the quantum yields of some NIR fluorophores were not reported in water. Presumably, these dyes have low aqueous quantum yield due to aggregation.³² Sulfonation can hugely enhance aqueous solubility; but, amongst the popular NIR fluorophore scaffolds discussed in **CHAPTER I**, only sulfonated BODIPYs and cyanines have been reported.^{34,44}

Sulfonated NIR BODIPYs are unstable in water.^{43,44} Most sulfonated cyanines have improved aqueous solubility and higher quantum yields.³⁴ This fact, along with their straightforward synthesis, has made cyanine derivatives the most commercially available NIR fluorophore. Although popular, cyanines have poor photostability, and larger cyanines, such as ICG are still largely insoluble in water. Despite carrying two sulfonates, the maximum solubility of ICG in PBS and water are 1 and 5 mg/ml, respectively.^{90–92} Taken together, the shortcomings of current NIR fluorophores highlight the urgency to develop novel compact NIR fluorophores with high photostability.

The excitation and emission wavelengths of a fluorophore can be red-shifted through the expansion of the π -conjugation.^{34,93} For example, the excitation and emission wavelengths of cyanines are red-shifted by approximately 100 nm for each additional methine group (double bond) (**Figure 3.1**). However, expansion of the π -conjugation increases hydrophobicity and in turn, leads to aggregation.

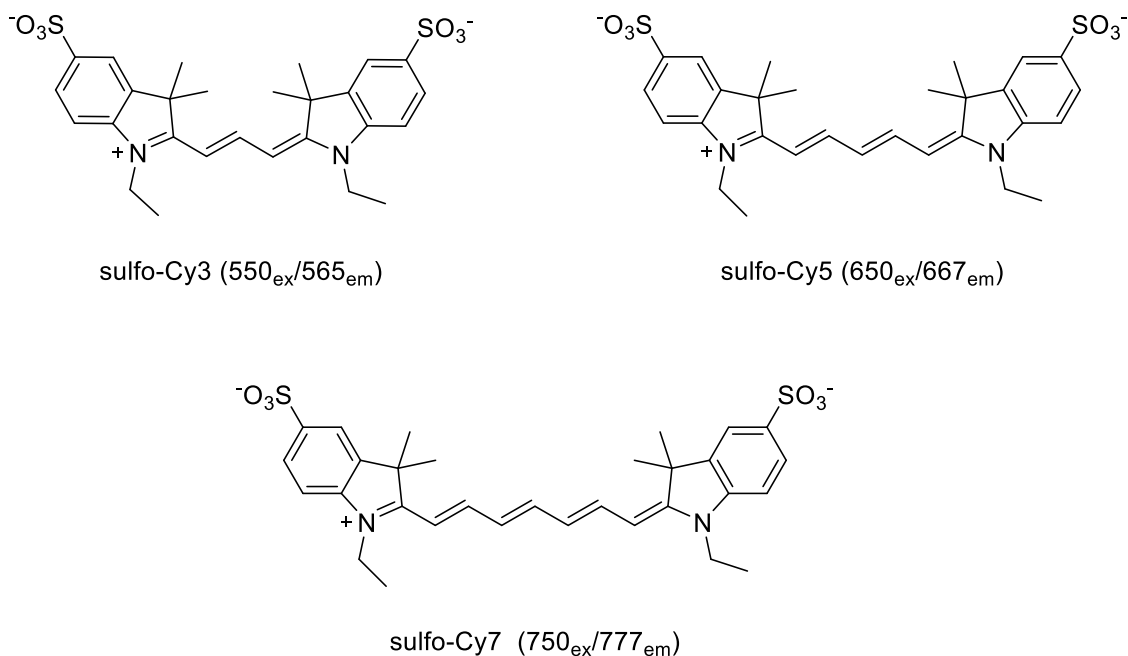


Figure 3.1: Expansion of π -conjugation red-shifts the fluorescence of cyanines. Each additional methine groups red-shifts both excitation and emission by approximately 100 nm. The name and optical properties are listed below each compound.

A more recent method for red-shifting fluorescence is oxygen to silicon substitution (silylation). The first reported silylated xanthene fluorophore is Pyronin Y, which yielded a noteworthy 90 nm bathochromic shift in both excitation and emission wavelengths (**Figure 1.11**). Shortly after the introduction of silylated Pyronin Y (SiP), a tsunami of silylated-rhodamines (SiR) and other substituted rhodamines emerged (**Figure 1.12**). Currently, the most red-shifted SiR is the SiR720 (720_{ex}/740_{em}), which absorbs and emits ~170 nm longer than tetramethylrhodamine (TMR) (**Figure 3.2**).^{47,57}

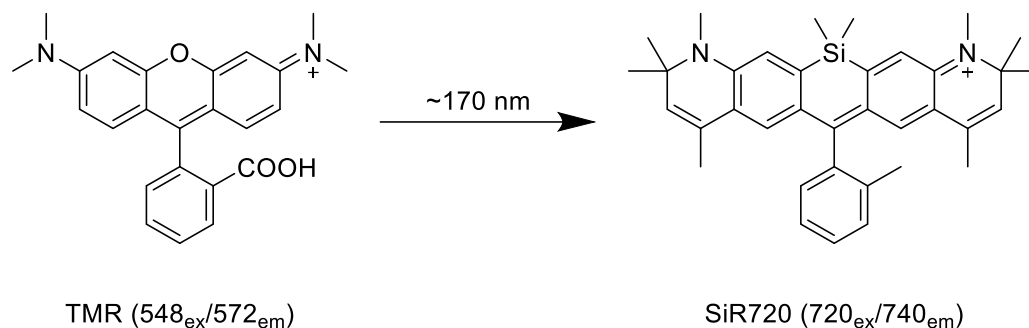


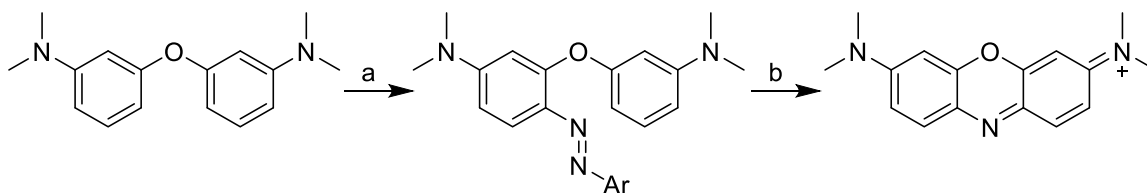
Figure 3.2: Excitation and emission wavelengths of SiR720 are red-shifted by ~170 nm compared to TMR

Oxygen to silicon substitution has been exclusively investigated in rhodamines. Oxazines are a class of NIR fluorophores that are structurally similar to rhodamines. The typical excitation and emission wavelengths of oxazines are between 640 and 670 nm. Like rhodamines, oxazines are compact and highly photostable, which are the two key attributes for an excellent imaging probe. Further, water-soluble, sulfonated oxazines have been reported.^{49,94} On the basis of structural similarities between rhodamines and oxazines, I hypothesized that silylation of oxazines would yield highly photostable azasiline fluorophores that absorb and emit over 700 nm. **(Figure 1.14).**

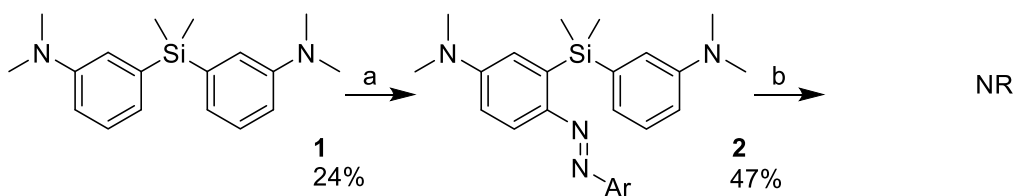
Results and Discussion

The synthesis of oxazines are well documented.^{49,94–96} One method to access oxazines is by reacting aryl ethers with a nitrogen donor, such as 4-nitrobenzenediazonium tetrafluoroborate. Subsequent acid-mediated cyclization readily yields the oxazine fluorophore.⁹⁴ I first attempted to access azasilines with a synthetic route analogous to the one use for oxazines (**Scheme 3.1**).

Oxazine synthesis:



Attempted azasiline synthesis:

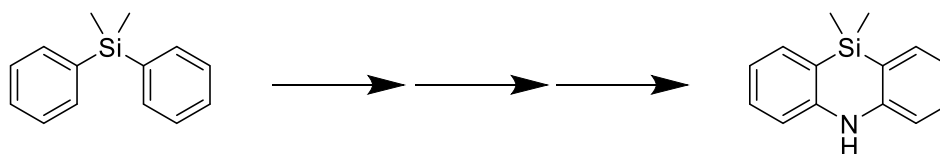


Scheme 3.1: Modeling azasiline synthesis after oxazines. Reported synthesis for oxazines (top) and analogous synthesis scheme for azasilines (bottom). Reaction conditions: (a) $\text{N}_2\text{PhNO}_2 \cdot \text{BF}_4$, aq. 2M HCl, MeOH, 0 °C; (b) aq. 2M HCl, EtOH, 80 °C. NR = No Reaction.

To access the azasiline, commercially available 3-Bromo-N,N-dimethylaniline was first treated with *n*-BuLi and then dichlorodimethylsilane (SiMe_2Cl_2) to form the aryl silane **3.1**. A diazo-nitrobenzene moiety was installed to yield **3.2**. Unfortunately, acid-mediated cyclization of **3.2** did not proceed to form the cyclized azasiline. The starting material remained unreacted even after overnight treatment with perchloric acid at 80 °C. Failure to cyclize **3.2** could be due to the increased bond length introduced by silicon and/or the lower nucleophilicity of silanes.

Although azasilines have not been utilized as NIR imaging probes, unsubstituted azasilines were previously reported as light emitters in OLED panels.^{97,98} Interestingly, the reported synthetic steps to access azasilines were in the reverse order as our initial scheme. Cyclization of those azasilines was achieved via silylation instead of the carbon-nitrogen bond formation (**Figure 3.3**).

Our initial scheme:



Reported scheme:

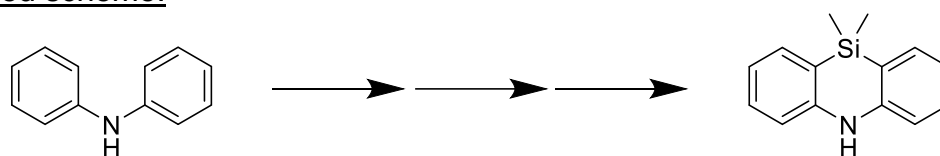
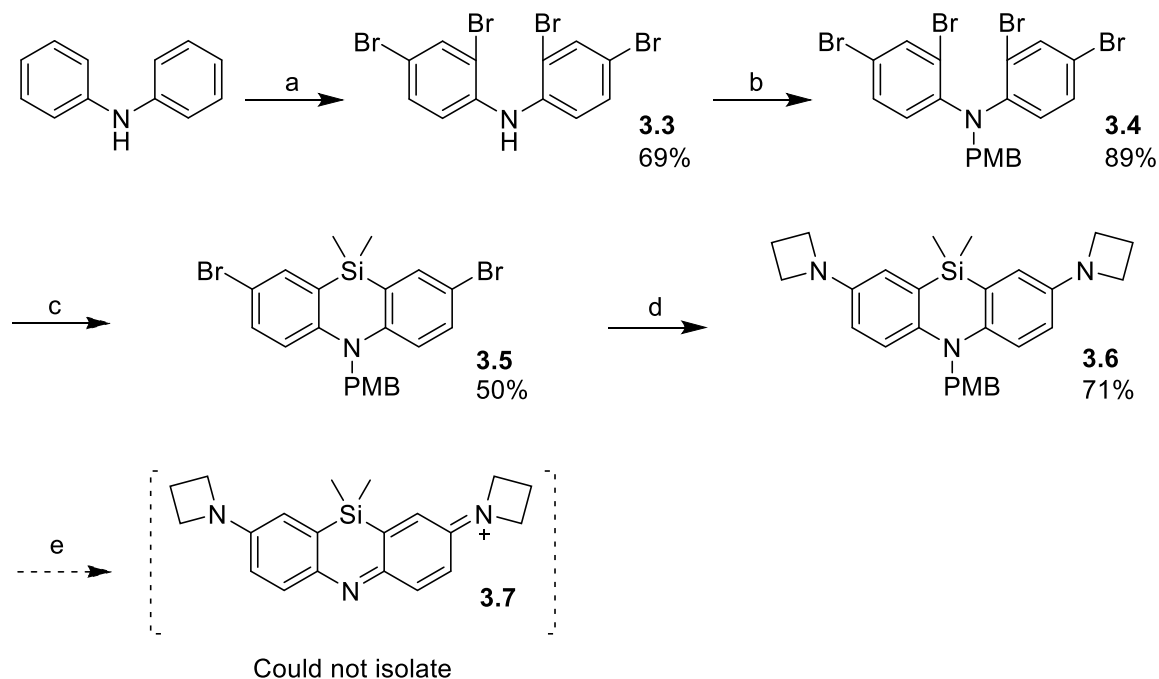


Figure 3.3: Possible approaches for accessing azasilines. Azasilines could be accessed starting from silanes and cyclized by forming the carbon-nitrogen bond (a) or starting from diphenylamine and cyclized via silylation (b).

In our revised scheme, diphenylamine was first tetrabrominated using Br₂ in acetic acid to yield **3.3**. Then nitrogen was protected with *para*-methoxybenzyl chloride (PMB-Cl) to yield **3.4**. Treatment with *n*-BuLi and SiMe₂Cl₂ afforded the cyclized PMB-protected azasilane **3.5**. Using palladium-catalyzed coupling chemistry, two azetidine groups, which were shown to increase quantum yield, were installed to yield **3.6**.⁴⁷ TFA treatment of **3.6** generated a more hydrophobic compound as observed on TLC, which was consistent with PMB deprotection. However, the product quickly decomposed from a bright yellow to a greenish-brown compound after solvent removal. One-pot PMB removal and oxidation of **3.6** with I₂ produced a compound with an absorption maxima of 730 nm. However, the putative product **3.7** isolated with HPLC again degraded after solvent removal possibly to yield a polymeric product that was insoluble in acetone, ethyl acetate, chloroform, DMSO, and water.

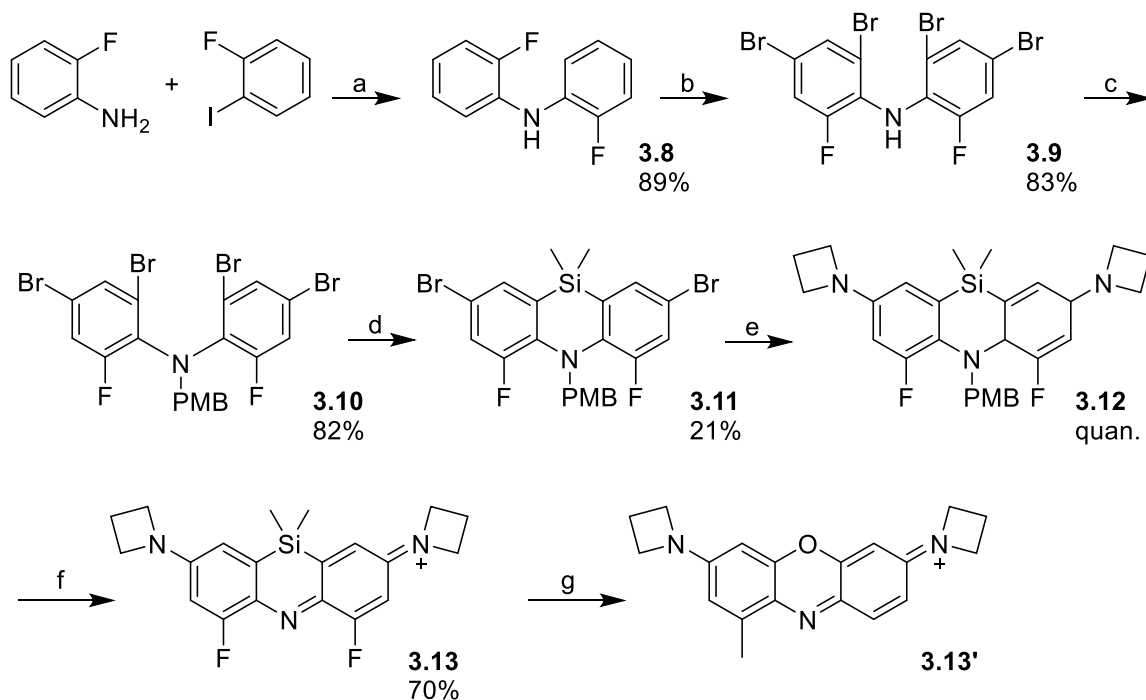


Scheme 3.2: Attempted synthesis of an azetidenyl-azasiline. Reaction conditions: (a) NBS, acetone, 0 °C, (b) NaH, PMB-Cl, DMF, RT. (c) *n*-BuLi, SiMe₂Cl₂, Et₂O -78 °C to RT. (d) azetidine, Pd₂(dba)₃, BINAP, NaOtBu, toluene, 110 °C. (e) I₂, MeOH, RT.

Despite the instability of the azasiline, the long absorption wavelength of the putative product reinforced our commitment to developing NIR azasiline fluorophores. Next, I tested whether the azasiline could be stabilized by altering the sterics and/ or electronics of the molecule. I designed two azasiline derivatives. The first contained inductively deactivating, but π -donating fluorine groups (**3.13**) and the second contained bulkier inductively donating methyl groups (**3.18**).

To access the difluoro-azasiline (**3.13**), palladium-catalyzed coupling was performed between commercially available 2-fluoroaniline and 1-bromo-2-fluorobenzene to yield the difluoro-diphenylamine **3.8**. Tetrabromination was achieved with Br₂ and acetic acid to yield **3.9**. The nitrogen was protected with PMB to yield **3.10**. Treatment with *n*-BuLi and SiMe₂Cl₂ afforded the cyclized dye precursor **3.11**. Using palladium-catalyzed coupling, two azetidines were installed to yield the *leuco*-dye **3.12**. One-pot PMB deprotection and oxidation with I₂ gave the final product **3.13** (ASiFluor710). Fortuitously, **3.13** readily oxidized and precipitated out of solution during I₂ treatment. Simple filtering and washing of the precipitant with hexanes and methanol afforded pure product (**Scheme 3.2**).

Encouraged by the successful synthesis of the ASiFluor710, I next determined its photophysical characteristics. In ethanol, the excitation and emission wavelengths of the ASiFluor710 were 712 and 719 nm, respectively, which is approximately 60 nm longer than those of Oxazine 1 (**Figure 3.4**). The quantum yield and extinction coefficient were determined as 0.11 and 60,000 M⁻¹ cm⁻¹, respectively (**Figure 3.5**). Lamentably, ASiFluor710 slowly degraded in PBS. HPLC and LCMS analyses of ASiFluor710 incubated in 50/50 ACN/PBS mixture for 48 hours revealed a degradation product with a peak absorption wavelength of 660 nm and a mass of 306, compared to the parent of 370 (**Figure 3.6 – 3.7**). The degradation product was subsequently isolated and characterized (**Figure 3.6c**). Consistent with the LCMS data, NMR and HRMS analyses revealed the structure of a methylated oxazine **3.13'** without any fluorine groups.



Scheme 3.3: Synthesis of a difluoro-azasiline (ASiFluor710). Reaction conditions: (a) Pd₂(dba)₃, Xantphos, NaOtBu, toluene, 110 °C. (b) AcOH, Br₂, 110 °C. (c) NaH, PMB-Cl, 15-Crown-5, THF, reflux. (d) *n*-BuLi, SiMe₂Cl₂, Et₂O -78 °C to RT. (e) azetidine, Pd₂(dba)₃, BINAP, NaOtBu, toluene, 110 °C. (f) I₂, MeOH, RT, (g) ACN/PBS, 48 hr, RT.

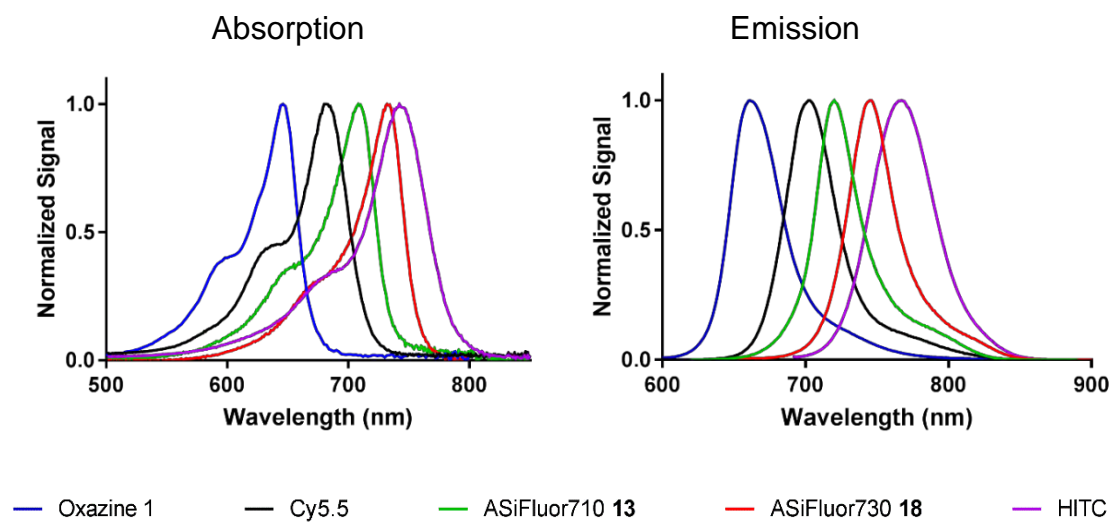
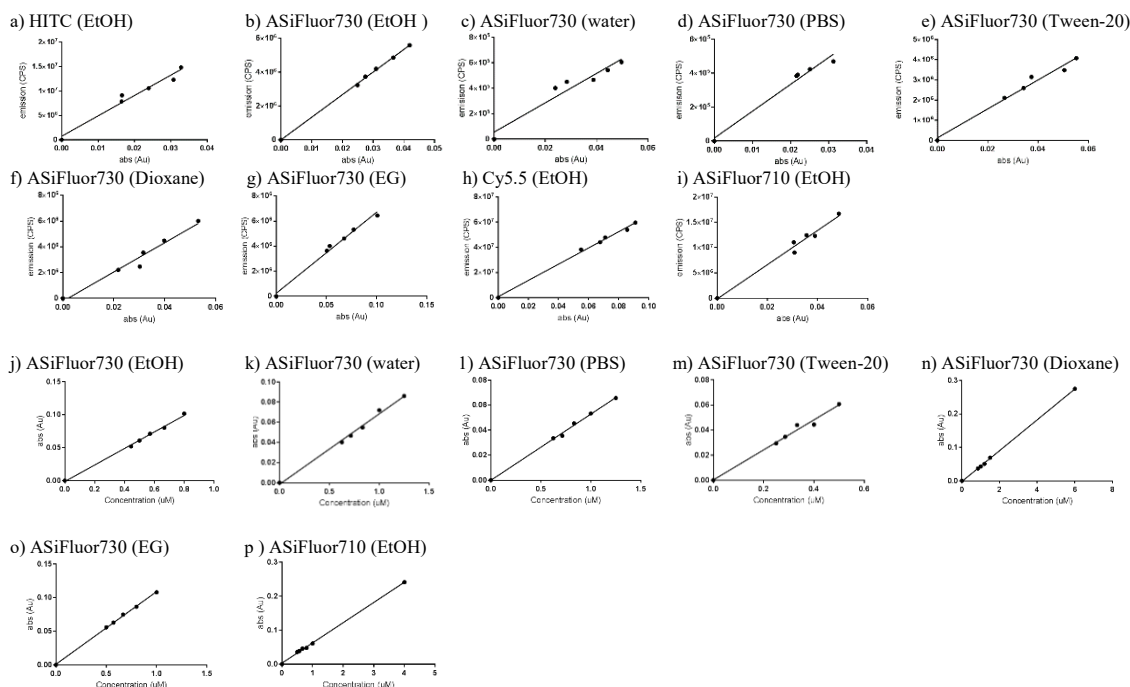


Figure 3.4: Excitation and emission of azasilines in ethanol. Absorbance (top left) and emission (top right) scans of various fluorophores. Peak absorbance and emission wavelengths are listed in the table.



Compound	Solvent	Slope	r^2	ϕ	ϵ ($M^{-1} cm^{-1}$)	r^2	Brightness
ASiFluor730	EtOH	133,500,434	0.9991	0.11	120,601	0.9998	13,817
	water	11,515,019	0.9337	0.01	69,980	0.9949	631
	PBS	15,807,667	0.9750	0.01	52,943	0.9941	549
	0.05% Tween-20	71,799,640	0.9802	0.06	95,030	0.9949	5,592
	ethylene glycol	132,590,701	0.9759	0.13	108,600	0.9999	13,661
	1,4-dioxane	120,154,108	0.9980	0.13	46,270	0.9990	5,942
ASiFluor710	EtOH	338,139,559	0.9788	0.11	59,570	0.9989	6,285
HITC	EtOH	349,572,566	0.9784	0.30			
Cy5.5	EtOH	641,024,853	0.9964	0.20			

Figure 3.5: Measurement of quantum yields and molar extinction coefficients of ASiFluors. Quantum yields (a-i) and molar extinction coefficients (l-p) of ASiFluors. Quantum yields were calculated using equation:

$$\phi_x = \phi_{ST} \left[\frac{(slope)_x}{(slope)_{ST}} \right] \left[\frac{n_x^2}{n_{ST}^2} \right]$$

where slope refers to the slope of absorbance vs. integrated emission and n was the refractive index of solvents if different solvents were used between the standard and sample x. HITC was used for ASiFluor730 and Cy5.5 was used for ASiFluor710 as references. Results are given in the table below the graphs.

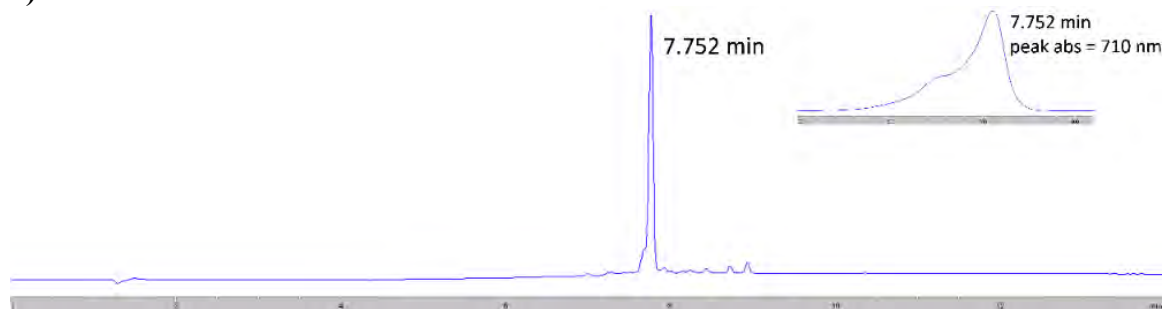
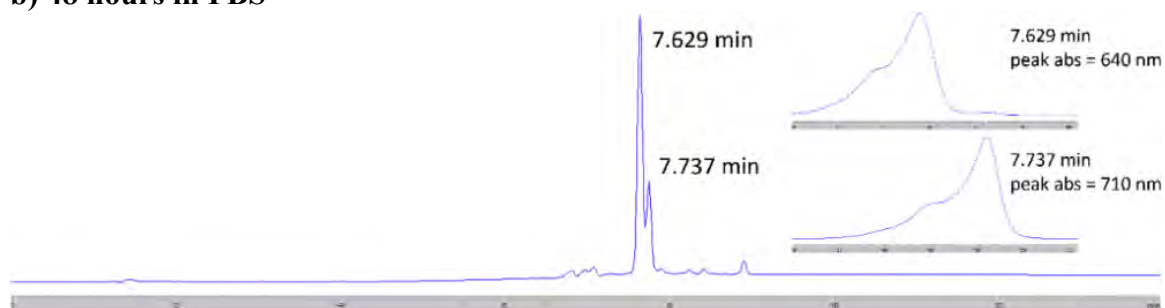
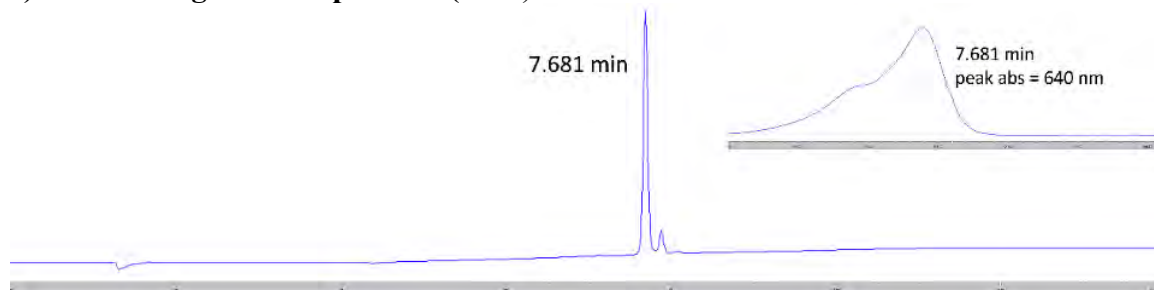
a) No treatment**b) 48 hours in PBS****c) Isolated degradation product (3.13')**

Figure 3.6: HPLC analysis of AsiFluor710 degradation. Before (a) and after (b) 48hr incubation in 50/50 ACN/PBS, and isolated degradation product (c). Each peak's corresponding photodiode array (PDA) spectrum is displayed on the right of each trace. HPLC detection wavelength was set 650 nm.

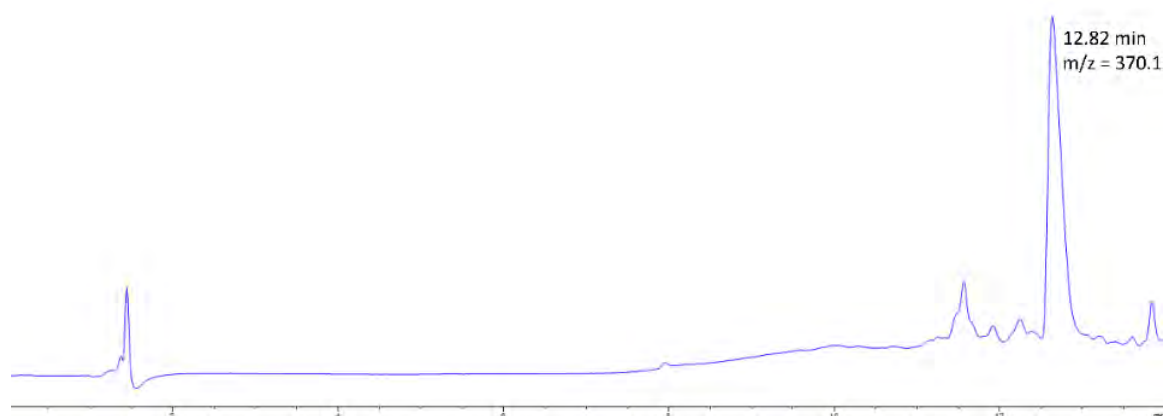
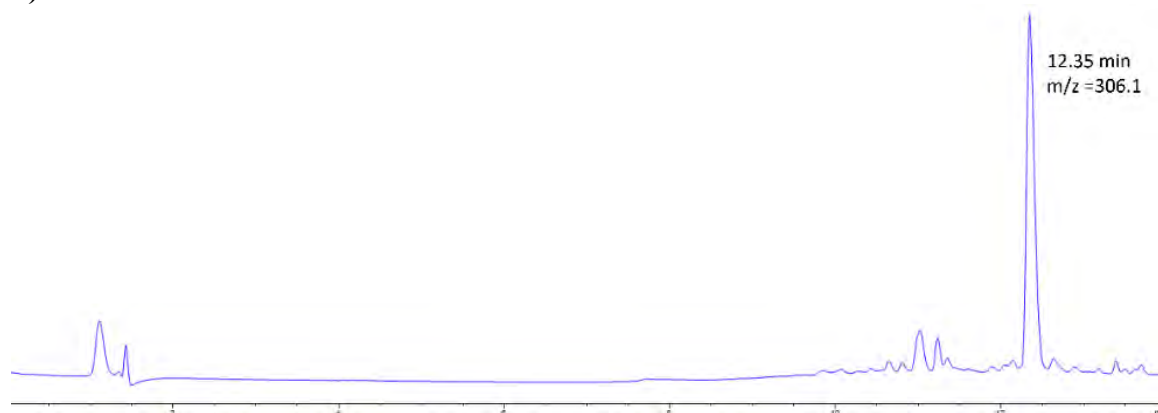
a) No treatment**b) 48 hours in PBS**

Figure 3.7: LCMS analysis of AsiFluor710 degradation. LCMS spectra of ASiFluor710 before (a) and after (b) 48 hour incubation in 50/50 ACN/PBS. Detected mass is reported below the retention time. LCMS detection wavelength was set to 280 nm.

Although the incorporation of fluorine groups promoted oxidation and allowed for the synthesis of azasilines, their electron-withdrawing effects likely increased aqueous lability. I predict that degradation was possibly initiated by the hydrolysis of fluorine, followed by fluorine-mediated reactions with silicon to form a silylated oxazine derivative, which underwent methyl transfer to form the final degradation product **3.13'** (**Figure 3.8**). In contrast, methyl groups are electron donating, which should increase aqueous stability.

The dimethyl-azasiline (**3.18**) was considerably more difficult to synthesize. Our initial synthetic route was analogous **Scheme 3.3**. However, this route failed at the PMB protection step, presumably due to the steric hindrance from the two methyl groups. I revisited my original synthetic scheme and postulated that cyclization can be achieved via palladium-catalyzed coupling (**Scheme 3.4**).

To access the dimethyl-azasiline, palladium-catalyzed coupling was first performed between commercially available azetidine and 3,5-dibromotoluene to yield the monobrominated azetindyl-toluene **3.14**. Treatment with *n*-BuLi and SiMe₂Cl₂ afforded the aryl silane **3.15**. Dibromination was achieved with NBS treatment to yield **3.16**. Ring closure was achieved with a palladium-catalyzed coupling between **3.16** and 4-methoxybenzylamine to yield the cyclized *leuco*-dye **3.17**. Finally, one-pot PMB deprotection and oxidation with I₂ treatment and subsequent HPLC purification afforded the final product **3.18** (ASiFluor730).

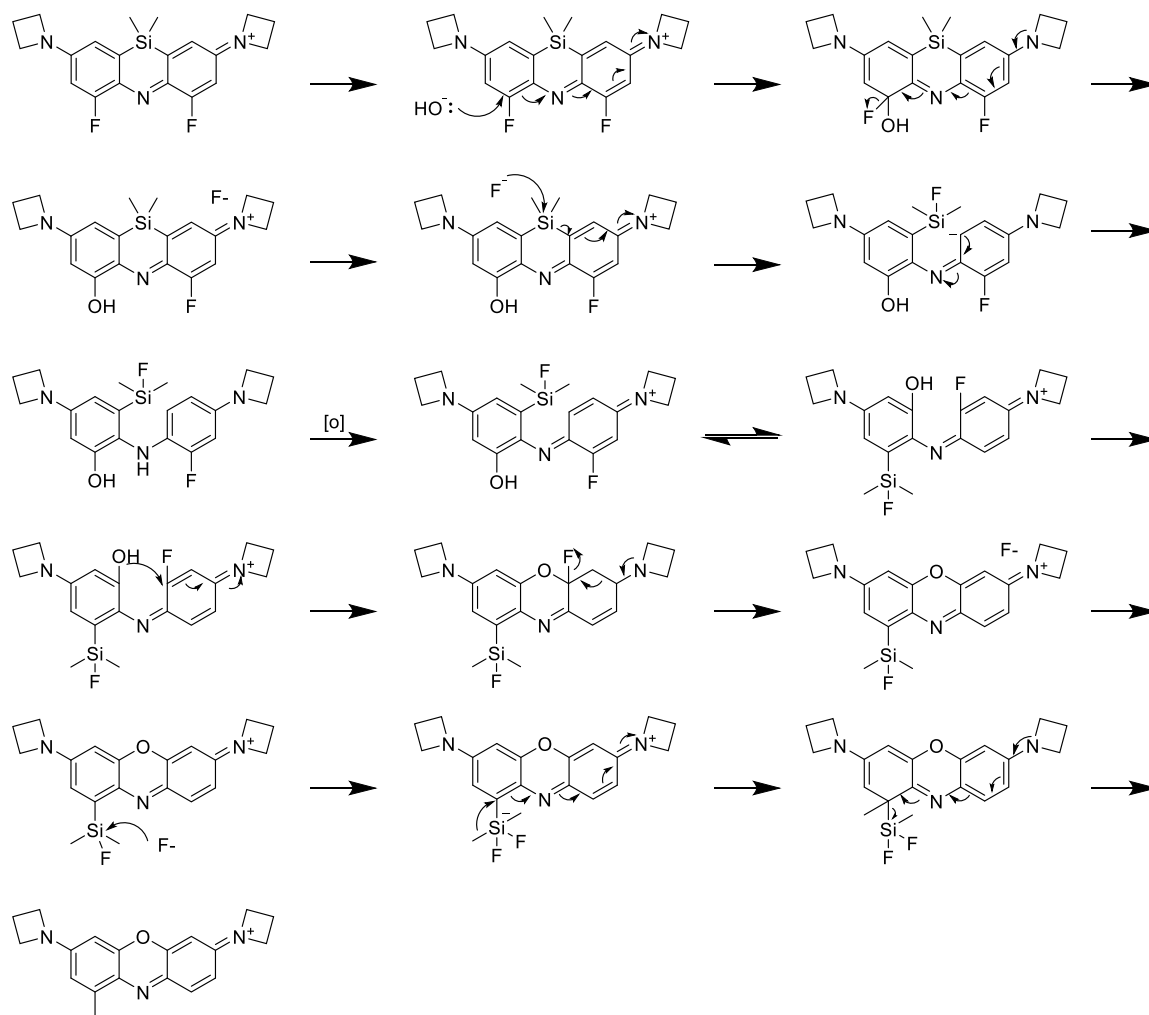
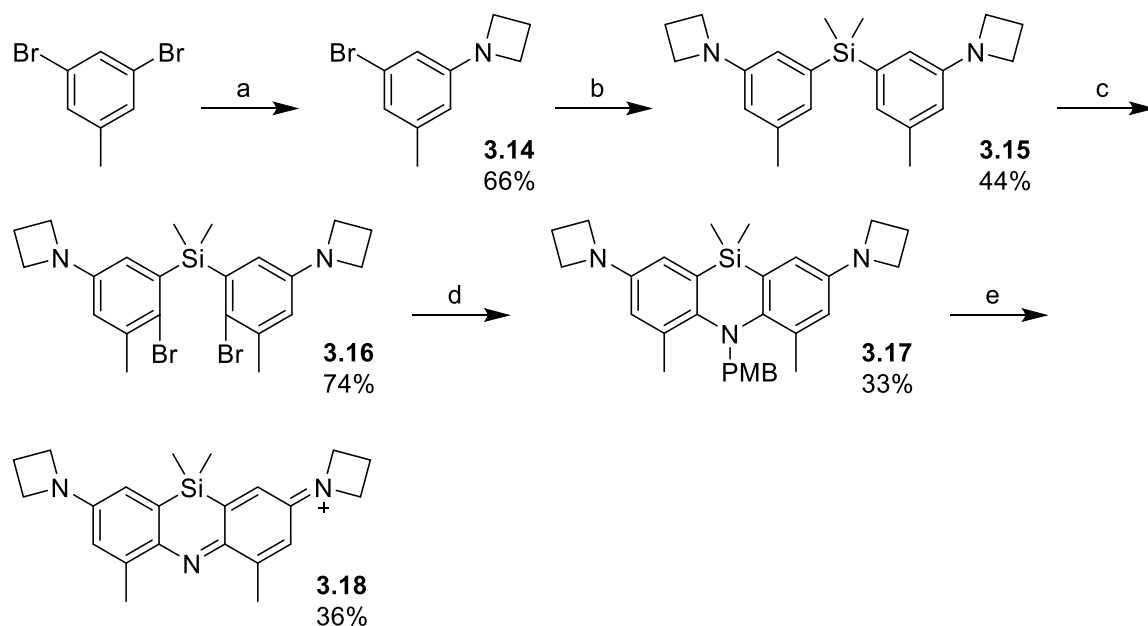


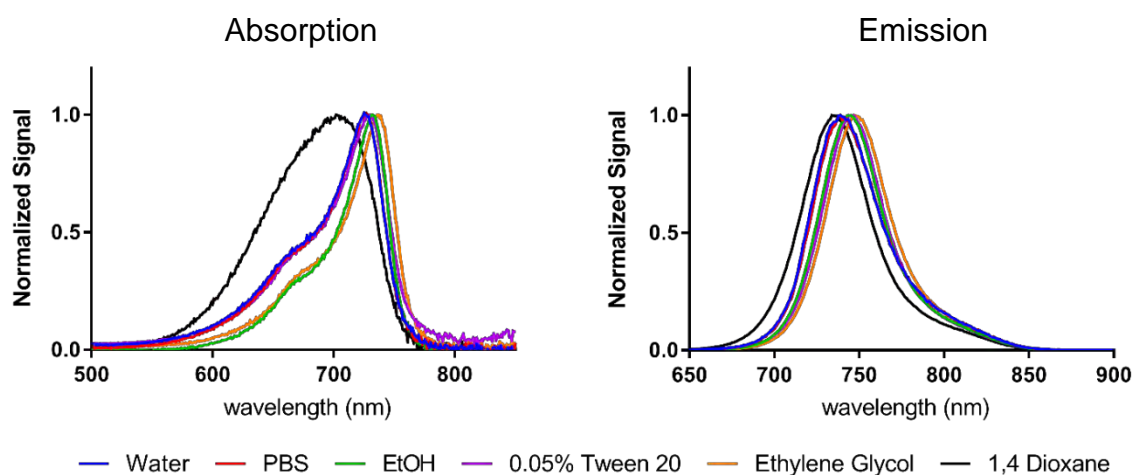
Figure 3.8: Proposed degradation mechanism of ASiFluor710.



Scheme 3.4: Synthesis of a dimethyl-azasiline (ASiFluor730). Reaction conditions: (a) azetidine, Pd₂(dba)₃, BINAP, NaOtBu, toluene, 110 °C. (b) *n*-BuLi, SiMe₂Cl₂, Et₂O/THF, -78 °C to RT. (c) NBS, DCM, 0 °C. (d) 4-Methoxybenzylamine, Pd₂(dba)₃, BINAP, NaOtBu, toluene, 110 °C. (e) I₂, MeOH, 0 °C.

ASiFluor730 displayed large bathochromic shifts of approximately 80 nm compared to Oxazine 1 (**Figure 3.4, 3.5 and 3.9**). Incubation in 50/50 ACN/PBS mixture for 48 hours did not degrade the compound (**Figure 3.10**). In ethanol, ASiFluor730 had a quantum yield and extinction coefficient of 0.11 and 120,000 M⁻¹cm⁻¹, respectively, which are comparable to those of Oxazine 1 (0.14 and 118,000 M⁻¹cm⁻¹).²⁹ In ethylene glycol and 1,4-dioxane, ASiFluor730 had a quantum yield of 0.13. However, the quantum yield of ASiFluor730 dropped to approximately 0.01 in deionized water and PBS, which is 11-fold lower than in ethanol. The addition of 0.05% Tween-20 restored the quantum yield to 0.06, implying that aggregation may be responsible for the reduced

quantum yield in aqueous solvents (**Figure 3.5**). Like cyanines, incorporation of polar groups such as sulfonates could enhance solubility and in turn, increase quantum yields.⁹³



Solvent	λ_{abs} (nm)	λ_{em} (nm)
Ethanol	732	745
Water	725	739
PBS	725	739
0.05% Tween 20	730	745
Ethylene Glycol	736	747
1,4-Dioxane	701	734

Figure 3.9: Excitation and emission of ASiFluor730 in various solvents. Absorbance (top left) and emission (top right) scans of ASiFluor730. Peak absorbance and emission wavelengths are listed in the table.

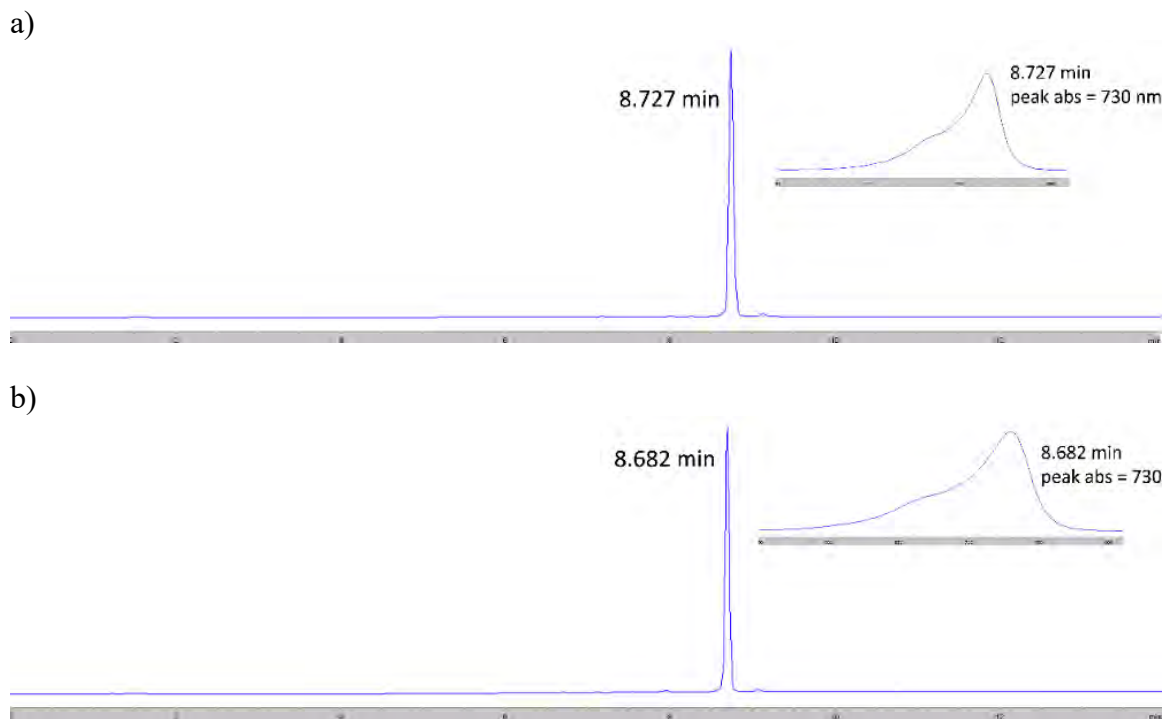


Figure 3.10: ASiFluor730 is stable in PBS. HPLC analysis of ASiFluor730 incubated in ACN/PBS. Before (a) and after (b) incubation after 48 hours. Each peak's corresponding Photodiode array (PDA) spectrum is displayed on the right of each trace. HPLC detection wavelength was set 650 nm.

Next, I compared the photostability of the ASiFluors to Oxazine 1 and Cy5.5, a cyanine derivative that absorbs and emit at similar wavelengths as the ASiFluors (**Figure 3.11**). Each fluorophore was irradiated for one hour at their peak absorption wavelength. Oxazine 1 and ASiFluor730 were photostable. ASiFluor710 displayed similar photostability in ethanol, but wasn't tested in PBS due to its aqueous lability. While Cy5.5 was photostable in ethanol, it lost ~60% of its fluorescence in PBS.

Although not as bright as NIR cyanines, azasilines are currently among the most compact NIR fluorophores (**Table 3.1**). Using molecular weight to excitation wavelength ratio (mw: λ_{ex}) as an estimate for compactness, azasilines are approximately twice as compact as ICG. Further, the ASiFluor730 was 1.4X more compact than SiR720, which is the most red-shifted SiR.

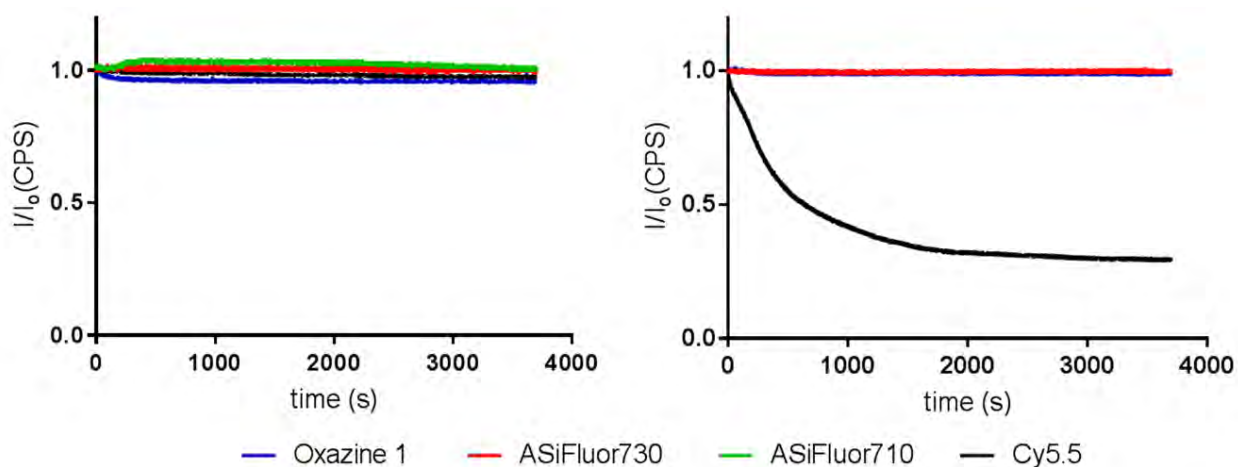


Figure 3.11: Azasilines retain the high photostability of oxazines. Each fluorophore was irradiated continuously for one hour at their max absorbance wavelength (Oxazine 1 = 646 nm; Cy5.5 = 684 nm; ASiFluor710 = 710 nm; ASiFluor730 = 730 nm) in ethanol (left panel) and PBS (right panel). ASiFluor710 was not tested in PBS due to its instability in aqueous solution.

Fluorophore	Ex (nm)	Em (nm)	MW	Length (Å)	Ex : Length	Ex : MW	Distance Between	Ref.
ASiFluor710	710	720	370	13.08	54.28	1.92	C(22)-C(25)	this work
ASiFluor730	730	740	362	13.08	55.81	2.02	C(24)-C(21)	this work
SiR700	691	712	423	11.93	57.92	1.63	C(8)-C(19)	99
SiR720	721	740	532	14.52	49.66	1.36	C(37)-C(33)	99
ICG	775	831	752	17.20	45.06	1.03	C(2)-C(30)	39
Cy5.5	679	696	483	14.89	45.60	1.41	C(2)-C(25)	39
Oxazine 1	646	662	324	14.39	44.89	1.99	C(19)-C(24)	29
HITC (Cy7)	743	772	409	18.03	41.21	1.82	C(2)-C(26)	29
TTAB	733	757	521	11.51	63.68	1.41	C(29)-C(22)	100
Sq2	729	739	521	14.27	51.09	1.40	C(35)-C(37)	101

Table 3.1: Size comparison of fluorophores. The length was calculated as the distance between the two outer most atoms using Chem3D. The excitation wavelength to molecular weight and excitation wavelength to length ratios estimate the compactness of the molecule. ICG = Indocyanine Green. TTAB and Sq2 are examples of NIR aza-BODIPY and squaraine fluorophores, respectively.

Lastly, I characterized ASiFluor730's behavior in HeLa cells. The cytotoxicity of ASiFluor730 was compared to that of Oxazine 1 using a standard cell proliferation assay called XTT. Oxazine 1 displayed low toxicity, cell density was decreased by only 25% at 100 μ M treatment. On the other hand, ASiFluor730 displayed moderate toxicity with a LD₅₀ of approximately 9.6 μ M (**Figure 3.12**).

Cationic dyes can accumulate in the mitochondria due the charge attraction between the negative membrane potential of the mitochondria and the positive charge of cationic dyes.¹⁰² Certain cationic dyes such as Rhodamine 123 have also been shown to cause mitochondrial depolarization that ultimately leads to apoptosis or autophagy via the inhibition of key enzymes in the electron transport chain.^{103–105} I speculate that

ASiFluor730 also confer cytotoxicity in a similar manner. Thus, the addition of polar anionic groups such as sulfonates could both increase aqueous solubility and lower the toxicity of ASiFluors.

Live HeLa cells were stained with ASiFluor730 (5 μM) and then imaged with fluorescent microscopy. Azasilines are cationic and thus, may migrate to the mitochondria due to the charge attraction between the negative potential of the mitochondria and the positive charge on the fluorophore.^{106–108} To test whether ASiFluor730 localizes to the mitochondria, cells were co-stained with MitoTracker Green.

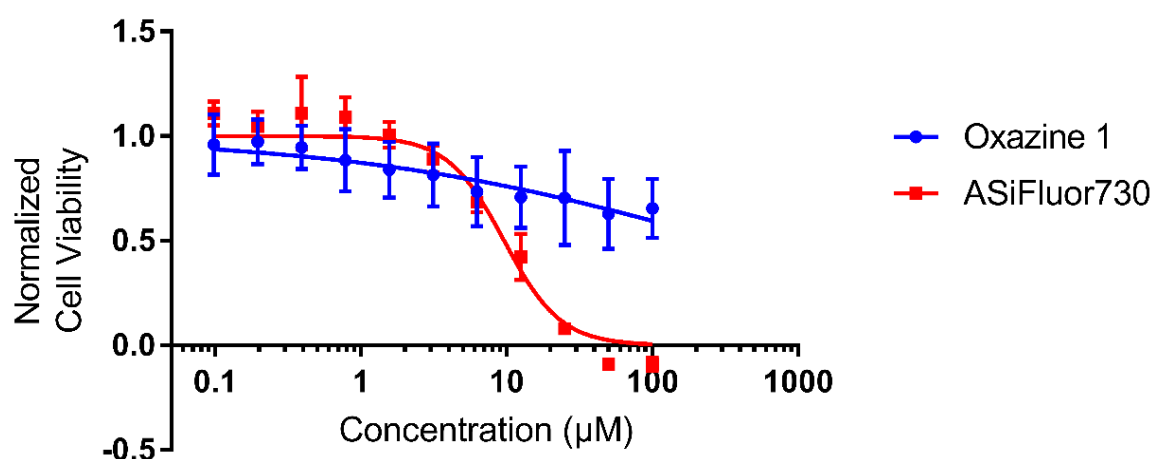


Figure 3.12: Cytotoxicity of ASiFluor730 in HeLa cell. Live HeLa cells were treated with different concentrations of ASiFluor730 (100 μM – 0.01 μM) for 1 hour. Toxicity was assessed using XTT cell proliferation assay 48 hours after treatment. Signals were normalized to the DMF vehicle control. Data was fitted with GraphPad Prism.

When used alone, ASiFluor730 gave a robust fluorescent signal, but does not access the nucleus (**Figure 3.13**). MitoTracker Green and ASiFluor730 showed identical staining patterns in co-stained HeLa cells, confirming that ASiFluor indeed migrates to the mitochondria (**Figure 3.13**).

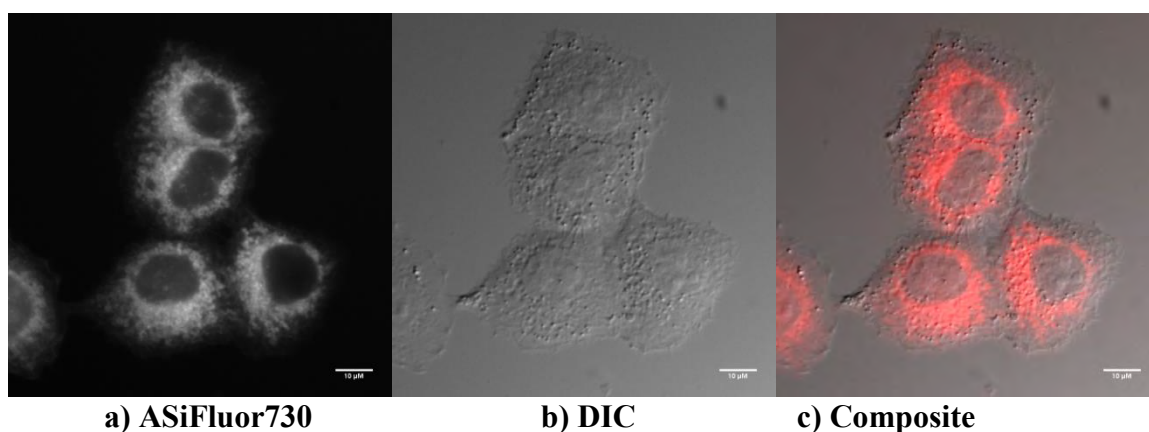


Figure 3.13: HeLa cells stained with ASiFluor730. Live HeLa cells were incubated with ASiFluor730 (5 μ M) for 15 minutes and imaged under a fluorescence microscope. Fluorescence image of ASiFluor730 (a), DIC (b) and composite (c).

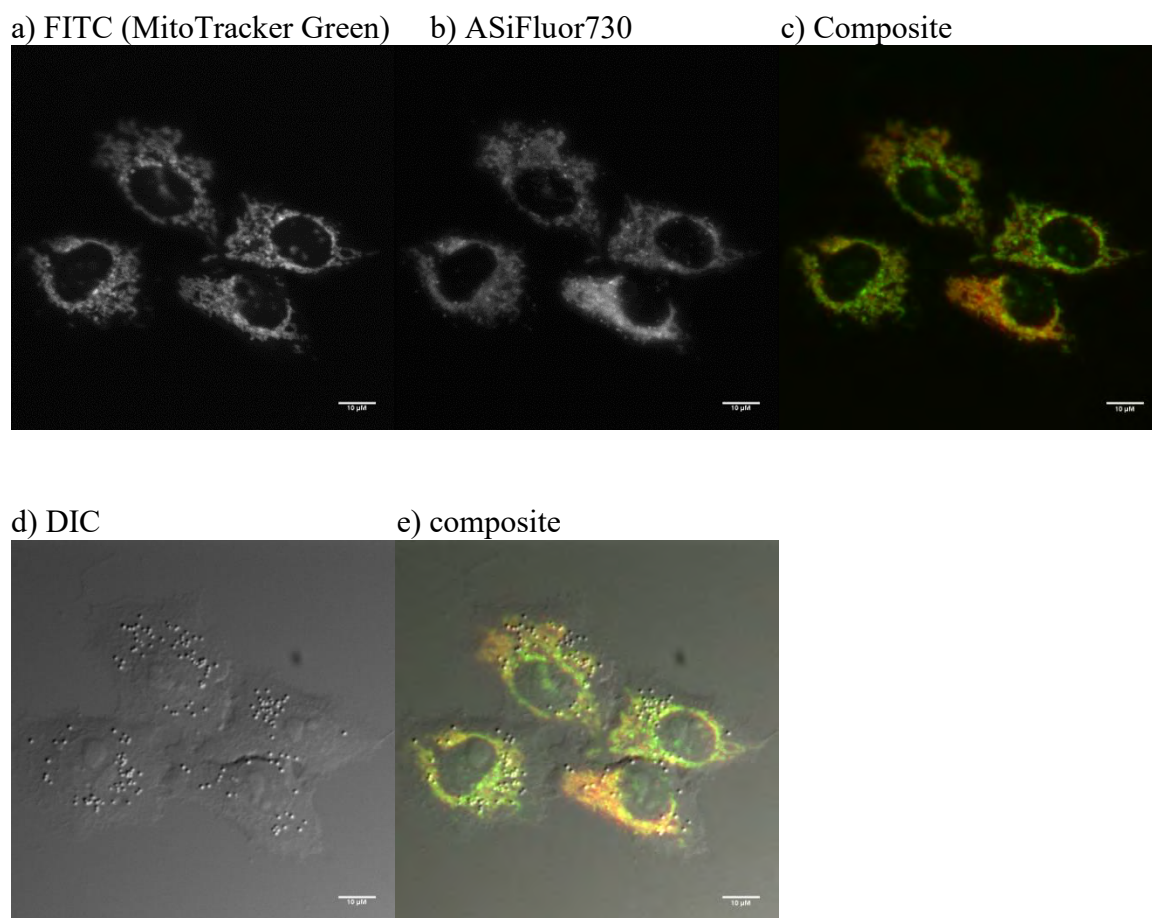


Figure 3.13: ASiFluor730 and MitoTracker Green co-localized in the mitochondria.

Live HeLa cells were first treated with MitoTracker Green (100 nM) for 15 minutes, followed by ASiFluor730 (5 μ M) for an additional 15 minutes. Fluorescence image of MitoTracker Green (a) and ASiFluor730 (b), composite fluorescence image (c), DIC (d), and composite of DIC and fluorescence image (e).

Conclusions

Silicon to oxygen substitution can dramatically red shift both excitation and emission wavelengths without substantially increasing molecular size. However, this phenomenon has only been investigated in rhodamines. Using this method of oxygen to silicon substitution I introduced two novel azasiline NIR fluorophores based on the oxazine scaffold.

Both azasilines displayed large bathochromic shifts, similar to those seen in SiR. The emission wavelengths of ASiFluor710 (712_{ex}/719_{em}) and ASiFluor730 (732_{ex}/745_{em}) are 57 and 83 nm longer than those of Oxazine 1 (646_{ex}/662_{em}), respectively. Although ASiFluor710 was unstable and degraded into a methylated oxazine in PBS, it had a respectable quantum yield of 0.11 in ethanol.

ASiFluor730 did not degrade in PBS and inherited the high photostability of oxazines. In ethanol, ASiFluor730 exhibited similar photophysical properties as Oxazine 1. The quantum yield in water was low, but was largely restored with the addition of 0.05% Tween 20. Although ASiFluor730 has a low quantum yield in water and showed moderate toxicity in Hela cells (LD₅₀ = 9.6 μ M), it still robustly stained cells.

The azasiline scaffold is one of the most compact NIR fluorophore scaffolds. Moreover, the azasiline scaffold contains multiple sites amendable for anchoring linkers, affinity tags, and installing water-soluble, polar groups (**CHAPTER IV**). Combined with the NIR fluorescence wavelengths and stability, I envision azasilines will find broad

applications in any fluorescence-based assays, including deep tissue imaging, and inspire the design of other silylated luminescent probes.

Materials and Methods

General:

Commercially available products were used without purification and purchased from Combi-Block, Chem-Impex, Sigma-Aldrich, Acros or Oakwood Chemicals. Palladium catalysts and ligands were purchased from Combi-Blocks and Chem-Impex. Cy5.5 free carboxylic acid was purchased from Lumiprobe. Anhydrous solvents were purchased from Acros. Compounds were purified with the CombiFlash Rf+ system and HPLC-grade ChromoSolv solvents were purchased from Sigma-Aldrich.

All NMR spectra (^1H , ^{19}F , and ^{13}C) were obtained on a Bruker Ascend 500. Analytical HPLC was performed on an Agilent 1100 equipped with a Zorbex C8 column and a PDA detector (G1315A DAD). Preparatory HPLC was performed on a Varian ProStar equipped with Agilent 10-Prep C18 21.2 x 250 mm Column. LCMS was performed on an Agilent 1260 Infinity equipped with a Zorbex SB-C18 column and a 6130 Quadrupole detector. High resolution mass-spec data were obtained on an Agilent 6520 Q-TOF. Absorption and emission data were obtained on Cary-50 and Fluoromax-4 instruments, respectively. Data were graphed and fitted using Graphpad Prism 7. NMR spectra were analyzed with MestReNova. Images were acquired with a Nikon Eclipse E600 and analyzed with ImageJ.

Excitation and Emission Spectra of Fluorophores

For excitation (absorption), compounds were diluted until the spectrums were smooth. For emission, compounds were diluted until the peak signal is below 1×10^6 CPS. The temperature was maintained at 20°C and slit widths varied between compounds. All samples were blanked with their respective blanks prior to analysis.

Equipment and Conditions:

System: Horiba Scientific FluoroMax-4

Temperature Controller: Newport Model 350B

Acquisition software: FluorEssence

Temperature: 20 °C

System: Horiba Scientific Cary 50

Acquisition software: Cary Win UV

Live Cell Imaging

Cell culture

HeLa cells were cultured with DMEM containing 10% FBS and 1% Pen/Strep at 37 °C. Cells were first cultured in T-75 TC flasks to 70% confluency, then trypsinized and diluted to 50,000 cells/mL. Coverslips (#1.5 18 mm) were seeded in a 10 cm petri dish using 10 mL of cell solution. Cells were allowed to adhere for 20 hours at 37 °C.

Staining

Coverslips were washed HBSS (3 X) and placed in a 35 mm petri plate containing 5 μ M of ASiFluor730 in HBSS (2 mL) and then incubated for 15 minutes at 37 °C. After incubation, the coverslips were washed with HBSS (3 X) and mounted using a technique adapted from Chazotte.⁸⁸ Instead of using VALAP, Vaseline was used to seal the chamber and 200 μ L of HBSS was used to fill the chamber to prevent the formation air bubbles.

Co-staining

Coverslips were washed HBSS (3 X) and placed in a 35 mm petri plate containing HBSS (2 mL). MitoTracker Green (1 μ l of a 200 μ M stock) was added to achieve a final concentration of 100 nM and then incubated for 15 minutes at 37 °C. After incubation, the coverslips were washed with HBSS (3 X), placed in HBSS containing 5 μ M of ASiFluor730 and incubated for an additional 15 minutes at 37 °C. After the second incubation, the coverslips were washed with HBSS (3 X) and mounted using a technique

adapted from Chazotte.⁸⁸ Instead of using VALAP, Vaseline was used to seal the chamber and 200 μ L of HBSS was used to fill the chamber to prevent the formation air bubbles.

Image processing

Raw 16-bit images were cropped to the desired 2 square inch frames (600 dpi) and a scale bar was applied (7.85 pixel/ μ m). Composite pictures were prepared using the merge channel function in the FIJI software, and pseudocolored.

Equipment

Coverslips: Deckgläser No. 1.5, 18 mm round glass

Microscope slides: Fisherfinest Premium Plain

Microscope: Nikon Eclipse E600

Camera: Hamamatsu Orca-ER with controller

Objective: Nikon Plan 50x oil immersion

Filter Set: Nikon UV-2A (330-380 nm bandpass excitation; 420 nm longpass emission)

Filter set: Custom filter cube (Ex: 665/40, FF685 Di02. Em: 747/33)

Light Source: Chiu Technical Corporation 100W Mercury Lamp

Exposure time: 100 ms

Imaging processing software: FIJI

HPLC Analysis of ASiFluor Degradation (analytical)

Compounds (1 μL of a 10 μM stock) were diluted in 50/50 ACN/PBS (1 mL) and incubated in the dark at room temperature for 48 hours. 50 μL was injected into the HPLC after filtration through a 0.45 μM PTFE syringe filter. Control samples were diluted in ACN, filtered and injected immediately. The HPLC column was equilibrated for at least 25 minutes at 1.4 mL/min prior to sample injection.

Equipment and Conditions:

Injection volume: 200 μL

HPLC system: Agilent Series 1100

Filter: 13mm 0.45 μM PTFE

Column: Agilent Zorbax XDB-C8 μm 4.6 mm x 150 mm

Wavelength monitored: 650 nm / 800 nm (reference)

System: 0.1% TFA H_2O /acetonitrile

Ramp:

Time (m)	% Acetonitrile	Flow rate (mL/ min)
2	0	1.4
12	100	1.4
15	100	1.4

HPLC (preparatory)

Samples (5 mL) dissolved in 50/50 ACN/H₂O were injected into the HPLC after filtration through a 0.45 μ M PTFE syringe filter. The HPLC column was equilibrated for at least 10 minutes at 20 mL/min prior to sample injection.

Equipment and Conditions:

Injection volume: 5 mL

HPLC system: Varian ProStar

Filter: 13mm 0.45 μ M PTFE

Column: Agilent 10-Prep C18 21.2 x 250 mm

Wavelength monitored: 650 nm

System: 0.1% TFA H₂O/acetonitrile

Ramp:

Time (m)	% Acetonitrile	Flow rate (mL/ min)
5	0	20
40	65 (3.13') or 85 (3.18)	20
42	100	20
47	100	20

LCMS Analysis of ASiFluor Degradation

Compounds (1 μ L of a 10 μ M stock) were diluted in 50/50 ACN/PBS (1 mL) and incubated in the dark at room temperature for 48 hours. 10 μ L was injected into the LCMS after filtration through a 0.45 μ M PTFE syringe filter. Control samples were diluted in ACN, filtered and injected immediately. The LCMS column was equilibrated for at 5 minutes at 0.5 mL/min prior to sample injection.

Equipment and Conditions:

Injection volume: 10 μ L

LCMS system: Agilent 1260 Infinity with auto-sampler, 6130 Quadrupole LC/MS

Column: Zorbex SB-C18 2.1x50 mm 1.8 μ m

Wavelength monitored: 280 nm / 595 nm (reference)

System: 0.1% aq. formic acid/acetonitrile

Ramp:

Time (m)	% Acetonitrile	Flow rate (mL/ min)
2	0	0.5
12	100	0.5
14	100	0.5
Post-run (5 minutes)	0	0.5

Photostability of ASiFluors

Each fluorophore was diluted from a 10 mM DMSO stock to 3.3 μM in ethanol or 10 μM in PBS. The excitation wavelength was set to match each fluorophore's absorption maxima with a 20 nm slit width. The emission detection wavelength was set to 40 nm away from the absorption maxima at the indicated slit width. The fluorescence signal was collected every 0.1 seconds for 3700 seconds and normalized to the initial signal. The average μAs are listed as an estimate of the relative irradiation intensity at each wavelength.

Compound	[μM]	Solvent	Excitation	Slit	Emission	Slit	Avg. μA
Oxazine 1	10	PBS	646	20	686	1	116
	3.3	EtOH				1	
ASiFluor730 (18)	10	PBS	730		770	10	95
	3.3	EtOH				2	
Cy5.5	10	PBS	684		724	2	141
	3.3	EtOH				1	
ASiFluor710 (13)	3.3	EtOH	710		750	2	105

Quantum Yield and Extinction Coefficient Determination

Compounds were first diluted from a 10 mM DMSO stock into the desired solvent (e.g. PBS, water, EtOH, 1,4-Dioxane, 0.05% Tween-20 or ethylene glycol). The first dilution solution was allowed to equilibrate in the dark at room temperature for 15 minutes before a second dilution was made. The second dilution was allowed to equilibrate in the dark at room temperature for another 15 minutes before the absorption or fluorescence signal was read. Absorbance readings were kept below 0.1 for quantum yield samples. Slit widths were set to 2 nm (ex) and 5 nm (em) with 0.1s integration time for fluorescence measurements.

Toxicity Assay

Cell culture

HeLa cells were cultured with DMEM containing 10% FBS and 1% Pen/Strep at 37 °C. Cells were first cultured in T-75 TC flasks to 70% confluency, then trypsinized and diluted to 50,000 cells/mL. Clear 96-well plates were seeded with 5000 cells/well. Cells were allowed to adhere for 24 hours at 37 °C.

XTT Assay

DMEM medium was removed via aspiration and the cells were washed once with HBSS (100 µL). After washing, the wells were filled with HBSS (50 µL). Compounds (50 µL) were added and incubated for 1 hr at 37 °C. After treatment, the compounds were removed via aspiration and the cells were washed once with HBSS (100 µL). The cells were supplied with fresh DMEM (100 µL) and allowed to proliferate for 48 hours at 37 °C. Activated XTT reagent (50 µL) were added and incubated at 37 °C for 4 hour. Wells were read at 490 nm and 660 nm.

Compounds at 10 mM stock concentration in DMSO were first diluted in HBSS (10 µL in 1 mL), then serially diluted (1:2) in HBSS. Concentrations ranged from 100 µM to 1 µM at 2X.

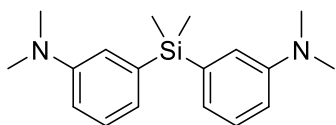
Equipment

Plates: BD 35-3072

Plate Reader: BioRad IMark

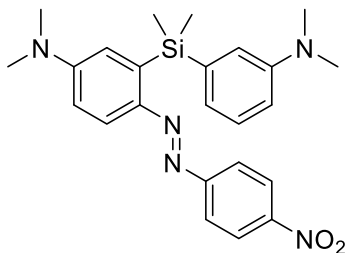
XTT Reagent: ATCC XTT Kit 30-1011K

Synthetic Methods



3,3'-(Dimethylsilanediyl)bis(N,N-dimethylaniline) (3.1)

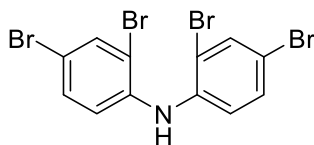
In a 50 mL oven dried round bottom flask, 3-bromo-N,N-dimethylaniline (200 mg, 1 mmol) was dissolved in anhydrous diethyl ether (10 mL) and anhydrous THF (0.5 mL) at room temperature and then cooled to 0 °C. *n*-BuLi (0.49 ml of 2.5 M, 1.2 mmol) was added drop-wise to the reaction. After 1 hour, dichlorodimethylsilane (77 mg, 0.6 mmol) was added and the reaction was warmed to room temperature. After 16 hours, the reaction was poured into water (20 mL), and the product was extracted with diethyl ether (25 mL). The combined organic layers were washed with water (50 mL) and brine (50 mL), then dried over Na₂SO₄. The solvent was removed under reduced pressure and the product was purified by silica gel chromatography (0-30% EtOAc/hexanes) to afford the product as a yellow oil (37 mg, 0.12 mmol, 24%). ¹H NMR (500 MHz, CDCl₃) δ 7.30 – 7.27 (m, 2H), 6.98 (d, *J* = 2.7 Hz, 2H), 6.95 (m, 2H), 6.80 (ddd, *J* = 8.2, 2.7, 0.6 Hz, 2H), 2.96 (s, 12H), 0.57 (s, 6H). ¹³C NMR (126 MHz, CDCl₃) δ 150.1, 139.1, 128.6, 122.9, 118.5, 113.7, 40.8, -2.0. HR-EIMS *m/z* calculated for C₁₈H₂₇N₂Si [M + H]⁺: 299.1938, found: 299.1917.



(E)-3-((3-(Dimethylamino)phenyl)dimethylsilyl)-N,N-dimethyl-4-((4-nitrophenyl)diazenyl) aniline (3.2)

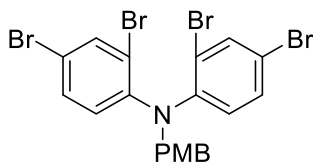
In a 100 mL round bottom flask, compound **3.1** (149 mg, 0.5 mmol) was dissolved in aq 2 M HCl (25 mL) and MeOH (10 mL) at 0 °C. 4-Nitrobenzenediazonium tetrafluoroborate (119 mg, 0.5 mmol) was separately dissolved in aq 2 M HCl (1 mL) and MeOH (5 mL) and added dropwise with an addition funnel, then stirred at 4 °C. After 16 hours, the reaction was poured into sat'd NaHCO₃ (100 mL), and the product was extracted with ethyl acetate (3 X 20 mL). The combined organic layers were washed with NaHCO₃ (50 mL) and brine (50 mL), then dried over Na₂SO₄. The solvent was removed under reduced pressure and the product was purified by silica gel chromatography (0-20% EtOAc/hexanes) to afford the product as a purple solid (105 mg, 0.23 mmol, 47%).

¹H NMR (500 MHz, CDCl₃) δ 8.21 (d, *J* = 8.9 Hz, 2H), 7.91 (d, *J* = 9.1 Hz, 1H), 7.60 (d, *J* = 8.9 Hz, 2H), 7.22 (t, *J* = 7.7 Hz, 1H), 6.95 (d, *J* = 2.2 Hz, 1H), 6.92 (d, *J* = 7.2 Hz, 1H), 6.87 (d, *J* = 2.8 Hz, 1H), 6.78 – 6.71 (m, 2H), 3.08 (s, 6H), 2.88 (s, 6H), 0.61 (s, 6H). ¹³C NMR (126 MHz, CDCl₃) δ 157.0, 152.5, 150.2, 148.3, 147.2, 145.3, 140.0, 128.5, 124.7, 123.0, 122.9, 118.6, 118.2, 117.4, 113.6, 113.1, 40.9, 40.3, -0.2. HR-EIMS *m/z* calculated for C₂₄H₃₀N₅O₂Si [M + H]⁺: 488.2163, found: 488.2143.



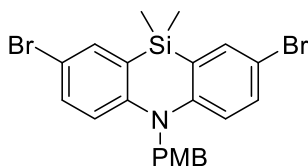
Bis(2,4-dibromophenyl)amine (**3.3**)

In a 1 L round bottom flask, diphenylamine (5 g, 29.9 mmol) was dissolved in acetone (225 mL) at room temperature. The temperature was lowered to 0 °C, then NBS (23.2 g) was added in small portions. After 15 minutes, H₂O (225 mL) was added to the reaction and the white solid was filtered and washed with 50/50 acetone/H₂O (400 mL). Finally, the white solid was recrystallized in toluene (300 mL) giving **3** as a white solid (9.75 g, 20.1 mmol, 69%). ¹H NMR (500 MHz, C₆D₆) δ 7.45 (d, *J* = 2.2 Hz, 2H), 6.88 (dd, *J* = 8.7, 2.2 Hz, 2H), 6.39 (d, *J* = 8.7 Hz, 2H), 6.15 (s, 1H). ¹³C NMR (126 MHz, C₆D₆) δ 139.0, 135.6, 131.3, 119.2, 115.3, 114.2. HR-EIMS *m/z* calculated for C₁₂H₈Br₄N [M + H]⁺: 485.7344, found: 485.7339.



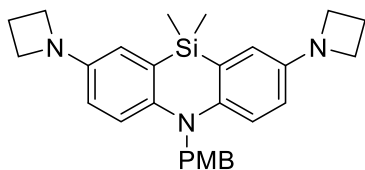
2,4-Dibromo-N-(2,4-dibromophenyl)-N-(4-methoxybenzyl)aniline (3.4)

In a 500 mL round bottom flask, compound **3.3** (9.75 g, 20.1 mmol) was dissolved in THF (250 mL) at 0 °C. Sodium hydride (2.4 g, 100 mmol) was added to the reaction in small portions. After one hour, *p*-methoxybenzyl chloride (PMB-Cl) (4.1 mL, 30.1 mmol) was added, then the reaction was warmed to room temperature and stirred for 72 hours. The solvent was then removed under reduced pressure. The resulting solid was triturated in MeOH (10 mL) and the product was collected by filtration (10.8 g, 17.9 mmol, 89%). ¹H NMR (500 MHz, CDCl₃) δ 7.74 (d, *J* = 2.0 Hz, 2H), 7.40 (d, *J* = 8.4 Hz, 2H), 7.36 – 7.21 (m, 2H), 6.83 (d, *J* = 8.5 Hz, 4H), 4.72 (s, 2H), 3.78 (s, 3H). ¹³C NMR (126 MHz, CDCl₃) δ 158.8, 145.8, 136.7, 131.1, 128.8, 128.7, 126.5, 122.0, 117.2, 114.0, 56.1, 55.2. HR-EIMS *m/z* calculated for C₂₀H₁₄Br₄NO [M - H]⁺: 603.7762, found: 603.7756. The NMR is consistent with previously reported values.⁹⁷



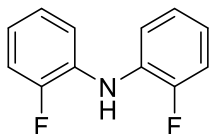
2,4-Dibromo-N-(2,4-dibromophenyl)-N-(4-methoxybenzyl)aniline (3.5).

In a 100 mL oven-dried round bottom flask, compound **3.4** (1.2 g, 1.99 mmol) was dissolved in anhydrous diethyl ether (25 mL) at room temperature and then cooled to 0 °C. *n*-BuLi (2.6 mL of 1.6 M) was added drop-wise to the reaction. After 1 hour, dichlorodimethylsilane (460 mg, 3.6 mmol) was added and the reaction mixture was warmed to room temperature. After 16 hours, the product was extracted with ether (50 mL), washed with water (50 mL) and brine (50 mL), and finally purified with silica gel chromatography (0-50% DCM/hexanes) to afford a white solid (515 mg, 1 mmol, 50%). ¹H NMR (500 MHz, CDCl₃) δ 7.55 (d, *J* = 2.5 Hz, 2H), 7.30 (dd, *J* = 9.0, 2.5 Hz, 2H), 7.11 (d, *J* = 8.7 Hz, 2H), 6.90 – 6.85 (m, 2H), 6.78 (d, *J* = 9.0 Hz, 2H), 5.09 (s, 2H), 3.81 (s, 3H), 0.47 (s, 6H). ¹³C NMR (126 MHz, CDCl₃) δ 158.9, 148.4, 135.8, 133.2, 128.7, 127.4, 124.5, 118.3, 114.5, 113.9, 55.6, 55.5, -0.8. HR-EIMS *m/z* calculated for C₂₂H₂₂Br₂NOSi [M + H]⁺: 503.9811, found: 503.9805.



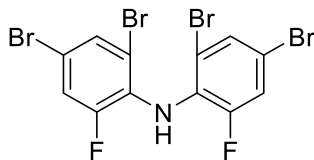
2,8-Di(azetidin-1-yl)-5-(4-methoxybenzyl)-10,10-dimethyl-5,10-dihydrodibenzo[b,e][1,4] azasiline (3.6)

In a 15 mL sealed tube, compound **3.5** (200 mg, 0.4 mmol), $\text{Pd}_2(\text{dba})_3$ (18.3 mg, 0.02 mmol), BINAP (25 mg 0.04 mmol), sodium *tert*-butoxide (92 mg, 0.96 mmol) and azetidine (50 mg, 0.87 mmol) were dissolved in anhydrous toluene (10 mL). The reaction tube was flushed with argon, then heated to 80 °C for 24 hours. The reaction was filtered through Celite and the product was purified with silica gel chromatography (0-30% EtOAc/hexanes) to afford a yellow-tinted solid (129 mg, 0.28 mmol, 71%). ^1H NMR (500 MHz, CDCl_3) δ 7.17 (d, J = 8.6 Hz, 2H), 6.88 – 6.84 (m, 2H), 6.78 (d, J = 8.9 Hz, 2H), 6.60 (d, J = 2.9 Hz, 2H), 6.41 (dd, J = 8.9, 2.9 Hz, 2H), 5.05 (s, 2H), 3.83 (t, J = 7.1 Hz, 8H), 3.80 (s, 3H), 2.33 (p, J = 7.1 Hz, 4H), 0.45 (d, J = 3.2 Hz, 6H). ^{13}C NMR (126 MHz, CDCl_3) δ 158.5, 146.0, 142.8, 131.1, 127.6, 122.1, 116.5, 115.8, 114.4, 114.2, 55.6, 55.4, 53.2, 17.3, -0.7. HR-EIMS m/z calculated for $\text{C}_{28}\text{H}_{34}\text{N}_3\text{OSi}$ $[\text{M} + \text{H}]^+$: 456.2466, found: 456.2436.



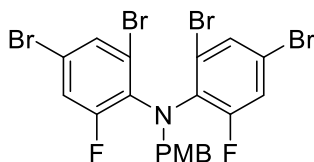
Bis(2-fluorophenyl)amine (3.8)

In a 100 mL round bottom flask equipped with a reflux condenser, 2-fluoroaniline (2 g, 18 mmol), 1-bromo-2-fluorobenzene (3.5 g, 19.8 mmol), $\text{Pd}_2(\text{dba})_3$ (833 mg, 0.9 mmol), Xantphos (1 g, 1.8 mmol), and sodium *tert*-butoxide (2.1 g, 21.8 mmol) were dissolved in anhydrous toluene (15 ml). The reaction was refluxed at 110 °C. After 16 hours, the reaction was filtered through Celite and the solvent was removed under reduced pressure. The product was purified with silica gel chromatography (0-5% DCM/hexanes) to afford a clear oil (3.3 g, 16 mmol, 89%). ^1H NMR (500 MHz, CDCl_3) δ 7.33 (dt, $J = 8.3, 1.4$ Hz, 2H), 7.19 – 7.12 (m, 2H), 7.12 – 7.06 (m, 2H), 6.98 – 6.91 (m, 2H), 5.90 (s, 1H). ^{19}F NMR (471 MHz, CDCl_3) δ -131.24 (ddd, $J = 11.6, 8.6, 4.9$ Hz). ^{13}C NMR (126 MHz, CDCl_3) δ 153.7 (d, $J_{\text{CF}} = 242.2$ Hz), 130.7 (d, $J_{\text{CF}} = 11.1$ Hz), 124.4 (d, $J_{\text{CF}} = 3.8$ Hz), 121.7 (d, $J_{\text{CF}} = 7.3$ Hz), 118.3 (d, $J_{\text{CF}} = 1.8$ Hz), 115.8 (d, $J_{\text{CF}} = 19.2$ Hz). HR-EIMS m/z calculated for $\text{C}_{12}\text{H}_{10}\text{F}_2\text{N}$ $[\text{M} + \text{H}]^+$: 206.0776, found: 206.0776.



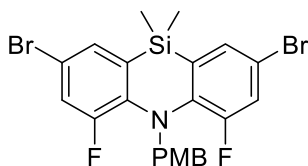
Bis(2,4-dibromo-6-fluorophenyl)amine (3.9)

In a 50 mL round bottom flask, compound **3.8** (2 g, 9.74 mmol) was dissolved in acetic acid (20 mL). The reaction temperature was raised to 110 °C, followed by the addition of bromine (2.1 mL, 58.4 mmol). After 10 minutes, the reaction was cooled to room temperature to allow for crystallization of the product. The product was filtered and washed with acetic acid (60 mL) and H₂O (200 mL) to afford a white solid (4.21 g, 8.1 mmol, 83%). ¹H NMR (500 MHz, CDCl₃) δ 7.57 – 7.50 (m, 2H), 7.18 (dd, *J* = 10.6, 1.9 Hz, 2H), 5.64 (s, 1H). ¹⁹F NMR (471 MHz, CDCl₃) δ -119.23 (d, *J* = 10.4 Hz). ¹³C NMR (126 MHz, CDCl₃) δ 154.4 (dd, *J*_{CF} = 254.0, 2.3 Hz), 130.6 (d, *J*_{CF} = 2.8 Hz), 128.8 (dd, *J*_{CF} = 11.7, 2.0 Hz), 119.0 (d, *J*_{CF} = 23.5 Hz), 116.9 – 116.4 (m), 114.4 – 114.1 (m). HR-EIMS *m/z* calculated for C₁₂H₆Br₄F₂N [M + H]⁺: 521.7155, found: 521.7135.



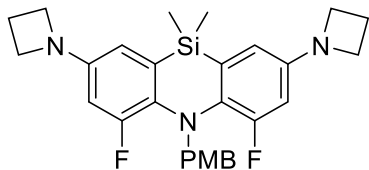
2,4-Dibromo-N-(2,4-dibromo-6-fluorophenyl)-6-fluoro-N-(4-methoxybenzyl)aniline (3.10)

In a 100 mL round bottom flask, compound **3.9** (2 g, 3.9 mmol) and 15-Crown 5 (1.6 mL, 7.8 mmol) were dissolved in THF (40 mL). Sodium hydride (120 mg, 5 mmol) was added to the reaction in small portions. After 1 hour, *p*-methoxybenzyl chloride (529 μ L, 5.85 mmol) was added to the solution and refluxed at 75 °C. After 24 hours, the reaction was poured into brine (100 mL) and extracted with EtOAc (3 X 50 mL). The combined organic layers were washed with brine (100 mL) and dried over sodium sulfate. The solvent was removed under reduced pressure and the product was purified by silica gel chromatography (0-100% DCM/hexanes) to afford a white solid (2.07 g, 3.22 mmol, 82%). ^1H NMR (500 MHz, CDCl_3) δ 7.47 – 7.44 (m, 2H), 7.41 (d, J = 8.6 Hz, 2H), 7.11 (dd, J = 10.9, 2.2 Hz, 2H), 6.80 – 6.72 (m, 2H), 4.82 (s, 2H), 3.75 (s, 3H). ^{19}F NMR (471 MHz, CDCl_3) δ -111.59. ^{13}C NMR (126 MHz, CDCl_3) δ 160.1 (d, J_{CF} = 256.5 Hz), 159.6, 133.1 (d, J_{CF} = 11.9 Hz), 132.2 (d, J_{CF} = 3.4 Hz), 129.7, 128.4, 123.4 (d, J_{CF} = 3.9 Hz), 119.6 (d, J_{CF} = 25.3 Hz), 117.8 (d, J_{CF} = 11.0 Hz), 113.7, 56.7 (t, J_{CF} = 5.67 Hz), 55.3. HR-EIMS m/z calculated for $\text{C}_{20}\text{H}_{12}\text{Br}_4\text{F}_2\text{NO}$ $[\text{M} - \text{H}]^+$: 639.7574, found: 639.7564.



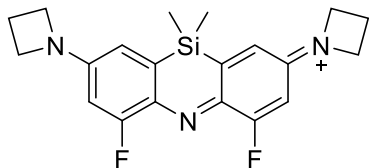
2,8-Dibromo-4,6-difluoro-5-(4-methoxybenzyl)-10,10-dimethyl-5,10-dihydrodibenzo[b,e][1,4] azasiline (3.11)

In a 50 mL oven-dried round bottom flask, compound **3.10** (642 mg, 1 mmol) was dissolved in anhydrous diethyl ether (25 mL) at room temperature and then cooled to -78 °C. *n*-BuLi (0.96 ml of 1.6 M, 2.4 mmol) was added drop-wise to the reaction. After 1 hour, dichlorodimethylsilane (645 mg, 5 mmol) was added and the reaction mixture was warmed to room temperature. After 4 hours, the product was extracted with ether (25 mL) and then washed with water (50 mL) and brine (50 mL) and dried over Na₂SO₄. The solvent was removed under reduced pressure and the product was purified by silica gel chromatography (0-50% DCM/hexanes). The resulting white solid was washed with MeOH (2 mL) and filtered to afford the product (114 mg, 0.21 mmol, 21%). ¹H NMR (500 MHz, CDCl₃) δ 7.30 (dd, *J* = 11.7, 2.2 Hz, 2H), 7.21 (d, *J* = 2.1 Hz, 2H), 6.80 – 6.73 (m, 2H), 6.71 – 6.62 (m, 2H), 4.86 (s, 2H), 3.70 (s, 3H), 0.46 (s, 3H), -0.26 (s, 3H). ¹⁹F NMR (471 MHz, CDCl₃) δ -113.89 (d, *J* = 11.6 Hz). ¹³C NMR (126 MHz, CDCl₃) δ 159.3, 156.2, 154.2, 137.9 (d, *J*_{CF} = 6.4 Hz), 134.0, 131.1 (d, *J*_{CF} = 4.0 Hz), 130.6, 129.4, 121.0 (d, *J*_{CF} = 24.8 Hz), 116.0 (d, *J*_{CF} = 7.6 Hz), 113.8, 58.0 (t, *J*_{CF} = 9.2 Hz), 55.4. HR-EIMS *m/z* calculated for C₂₂H₂₀Br₂F₂NOSiNa [M + Na]⁺: 561.9442, found: 561.9432.



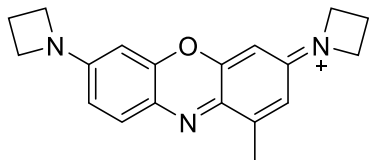
2,8-Di(azetidin-1-yl)-4,6-difluoro-5-(4-methoxybenzyl)-10,10-dimethyl-5,10-dihydrodibenzo [b,e][1,4]azasiline (3.12)

In a 15 mL sealed tube, compound **3.11** (50 mg, 0.093 mmol), $\text{Pd}_2(\text{dba})_3$ (4.2 mg, 0.0046 mmol), BINAP (5.8 mg, 0.009 mmol), sodium *tert*-butoxide (21 mg, 0.22 mmol) and azetidine (21 mg, 0.37 mmol) were dissolved in anhydrous toluene (2 mL). The reaction tube was flushed with argon, then heated to 110 °C. After 24 hours, the reaction mixture was filtered through Celite. The solvent was removed under reduced pressure and the product was purified by silica gel chromatography (0-30% EtOAc/hexanes) to afford a light yellow solid (46 mg, 0.093 mmol, quantitative). ^1H NMR (500 MHz, CDCl_3) δ 6.71 – 6.53 (m, 4H), 6.29 (dd, $J = 13.9, 2.5$ Hz, 2H), 6.13 (d, $J = 2.5$ Hz, 2H), 4.71 (s, 2H), 3.85 (t, $J = 7.2$ Hz, 8H), 3.69 (s, 3H), 2.34 (p, $J = 7.5$ Hz, 4H), 0.36 (s, 3H), -0.47 (s, 3H). ^{19}F NMR (471 MHz, CDCl_3) δ -117.72 (d, $J = 13.9$ Hz). ^{13}C NMR (126 MHz, CDCl_3) δ 158.9, 156.3 (d, $J_{\text{CF}} = 249.5$ Hz), 149.2 (d, $J_{\text{CF}} = 8.6$ Hz), 133.2, 130.9, 130.5 (t, $J_{\text{CF}} = 3.6$ Hz), 113.4, 110.1 (d, $J_{\text{CF}} = 3.1$ Hz), 101.6 (d, $J_{\text{CF}} = 24.9$ Hz), 58.5 (t, $J_{\text{CF}} = 7.4$ Hz), 55.3, 52.9, 17.0, -1.0, -2.6. HR-EIMS m/z = calculated for $\text{C}_{28}\text{H}_{32}\text{F}_2\text{N}_3\text{OSi}$ $[\text{M} + \text{H}]^+$: 492.2277, found: 492.2257.



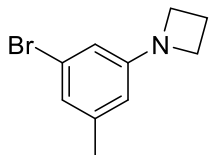
2,8-Di(azetidin-1-yl)-4,6-difluoro-5-(4-methoxybenzyl)-10,10-dimethyl-5,10-dihydrodibenzo[b,e][1,4]azasiline (3.13), ASiFluor710

In a 25 mL round bottom flask, compound **3.12** (20 mg, 0.04 mmol) was dissolved in MeOH (10 mL) at 0 °C. Iodine (21 mg, 0.08 mmol) was separately dissolved in MeOH (5 mL) and added to the reaction. After 20 minutes, the resulting green solid was collected by filtration and washed with hexane (10 mL). The product can used without further purification (13 mg, 0.028 mmol, 70%). To increase solubility 10 mg (0.021 mmol) was eluted through a reverse phase C18 column (20-85% ACN/H₂O, 0.1% TFA) to afford the TFA salt (4 mg, 0.008 mmol, 40%). ¹H NMR (500 MHz, CD₃CN) δ 6.83 (d, *J* = 2.3 Hz, 2H), 6.39 (dd, *J* = 12.3, 2.3 Hz, 2H), 4.62 – 4.20 (m, 8H), 2.53 (p, *J* = 8.0 Hz, 4H), 0.48 (s, 6H). ¹⁹F NMR (471 MHz, CD₃CN) δ -105.67 (d, *J* = 12.4 Hz). ¹³C NMR (126 MHz, CD₃CN) δ 166.5 (d, *J*_{CF} = 272.2 Hz), 157.3 (d, *J*_{CF} = 14.2 Hz), 140.1 (d, *J*_{CF} = 2.2 Hz), 134.9 (d, *J*_{CF} = 7.1 Hz), 120.5, 100.2 (d, *J*_{CF} = 25.2 Hz), 55 – 54 (m), 16.4, -1.0. HR-EIMS *m/z* [M]⁺ calculated for C₂₀H₂₂F₂N₃Si [M + H]⁺: 370.1546, found: 370.1545.



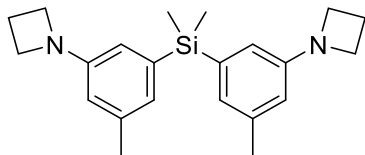
1-(7-(Azetidin-1-yl)-1-methyl-3H-phenoxazin-3-ylidene)azetidin-1-ium (3.13')

In a 50 mL round bottom flask, compound **3.13** (6 mg, 0.01 mmol) was dissolved in acetonitrile (10 mL) and PBS (10 mL) and stirred in the dark at room temperature. After 48 hours, the reaction was poured into brine (50 mL) and extracted with acetonitrile (3 X 20 mL). The combined organic layers were washed with brine (50 mL) and dried over sodium sulfate. The solvent was removed under reduced pressure and the product was purified by preparatory HPLC (0-65% 0.1% TFA ACN/H₂O) to afford a blue solid (>1 mg). ¹H NMR (500 MHz, MeOD) δ 7.75 (d, J = 9.2 Hz, 1H), 6.87 (dd, J = 9.2, 2.4 Hz, 1H), 6.83 – 6.79 (m, 1H), 6.46 (d, J = 2.4 Hz, 1H), 6.40 (d, J = 2.4 Hz, 1H), 4.52 – 4.32 (m, 8H), 2.64 – 2.49 (m, 7H). HR-EIMS m/z calculated for C₁₉H₂₀N₃O M⁺: 306.1601, found: 306.1596.



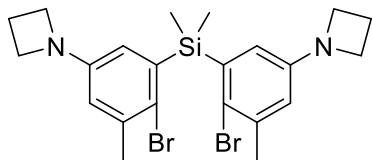
1-(3-Bromo-5-methylphenyl)azetidine (3.14)

In a 75 mL sealed pressure tube, 2,5-dibromotoluene (4 g, 16 mmol), azetidine (457 mg, 8 mmol), $\text{Pd}_2(\text{dba})_3$ (366 mg, 0.4 mmol), BINAP (498 mg, 0.8 mmol), and sodium *tert*-butoxide (921 mg, 9.6 mmol) were dissolved in anhydrous toluene (62 mL). The reaction was heated to 110 °C for 24 hours. The reaction was then filtered through Celite and the solvent was removed under reduced pressure. The product was purified with silica gel chromatography (0-30% EtOAc/hexanes) to afford a white solid (1.2 g, 5.3 mmol, 66%). ^1H NMR (500 MHz, CDCl_3) δ 6.68 (s, 1H), 6.39 – 6.35 (m, 1H), 6.14 (s, 1H), 3.85 (t, $J = 7.2$ Hz, 4H), 2.35 (p, $J = 7.5$ Hz, 2H), 2.25 (s, 3H). ^{13}C NMR (126 MHz, CDCl_3) δ 153.1, 140.5, 122.8, 120.9, 111.3, 110.6, 52.3, 21.4, 16.9. HR-EIMS m/z calculated for $\text{C}_{10}\text{H}_{13}\text{BrN}$ $[\text{M} + \text{H}]^+$: 226.0226, found: 226.0197.



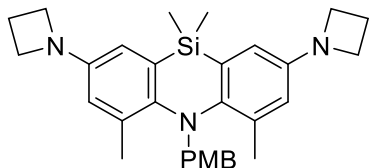
Bis(3-(azetidin-1-yl)-5-methylphenyl)dimethylsilane (3.15)

In a 100 mL oven-dried round bottom flask, compound **3.14** (500 mg, 2.21 mmol) was dissolved in anhydrous diethyl ether (50 mL) and anhydrous THF (1 mL) at room temperature and then cooled to 0 °C. *n*-BuLi (1.76 ml of 2.5 M, 4.4 mmol) was added drop-wise to the reaction. After 1 hour, dichlorodimethylsilane (171 mg, 1.3 mmol) was added and the reaction was warmed to room temperature. After 16 hours, the reaction was poured into water (20 mL), and the product was extracted with diethyl ether (25 mL). The combined organic layers were washed with water (50 mL) and brine (50 mL), then dried over Na₂SO₄. The solvent was removed under reduced pressure and the product was purified by silica gel chromatography (0-50% DCM/hexanes) to afford a yellow solid (170 mg, 0.49 mmol, 44%). ¹H NMR (500 MHz, CDCl₃) δ 6.72 (s, 2H), 6.44 (d, *J* = 2.2 Hz, 2H), 6.38 – 6.25 (m, 2H), 3.85 (t, *J* = 7.2 Hz, 8H), 2.33 (p, *J* = 7.5 Hz, 4H), 2.28 (s, 6H), 0.48 (s, 6H). ¹³C NMR (126 MHz, CDCl₃) δ 151.8, 138.9, 137.9, 124.4, 114.2, 113.1, 52.6, 21.8, 17.2, -2.0. HR-EIMS *m/z* calculated for C₂₂H₃₁N₂Si [M + H]⁺: 351.2251, found: 351.2261.



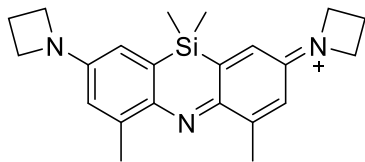
Bis(5-(azetidin-1-yl)-2-bromo-3-methylphenyl)dimethylsilane (3.16)

In a 50 ml round bottom flask, **3.15** (170 mg, 0.48 mmol) was dissolved in dichloromethane (19 mL) at 0 °C. NBS (172 mg, 0.97 mmol) was separately dissolved in dichloromethane (1 mL) and added dropwise to the reaction. After 15 minutes, the solvent was removed under reduced pressure and the product was purified by silica gel chromatography (0-20% EtOAc/hexanes) to afford a white solid (170 mg, 0.35 mmol, 74%). ¹H NMR (500 MHz, CDCl₃) δ 6.39 (d, *J*=2.8 Hz, 2H), 6.33 (d, *J*= 2.7, 2 H), 3.80 (t, *J*= 7.2 Hz, 8H), 2.37 – 2.27 (m, 10H), 0.71 (s, 6H). ¹³C NMR (126 MHz, CDCl₃) δ 150.8, 140.2, 138.2, 120.5, 118.4, 115.0, 52.6, 24.3, 17.1, -0.2. HR-EIMS *m/z* calculated for C₂₂H₂₉Br₂N₂Si [M + H]⁺: 509.0441, found: 509.0457.



2,8-Di(azetidin-1-yl)-5-(4-methoxybenzyl)-4,6,10,10-tetramethyl-5,10-dihydrodibenzo [b,e][1,4]azasiline (3.17)

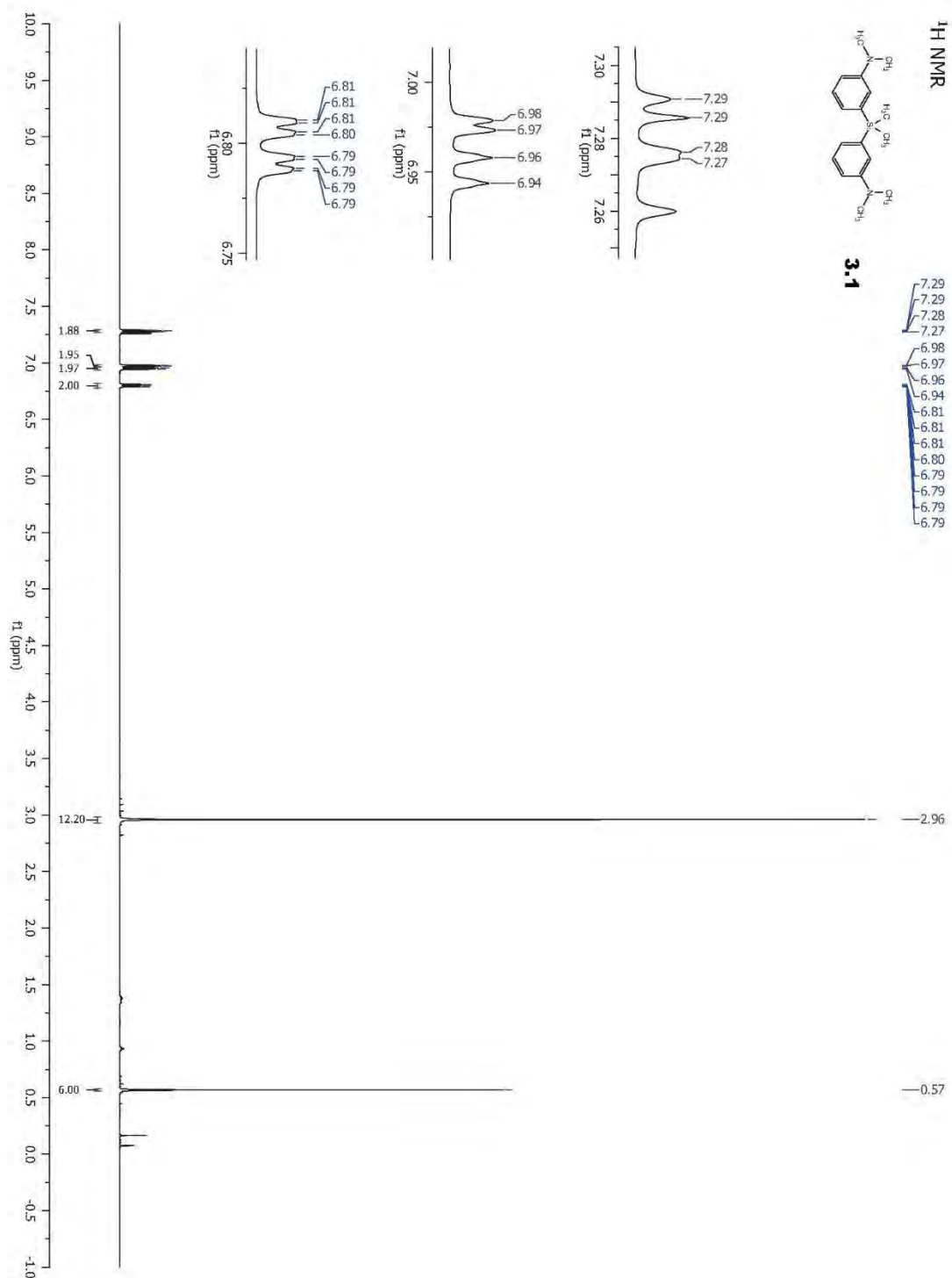
In a 15 mL sealed tube, compound **3.16** (150 mg, 0.3 mmol), $\text{Pd}_2(\text{dba})_3$ (13.7 mg, 0.015 mmol), BINAP (18.4 mg 0.03 mmol), sodium *tert*-butoxide (68 mg, 0.71 mmol) and 4-methoxybenzylamine (49 mg, 0.35 mmol) were dissolved in anhydrous toluene (3 mL). The reaction tube was flushed with argon, then heated to 110 °C. After 48 hours the reaction mixture was filtered through Celite. The solvent was removed under reduced pressure and the product was purified by silica gel chromatography (0-20% EtOAc/hexanes) to afford a yellow solid (50 mg, 0.1 mmol, 33%). ^1H NMR (500 MHz, CDCl_3) δ 6.61 (d, J = 8.6 Hz, 2H), 6.51 (d, J = 8.6 Hz, 2H), 6.37 (d, J = 2.6 Hz, 2H), 6.34 (d, J = 2.7 Hz, 2H), 4.15 (s, 2H), 3.85 (t, J = 7.1 Hz, 8H), 3.72 (s, 3H), 2.40 (s, 6H), 2.33 (p, J = 7.0 Hz, 4H), 0.31 (s, 3H), -0.24 (s, 3H). ^{13}C NMR (126 MHz, CDCl_3) δ 158.8, 148.6, 144.9, 134.5, 134.1, 132.0, 130.2, 115.8, 113.8, 113.2, 61.8, 55.4, 52.9, 19.6, 17.2, -0.4, -1.5. HR-EIMS m/z calculated for $\text{C}_{30}\text{H}_{38}\text{N}_3\text{OSi}$ $[\text{M} + \text{H}]^+$: 484.2779, found: 484.2762.

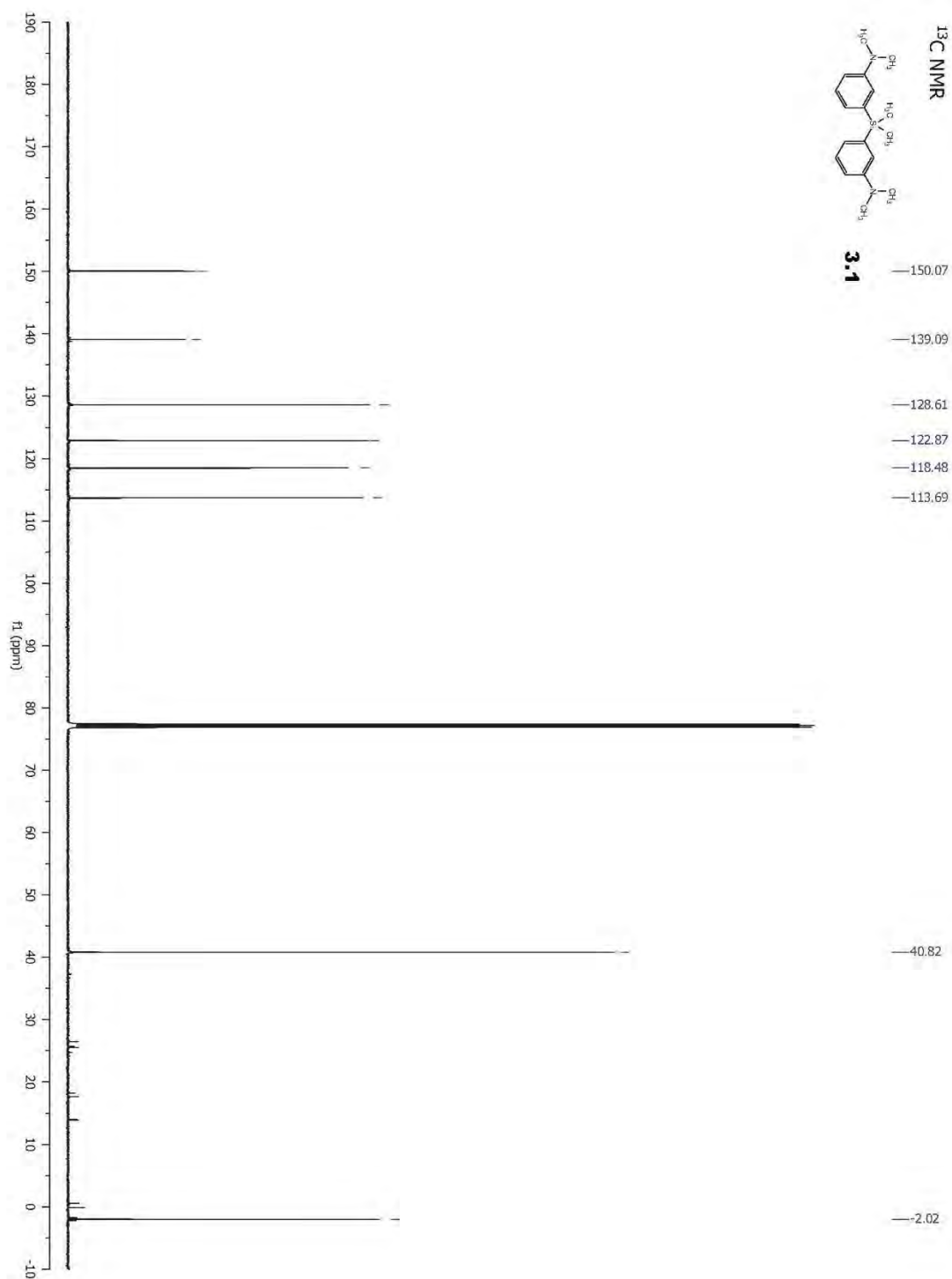


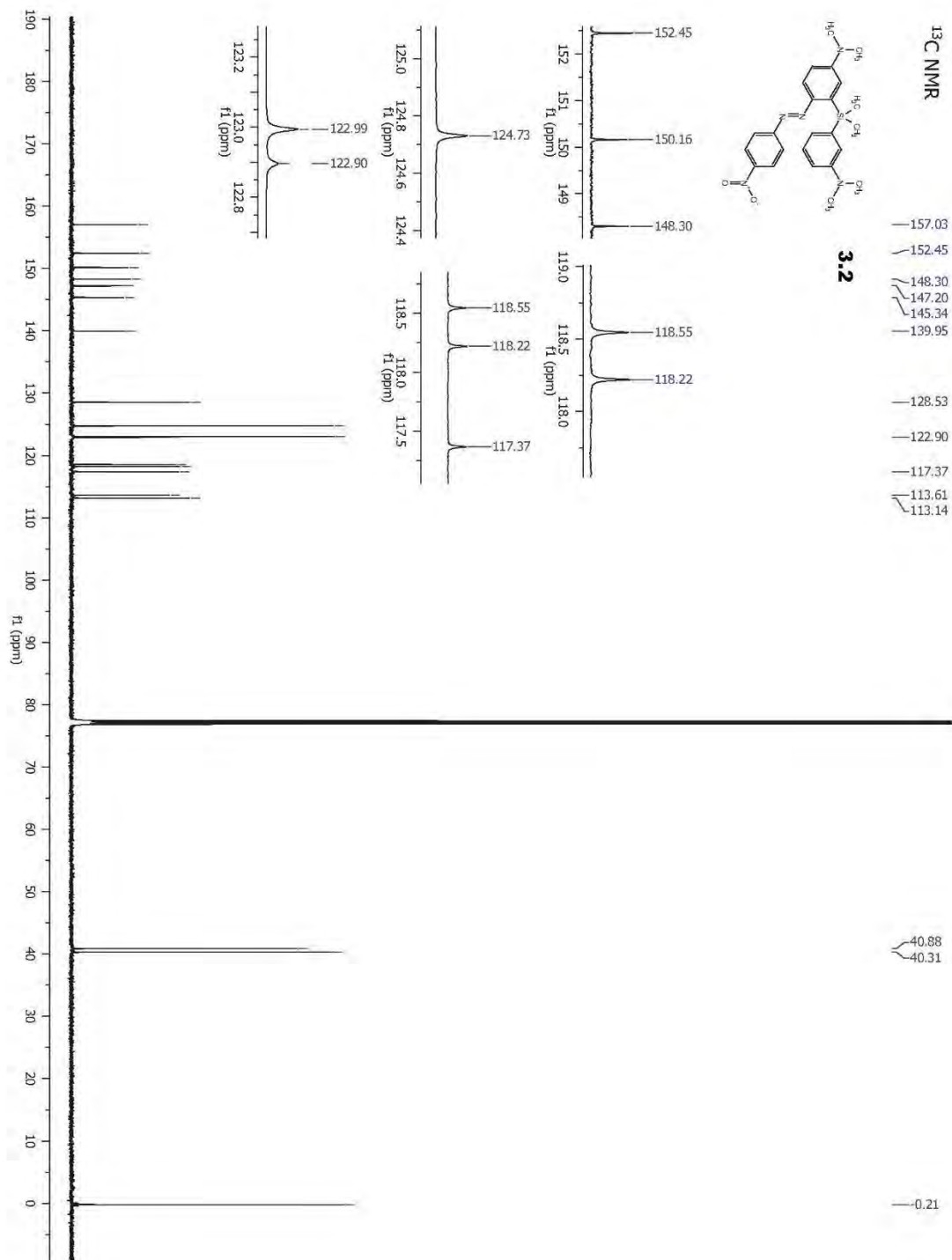
1-(8-(Azetidin-1-yl)-4,6,10,10-tetramethyldibenzo[b,e][1,4]azasilin-2(10H)-ylidene)azetidin-1-ium (3.18), ASiFluor730

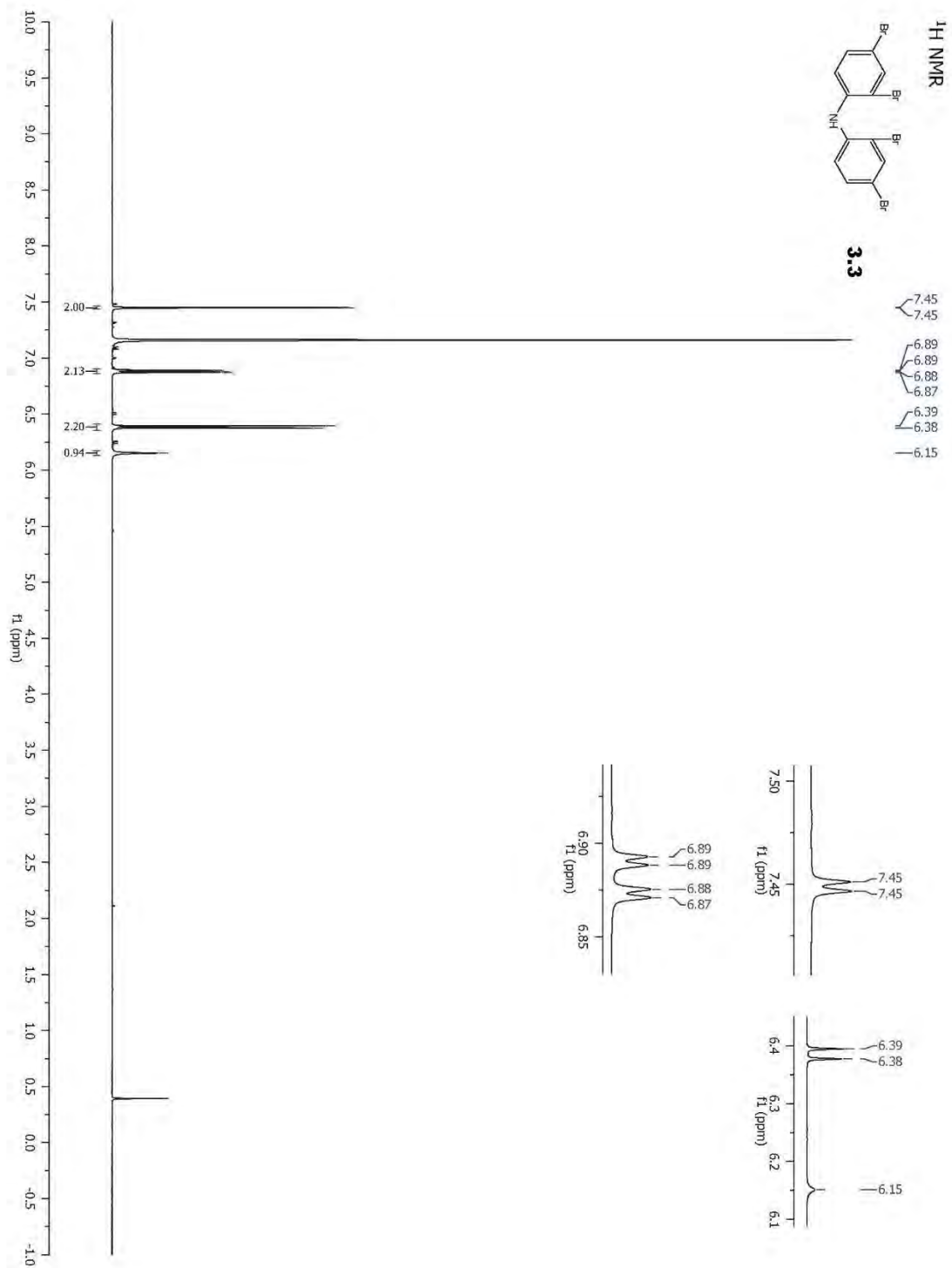
In a 25 mL round bottom flask, compound **3.17** (8.5 mg, 0.018 mmol) was dissolved in MeOH (1 mL) at 0 °C. Iodine (4.4 mg, 0.176 mmol) was separately dissolved in MeOH (5 mL) and then added to the reaction. After 15 minutes, the solvent was removed under reduced pressure and the product was purified by silica gel chromatography (0-20% MeOH/DCM). The product was further purified with preparatory HPLC (20-85% 0.1% TFA ACN/H₂O) to afford a green solid (3 mg, 0.006 mmol, 36%). ¹H NMR (500 MHz, MeOD) δ 6.88 (d, *J* = 2.6 Hz, 2H), 6.59 – 6.55 (m, 2H), 4.47 (t, *J* = 7.7 Hz, 8H), 2.57 (p, *J* = 7.5 Hz, 4H), 2.50 (s, 6H), 0.44 (s, 6H). ¹³C NMR (126 MHz, MeOD) δ 155.2, 154.2, 144.4, 140.5, 121.3, 115.0, 53.7, 19.8, 16.7, -1.4. HR-EIMS *m/z* calculated for C₂₂H₂₈N₃Si M⁺: 362.2047, found: 362.2043.

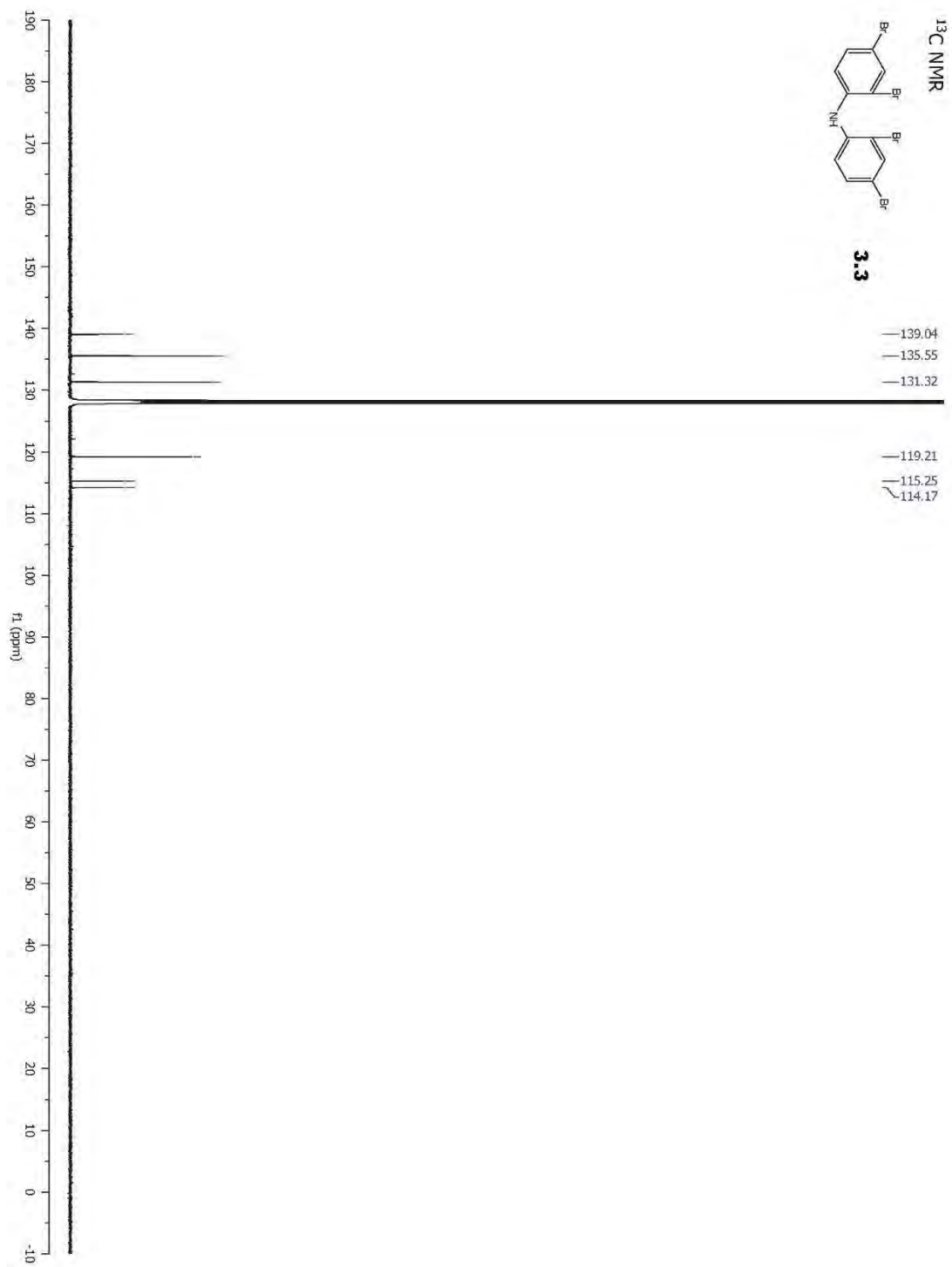
NMR Spectra

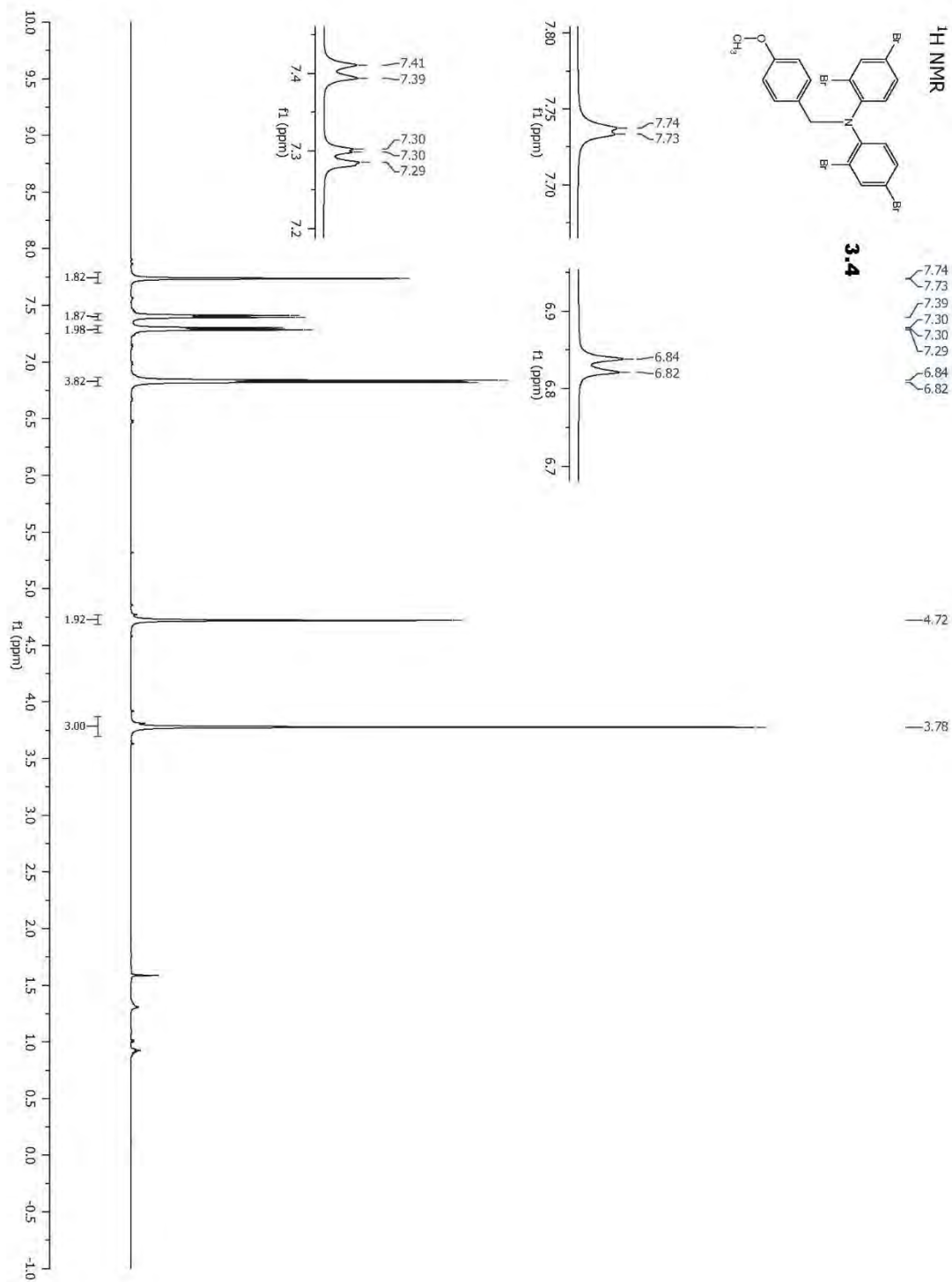


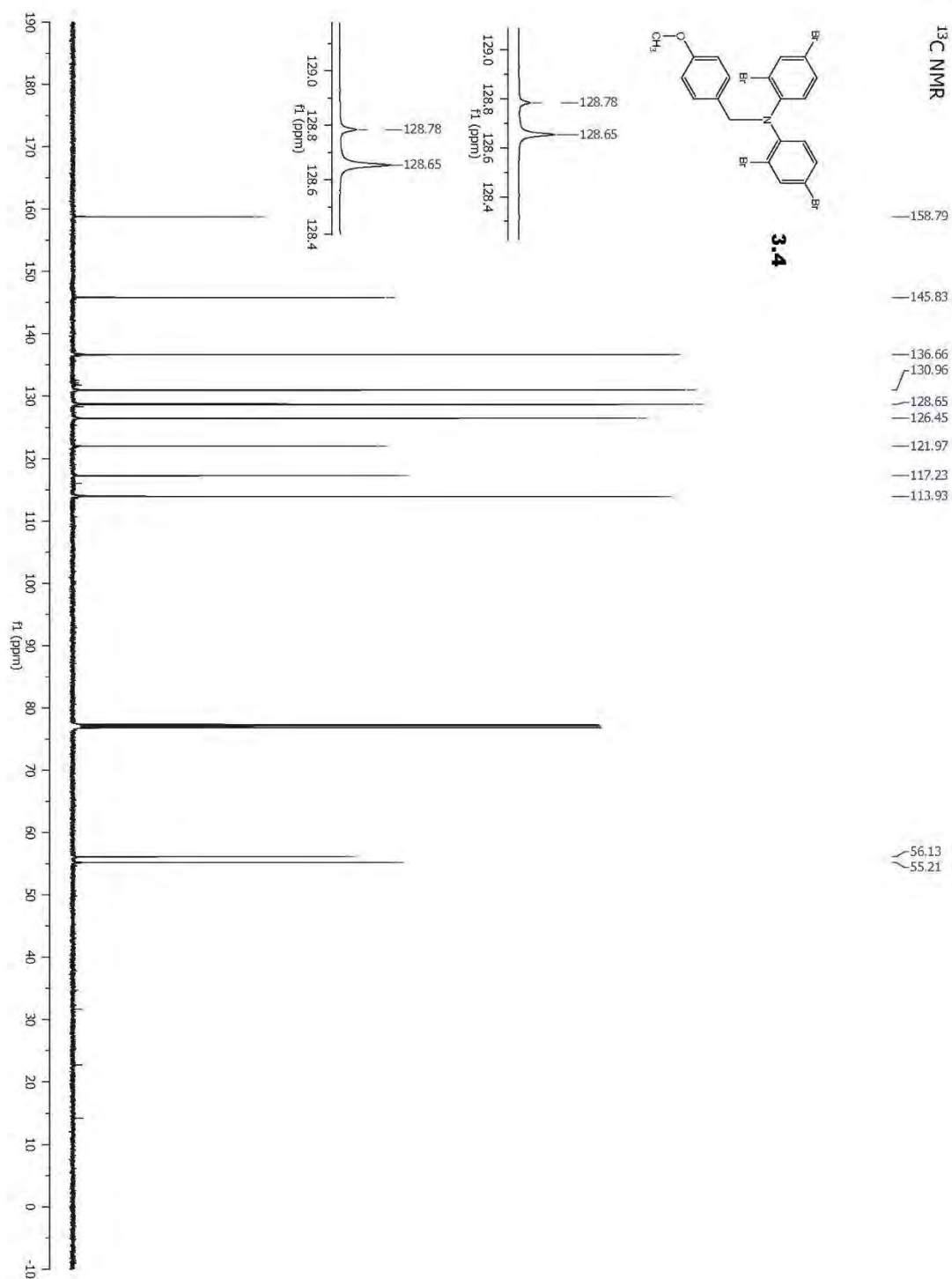


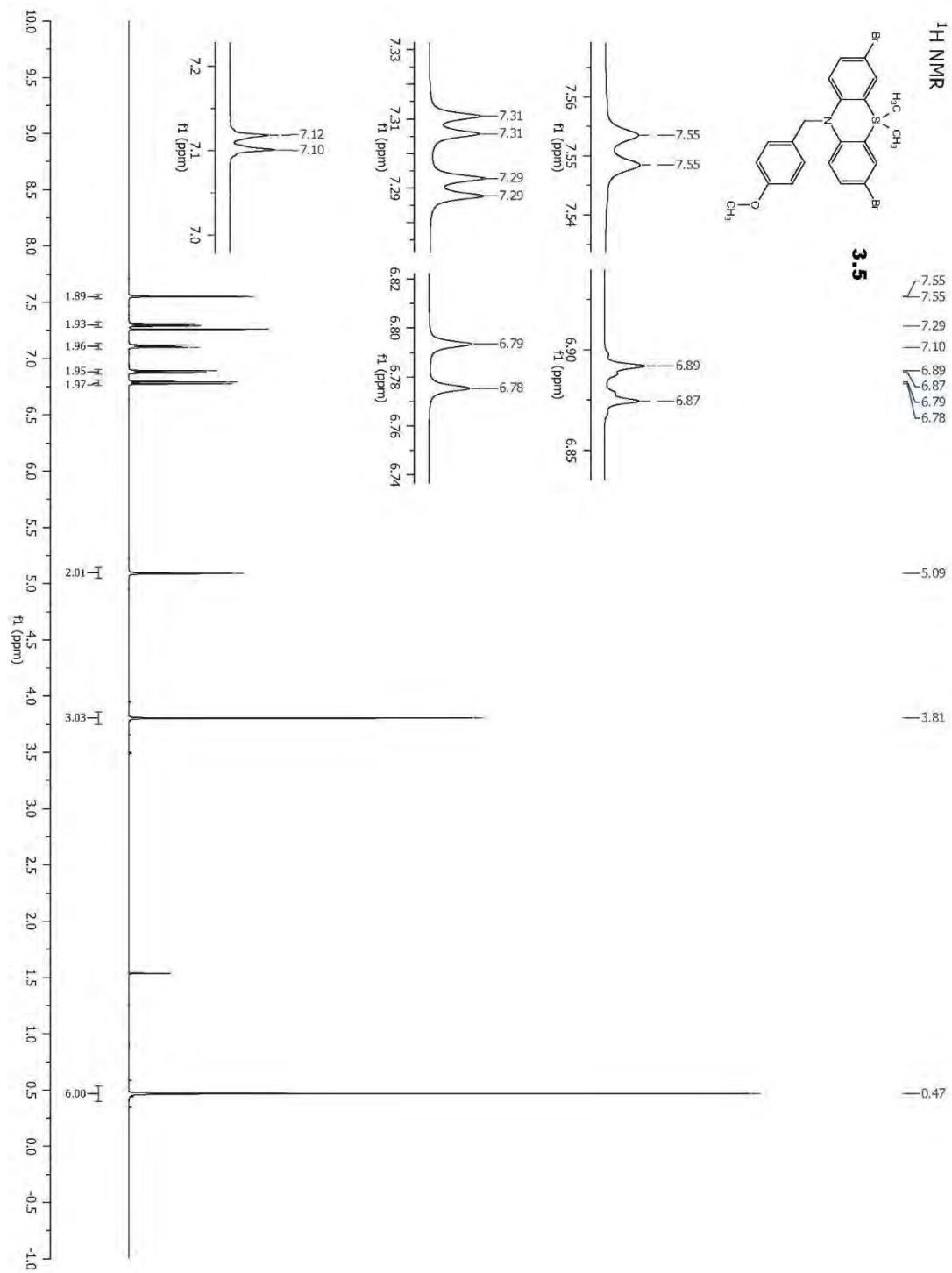


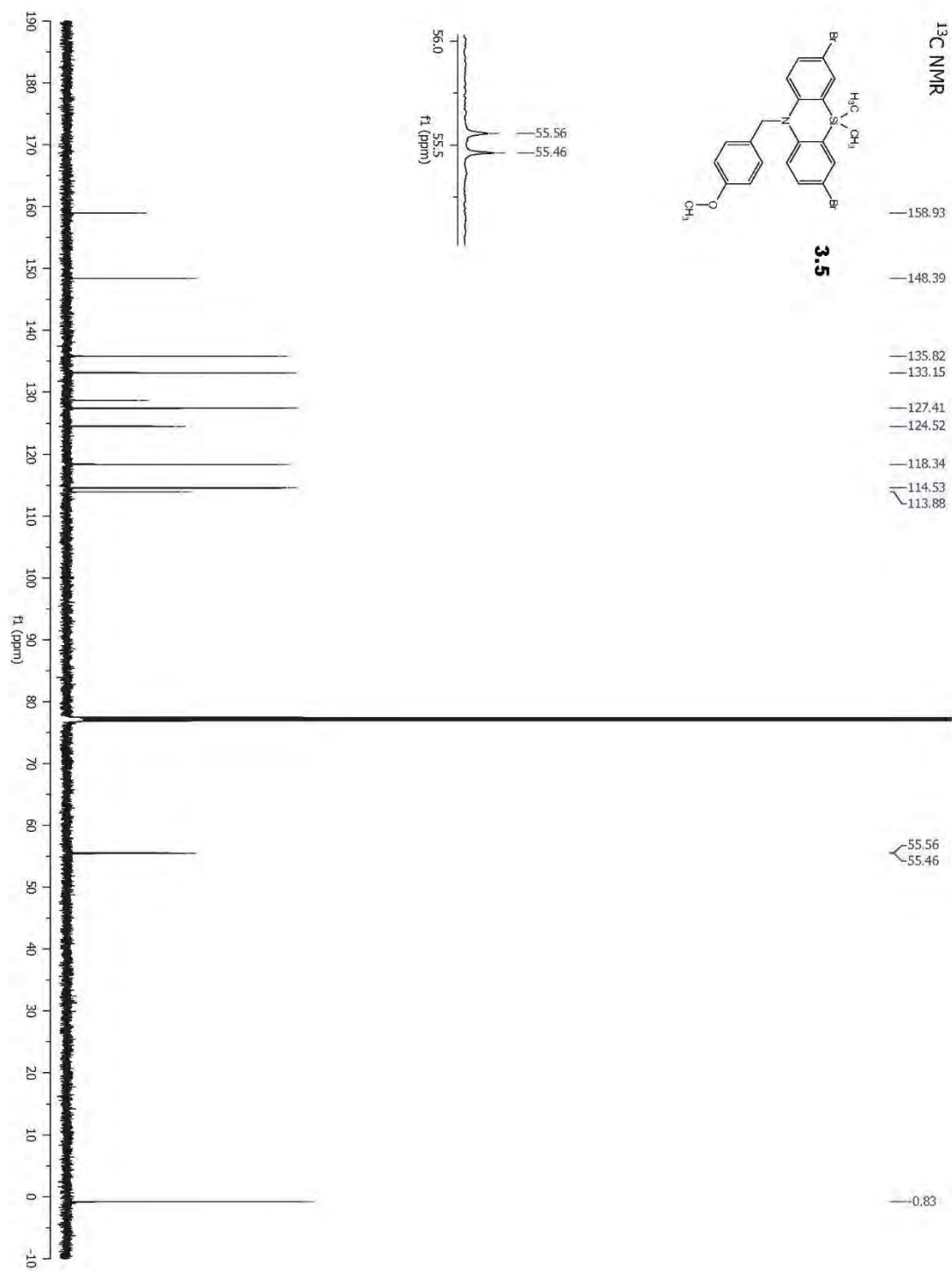


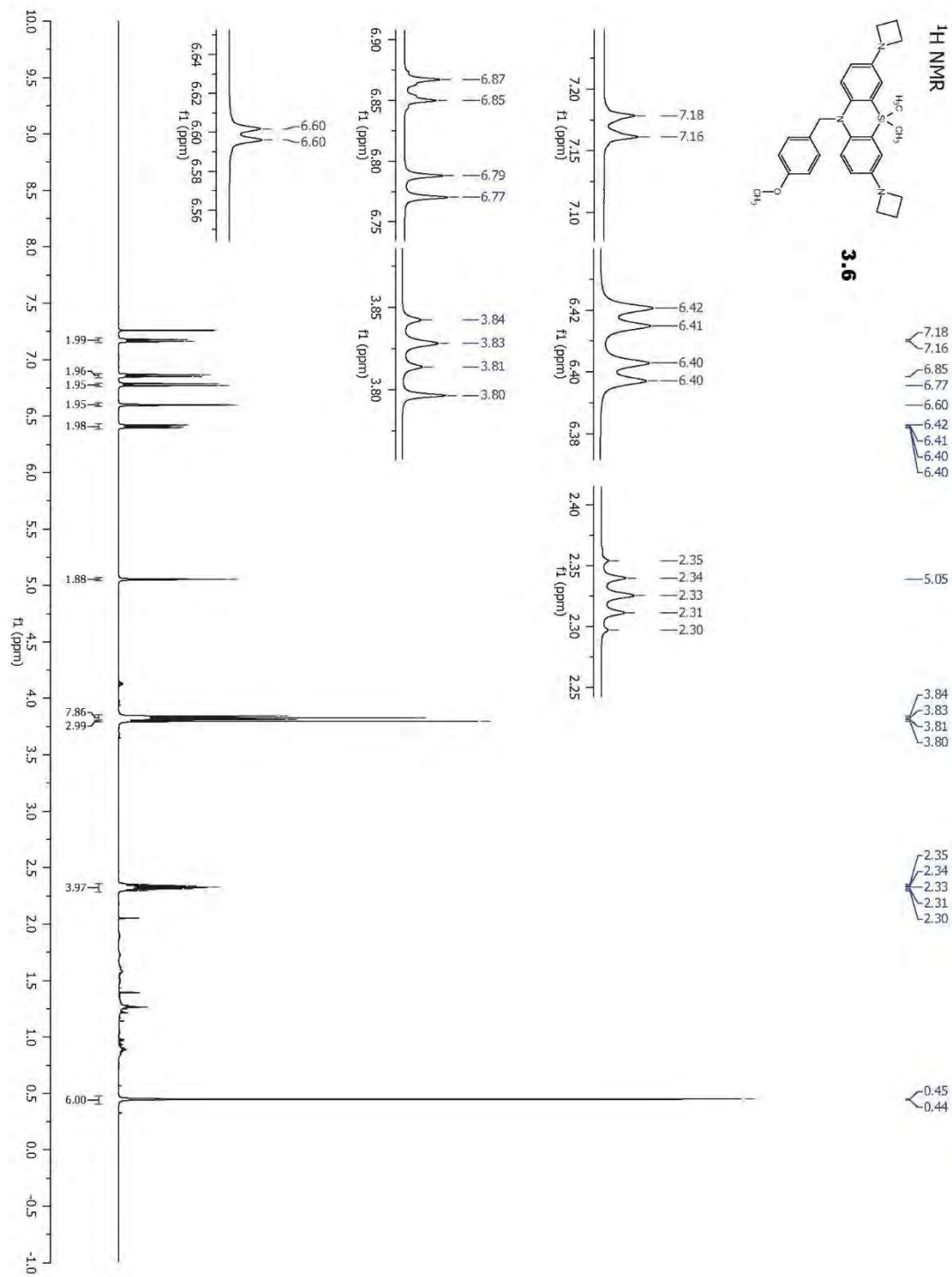


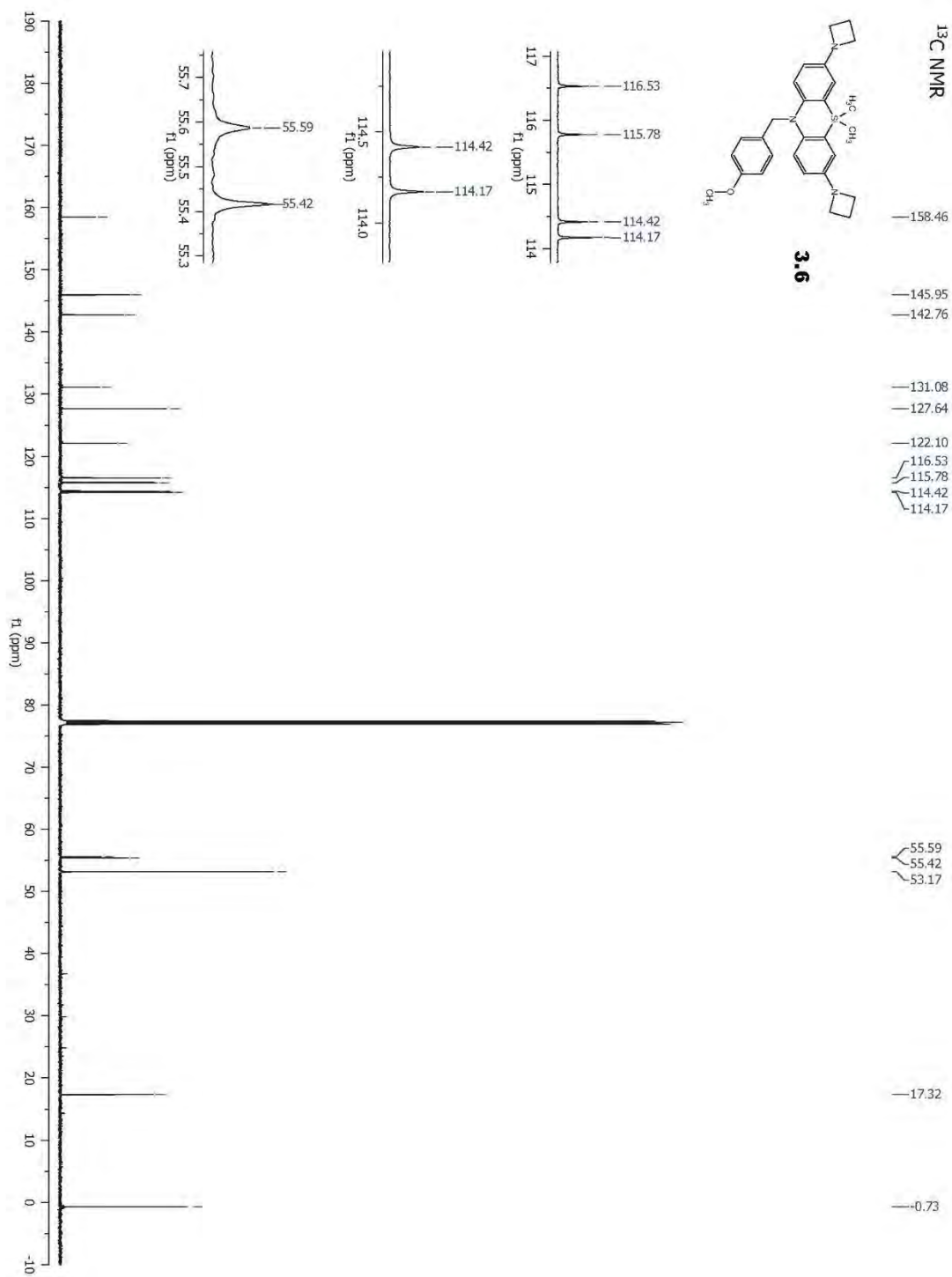


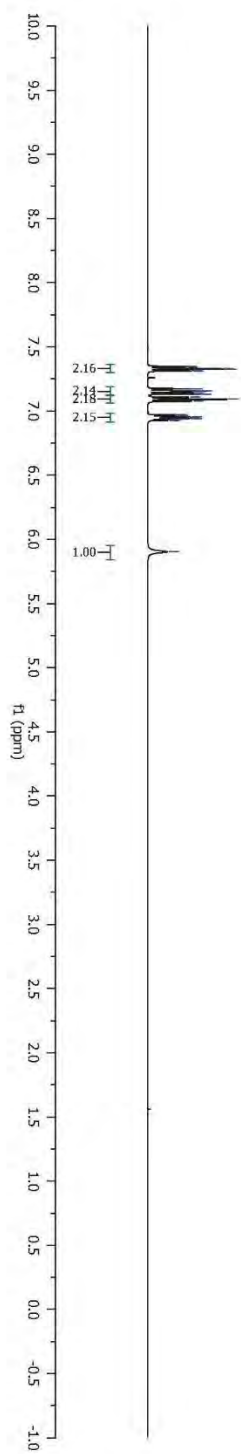
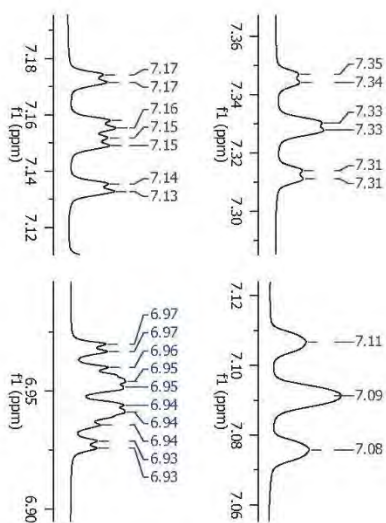
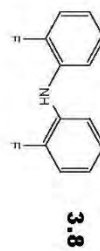


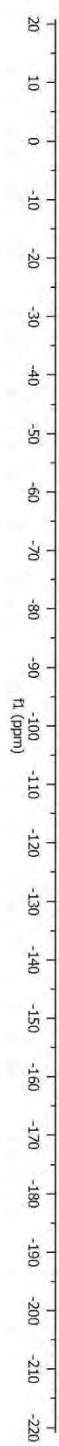
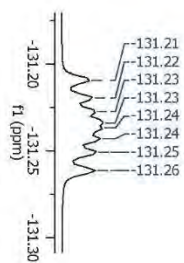
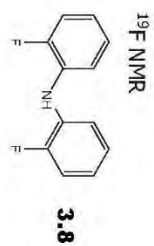


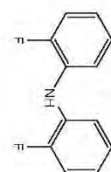
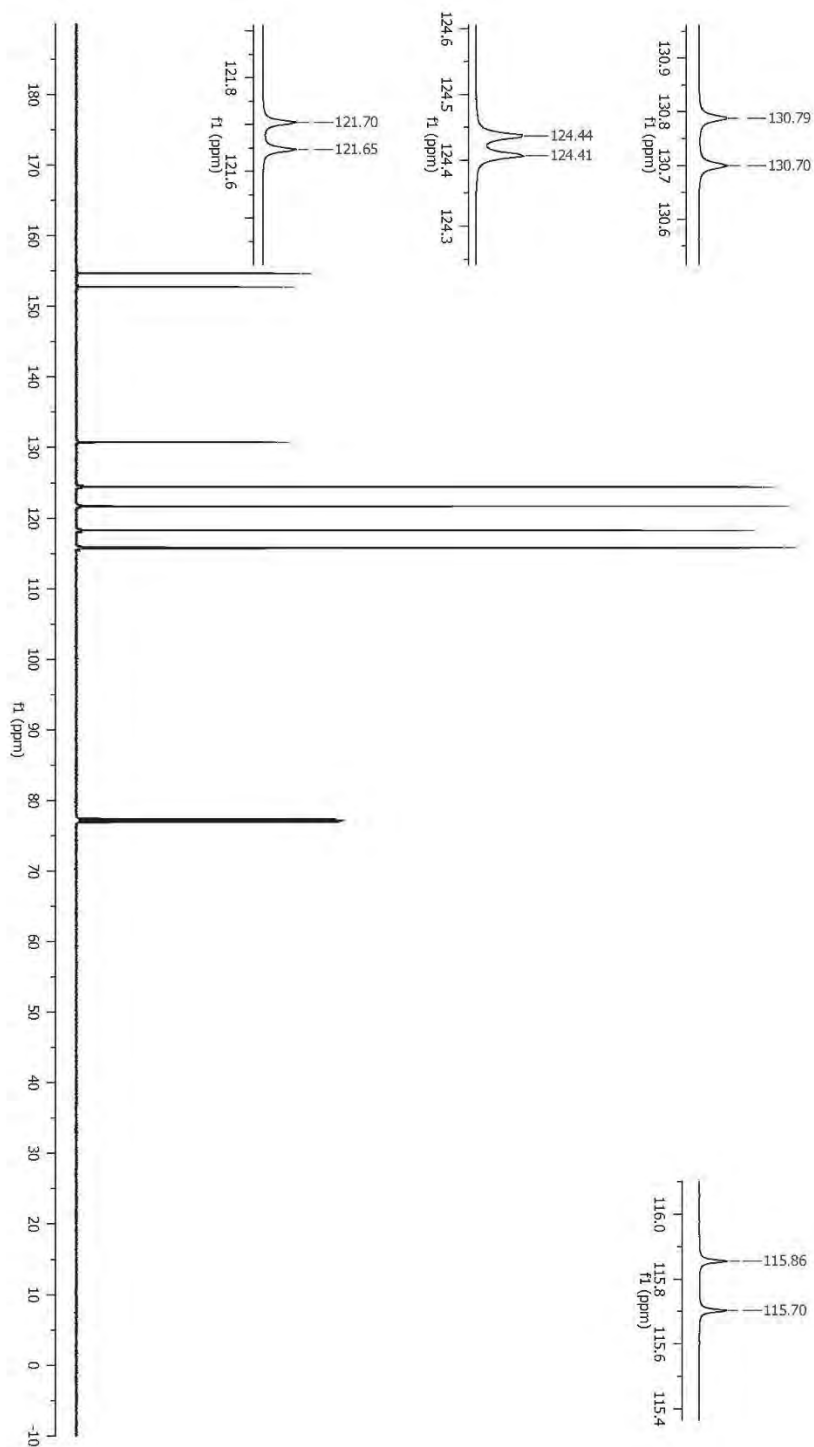


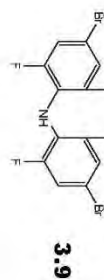






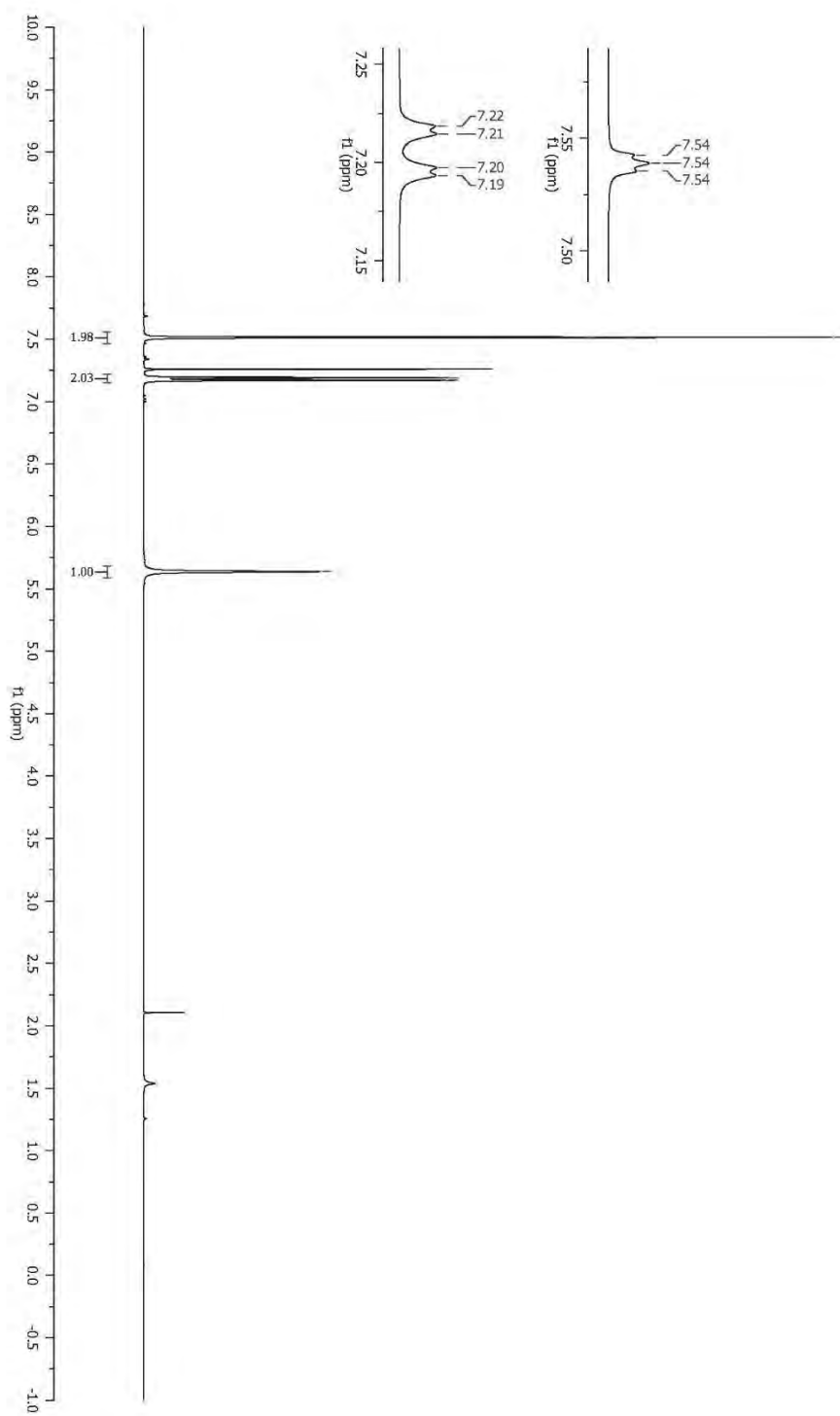


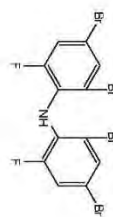
^{13}C NMR**3.8**154.68
152.76130.79
130.70
124.44
124.41
121.65
118.27
118.26
115.86
115.70

¹H NMR

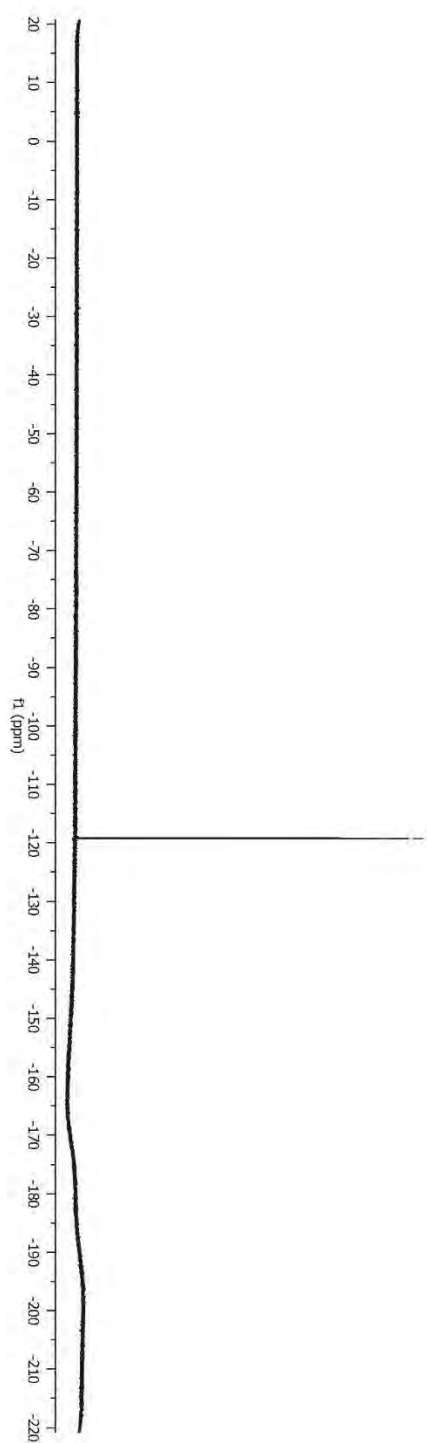
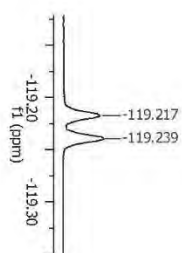
7.52
7.51
7.51
7.19
7.19
7.17
7.17

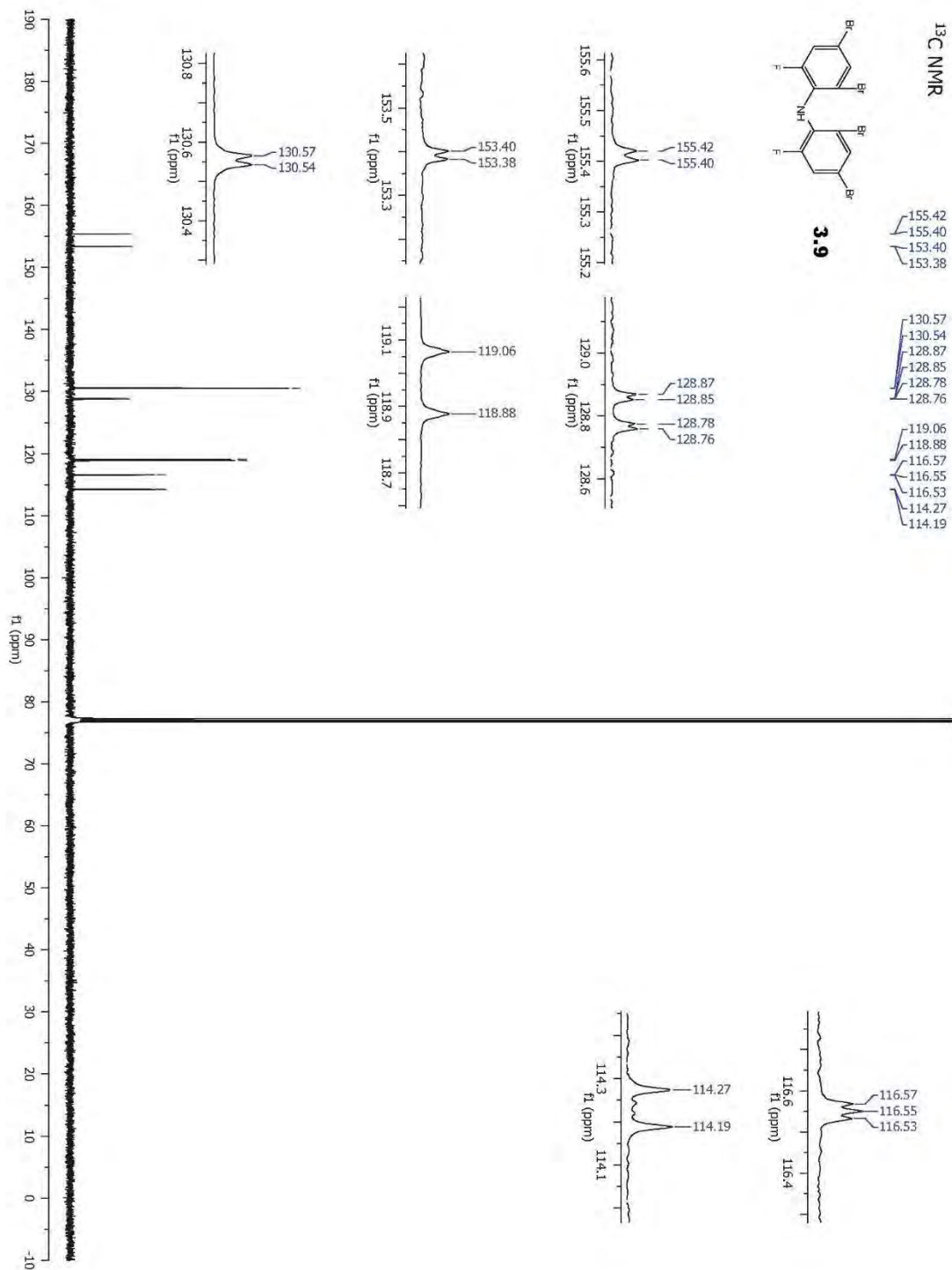
5.64

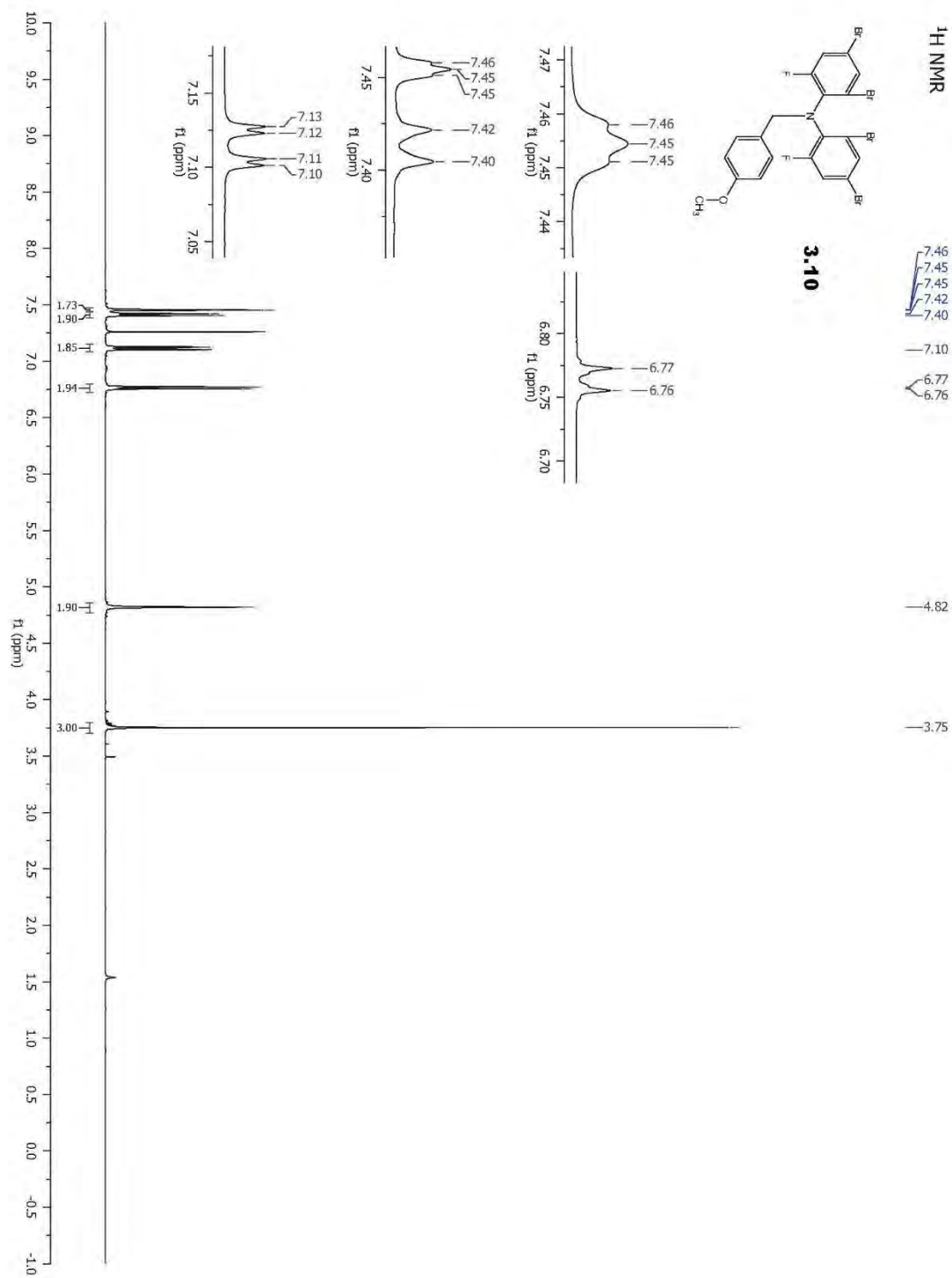


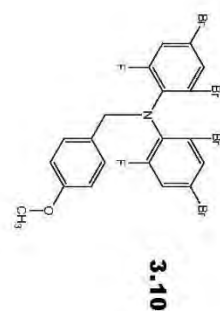
¹⁹F NMR**3.9**

-119.22
-119.24

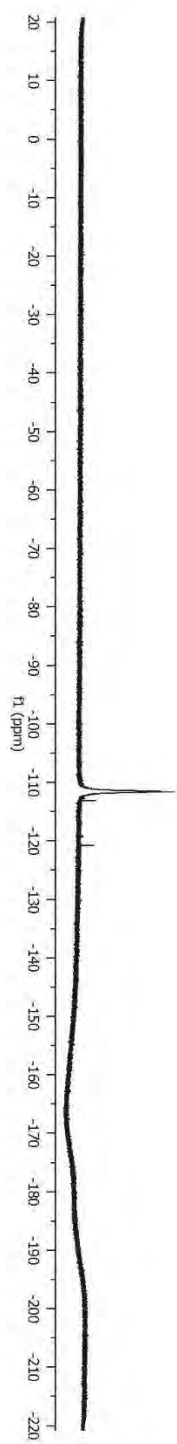
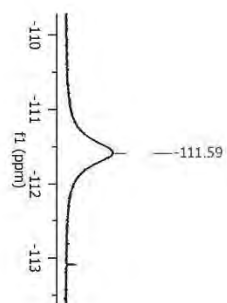


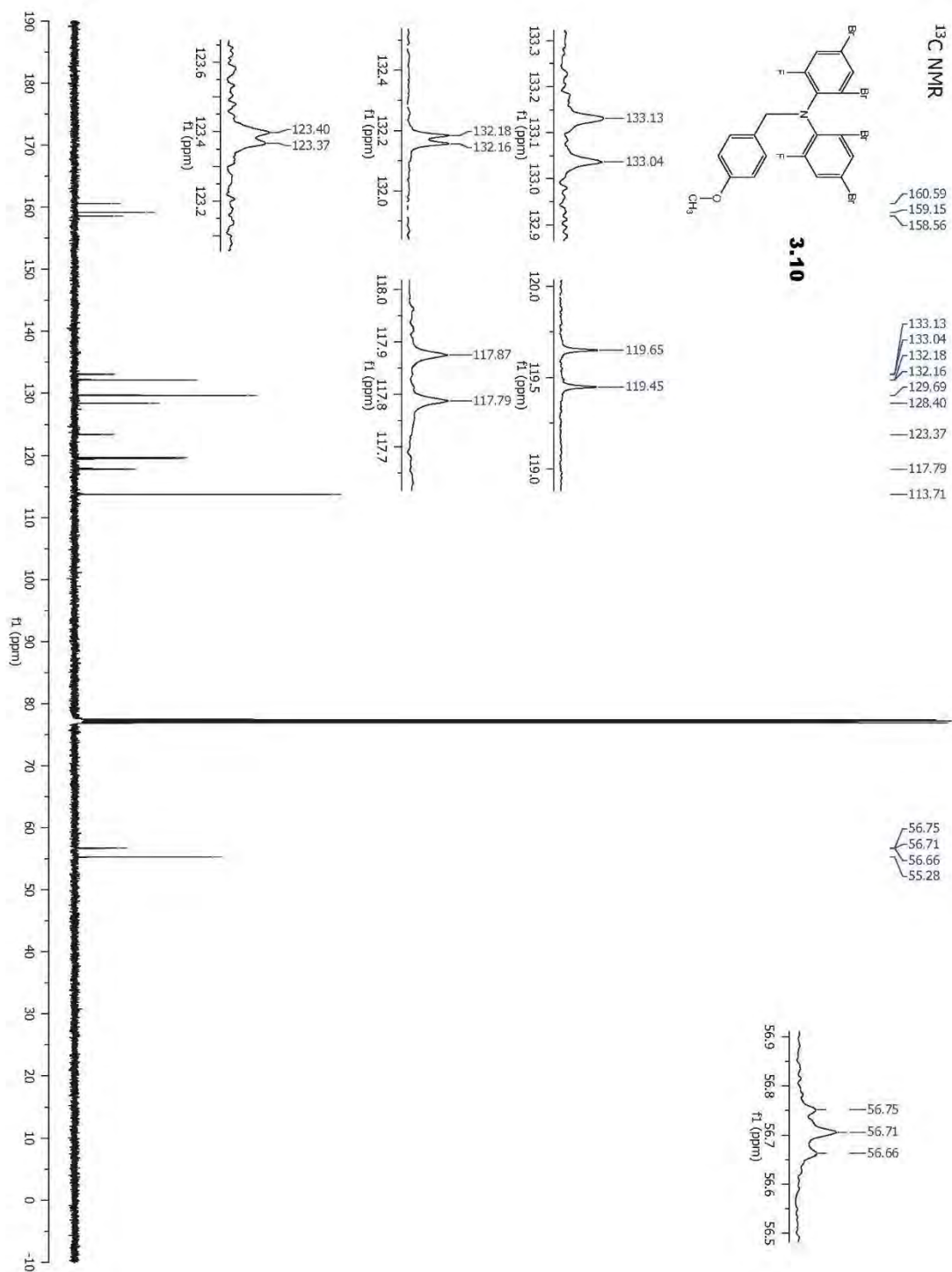


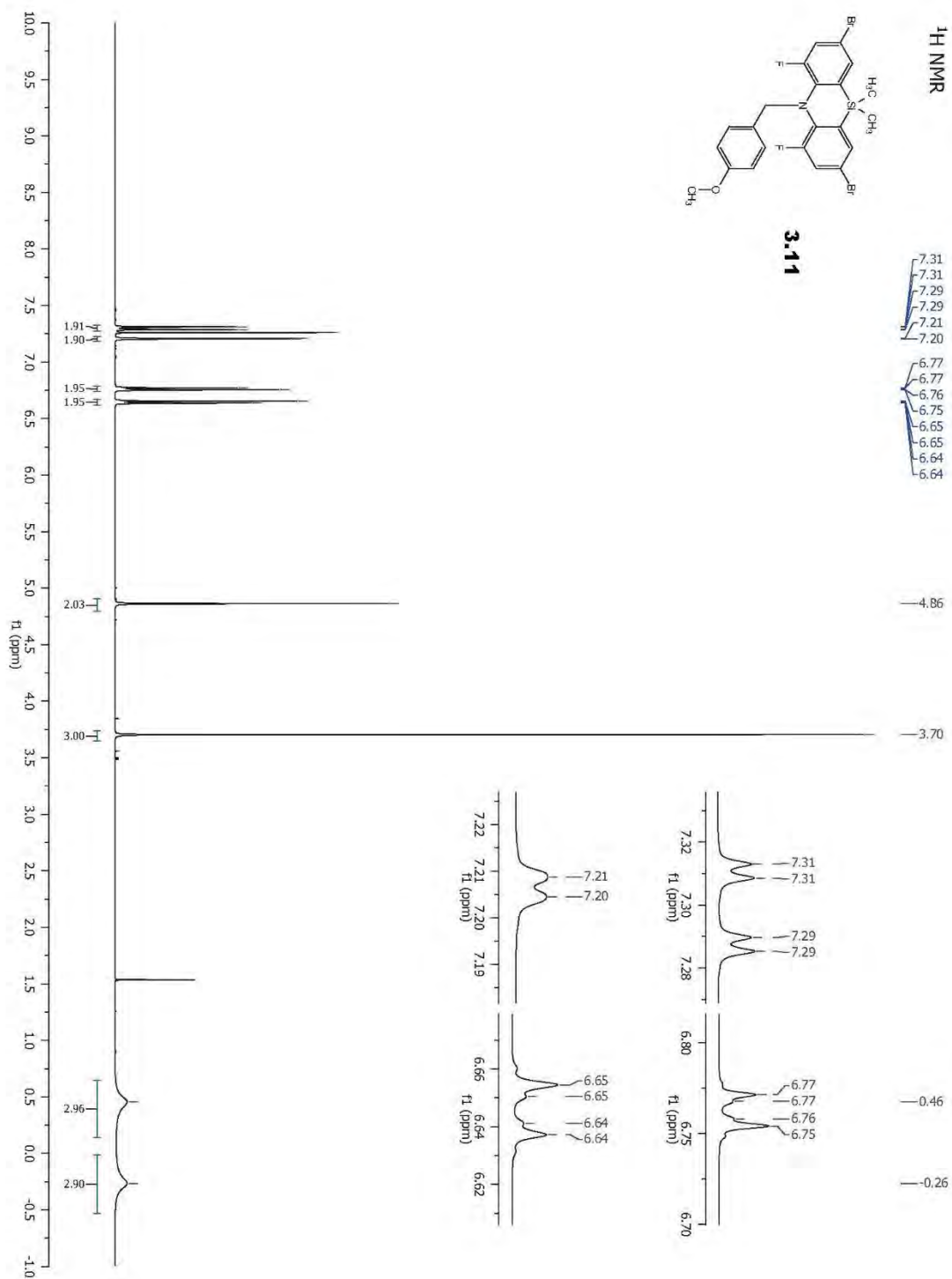


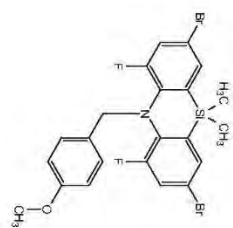
¹⁹F NMR

-111.59

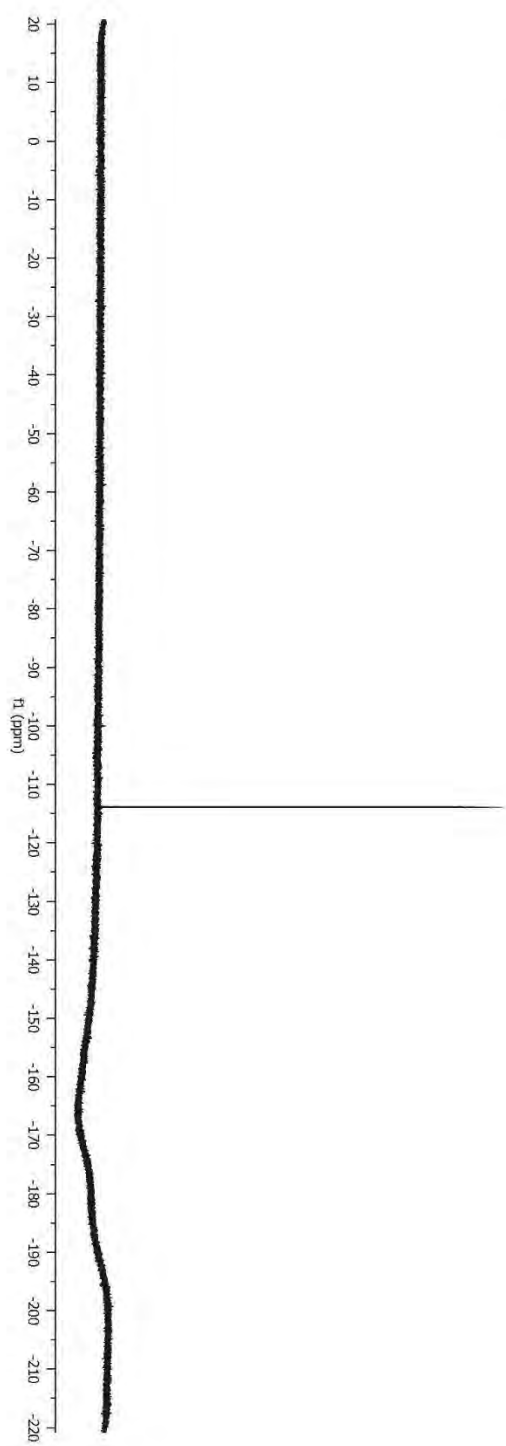
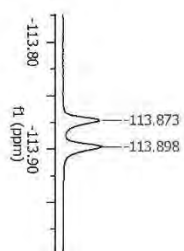


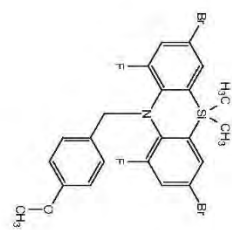
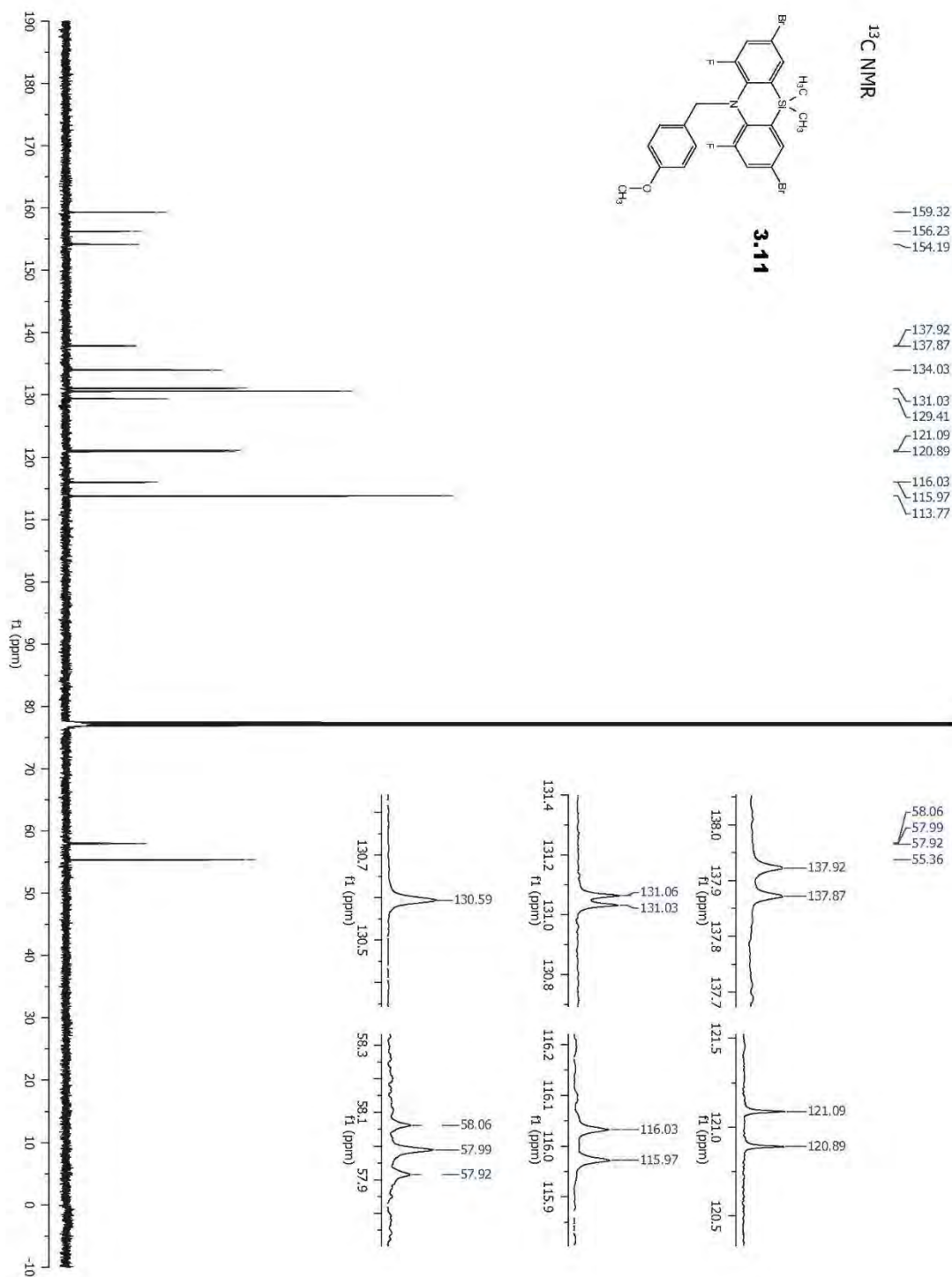


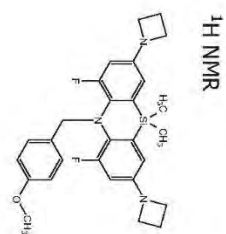


¹⁹F NMR**3.11**

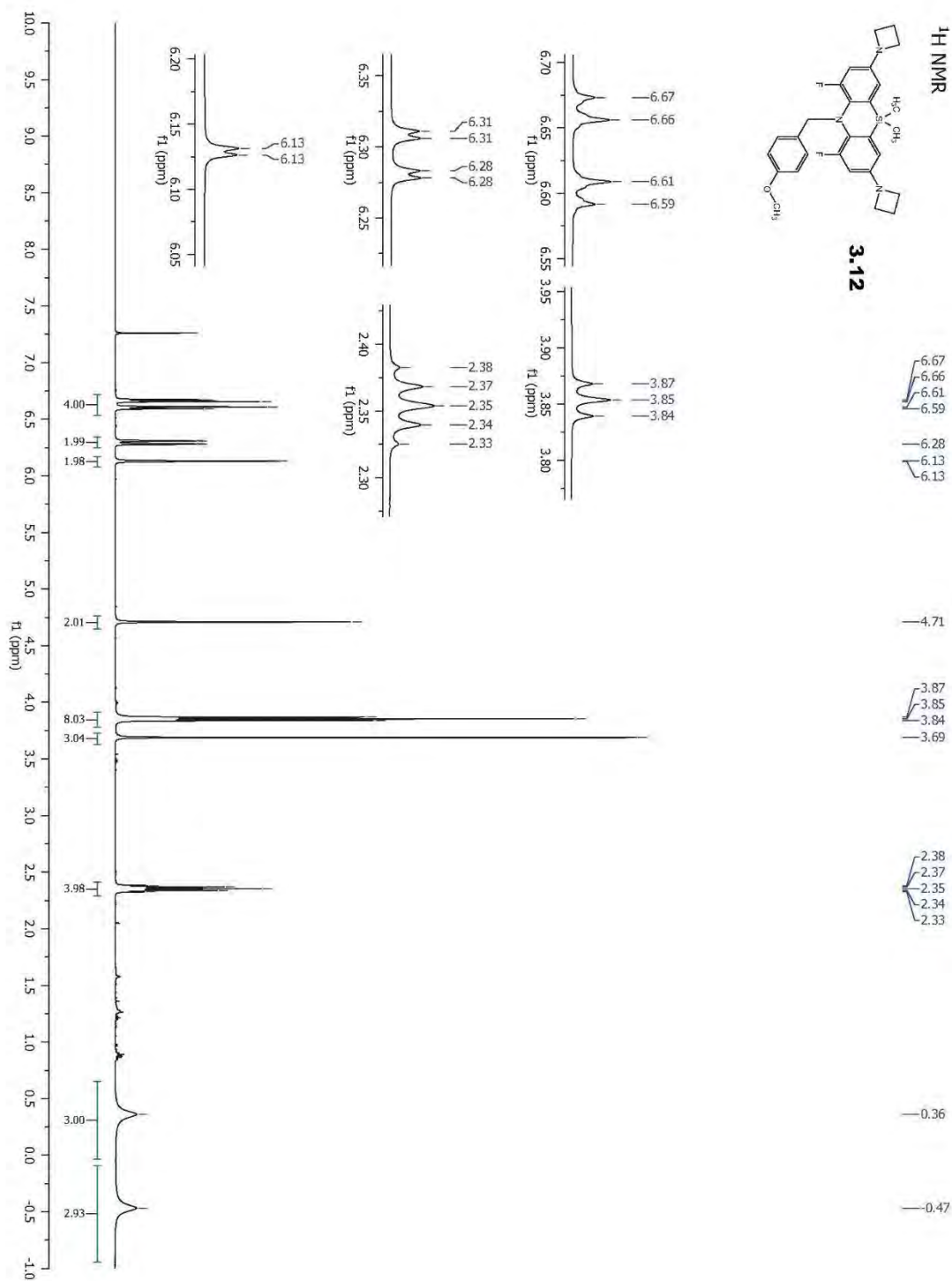
-113.87
-113.90

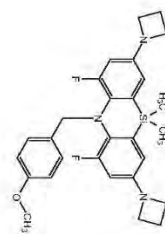


¹³C NMR**3.11**

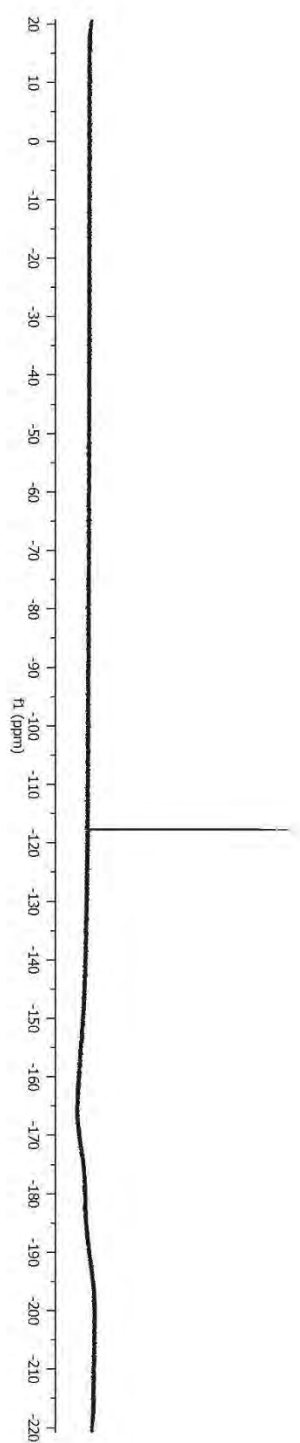
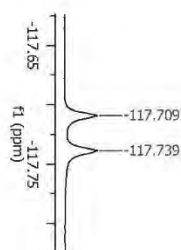


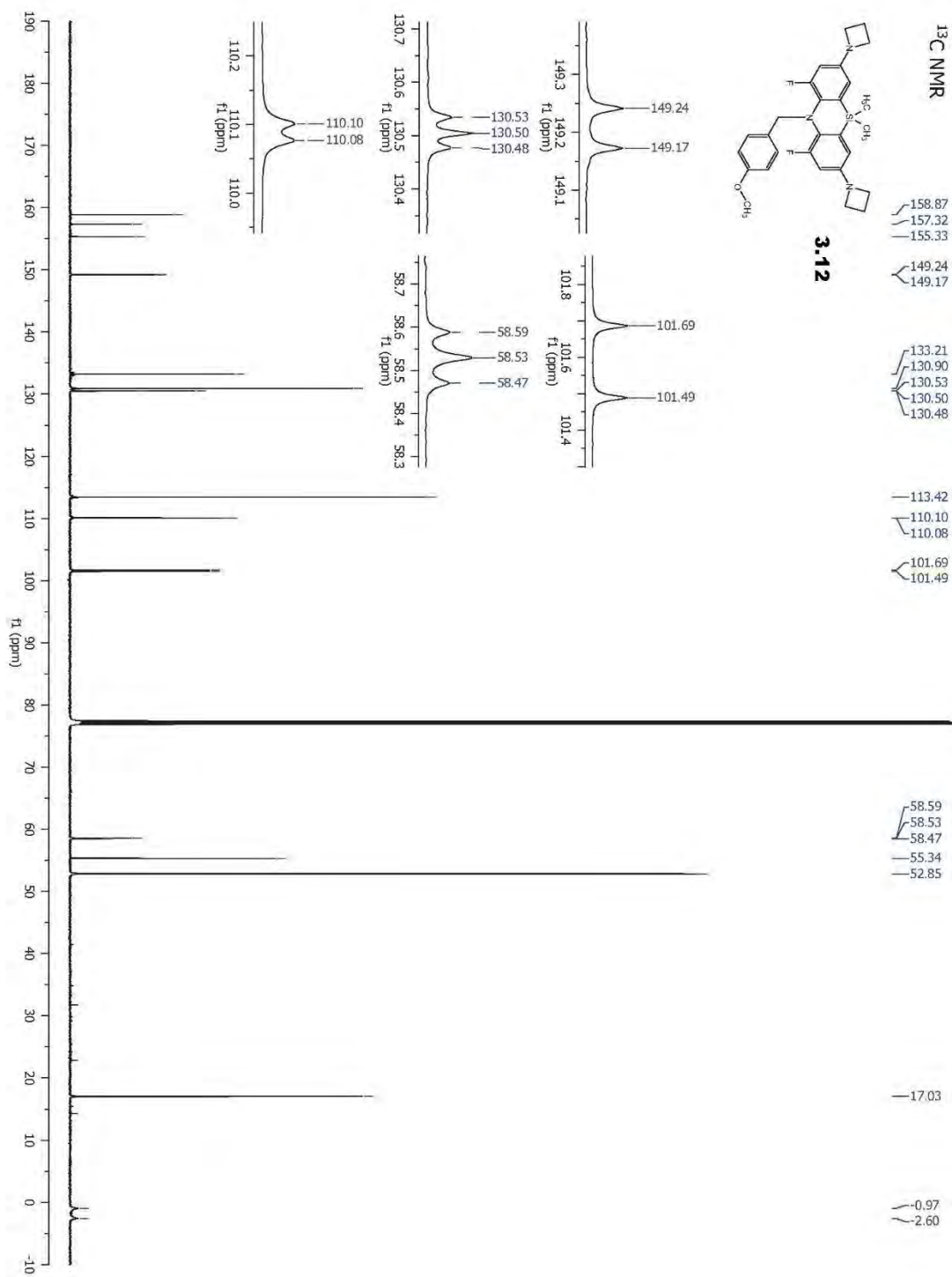
3.12

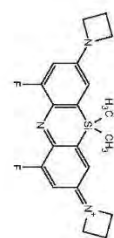
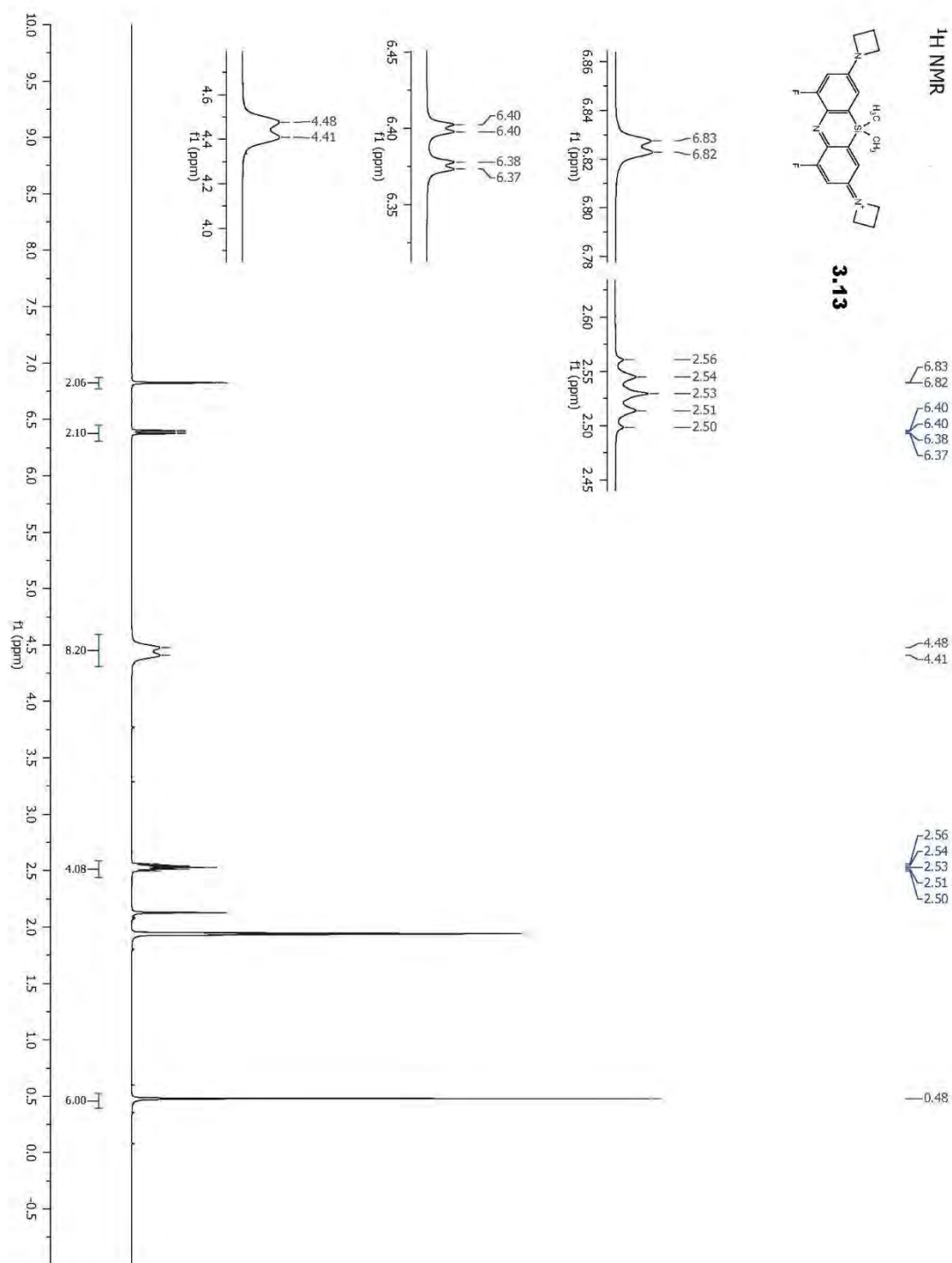


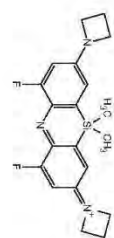
¹⁹F NMR**3.12**

-117.71
-117.74

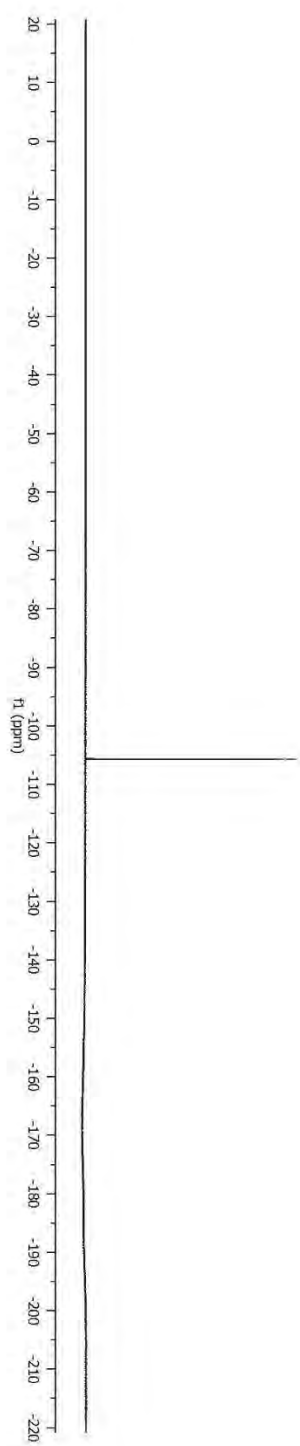
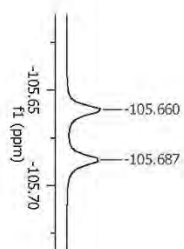


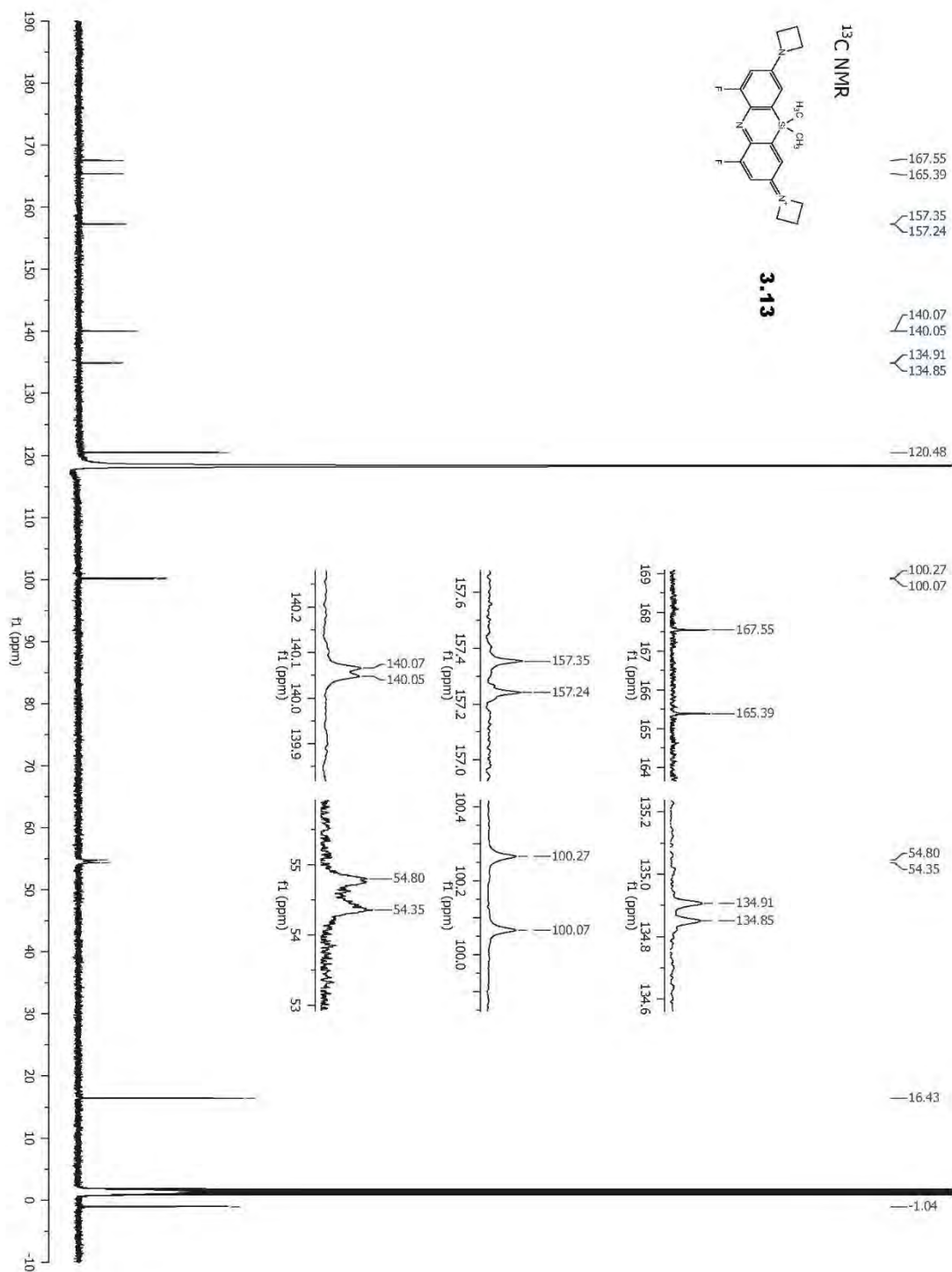


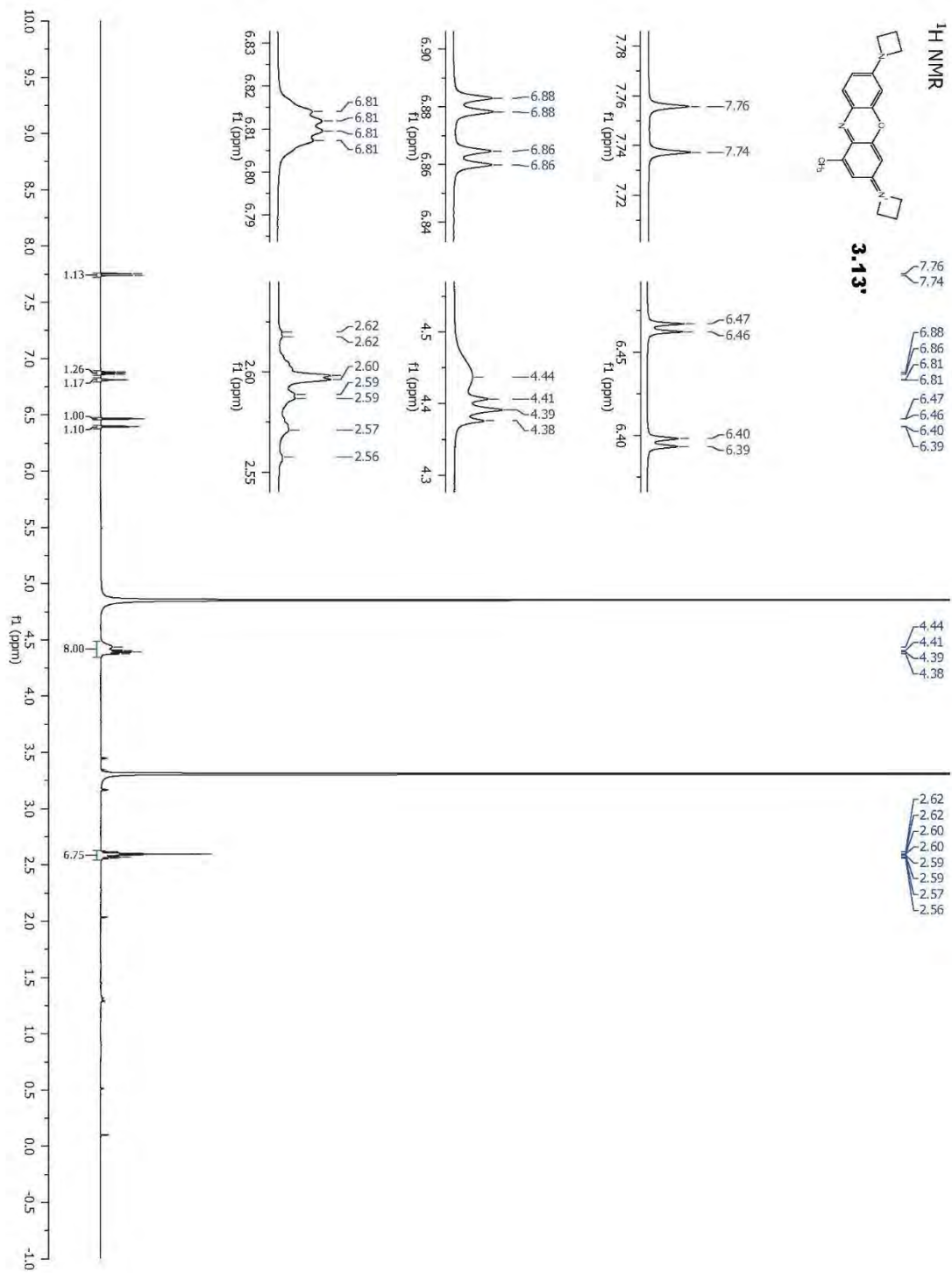
¹H NMR**3.13**

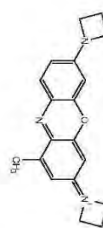
¹⁹F NMR**3.13**

-105.66
-105.69

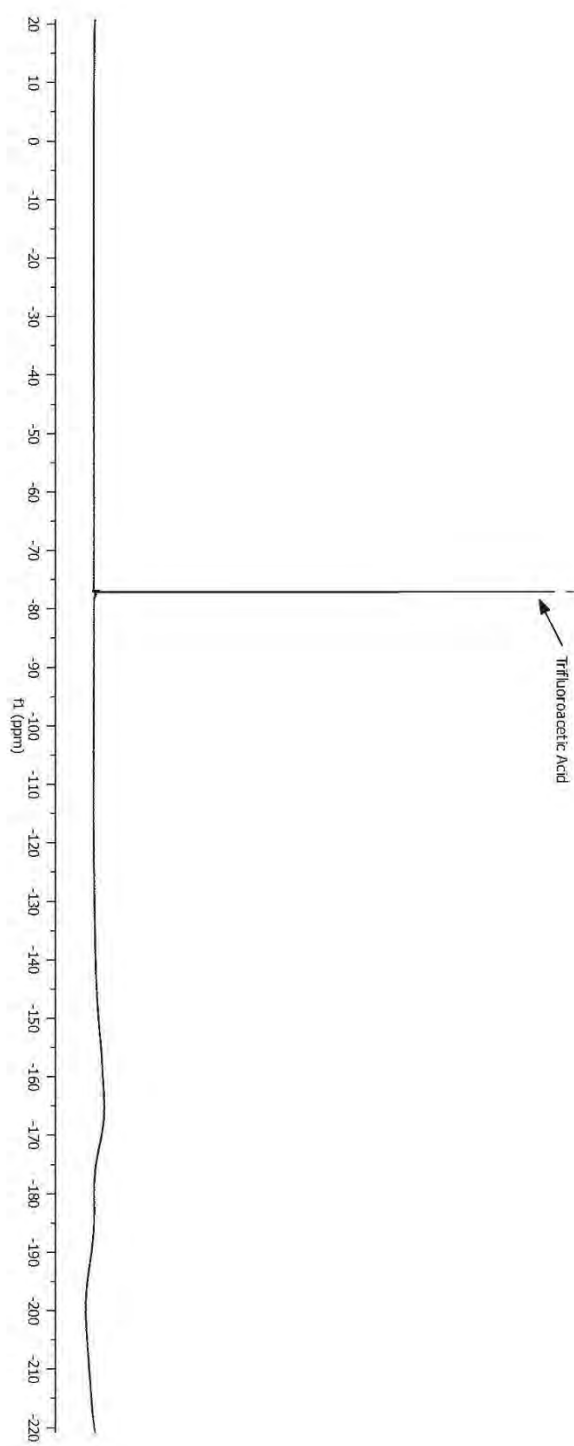


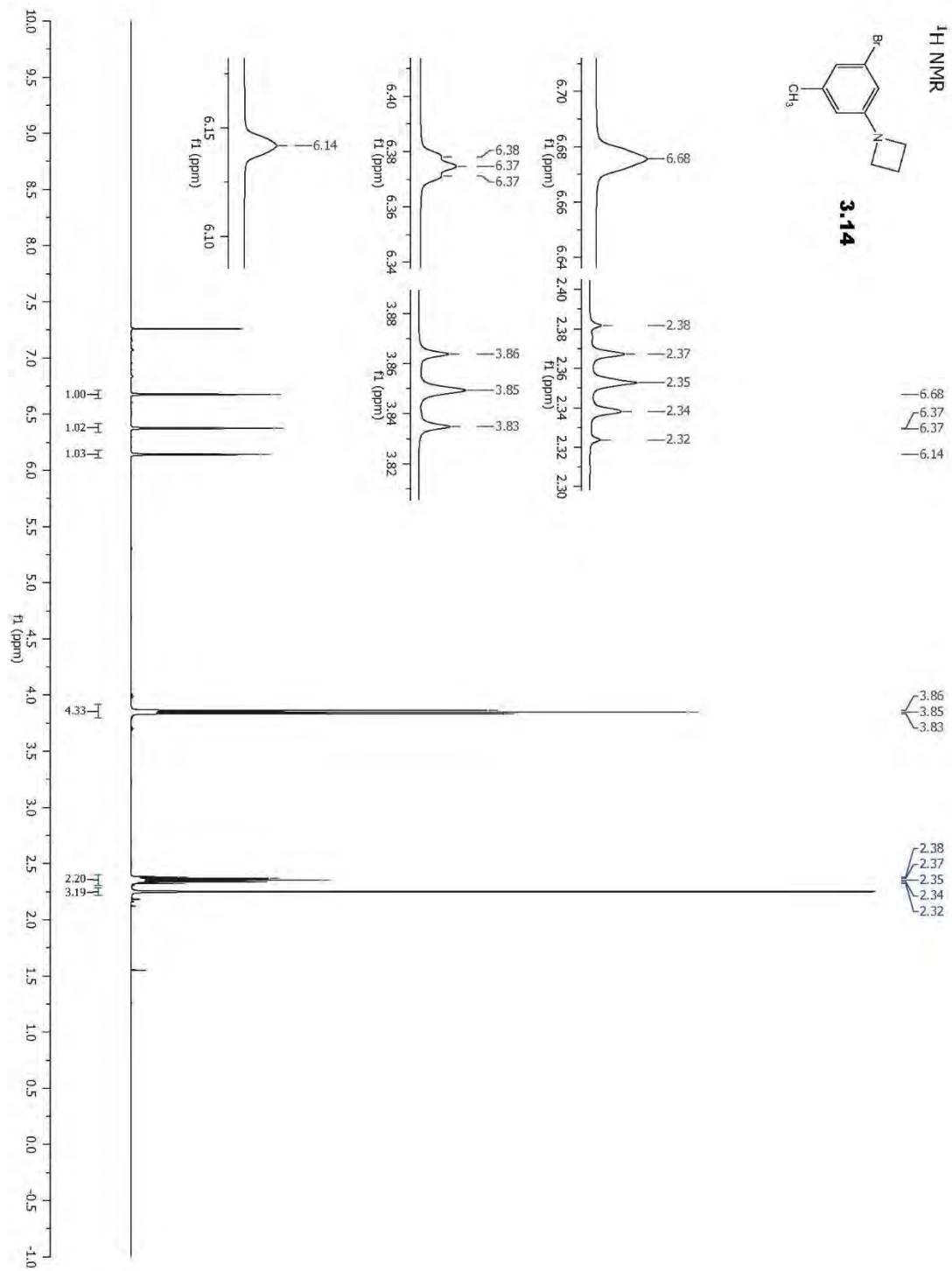


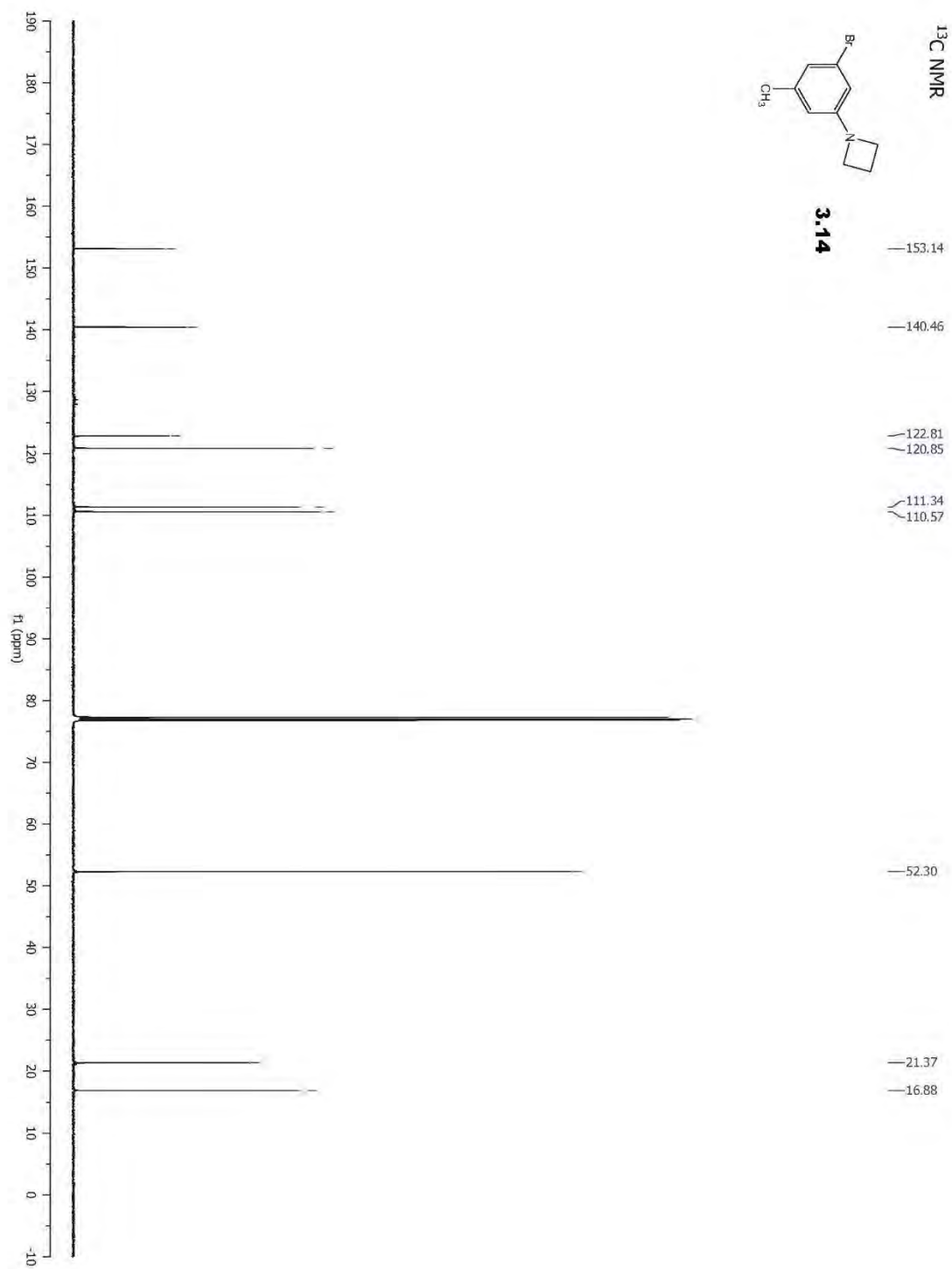


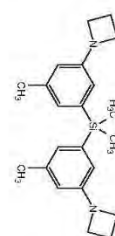
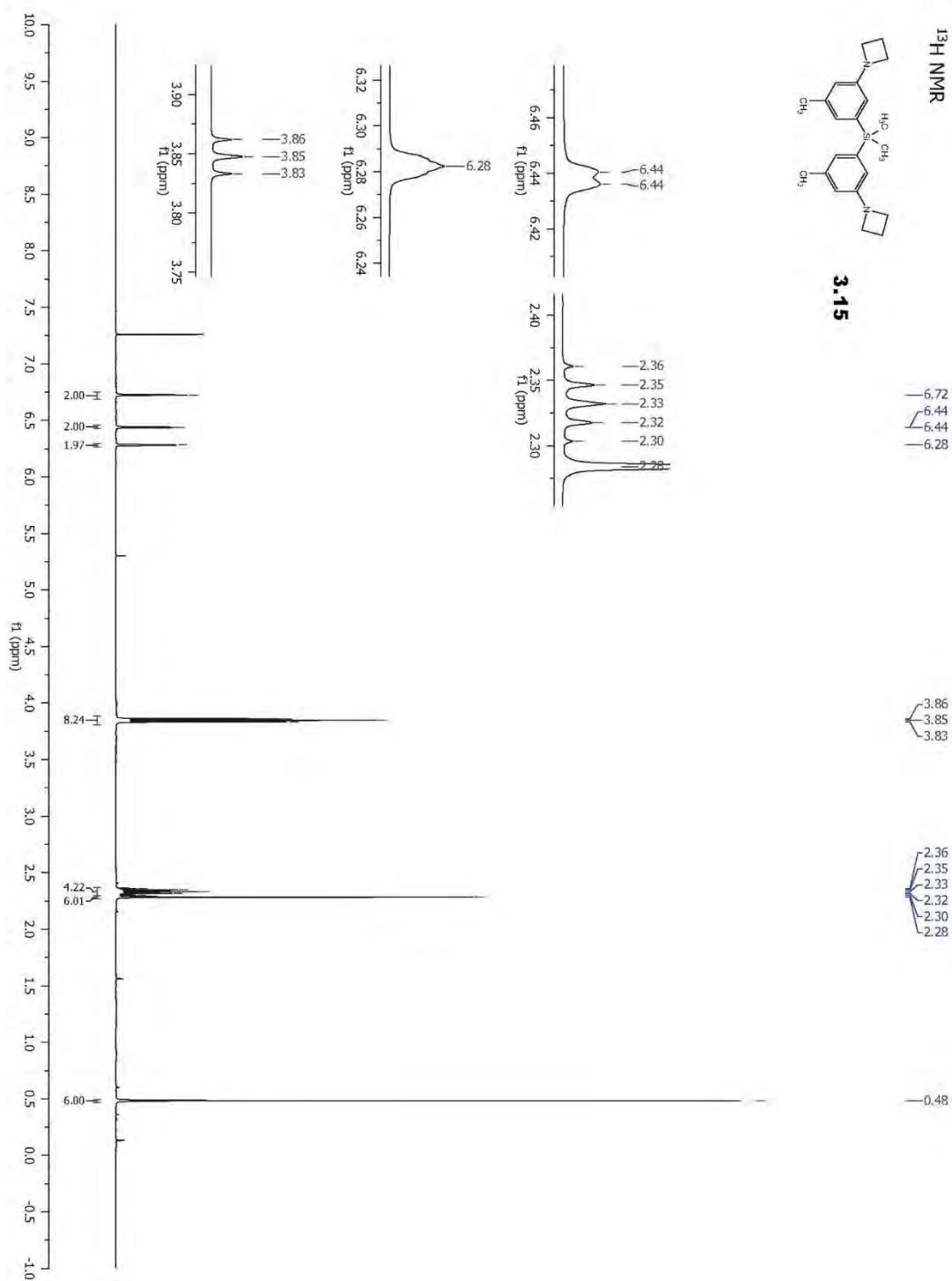
¹⁹F NMR**3.13'**

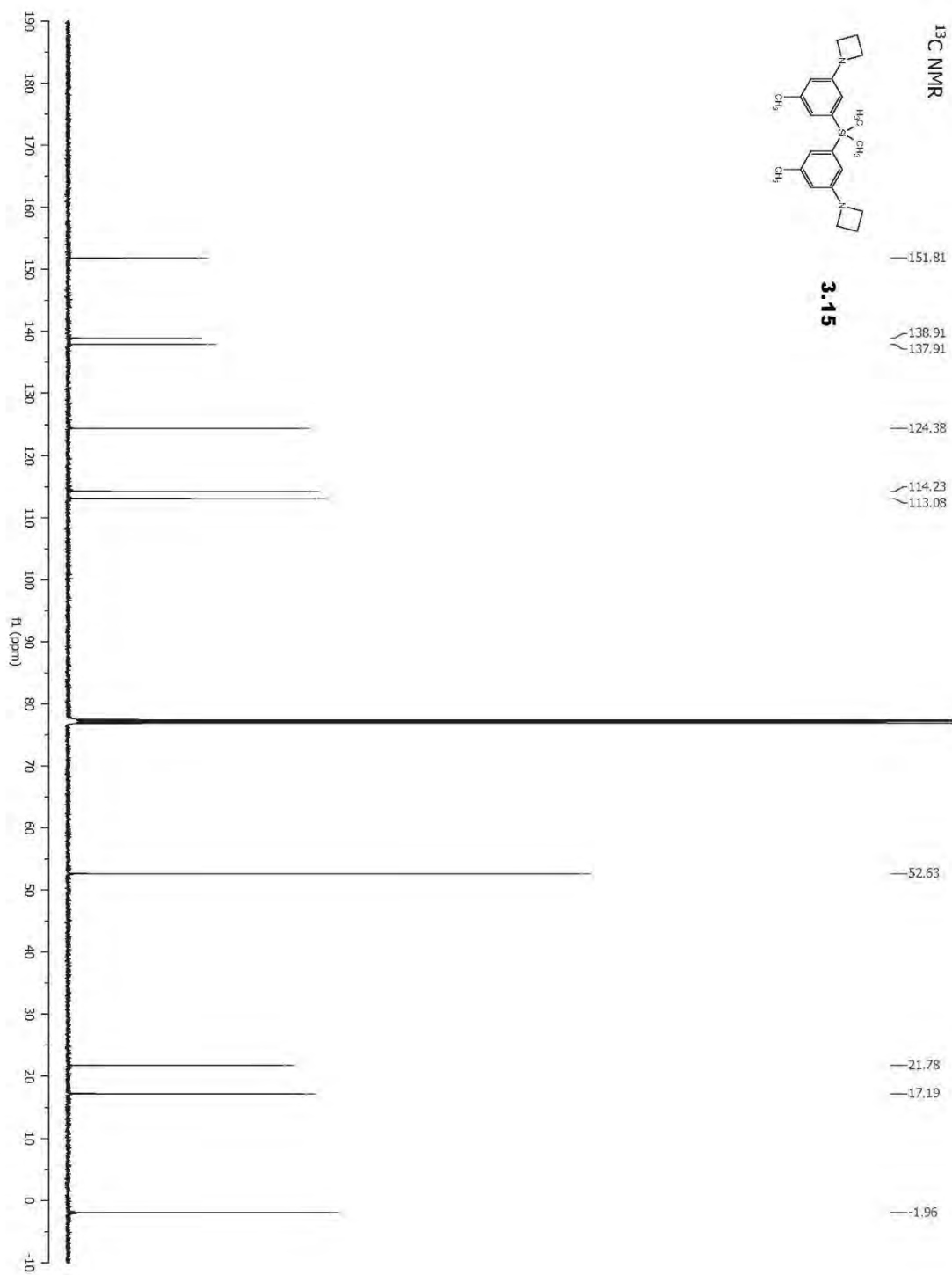
-77.11

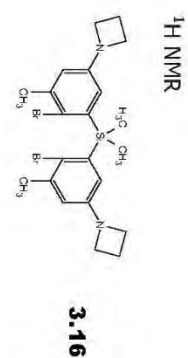






^1H NMR**3.15**



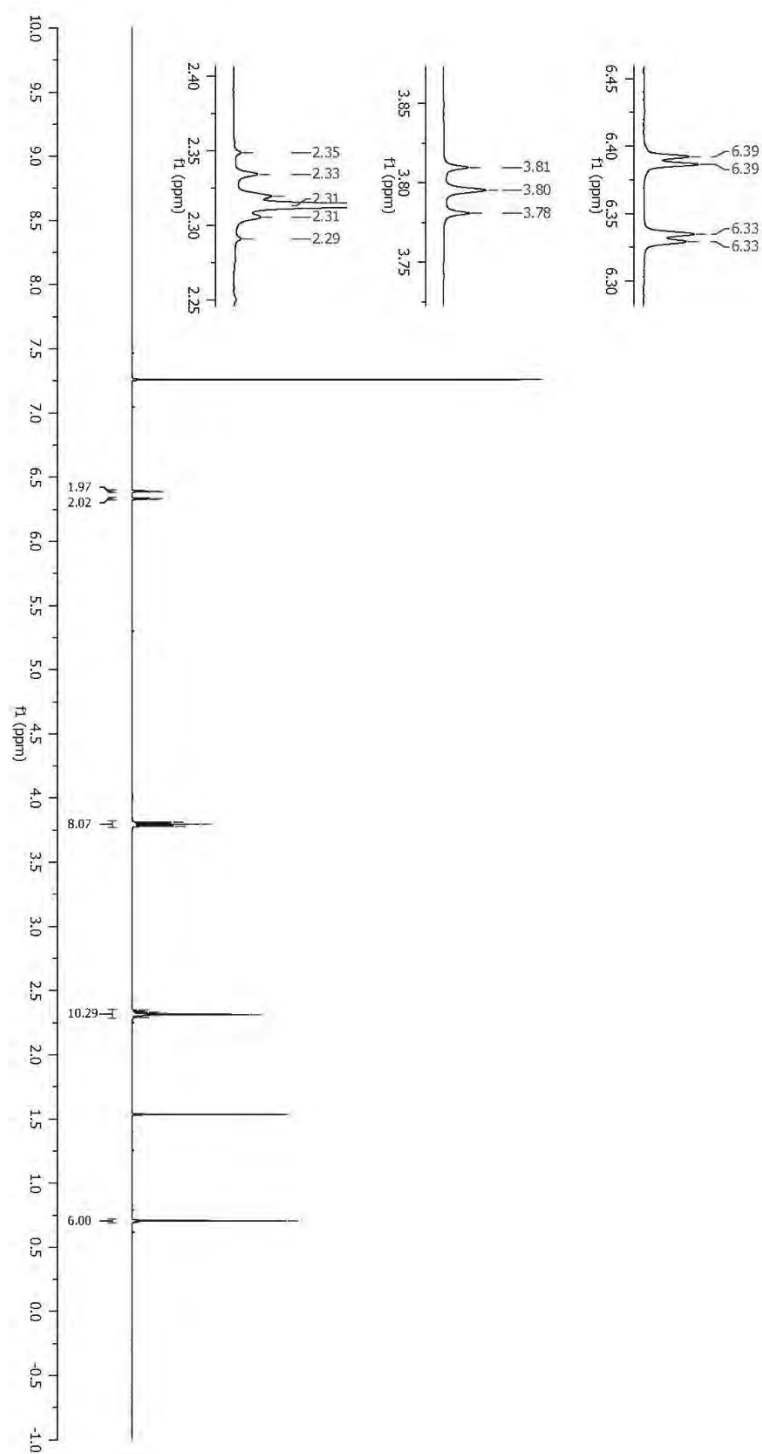


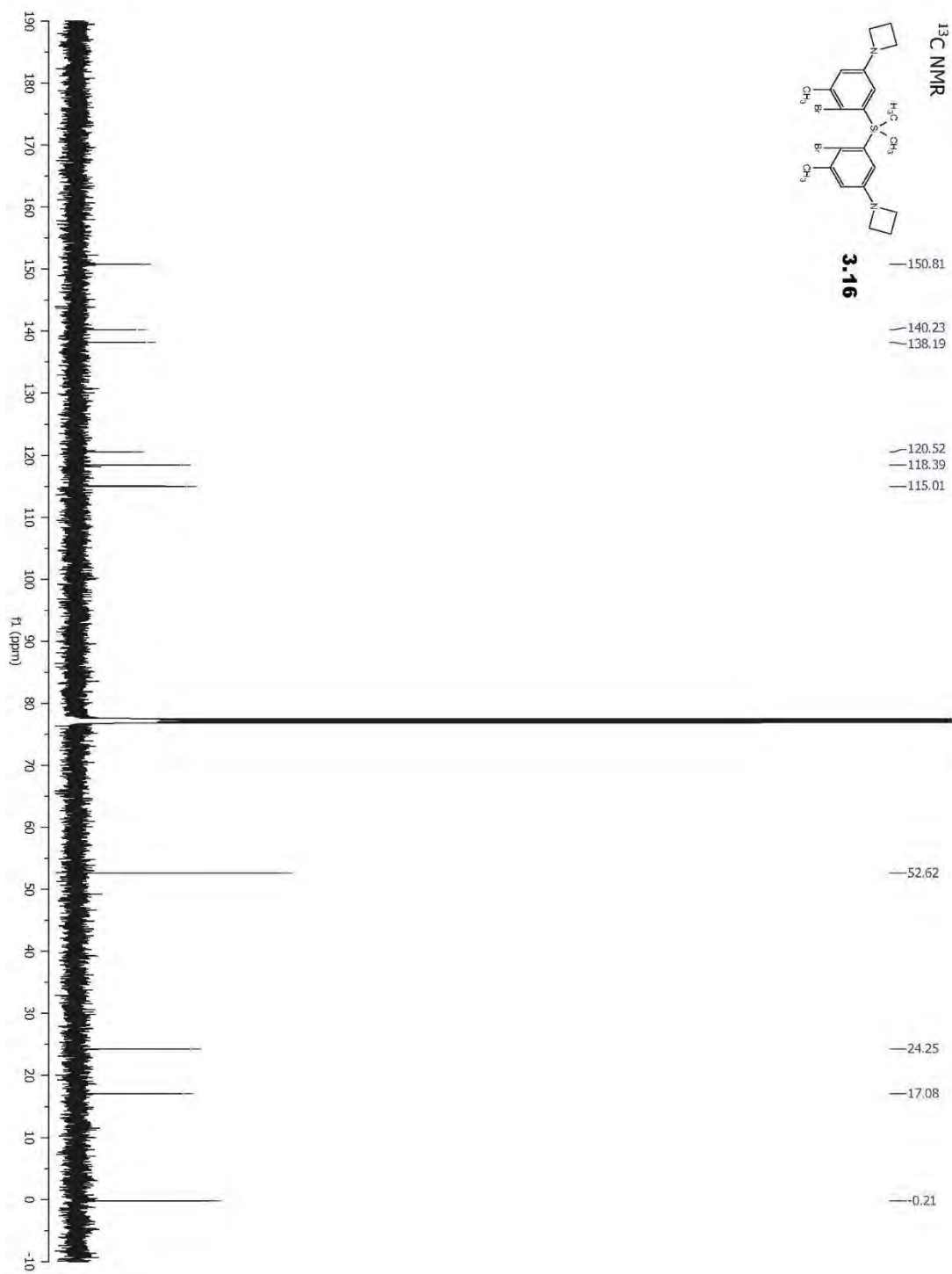
6.39
6.39
6.33
6.33

3.81
3.80
3.78

2.35
2.33
2.32
2.31
2.29

—0.71





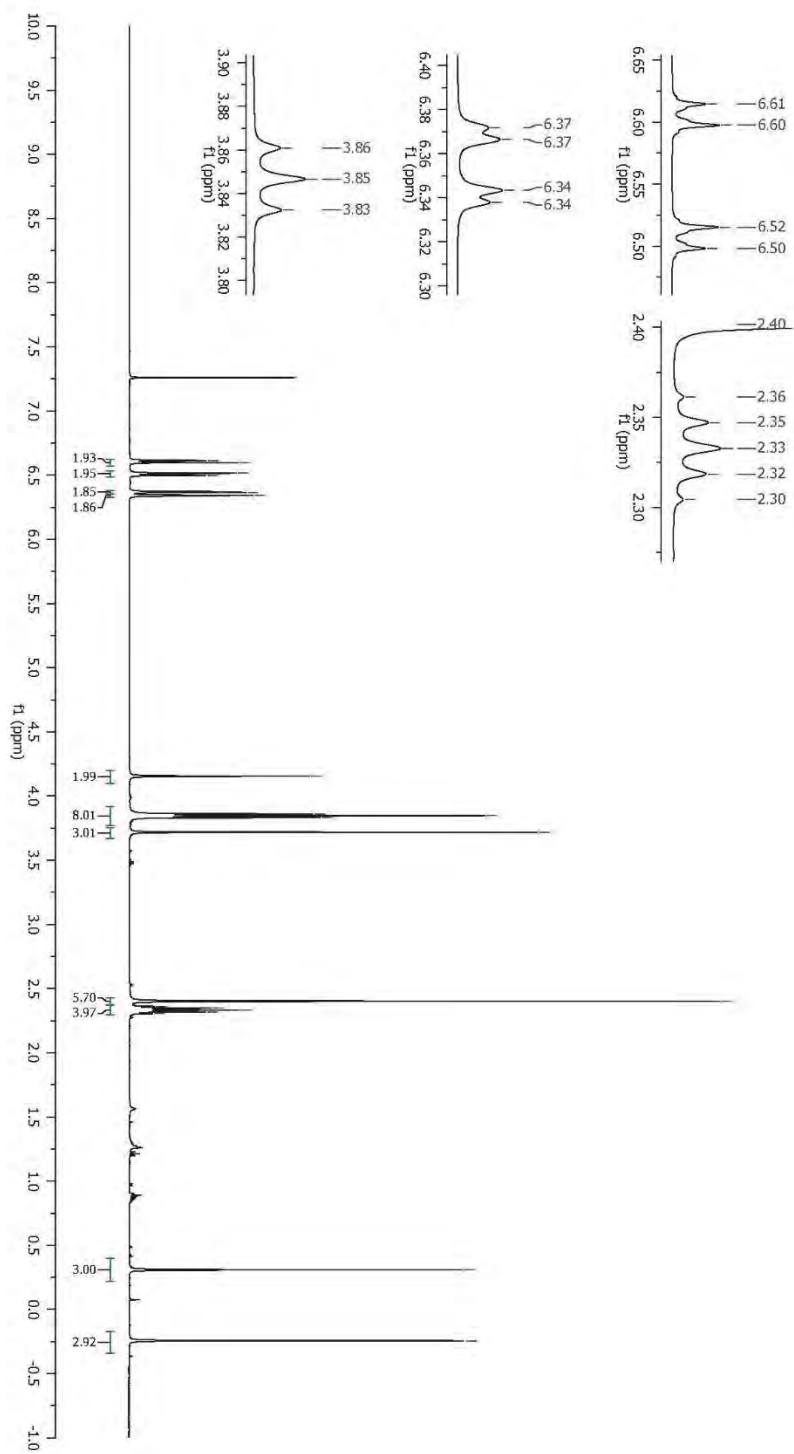
6.61
6.60
6.52
6.50
6.37
6.37
6.34
6.34

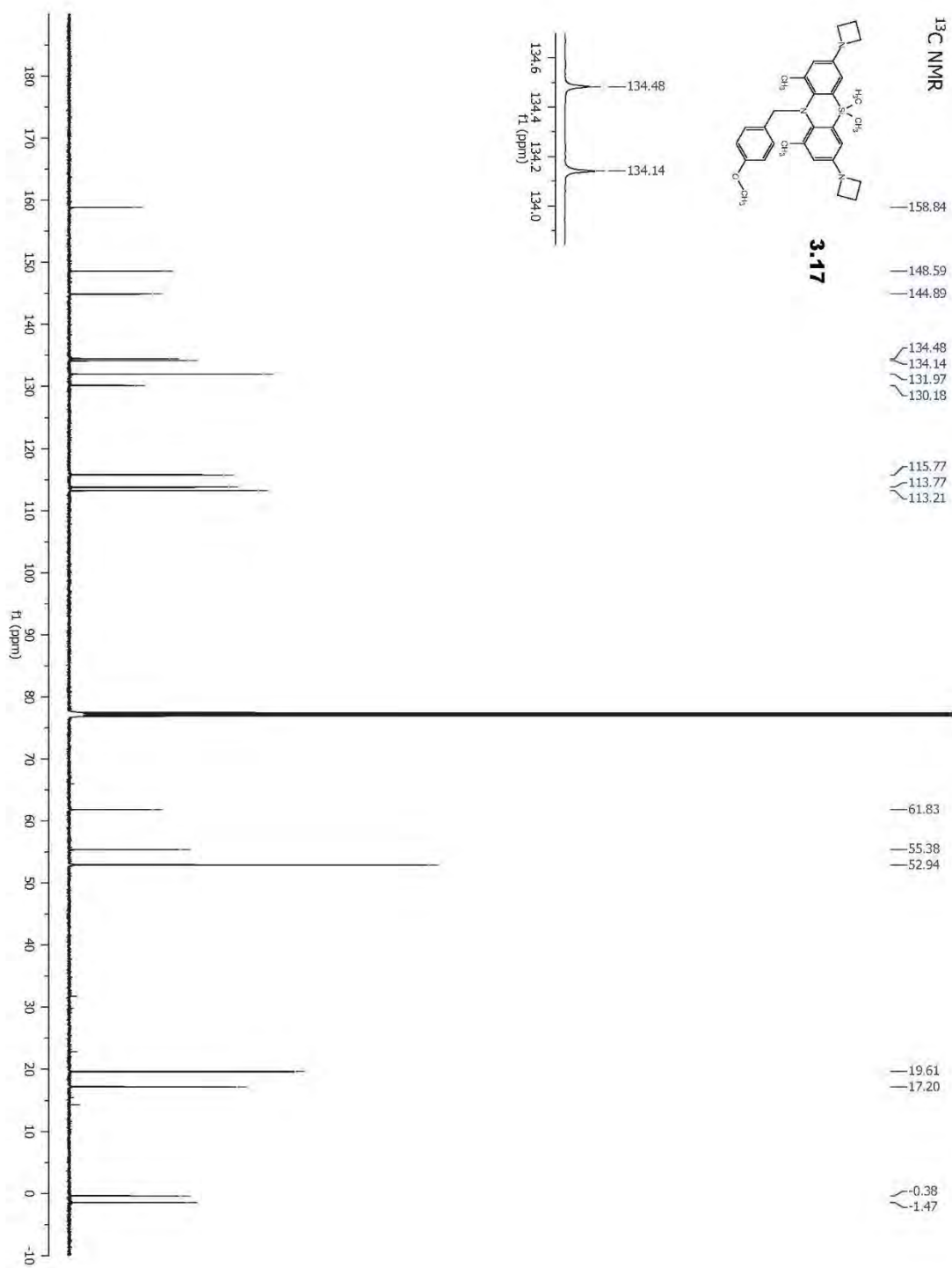
—4.15
 { 3.86
 { 3.85
 { 3.83
 { 3.72

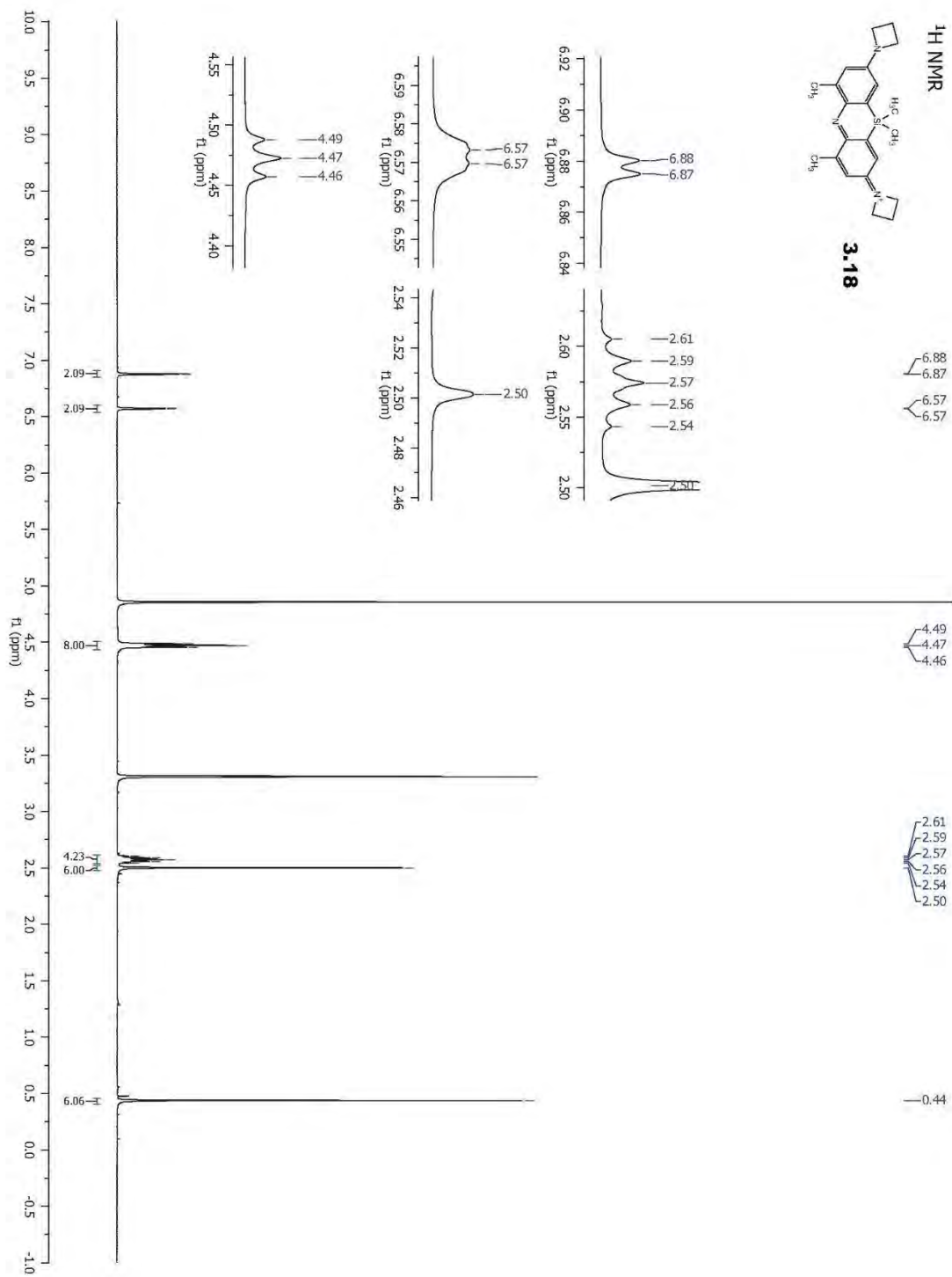
$\left\{ \begin{array}{l} 2.40 \\ 2.36 \\ 2.35 \\ 2.33 \\ 2.32 \\ 2.30 \end{array} \right.$

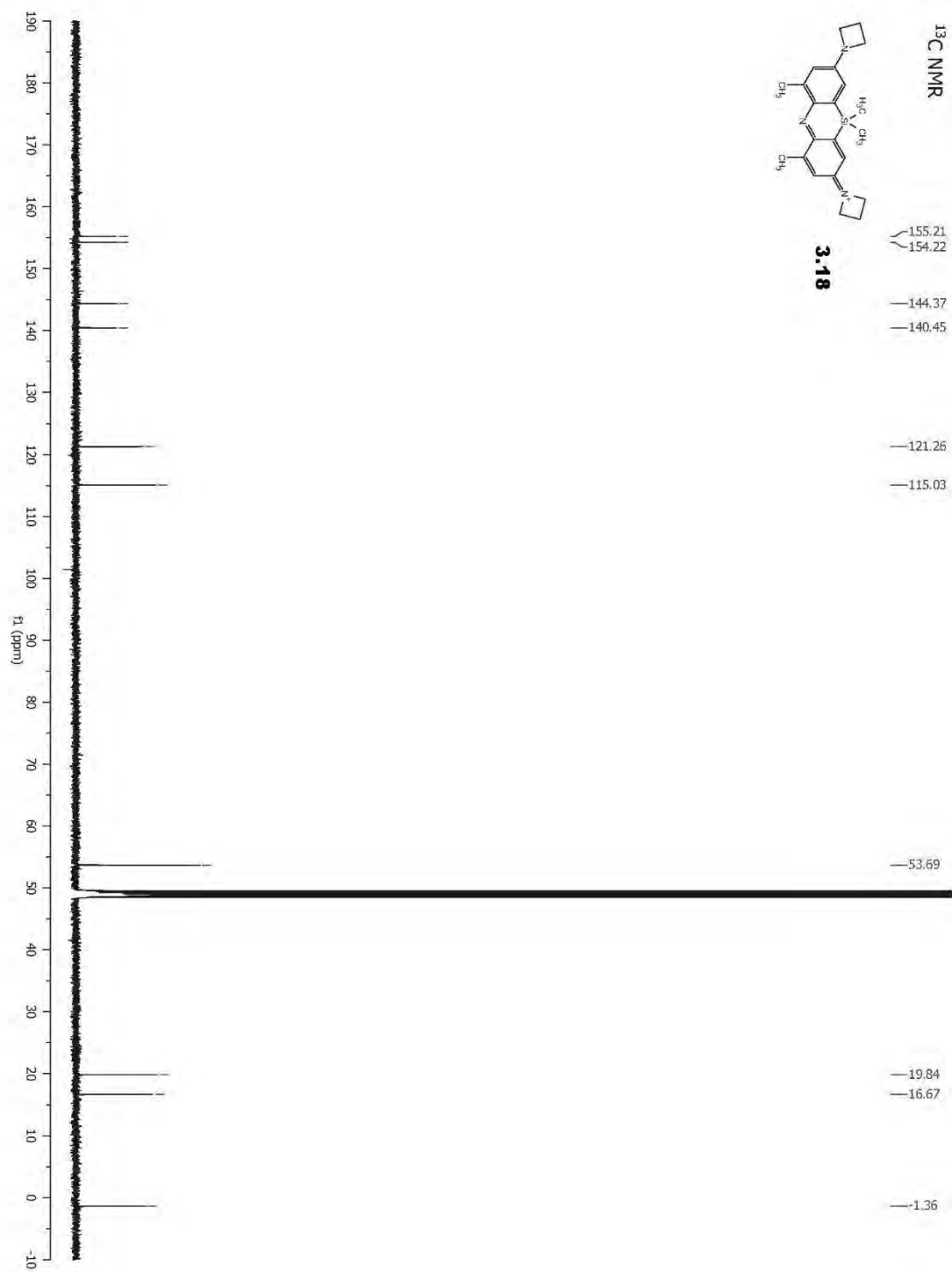
—0.31

—0.24









CHAPTER IV:

Discussions and Future Directions

Since the first discovery of fluorescence, researchers have used fluorescent probes to interrogate important biological and chemical processes.^{109,110} The arsenal of fluorescent probes in modern science includes numerous fluorescent proteins, organic dyes, and more recently, quantum dots.¹¹¹ Efforts to refine fluorescent techniques and probes, coupled with advances in microscopy, have positioned these tools at the vanguard of scientific progress. While fluorescent probes have made great strides in recent history, important limitations still exist, especially in regards to solubility, photostability, and light penetrance. Regardless of type, NIR fluorescent probes produce the cleanest signal, owing to the high penetrance of NIR light.^{22,27} However, as discussed in **CHAPTER I**, current NIR probes are far from perfect. Most NIR fluorophores have low aqueous solubility, due to their extended π -conjugation. Addition of polar sulfonates could impart aqueous solubility, but often at the expense of membrane permeability. However, Rusha and Miller showed that aqueous solubility and membrane permeability are not mutually exclusive. Using AcOTFMB, they delivered a dansyl-sulfonate fluorophore into live cells with intact membranes.⁴⁸

In **CHAPTER II**, I aimed to expand the repertoire of TFMB-based sulfonate protecting groups to include biocompatible chemically-labile triggers, with the goal of extending the applications of sulfonated molecules to living cells. Specifically, I am interested in creating reductively labile protecting groups that can exploit the high reductive activity of cytosolic GSH. To that end, I created two reductively-labile protecting groups (RLPG): MeSSTFMB and MeSSTFMP. The synthetic conditions to access both MeSSTFMB and MeSSTFMP were mild and straightforward.. MeSSTFMP

resulted in a high percentage of sulfonate delivery into cells. MeSSTFMB, while delivering a lower percentage of sulfonates when compared to MeSSTFMP, did not show any appreciable toxicity in Hela cells, demonstrating its potential in long exposure experiments.

MeSSTFMP-Dan achieved complete cleavage within three minutes *in vitro* and yielded bright diffusive fluorescence in Hela cells. Moreover, the observed LD₅₀ for MeSSTFMP-Dan was higher than AcOTFMB-Dan. I hypothesize thioquinone methides are intrinsically less toxic than quinone methides, which tend to form nucleophilic adducts. Thioquinone methides preferentially form the two-electron reduction product, which may impart transient oxidative stress, whereas alkylation can impart irreversible cell damage.^{48,86,87} If true, then perhaps the toxicity of AcOTFMB could be decreased if the acetoxy group is replaced with a thioester group (**Figure 4.1**).

The rate of (thio)methide generation may also contribute to toxicity. Presumably, reduction of MeSSTFMB and MeSSTFMP would form *p*-thioquinone methides with similar toxicity. However, as previously observed, the slow cleaving MeSSTFMB-Dan was not cytotoxic, implying a correlation between cleavage rate and toxicity.

To elucidate the source(s) of cytotoxicity, one could make two comparisons. First, compare the toxicity between different esterase-labile TFMB groups. Since structure dictates enzyme recognition, different esters should cleave at different rates, which in turn generates quinone methides at different rates. Second, compare the toxicity of the proposed S-AcOTFMB and AcOTFMB. Assuming their cleavage rates are similar, this

would allow one to directly compare the toxicity between thioquinone methide and quinone methide.

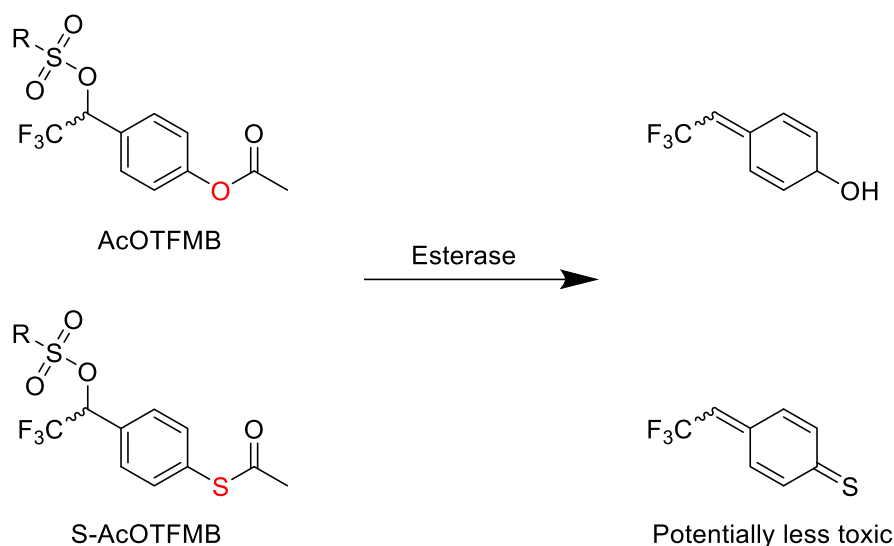


Figure 4.1: Thioester AcOTFMB (S-AcOTFMB) could be less cytotoxic. AcOTFMB and S-AcOTFMB form a quinone methide and thioquinone methide, respectively. The thioquinone methide is potentially less cytotoxic than the quinone methide

Shortly after the full characterization of MeSSTFMP, I sought to append it to other sulfonated fluorophores. Given the popularity of cyanine fluorophores, I was interested in synthesizing the bis-MeSSTFMP-Cy5. However, I quickly realized the inherent difficulties in protecting multiple sulfonates simultaneously. Sulfonate-esters are generally synthesized through sulfonyl chloride intermediates, which are prone to hydrolysis.^{112–114} Fully aware of their instability, the Cy5 sulfonyl chloride was used immediately after its synthesis and solvent removal. Disturbingly, esterification with MeSSTFMP still resulted in partial or complete hydrolysis of the sulfonyl chlorides,

despite my best efforts in maintaining an anhydrous environment. Mass spectrometry analysis revealed only trace amounts of the desired bis-sulfonate ester and the major product as the mono-sulfonate ester (**Figure 4.2**). Through optimization, the desired bis-MeSSTFMP-Cy5 was eventually isolated, albeit with low yield. Hence, inefficient synthetic routes to access sulfonate esters remain a major obstacle to the applications of RLPGs.

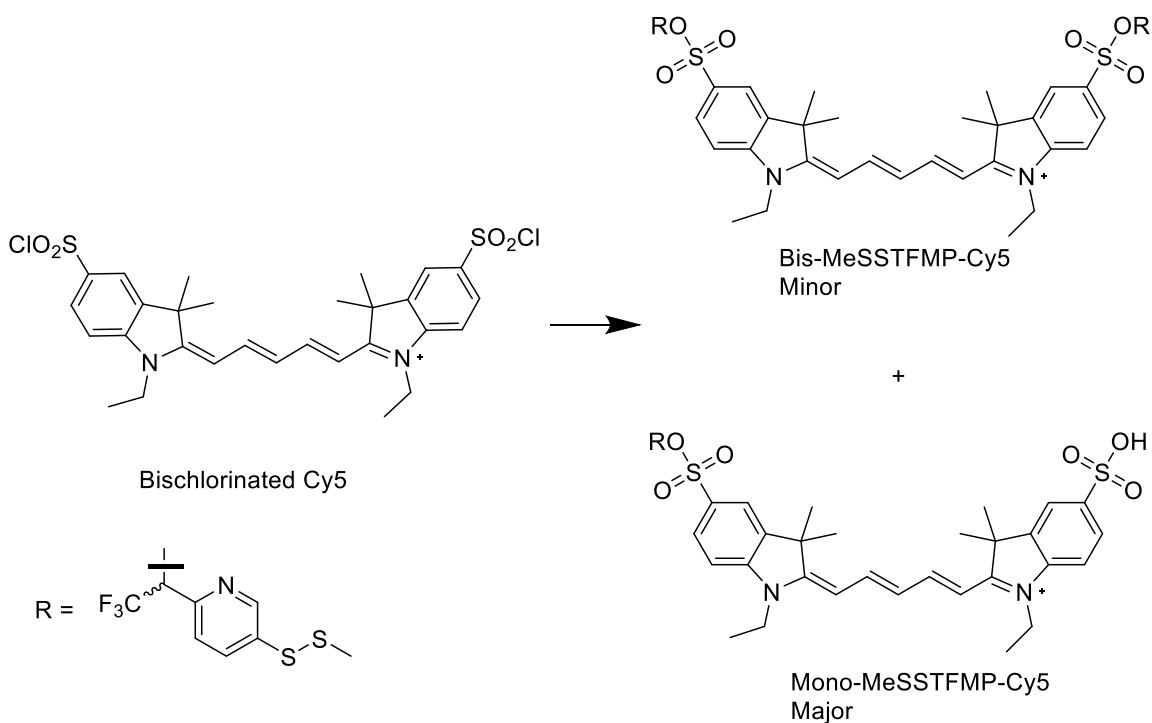


Figure 4.2: Protection of sulfo-Cy5 with MeSSTFMP typically yields the monoester as the major product. Sulfonyl chlorides are prone to hydrolysis. Esterification of multiple sulfonates via sulfonyl chloride intermediates generally yields the mono-ester and diester as the major and minor product, respectively.

Sulfonyl chlorides are unstable and easily hydrolyzed into sulfonates.¹¹⁵ Thus, the sulfonate-ester should either be formed at the beginning or the end of synthesis. Sulfonate-esters formed at the beginning must withstand harsh synthetic conditions, which are presumably incompatible with our RLPGs that are cleaved under mild biological conditions. Forming the ester at the end is plausible, though this approach comes with limitations, as not all compounds are stable under chlorination conditions. Moreover, as previously observed, trace amounts of moisture can completely quench the reaction. Further, purification of sulfonated compounds could be more difficult due to their polarity.

Clearly, neither method is ideal for appending RLPGs to compounds with multiple sulfonates. However, a third option is possible, where a chemically stable protecting group is first installed, followed by its conversion into a RLPG. For example, mono-sulfonated intermediates could be first converted to sulfonate esters with a chemically-stable RLPG precursor, such as 4-bromo-TFMP. Early esterification simplifies the reaction and purification conditions and eliminates the need for simultaneous esterification of multiple sulfonates. After total synthesis of the molecule, the aryl bromide could be converted to a thiosulfate group (Bunte salt), which, in turn, could form a disulfide (**Figure 4.3**).^{116–119} Since the thiosulfonate ester to disulfide conversion proceeds via a S_N2 mechanism, it should not lead to deprotection of the sulfonates.¹¹⁶

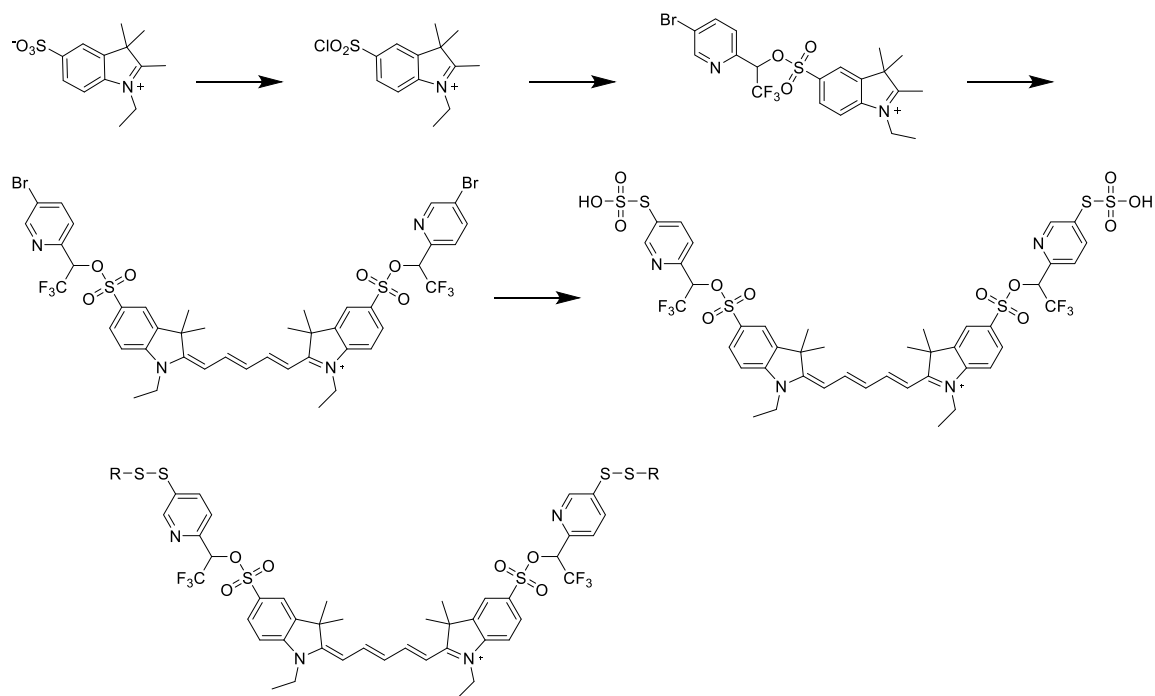


Figure 4.3: Accessing RLPG protected sulfo-Cy5 via a Bunte salt intermediate. Mono-sulfonated intermediates are chlorinated and esterified with a chemically stable protecting group. After the complete synthesis of the parent molecule, the aryl-bromide is converted into a Bunte salt and then into a disulfide to yield the RLPG.

To deliver the polar anionic dansyl sulfonate fluorophore in the living cells, I synthesized reductively-labile protecting groups. As predicted, both RLPGs successfully drove intracellular delivery of dansyl-sulfonate. However, the solubility of MeSSTFMB-Dan was rather low, aggregation on cell membranes was visible at concentrations as low as 10 μ M, reflecting the importance of the balance between hydrophilicity and hydrophobicity. Given the modularity of the TFMP and TFMB, one would expect that polarity could be optimized by the attachment of a hydrophilic group. While true, a quick survey of commercially available thiosulfonate S-esters, the key thiol group donor in our

synthetic schemes, quickly reveals their scarcity. Besides S-methyl or S-ethyl, other sulfonate S-esters are either unavailable or cost prohibitive. Given their importance in generating disulfides, I propose two feasible routes to access thiosulfonate S-esters.

Both routes undergo S_N2 reactions to form the desired thiosulfonate S-esters. However, the first route utilizes toluene-thiosulfonate, whereas, the second route, utilizes thiolates as nucleophiles (**Figure 4.4**). The generality of these methods should greatly improve the feasibility of accessing different disulfides, despite the commercial shortage of thiosulfonate S-esters. Besides solubilizing groups, one could also use these methods to append a myriad of linkers and targeting moieties on TFMP and TFMB to form a library of RLPGs.

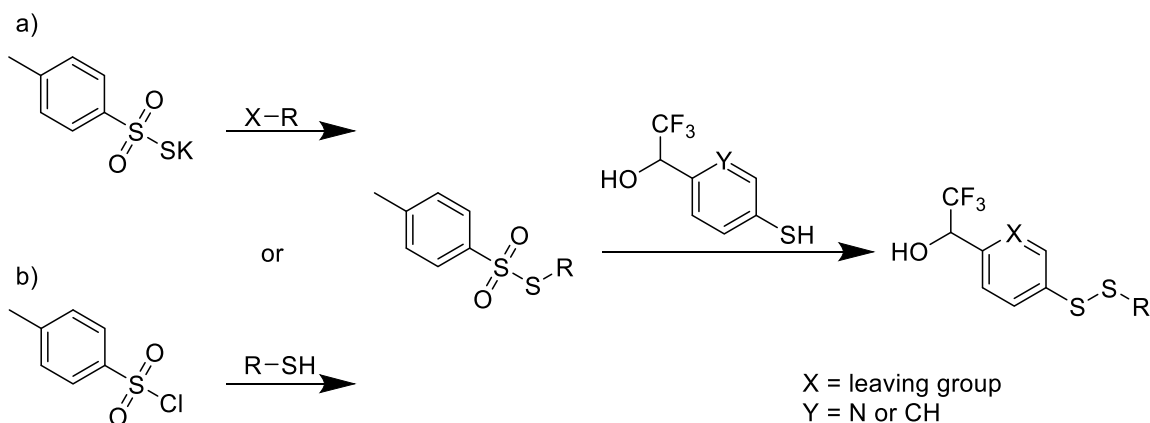


Figure 4.4: Different ways to access thiosulfonates intermediates. Reaction between *p*-toluenethiosulfonate and an alkyl halide (a) or tosyl chloride and a thiol (b) affords the thiosulfonate ester, which then can react to form RLPGs. For clarity, the R-group is depicted as a propyl group.

In **CHAPTER III**, I proceeded to address the deficiencies of current NIR fluorophores. Most NIR fluorophores have low aqueous solubility without solubilizing groups such as sulfonates. However, the ginormous ICG fluorophore is only sparingly soluble in water, even with two sulfonates.^{90–92} Clearly, molecular size can override the solubilizing effects of sulfonates. Moreover, the selection of NIR fluorescent probes is generally limited to cyanines, which have poor photostability. To combat the adverse effect of molecule size, while also achieving NIR fluorescence and maintaining high photostability, I substituted oxygen with silicon in oxazine fluorophores to form azasilines.

In total, I attempted to synthesize three different azasiline derivatives: an azetidiny (unsubstituted), a difluoro (ASiFluor710), and a dimethyl (ASiFluor730) derivative. Only the ASiFluor710 and ASiFluor730 could be synthesized and isolated, presumably due to the electron-donating effects of the R-groups. It is worth noting that ASiFluor710 was isolated without purification and thus, could be synthesized in large scale. Unfortunately, the fluorine groups on ASiFluor710 may have decreased aqueous stability. Although the precise mechanism of degradation wasn't determined, the formation of an oxazine implies that degradation was initiated by the replacement of fluorine by water (hydrolysis) (**Figure 4.5**).¹²⁰ Potentially, ASiFluor710 could be stabilized by replacing fluorine with a weaker leaving group, such as chlorine.

Not all fluorinated compounds are unstable in water. Stable fluorinated fluorescein and Si-rhodamines have been reported.^{55,121} Interestingly, these reports show that fluorine groups can change the photophysical properties of the dye molecule when installed in certain positions of the ring. Perhaps, changing fluorination positions on the azasiline can promote aqueous stability.

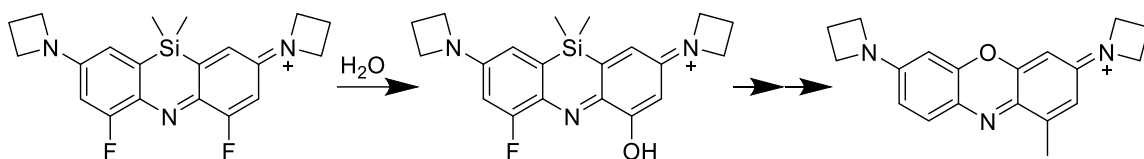


Figure 4.5: Possible initiation step of ASiFluor710 degradation. Nucleophilic aromatic substitution of fluorine by water ultimately leads to the formation of a methylated oxazine.

ASiFluor730 was photostable and showed impressive bathochromic shifts of over 80 nm compared to Oxazine 1. It also had a noteworthy quantum yield of 0.11, only 22% lower than oxazine 1 (0.14). Besides Oxazine 1, other oxazine derivatives that have higher quantum yields and/or longer emission wavelengths have been reported (**Figure 4.6**). For example, some rigidified oxazines have quantum yields of ≥ 0.20 and emission wavelengths of up to 717 nm.^{94,122} With that in mind, the optical properties of azasilines could be further optimized through modification.

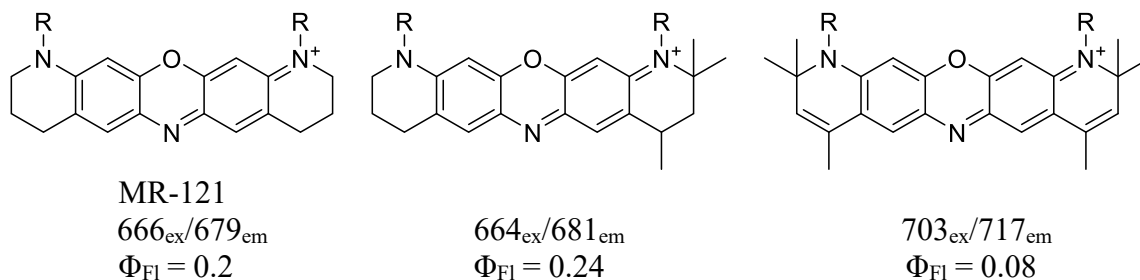


Figure 4.6: Optical properties of oxazine derivatives. Substituents alters the fluorescence and quantum yield of oxazines. The name (if available), excitation and emission wavelengths, and fluorescence quantum yield are listed below each molecule.

The increase in quantum yield after the addition of 0.05% Tween 20 implies the addition of polar groups could improve quantum yields in aqueous media. The azasiline scaffold has multiple sites amenable to functionalization. For example, the key aryl halide intermediate can undergo palladium-catalyzed coupling with amines. In **CHAPTER III**, I chose to install azetidines with the intention of increasing quantum yields. However, palladium-catalyzed coupling of aryl halides is not limited to azetidines; other substituted amines, such as ones that endow aqueous solubility are also compatible. Primary amines may also participate in palladium-catalyzed coupling to form secondary aryl amines, which could be further modified to form the final tertiary amines (**Figure 4.7**).^{123,124}

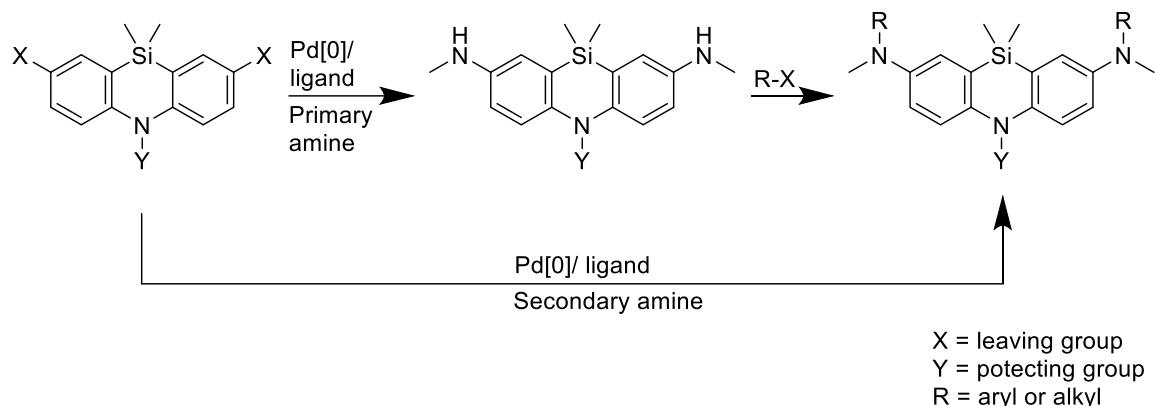


Figure 4.7: Modifying azasilines via aryl-halide intermediates. Palladium-catalyzed coupling of secondary or primary amines followed by N-alkyl or arylation yields functionalized azasilines.

Unlike oxygen, silicon is a group 14 element that can form four bonds without gaining a formal charge. Two of the four bonds are used to form the azasiline, leaving two for potential modifications. While commercially available dichloro-silane derivatives are limited, 3-chloropropylmethyldichlorosilane is available. Cyclization using 3-chloropropylmethyldichlorosilane yields an azasiline with a chloropropyl chain directly attached to the silicon. Potentially, the chloride could be replaced by an iodide with the Finklestein reaction, providing another site for modification.¹²⁰ Alkyl iodides are excellent leaving groups; simple S_N2 displacement should readily yield the azasilines bearing affinity ligands, such as HaloTag, SNAP-Tag, CLIP-Tag, and azido groups to support Click chemistry (**Figure 4.8**).^{125–127}

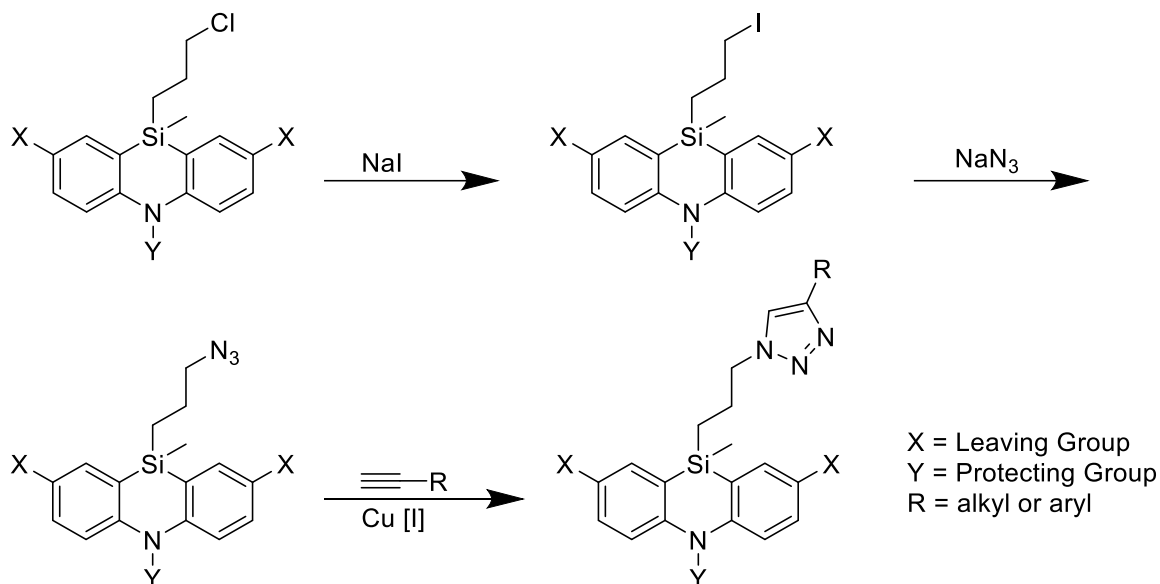
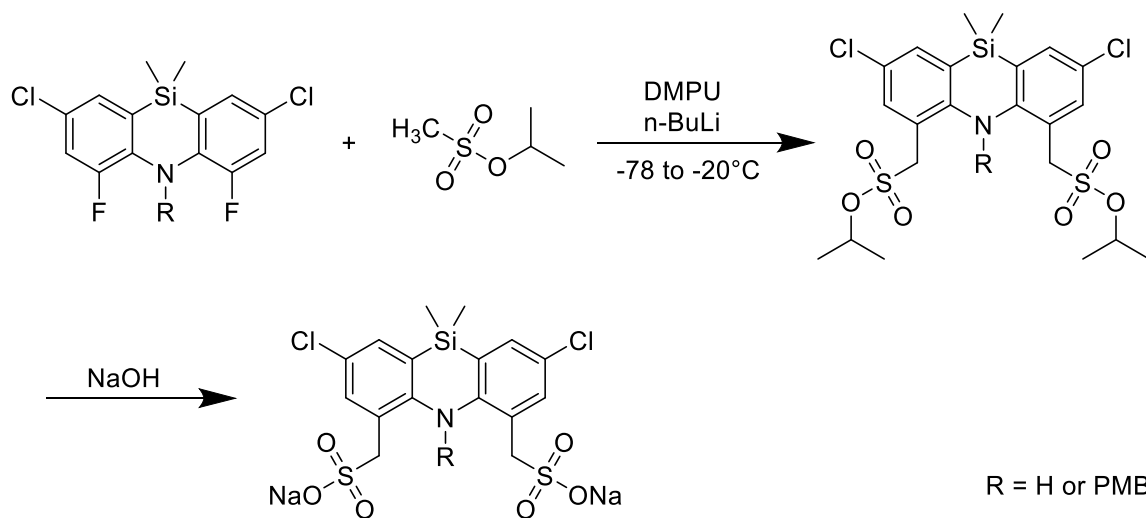


Figure 4.8: Potential R-group attachments on silicon of ASiFluors. Chloropropyl group installed on ASiFluors could be converted to an iodopropyl group and then to an azido group (N₃). Subsequent reaction with an alkyne (Click-chemistry) affords a functionalized R-group or tagged protein.

ASiFluor710 was easily synthesized, but labile to hydrolysis. Serendipitously, the electrophilic fluorine could potentially be used as yet another site for modification. The PMB-protected ASiFluor710 could react with carbanions to form alkylated azasilines. Carbon nucleophiles are not as common other nucleophiles, thus the modulatory could be limited. However, that position could be sulfonated via a lithiated carbanion intermediate (**Scheme 4.1**).¹²⁸ Finally, while modifications could be performed individually, all three sites could be utilized simultaneously for maximum versatility (**Figure 4.9**). One could install azetidines, an azido group, and sulfonates to concomitantly enhance the quantum yield, use Click Chemistry, and maximize aqueous solubility, respectively.



Scheme 4.1: Purposed sulfonation method for ASiFluors. Lithiated methyl sulfonate ester replaces the fluorine groups on an ASiFluor710 precursor. Subsequent based mediated hydrolysis forms the sulfonates.

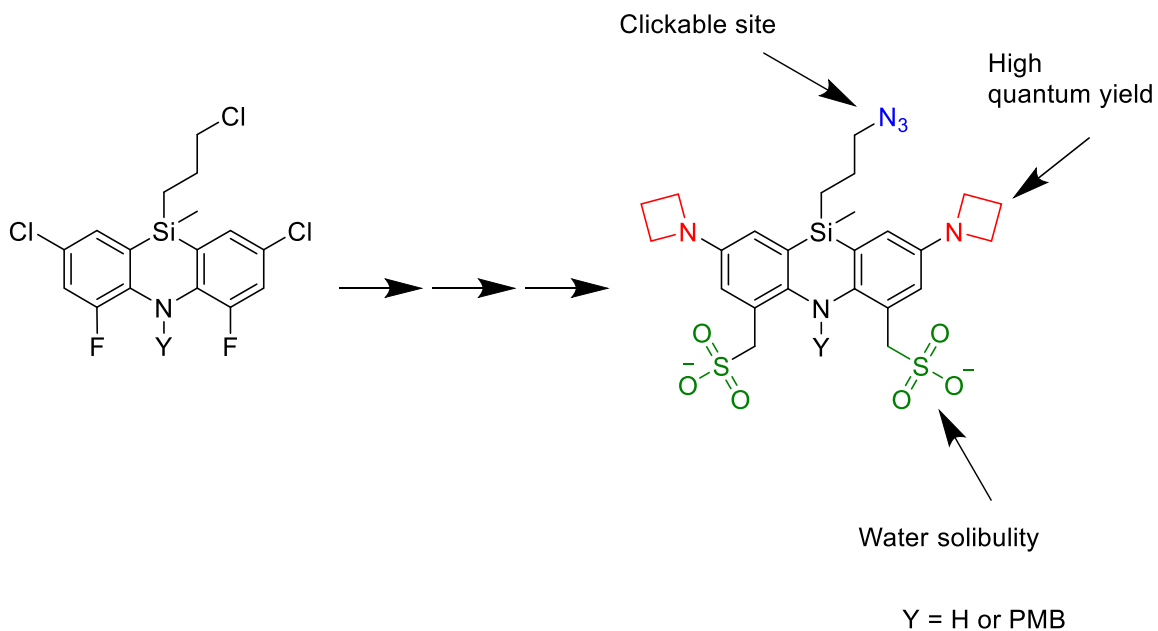


Figure 4.9: Azasilines can accommodate multiple modifications simultaneously. Modifications and their effects are labeled in color and below the structure, respectively. Azetidines (red) increase quantum yield, azido groups (blue) allow participation in Click Chemistry, and sulfonates (green) maximize aqueous solubility.

ASiFluor730 displayed higher cytotoxicity than Oxazine 1 in HeLa cells. Lipophilic cationic dyes are attracted to and accumulate in the mitochondria. Cationic dyes such as Rhodamine 123 can also depolarize the mitochondria and induce cytotoxicity.¹²⁹ Given the high reduction potential of azasilines, exemplified by the azatidenyl azasiline's recalcitrance to oxidation, toxicity could be caused from depolarization of the mitochondria. Thus, appending negatively charged polar groups such as sulfonates may improve solubility and lower cytotoxicity.

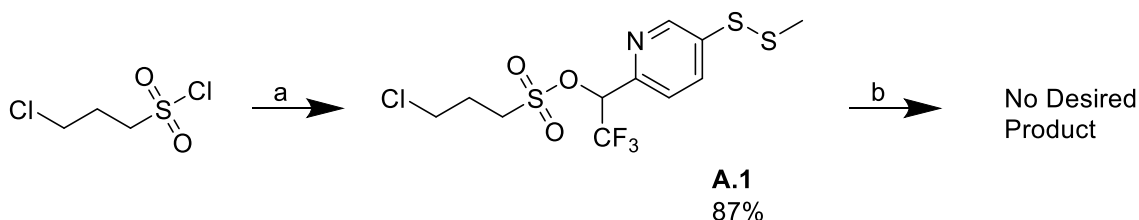
In addition to their use as imaging probes, azasilines have functionality in a variety of biological and medical applications. For example, azasilines could be modified into quenchers to participate in FRET experiments, or photosensitizers that deliberately release ROS to participate in photodynamic therapy (PDT).^{6,130} Like their imaging probe counterparts, the long adsorption wavelength enables deep tissue applications of the azasiline based quenchers and photosensitizers.

In summary, the main focus of my work has been to increase the utility of NIR fluorophores and to develop compact, photostable NIR probes. The employment of RLPGs extends the applications of sulfonated molecules to living cells. In **CHAPTER II**, I introduced two RLPGs capable of delivering sulfonated molecules across the cellular membrane of live cells. My MeSSTFMB and MeSSTFMP allow for the slow and rapid release of sulfonates, respectively. Compared to the reported AcOTFMB, my RLPGs were notably less cytotoxic, emphasizing their potential as intracellular delivery scaffolds. Additionally, I aimed to address the flaws of current NIR fluorophores, namely size and photostability. In **CHAPTER III**, I introduced synthetic methods to access novel NIR azasiline fluorophores. More importantly, I have shown that large bathochromic shift witnessed from oxygen to silicon substitution isn't exclusive to rhodamines, opening the possibility for the design of other long emitting silylated luminescent probes. ASiFluor730 was compact, photostable, and fluoresces beyond 730 nm. Nonetheless, the potential of these molecules has not been fully realized. With further optimization in both structural design and synthetic methods, I foresee these tools will play a pivotal role in illuminating the deep mysteries of biology, in cells and beyond.

APPENDIX

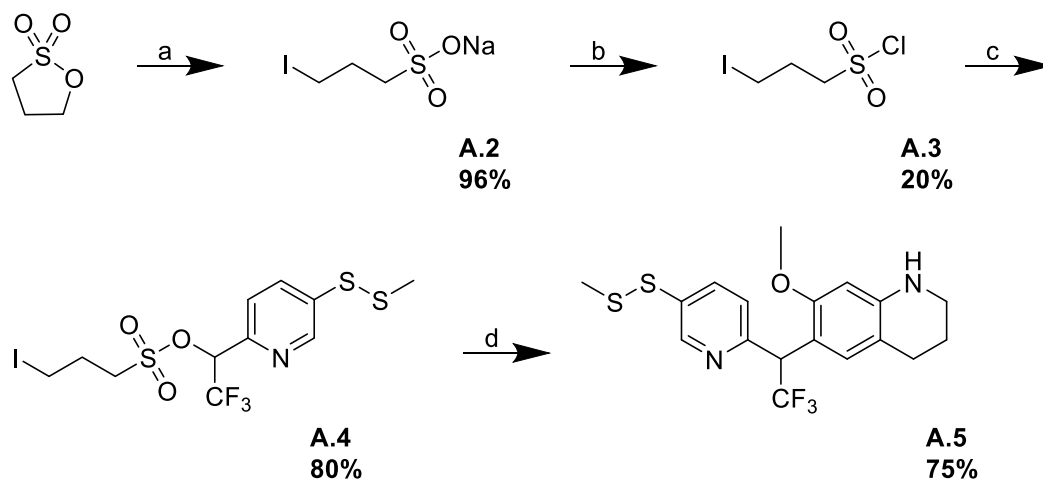
Conjugation of MeSSTFMP to NIR Fluorophores

After the synthesis of MeSSTFMP, I made tremendous efforts to append it onto NIR fluorophores, namely, oxazine and sulfo-Cy5. AcOTFMB protected oxazine had been reported, and cyanines are widely used as imaging agents.^{72,122} I first attempted to access the MeSSTFMP protected oxazines using a scheme modeled after AcOTFMB protection (**Scheme A1**).



Scheme A1: MeSSTFMP is labile to iodide. Reagent and conditions: (a) MeSSTFMP (**2.12**), TEA, DCM, 0 °C; MeSSTFMP; (b) NaI, acetone, reflux.

MeSSTFMP was treated with 3-chloropropane-1-sulfonyl chloride to form the sulfonate ester **A.1**. However, iodination under Finkelstein conditions deprotected the sulfonate, presumably due to nucleophilic attack on the disulfide by iodide. I circumvented this issue by installing an iodine group on the terminal carbon prior to esterification (**Scheme A.2**). 1,3-Propanesultone was treated with sodium iodide to yield 3-iodopropane-1-sulfonate **A.2**, which was subsequently chlorinated with oxalyl chloride to yield the sulfonyl chloride **A.3**. Esterification with MeSSTFMP afforded the protected sulfonate **A.4**. However, reaction with tetrahydroquinoline afforded an unexpected C-alkylated product **A.5**, instead of the desired N-alkylated product.



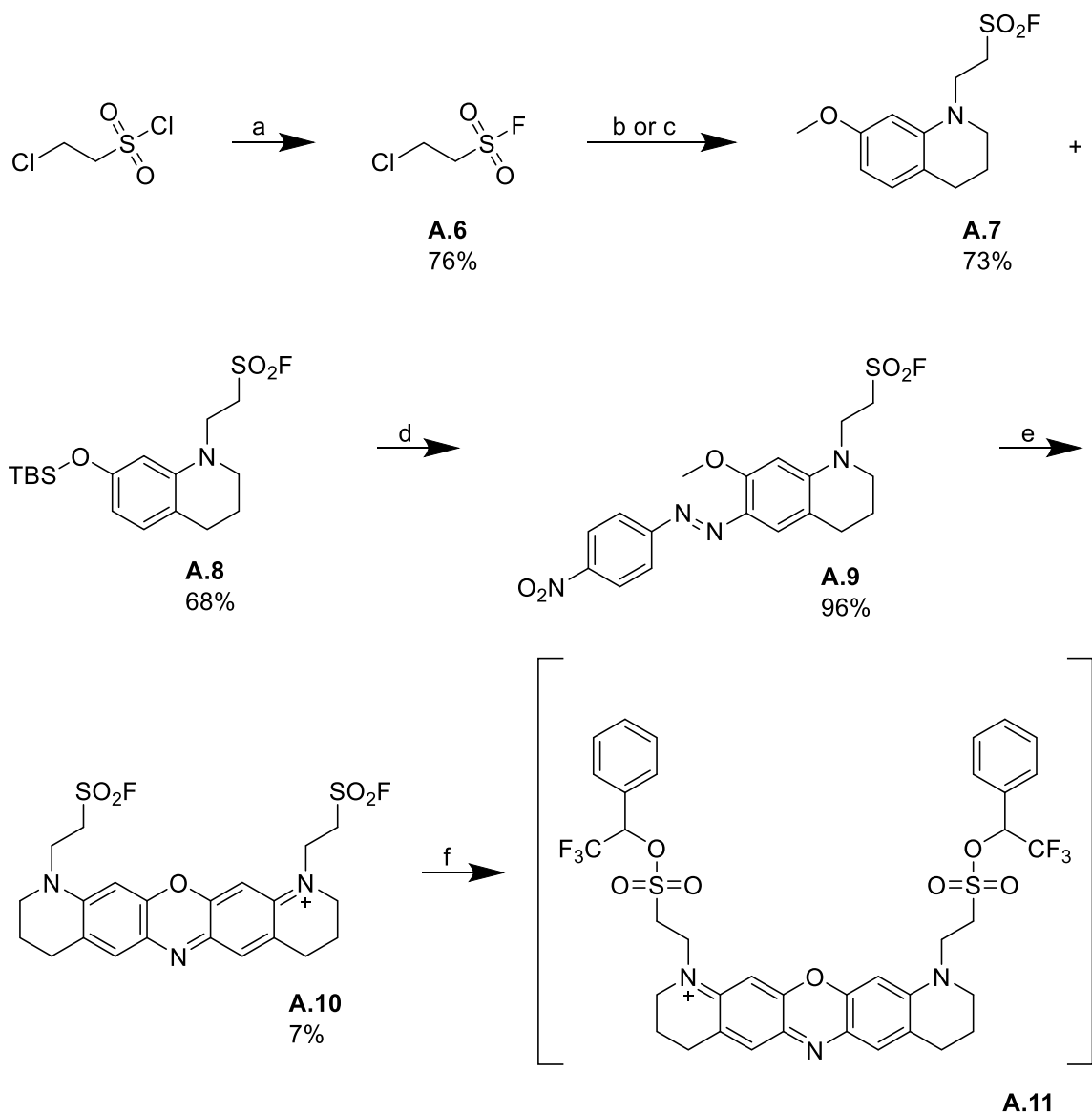
Scheme A2: MeSSTFMP ester forms adduct with methoxy tetrahydroquinoline.

Reagent and conditions: (a) NaI, acetone, reflux; (b) Oxalyl chloride, toluene, Na₂SO₄, DMF, 0 °C; (c) MeSSTFMP (**2.12**), TEA, DCM, 0 °C; (d) 7-methoxy-1,2,3,4-tetrahydroquinoline, DMF, K₂CO₃, 65 °C.

The *para* position of aniline derivatives is nucleophilic, which drives oxazine cyclization (**CHAPTER III**). Interestingly, the tetrahydroquinoline did not attack the disulfide, but instead attacked the α -carbon of the sulfonate ester, leaving the disulfide intact. These results suggest that the chemical reactivity of MeSSTFMP is distinct from TFMB derivatives.

Sulfonyl fluorides have been shown to replace sulfonyl chlorides in sulfonamide and sulfonate ester synthesis.¹³¹ Unlike sulfonyl chlorides, sulfonyl fluorides are less prone to hydrolysis and thus, can be installed at the beginning of the synthesis. To integrate sulfonyl fluorides into our scheme, I prepared the sulfonyl fluoride **A.6**, as reported, and subsequently attached it to the two tetrahydroquinoline derivatives to yield **A.7** and **A.8**.¹³¹ A diazonitrobenzene moiety was installed on **A.7** to yield **A.9**. Acid-mediated

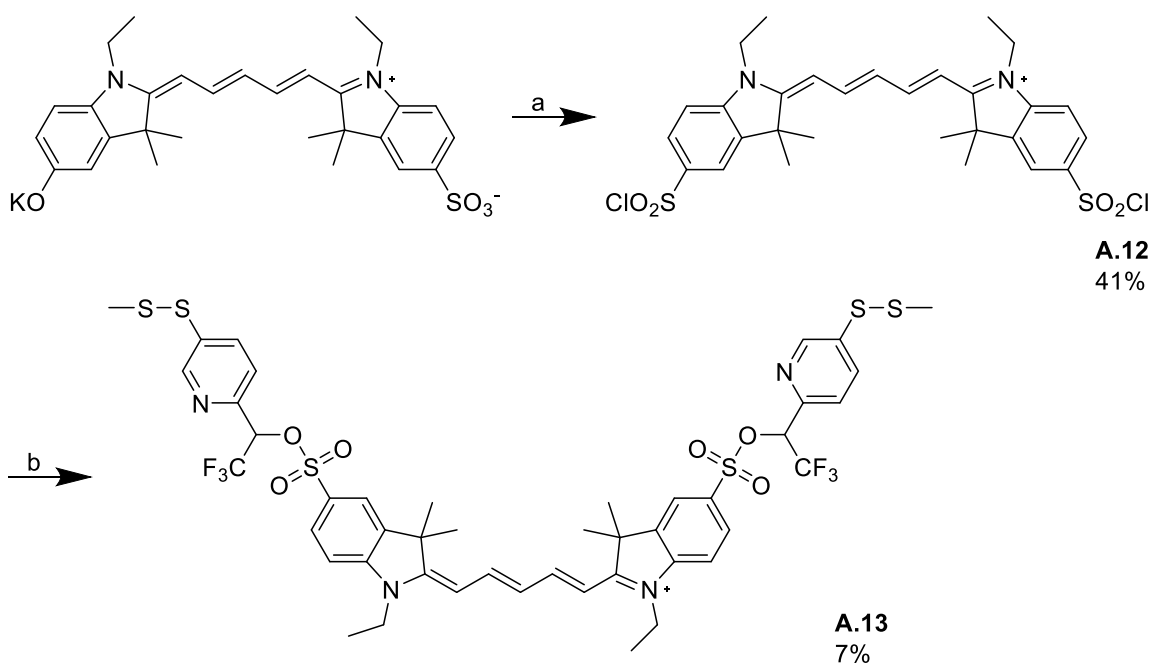
cyclization between **A.8** and **A.9**, followed by HPLC purification afforded the sulfonyl fluoride oxazine derivative **A.10**. For convenience, and as a pilot study, I attempted to append TFMB to the oxazine to yield **A.11**.¹³¹ Regrettably, esterification using reported conditions did not yield appreciable amounts of desired product (**Scheme A3**). Like sulfonyl chlorides, sulfonyl fluorides can form sulfene intermediaries under basic conditions, which are prone to hydrolysis and may explain the low yield.^{131–133}



Scheme A3: Synthesis of MeSSTFMP protected oxazine via sulfonyl fluorides.

Reagent and conditions: (a) HF_2K , pH 3 buffer, THF; (b) $\text{C}_{10}\text{H}_{13}\text{NO}$, MgO , H_2O , THF, 35°C ; (c) $\text{C}_{15}\text{H}_{25}\text{NOSi}$, MgO , H_2O , THF 35°C ; (d) 4-Nitrobenzenediazonium tetrafluoroborate, MeOH, 10% H_2SO_4 ; (e) conc. HCl , EtOH, 80°C ; (f) TMS-TFMB (**A.14**), DBU, ACN.

Unlike oxazines, the synthesis of sulfo-Cy5 does not require column purification, which is ideal for optimizing esterification conditions. The sulfo-Cy5 was prepared as reported.⁹³ Chlorination with phosphorous oxychloride (POCl_3) afforded the bis-chlorinated Cy5 **A.12**. Unfortunately, esterification using DABCO in dichloromethane generally afforded the mono-sulfonate ester with trivial amounts the desired bis-MeSSTFMP Cy5 **A.12**. Through several rounds of optimizations, **A.13** was finally synthesized with newly prepared **A.12** in anhydrous dichloromethane and anhydrous DABCO solution. Although successful, our esterification conditions remain inefficient (7% yield), underlining the necessity for further optimization.



Scheme A4: Synthesis of MeSSTFMP-protected sulfo-Cy5. Reagent and conditions: (a) POCl_3 , BTAC, ACN, reflux; (b) MeSSTFMP (**2.12**), DABCO, DCM, 0 °C.

Identification of Cuticle Permeable Scaffolds in *C. elegans*

Nematodes are responsible for many diseases in human and livestock and remain an economic burden in many third world countries. For example, according to the Centers for Disease Control (CDC), approximately 123 million people, mainly in Africa, are infected with *O. volvulus*, the causative agent of river blindness. Currently, approximately 300,000 people are blinded and another 800,000 visually impaired by the disease.¹³⁴ While the life cycle of parasitic nematodes vary, their cuticle composition is largely evolutionarily conserved.^{135–138} Using *C. elegans*, a free-living nematode, as a model for parasitic nematodes, I aimed to identify cuticle permeable scaffolds for the design of broad-spectrum anthelmintics.

To rapidly identify cuticle permeable scaffolds, I designed a high throughput screen (HTS) using live *C. elegans*. Our screen utilized an ATP dependent bioluminescent reaction to measure intracellular ATP concentrations. Since the generation and maintenance of ATP levels represent a complex network, involving multiple pathways and multiple enzymes, I hypothesized that this screening approach would yield inhibitors from different structural classes and thus, a diverse set of cuticle permeable structural features.

C. elegans strain PE254, that constitutively and ubiquitously expresses firefly luciferase was cultured and synchronized at the L1 stage using standard methods. Using a fluid dispenser, the L1 larvae were seeded into 96 well plates and allowed to mature into the L4 larval stage in the presence of the bacteria. The L4 larva displays a recognizable

vulva morphology (white spot) and thus, was selected for staging purposes.¹³⁹ The uniformity of worm distribution was evaluated based on the variation (% CV) in bioluminescence signals after the addition of D-luciferin (**Eq. A1**). High variation in the background population increases the noise, which, in turn, decreases the Z' , which is a statistical estimate of signal to noise ratio in an HTS (**Eq. A2**).¹⁴⁰ A perfect assay without any noise will have a Z' of 1. Ideally, an excellent chemical screen will have a Z' of 0.7 or above.¹⁴⁰

Our initial results showed poor signal distribution within plates and inconsistent average signal values between plates. The firefly luciferase gene is integrated into the genome of PE254, thus I predicted that the poor signal distribution was the direct result of poor worm distribution. To visualize the worm distribution under a microscope, clear 96 well plates were seeded under identical conditions. As predicted, the worm count was inconsistent between wells.

Sporadic worm distribution could be due to either inadequate worm mixing in the reservoir and/ or worm adhesion to plastic tubing during seeding.^{141,142} To address these issues, I optimized several parameters, including mix speed, size of stir bar and flask, and the addition of PEG-3000 to prevent adhesion. Although substantial improvements were made, the variation in the background signal remained unsatisfactory. Using **Eq. A3**, which assumes low signal variation from hit compounds, the Z' was estimated to be at most 0.58. For this reason, I did not proceed with the screen. However, I believe this

bioluminescence screen holds great potential for identifying diverse cuticle permeable scaffolds for the design of novel of broad-spectrum anthelmintics.

$$\% CV = \frac{\sigma_n}{\mu_n} \quad [\text{Eq. A1}]$$

$$Z' = 1 - \frac{3(\sigma_p + \sigma_n)}{|\mu_p - \mu_n|} \quad [\text{Eq. A2}]$$

$$Z' = 1 - \frac{3(\sigma_n)}{|\mu_n|} \quad [\text{Eq. A3}]$$

Eq A1 – A3: Equation to for % CV and Z' calculation. σ and μ are the standard deviation and average signal of the hit compounds (p) and background population (n).

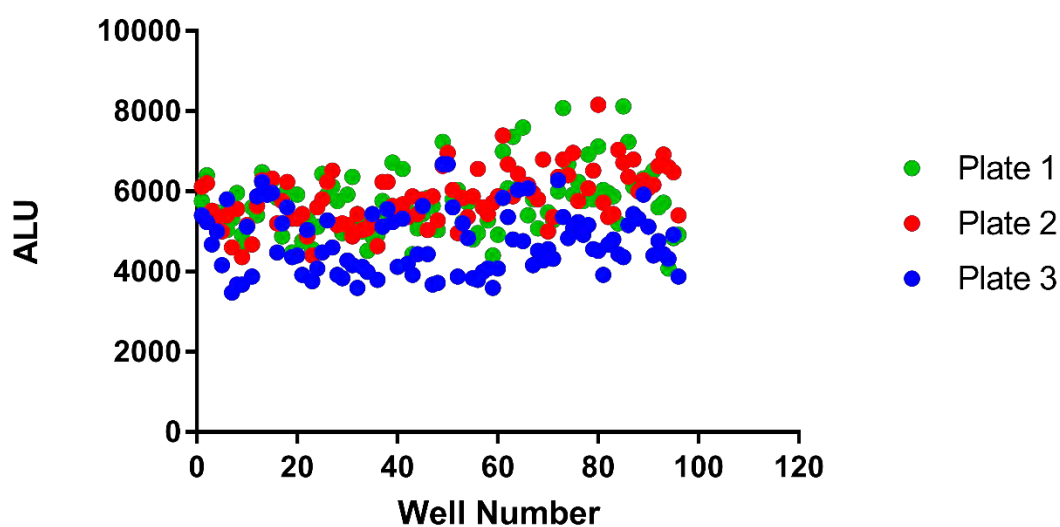


Plate	Avg	S.D	% CV	Z' estimate
1	5732.917	810.863	0.14144	0.58
2	5825.417	695.3226	0.11936	0.64
3	4736.667	769.6926	0.162497	0.51

Figure A1: Sporadic worm distribution lowers the Z'. Well number is plotted against its bioluminescence signal. % CV and Z' estimate are calculated with eq. A1 and eq. A3, respectively.

Materials and Methods

General:

Commercially available products were used without purification and purchased from Combi-Block, Chem-Impex, Sigma-Aldrich, Acros or Oakwood Chemicals. Palladium catalysts and ligands were purchased from Combi-Blocks and Chem-Impex. Anhydrous solvents were purchased from Acros. Compounds were purified with the CombiFlash Rf+ system and HPLC-grade ChromoSolv solvents were purchased from Sigma-Aldrich.

All NMR spectra (^1H , ^{19}F , and ^{13}C) were obtained on a Bruker Ascend 500.

Analytical HPLC was performed on an Agilent 1100 equipped with a Zorbex C8 column and a PDA detector (G1315A DAD). Preparatory HPLC was performed on a Varian ProStar equipped with Agilent 10-Prep C18 21.2 x 250 mm Column. High resolution mass-spec data were obtained on an Agilent 6520 Q-TOF. *C. elegans* were dispensed with aBioTek MultiFlo FX microplate dispenser and read with an EnVision plate reader. Data were graphed and fitted using Graphpad Prism 7. NMR spectra were analyzed with MestReNova.

Bacterial culture:

Single colonies of OP50-GFP were picked and cultured in LB broth containing 50 µg/ml carbenicillin at 37 °C overnight. The bacteria was precipitated via centrifugation at 6000 x g for 15 minutes and diluted in S Medium (1g/ mL). Newly grown bacteria was used for each experiment.

Worm Culture:

A mixed population of PE254 (*felS4*) was disinfected and synchronized using standard sodium hydroxide/ sodium hypochlorite solution. The population was allowed to mature on NGM plates containing OP50-GFP. Highly fluorescent roller L4 worms were transferred to fresh NGM agar plates containing OP50-GFP, where they matured and laid eggs. Once the progeny has become adults, their eggs were harvested using the synchronization method. The eggs were allowed to hatch and the population was synchronized to L1 in M9 media overnight. The L1s were washed with S Medium containing 0.25 % PEG 3000 three times via centrifugation/ aspiration. The worms were diluted to 3 worms per microliter, followed by OP50-GFP addition to a final concentration of 3 mg/ mL.

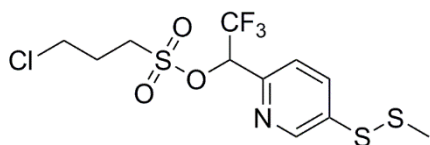
Plating

The worm solution (100 μ L) was mixed continuously with a stir bar and seeded into 96 wells white plates using a BioTek MultiFlo FX with a peristaltic pump. Once the seeding is completed, the plates were sealed with a breathable film and placed in a 20 °C incubator for 48 hours.¹⁴³

Bioluminescence Reading

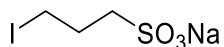
D-luciferin (2 μ L of 500 μ M stock) was added to each well using BioTek MultiFlo FX. The solution was allowed to equilibrate for 15 minutes, then read using the EnVision plate reader equipped with an ultra-sensitive luminescence cube.

Synthetic Methods



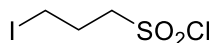
2,2,2-trifluoro-1-(5-(methyldisulfanyl)pyridin-2-yl)ethyl 3-chloropropane-1-sulfonate (A.1)

In a 25 mL round bottom flask, compound **2.11** (41 mg, 0.2 mmol) and TEA (41 mg, 0.4 mmol) were dissolved in anhydrous DCM (3 mL) at 0°C. 3-Chloropropanesulfonyl chloride (71 mg, 0.4 mmol) was separately dissolved in DCM (1 mL) and added dropwise to the reaction. The reaction was stirred at 0 °C for 2 hours and then poured in to aq. 1M HCl (20 mL). The product was extracted with DCM (3 x 20 mL) and the combined organic layers was washed with saturated NaHCO₃ (20 mL), brine (20 mL), then dried over Na₂SO₄. The solvent was removed under reduced pressure and the product was purified by silica gel chromatography (0-20% EtOAc/hex) to afford a pale yellow oil (69 mg, 0.17 mmol, 87%). ¹H NMR (400 MHz, CDCl₃) δ 8.73 (dd, *J* = 2.4, 0.7 Hz, 1H), 8.02 (dd, *J* = 8.3, 2.4 Hz, 1H), 7.59 (d, *J* = 8.3 Hz, 1H), 6.00 (q, *J* = 6.2 Hz, 1H), 3.65 (t, *J* = 6.0 Hz, 2H), 3.45 – 3.37 (m, 2H), 2.49 (s, 3H), 2.37 - 2.29 (m, 2H). ¹⁹F NMR (376 MHz, CDCl₃) δ -75.01 (d, *J* = 6.3 Hz). ¹³C NMR (125 MHz, CDCl₃) δ 147.8 – 147.7 (m), 137.0, 135.6, 122.0 (q, *J* = 280.0 Hz), 122.9, 77.7 (q, *J* = 22.5 Hz), 49.5, 42.1, 26.5, 22.9. HR-EIMS *m/z* calculated for C₁₁H₁₄ClF₃NO₃S₃⁺: 395.9771, found: 395.9755.



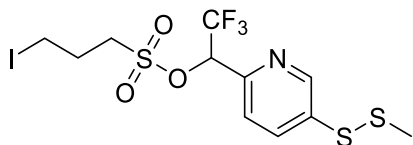
3-Iodopropane-1-sulfonate sodium salt (A.2)

In a 100 mL round bottom flask, sodium iodide (1.1 g, 7.3 mmol) and 1,3-Propanesultone (1 g, 8.1 mmol) were dissolved in acetone (20 mL), then refluxed. After 3 hours, the temperature was brought down to room temperature. The product was filtered and washed with acetone (50 mL) to afford X as a white solid (1.9 g, 7.0 mmol, 96%) ^1H NMR (500 MHz, MeOD) δ 3.39 (t, $J = 7.0$ Hz, 2H), 2.94 – 2.89 (m, 2H), 2.33 – 2.26 (m, 2H). ^{13}C NMR (126 MHz, MeOD) δ 49.6, 27.1, 1.4. ES-HRMS calcd for $\text{C}_3\text{H}_6\text{IO}_3\text{S}$ [$\text{M}-\text{Na}$] $^-$: 248.9088, found: 248.9079.



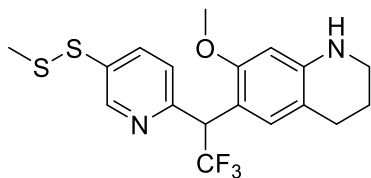
3-iodopropane-1-sulfonyl chloride (A.3)

In a 25 mL round bottom flask, **A.2** (200 mg, 0.76 mmol), Na₂SO₄ (162 mg, 1.14 mmol) and DMF (cat.) were dissolved in toluene (4 mL) at 0 °C. Oxalyl chloride (106 mg, 0.84 mmol) were added dropwise and the reaction was brought to temperature. After 1 hour, the suspension was filtered and the solid was washed with ethyl acetate (3 X 5 mL). The solvents were removed under reduced pressure to give a yellow oil (40 mg, 0.15 mmol, 20%). The compound was used without further purification. ¹H NMR (500 MHz, CDCl₃) δ 3.76 (t, *J* = 7.5 Hz, 2H), 3.27 (t, *J* = 6.5 Hz, 4H), 2.52 – 2.43 (m, 2H). ¹³C NMR (126 MHz, CDCl₃) δ 65.8, 28.0, 0.9.



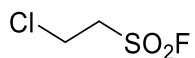
2,2,2-trifluoro-1-(5-(methyldisulfaneyl)pyridin-2-yl)ethyl 3-iodopropane-1-sulfonate (A.4)

In a 25 mL round bottom flask, compound **A.3** (171 mg, 0.64 mmol), compound **2.11** (122 mg, 0.58 mmol) were dissolved in anhydrous dichloromethane at 0 °C. Triethylamine (117 mg, 1.16 mmol) was then added dropwise. After 6 hours, the reaction mixture was poured in aq. 1M HCl (10 mL) and extracted with ethyl acetate (3 X 10 mL). The combined organic layers were washed with H₂O (3 X 10 mL) and brine (10 mL), then dried over sodium sulfate. The solvent was removed under reduced pressure and the product was purified by silica gel chromatography (0-20% EtOAc /hexanes) to afford a yellow oil (185 mg, 0.46 mmol, 80%). ¹H NMR (500 MHz, CDCl₃) δ 8.73 (d, *J* = 2.3 Hz, 1H), 7.99 (dd, *J* = 8.3, 2.3 Hz, 1H), 7.56 (d, *J* = 8.3 Hz, 1H), 5.93 (q, *J* = 6.2 Hz, 1H), 3.33 (t, *J* = 7.5 Hz, 2H), 3.25 (t, *J* = 6.6 Hz, 2H), 2.49 (s, 3H), 2.38 – 2.31 (m, 2H). ¹⁹F NMR (471 MHz, CDCl₃) δ -74.95 (d, *J* = 6.2 Hz). ¹³C NMR (126 MHz, CDCl₃) δ 147.96, 147.86, 137.11, 135.71, 123.0 (d, *J* = 0.8 Hz), 122.1 (d, *J* = 280.4 Hz), 77.9 (d, *J* = 33.9 Hz), 52.9, 27.1, 23.1, 2.0. ES-HRMS calcd for C₁₁H₁₄F₃INO₃S₃: 487.9127, found: 487.9115.

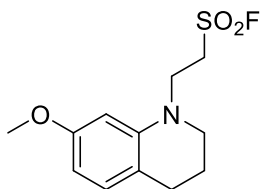


7-methoxy-6-(2,2,2-trifluoro-1-(5-(methylthio)pyridin-2-yl)ethyl)-1,2,3,4-tetrahydroquinoline (A.5)

In a 10 mL round bottom flask, compounds **A.11** (49 mg, 0.1 mmol), 7-methoxy-1,2,3,4-tetrahydroquinoline (19 mg, 0.12 mmol) and potassium carbonate (17 mg, 0.12 mmol) were dissolved in DMF (2 mL), then the temperature was raised to 65 °C. After 3 hours the reaction was poured in to brine (20 mL) and extracted with ethyl acetate (3 X 10 mL). The combined organic layers were washed with H₂O (3 X 10 mL) and brine (10 mL), then dried over sodium sulfate. The solvent was removed under reduced pressure and the product was purified by silica gel chromatography (0-30% EtOAc /hexanes) to afford a yellow oil (30 mg, 0.75 mmol, 75%). ¹H NMR (500 MHz, CDCl₃) δ 8.69 (dd, *J* = 2.3, 0.4 Hz, 1H), 7.80 (dd, *J* = 8.2, 2.5 Hz, 1H), 7.33 (d, *J* = 8.2 Hz, 1H), 7.10 (s, 1H), 6.00 (s, 1H), 5.38 (q, *J* = 10.1 Hz, 1H), 3.74 (s, 3H), 3.31 – 3.21 (m, 2H), 2.77 – 2.59 (m, 2H), 2.45 (s, 3H), 1.95 – 1.83 (m, 3H). ¹⁹F NMR (471 MHz, CDCl₃) δ -65.74 (d, *J* = 10.2 Hz). ¹³C NMR (126 MHz, CDCl₃) δ 156.4, 155.4 – 155.3 (m), 148.7, 145.6, 136.4, 132.8, 130.5, 126.3 (q, *J* = 281.1 Hz), 124.2 – 124.0 (m), 114.0, 110.8, 97.1, 56.0, 47.7 (q, *J* = 27.7 Hz), 41.9, 26.4, 23.1, 22.3. ES-HRMS calcd for C₁₈H₂₀F₃N₂OS₂: 401.0964, found: 401.0953.

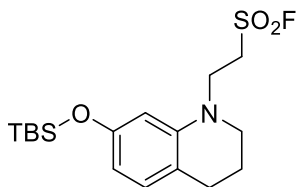
**2-chloroethane-1-sulfonyl fluoride (A.6)**

In a 50 ml round bottom flash, 2-chloroethyl sulfonyl chloride (2g, 12.7 mmol) was dissolved (1 mL). Potassium bifluoride (2g, 25.4 mmol) was separately dissolved in 0.1M pH 3 sodium acetate buffer (9 mL) and slowly added to the reaction. After 5 hours, the product was extracted with diethyl ether (3 X 20 mL). The combined organic layers were washed with H₂O (3 X 20 mL) and brine (20 mL), then dried over sodium sulfate. The solvent was removed under reduced pressure and the product to afford a brown oil (1.4 g, 9.65 mmol, 76%). NMR matches previously reported.¹³¹



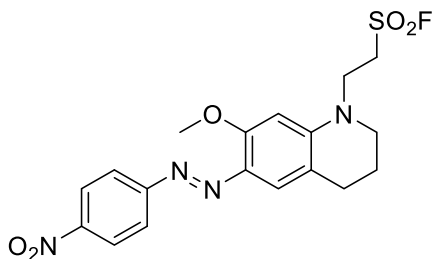
2-(7-methoxy-3,4-dihydroquinolin-1(2H)-yl)ethane-1-sulfonyl fluoride (A.7)

In a 10 mL round bottom flask, 7-methoxy-1,2,3,4-tetrahydroquinoline (300 mg, 1.8 mmol), compound **A.6** (390 mg, 2.7 mmol) and magnesium oxide (108 mg, 2.7 mmol) were dissolved in H₂O/THF (0.4/ 3.6 mL) mixture at 35 °C. After 5 hours, the product was extracted with ethyl acetate (3 X 20 mL). The combined organic layers were washed with H₂O (3 X 20 mL) and brine (20 mL), then dried over sodium sulfate. The solvent was removed under reduced pressure and the product was purified by silica gel chromatography (0-20% EtOAc /hexanes) to afford a yellow solid (360 mg, 1.32 mmol, 73%). ¹H NMR (500 MHz, CDCl₃) δ 6.91 (d, *J* = 8.2 Hz, 1H), 6.27 (dd, *J* = 8.2, 1.8 Hz, 1H), 6.14 (s, 1H), 3.89 (t, *J* = 6.5 Hz, 2H), 3.77 (s, 3H), 3.65 (dt, *J* = 6.5, 5.1 Hz, 2H), 3.32 (t, *J* = 5.5 Hz, 2H), 2.71 (t, *J* = 6.4 Hz, 2H), 2.02 – 1.91 (m, 2H). ¹³C NMR (126 MHz, CDCl₃) δ 159.4, 143.9, 130.3, 116.1, 101.8, 97.4, 55.2, 49.8, 47.0 (d, *J* = 13.6 Hz) 45.7, 26.9, 22.3. ES-HRMS calcd for C₁₂H₁₇FN₂O₃S: 274.0908, found: 274.0896.



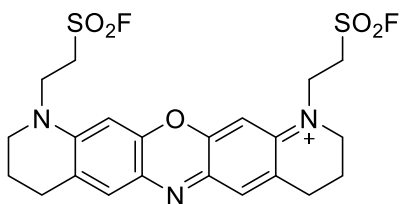
2-(7-((tert-butyldimethylsilyl)oxy)-3,4-dihydroquinolin-1(2H)-yl)ethane-1-sulfonyl fluoride (A.8)

In a 10 mL round bottom flask, 7-((tert-butyldimethylsilyl)oxy)-1,2,3,4-tetrahydroquinoline (300 mg, 1.3 mmol), compound **A.6** (261 mg, 1.8 mmol) and magnesium oxide (72 mg, 1.8 mmol) were dissolved in H₂O/THF (0.4/ 3.6 mL) mixture at 35 °C. After 5 hours, the product was extracted with ethyl acetate (3 X 20 mL). The combined organic layers were washed with H₂O (3 X 20 mL) and brine (20 mL), then dried over sodium sulfate. The solvent was removed under reduced pressure and the product was purified by silica gel chromatography (0-10% EtOAc /hexanes) to afford a yellow solid (330 mg, 0.88 mmol, 68%). ¹H NMR (500 MHz, CDCl₃) δ 6.82 (d, *J* = 8.0 Hz, 1H), 6.19 (d, *J* = 8.1 Hz, 1H), 6.05 (s, 1H), 3.85 (t, *J* = 6.5 Hz, 2H), 3.66 – 3.55 (m, 2H), 3.29 (t, 2H), 2.68 (t, *J* = 6.3 Hz, 2H), 2.01 – 1.85 (m, 2H), 0.98 (s, 9H), 0.20 (s, 6H). ¹³C NMR (126 MHz, CDCl₃) δ 155.2, 143.7, 130.2, 116.4, 109.2, 102.7, 49.7, 46.8 (d, *J* = 13.5 Hz), 45.7, 27.0, 25.7, 22.3, 18.2, -4.4. ES-HRMS calcd for C₁₇H₂₉FNO₃SSi: 374.1616, found: 274.1602.



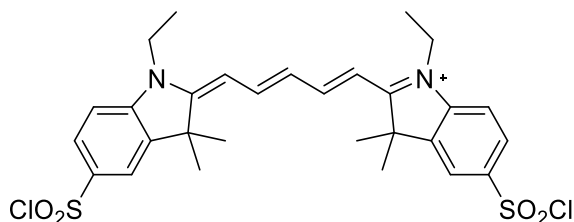
(E)-2-(7-methoxy-6-((4-nitrophenyl)diazenyl)-3,4-dihydroquinolin-1(2H)-yl)ethanesulfonyl fluoride (A.9)

In 50 mL round bottom flask, compound **A.7** (130 mg, 0.47 mmol) was dissolved in methanol (4.7 mL). 4-Nitrobenzenediazonium tetrafluoroborate (123 mg, 0.52 mmol) was separately suspended in aq. 10% H₂SO₄ and added to the reaction. After 1 hour, the reaction was poured into sat. NaHCO₃ (50 mL) and extracted with ethyl acetate (3 X 20 mL). The combined organic layers were washed with H₂O (3 X 20 mL) and brine (20 mL), then dried over sodium sulfate. The solvent was removed under reduced pressure and the product was purified by silica gel chromatography (0-100% EtOAc /hexanes) to afford a shiny purple solid (190 mg, 0.45 mmol, 96%). ¹H NMR (500 MHz, DMSO) δ 8.34 (d, *J* = 8.3 Hz, 2H), 7.85 (d, *J* = 8.4 Hz, 2H), 7.49 (s, 1H), 6.32 (s, 1H), 4.39 (dd, *J* = 12.3, 6.1 Hz, 2H), 4.04 (t, *J* = 6.5 Hz, 2H), 3.98 (s, 3H), 3.50 – 3.43 (m, 2H), 2.67 (t, *J* = 6.0 Hz, 2H), 1.92 – 1.81 (m, 2H). ¹³C NMR (126 MHz, DMSO) δ 160.1, 157.3, 150.9, 146.7, 133.6, 125.4, 122.7, 117.0, 116.6, 94.6, 56.3, 49.7, 47.5 (d, *J* = 11.8 Hz), 45.6, 26.9, 21.8. ES-HRMS calcd for C₁₈H₂₀FN₄O₅S: 423.1133, found: 274.1123.



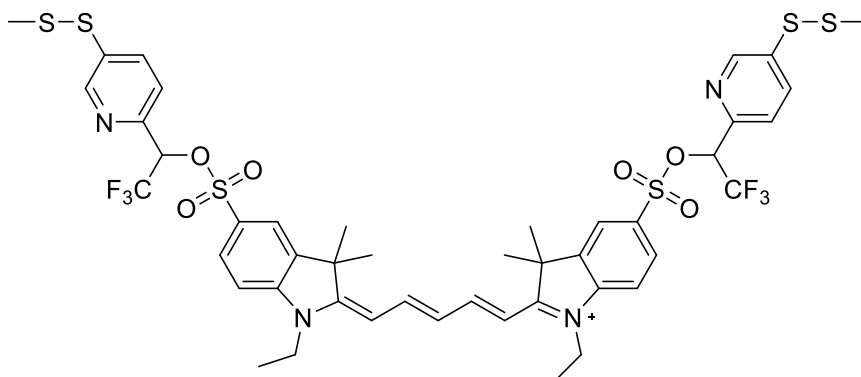
1,11-bis(2-(fluorosulfonyl)ethyl)-3,4,8,9,10,11-hexahydro-2H-dipyrido[3,2-b:2',3'-i]phenoxazin-1-ium (A.10)

In a 25 mL round bottom flask, compound **A.7** (112 mg, 0.27) and **A.8 Y** (100 mg, 0.27 mmol) were dissolved in concentrated HCl (1 mL) and ethanol (9 mL), then the temperature was raised to 80 °C. After 3 hours, the product was first purified by silica gel chromatography (0-10% MeOH/DCM), then followed by HPLC (0.1% TFA, 0-100% ACN/H₂O) to afford compound X as a blue solid (10 mg, 0.02 mmol, 7%). ¹H NMR (500 MHz, MeOD) δ 7.67 (t, *J* = 1.2 Hz, 2H), 7.06 (s, 2H), 4.36 – 4.23 (m, 8H), 3.80 (t, *J* = 6.0 Hz, 4H), 3.02 (t, *J* = 5.9 Hz, 4H), 2.15 – 2.06 (m, 4H). ¹³C NMR (126 MHz, MeOD) δ 156.2, 150.1, 136.4, 132.4, 131.3, 96.8, 52.3, 47.9, 47.8 (d, *J* = 16.4 Hz), 28.4, 21.7. ES-HRMS calcd for C₂₂H₂₄F₂N₃O₅S₂: 512.1120, found: 512.1107.



5-(chlorosulfonyl)-2-((1E,3E)-5-((E)-5-(chlorosulfonyl)-1-ethyl-3,3-dimethylindolin-2-ylidene)penta-1,3-dien-1-yl)-1-ethyl-3,3-dimethyl-3H-indol-1-ium (A.12)

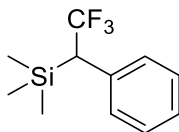
In a 3 neck flask equipped with a reflux condenser, sulfo-Cy5 potassium salt (65 mg, 0.1 mmol) and benzyltrimethylammonium chloride (BTAC) (91 mg, 0.4 mmol) was dissolved in anhydrous acetonitrile (6.5 mL). Phosphorous oxychloride (POCl_3) (396, 2.4 mmol) was injected via syringe and the reaction was refluxed 85 °C for 12 minutes. The reaction mixture was cooled to room temperature, transferred to a 100 mL round bottom flask and removed under reduced pressure. The residue was dissolved in cold CHCl_3 (20 mL), poured into ice water (50 mL) extracted with cold CHCl_3 (2X, 20 mL). The combined organic layers were washed with cold brine and dried over sodium sulfate. The solvent was removed under reduced pressure to yield X as a blue solid (30 mg, 0.041 mmol, 41%). The compound was used without further purification.



1-ethyl-2-((1E,3E)-5-((E)-1-ethyl-3,3-dimethyl-5-((2,2,2-trifluoro-1-(5-(methyldisulfaneyl)pyridin-2-yl)ethoxy)sulfonyl)indolin-2-ylidene)penta-1,3-dien-1-yl)-3,3-dimethyl-5-((2,2,2-trifluoro-1-(5-(methyldisulfaneyl)pyridin-2-yl)ethoxy)sulfonyl)-3H-indol-1-ium (A.13)

In a 100 mL round bottom flask, **A.12** (30 mg, 0.041 mmol) and **2.11** (31 mg, 0.92 mmol) were dissolved in anhydrous DCM that was dried under molecular sieves (3 Å) overnight, under argon atmosphere. The temperature was lowered to 0 °C and 1M DABCO in THF solution (82 µL, 0.082 mmol) was added dropwise. The reaction was allowed to warm to room temperature naturally in the ice bath and stirred for 16 hours. The reaction was poured into brine (20 mL) and extracted with DCM (3X, 20 mL). The combined organic layers were washed with H₂O (3 X 20 mL) and brine (20 mL), then dried over sodium sulfate. The solvent was removed under reduced pressure and the product was purified by silica gel chromatography (0-50% MeOH /DCM), followed by preparatory HPLC (0.1% TFA, 0-100% ACN/H₂O) to afford **A.12** as a blue solid (3.2 mg, 0.03 mmol, 7%). ¹H NMR (500 MHz, MeOD) δ 8.46 (dd, *J* = 2.4, 0.6 Hz, 2H), 8.37 (t, *J* = 13.1 Hz, 2H), 7.86 (m, 6H), 7.42 (d, *J* = 8.3 Hz, 2H), 7.34 (d, *J* = 8.4 Hz, 2H), 6.74 (t, *J* = 12.4 Hz, 1H), 6.40 (d, *J* = 13.7 Hz, 2H), 6.00 (q, *J* = 6.3 Hz, 2H), 4.11 (q, *J* = 7.2

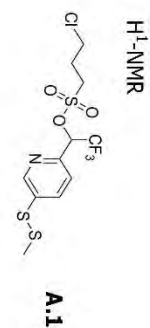
Hz, 4H), 2.41 (s, 6H), 1.66 (d, $J = 5.9$ Hz, 12H), 1.32 (t, $J = 7.2$ Hz, 6H). ^{19}F NMR (471 MHz, MeOD) δ -76.98 (d, $J = 6.4$ Hz). ^{13}C NMR (126 MHz, MeOD) δ 174.2, 156.7, 147.4, 146.8, 146.5, 142.4, 136.8, 135.1, 131.2, 130.2, 128.1, 123.6, 122.2 (q, $J = 281.0$ Hz), 110.9, 105.0, 77.9 (q, $J = 34.0$ Hz) 49.2, 39.1, 26.2, 26.1, 21.8, 11.1. ES-HRMS calcd for $\text{C}_{45}\text{H}_{47}\text{F}_6\text{N}_4\text{O}_6\text{S}_6^+$: 1045.1719, found: 1045.1671.



Trimethyl(2,2,2-trifluoro-1-phenylethyl)silane (A.14)

In a 50 mL round bottom flask, benzaldehyde (1 g, 9.4 mmol) and trimethyl(trifluoromethyl)silane (1 g, 11.3 mmol) were dissolved in anhydrous THF (20 mL) under argon. The temperature was lowered to 0 °C, followed by the dropwise addition of 1 M TBAF in THF (50 μ L, 0.05 mmol). The reaction was raised to room temperature and stirred for 30 minutes. The solvent was removed under reduced pressure and the product was purified by silica gel chromatography (0 – 5% EtOAc/hex) to afford a pale yellow oil (1.9 g, 8.2 mmol, 87%). ^1H NMR (500 MHz, CDCl_3) δ 7.36 – 7.31 (m, 2H), 7.27 – 7.22 (m, 3H), 4.80 (q, J = 6.6 Hz, 1H), -0.00 (s, 9H). ^{19}F NMR (471 MHz, CDCl_3) δ -78.40 (d, J = 6.7 Hz). ^{13}C NMR (126 MHz, CDCl_3) δ 135.8, 129.4, 128.6, 127.9, 124.6 (d, J = 282.2 Hz), 73.7 (q, J = 32.1 Hz), -0.0.

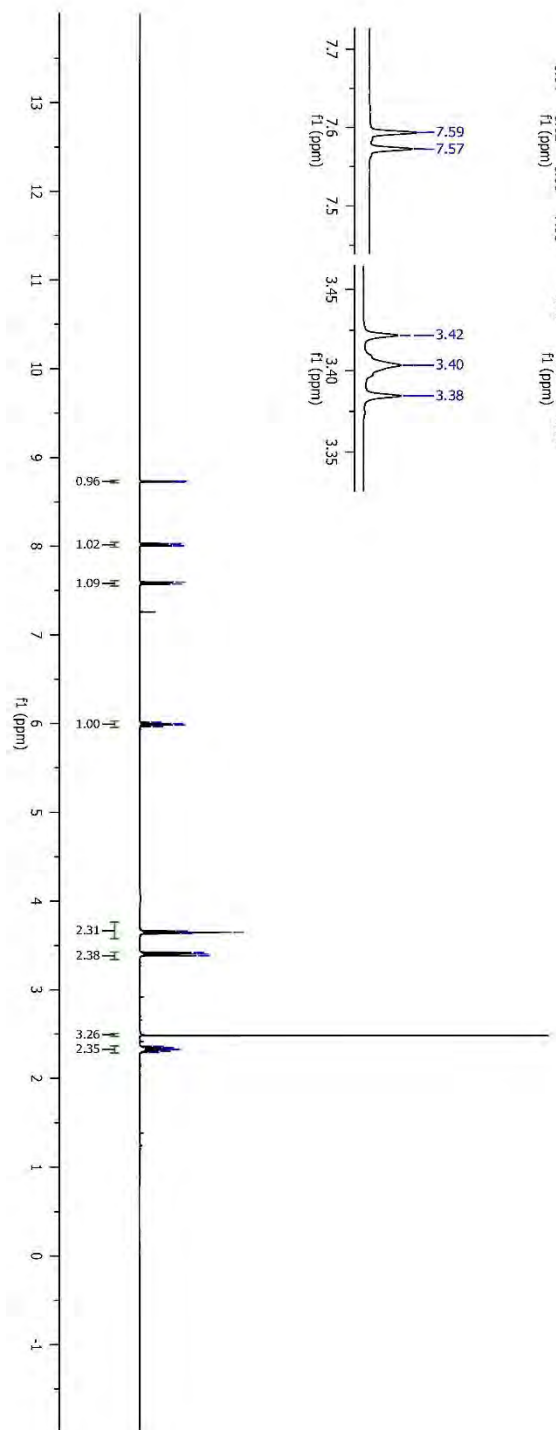
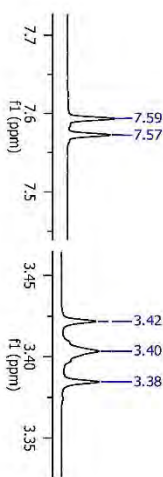
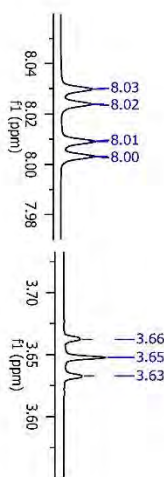
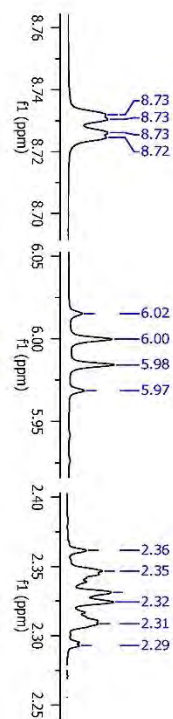
NMR Spectra

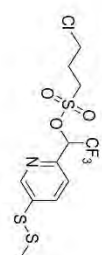


8.73
8.73
8.73
8.72
8.02
8.00

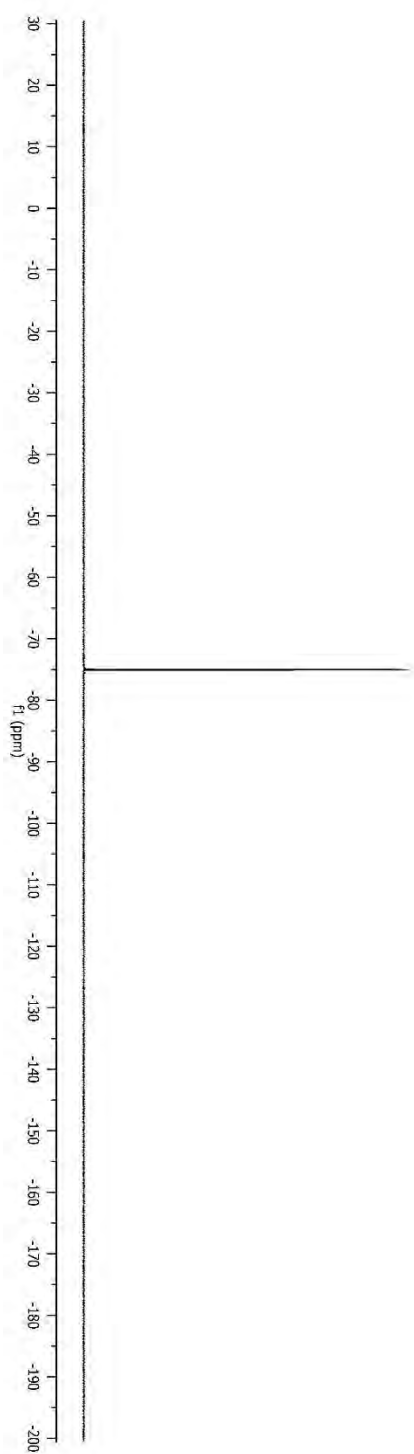
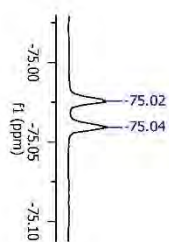
6.02
6.00
5.98
5.97

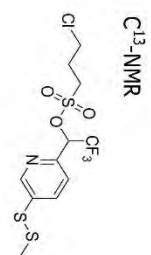
3.66
3.66
3.65
3.63
3.40
3.38
2.36
2.35
2.33
2.32
2.31
2.29



F^{19} -NMR**A.1**

-75.02
-75.04



**A.1**

147.76
147.74

137.04
135.64

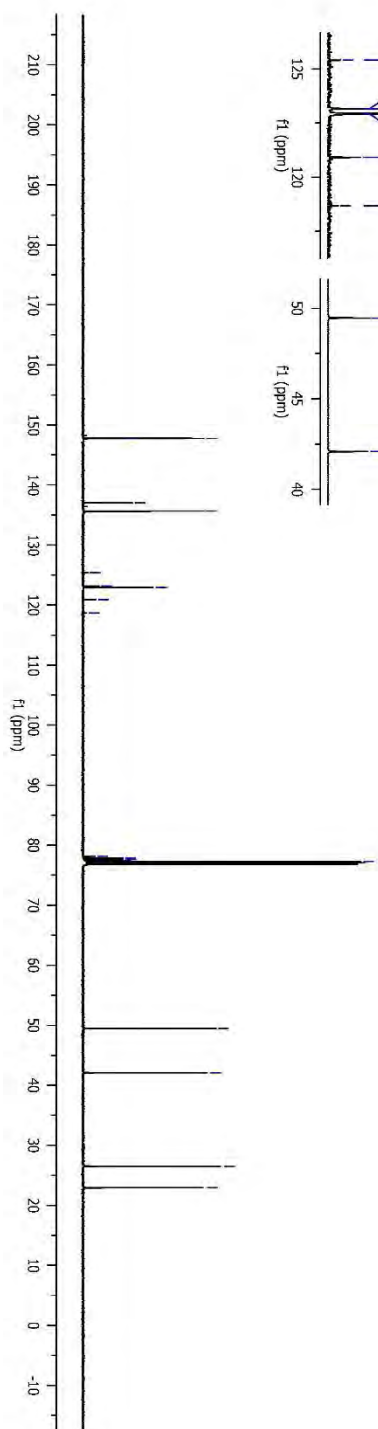
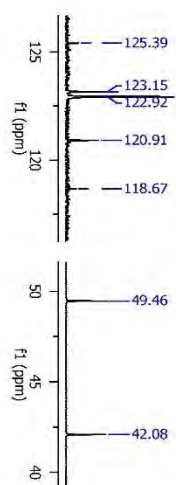
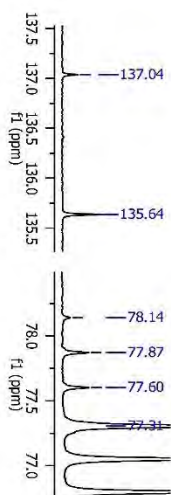
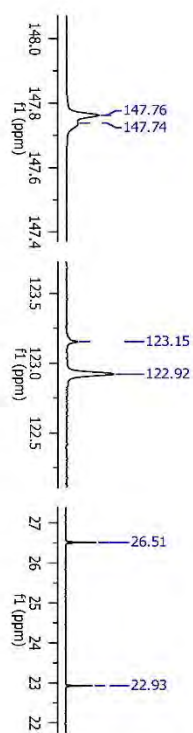
125.39
123.15
122.92
120.91
118.67

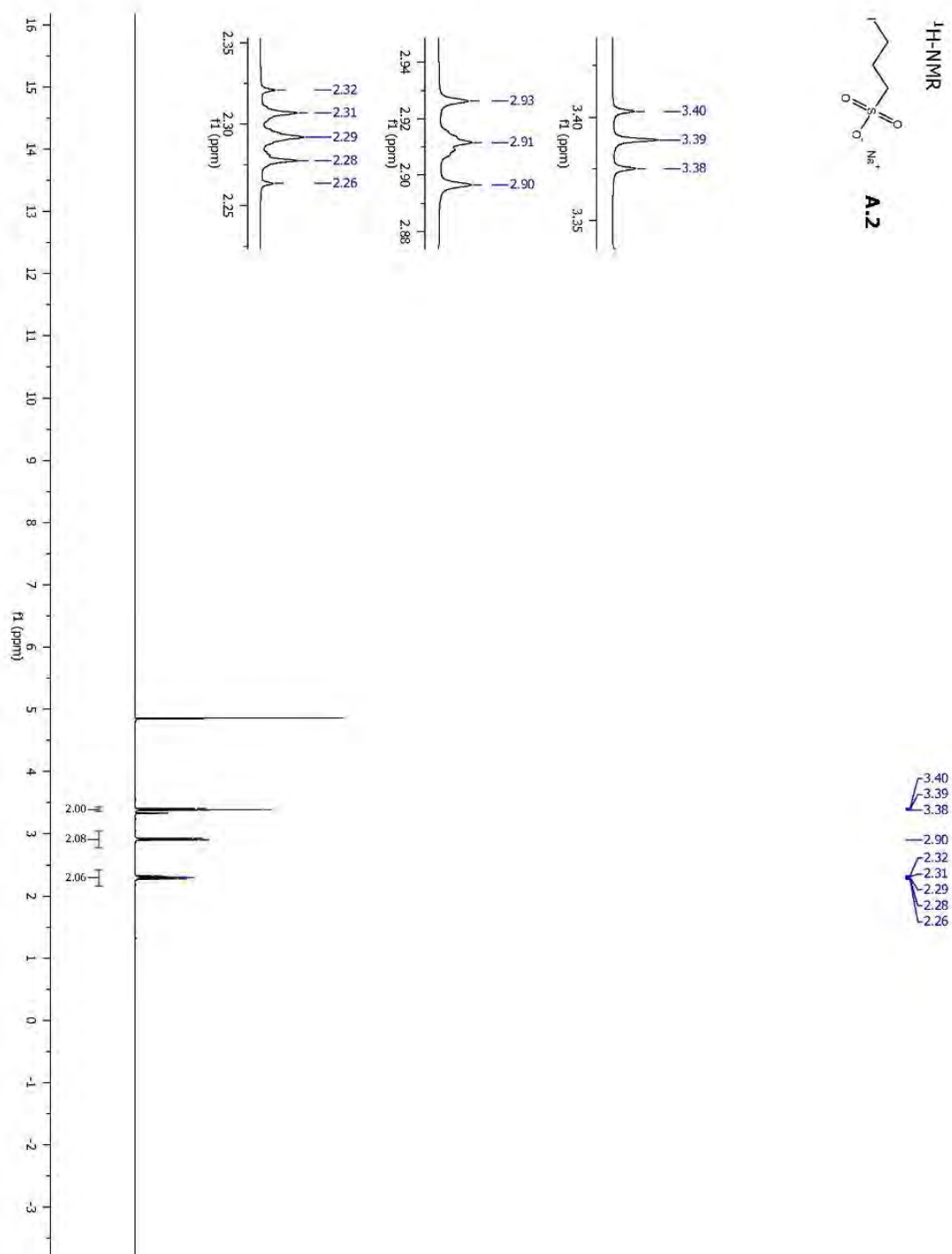
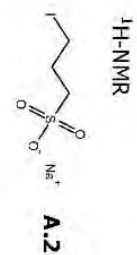
78.14
77.87
77.60
77.31

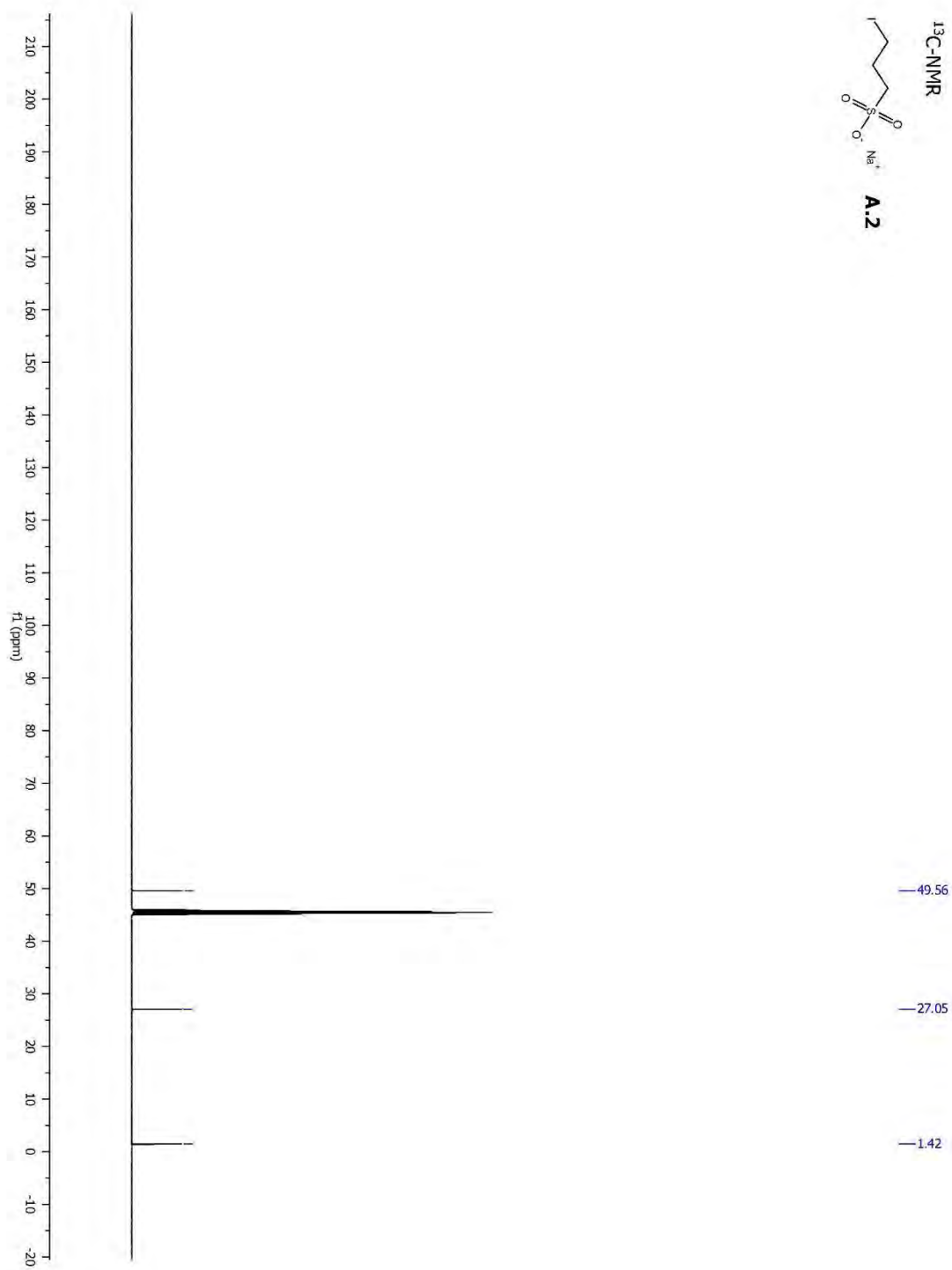
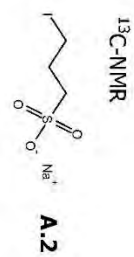
49.46

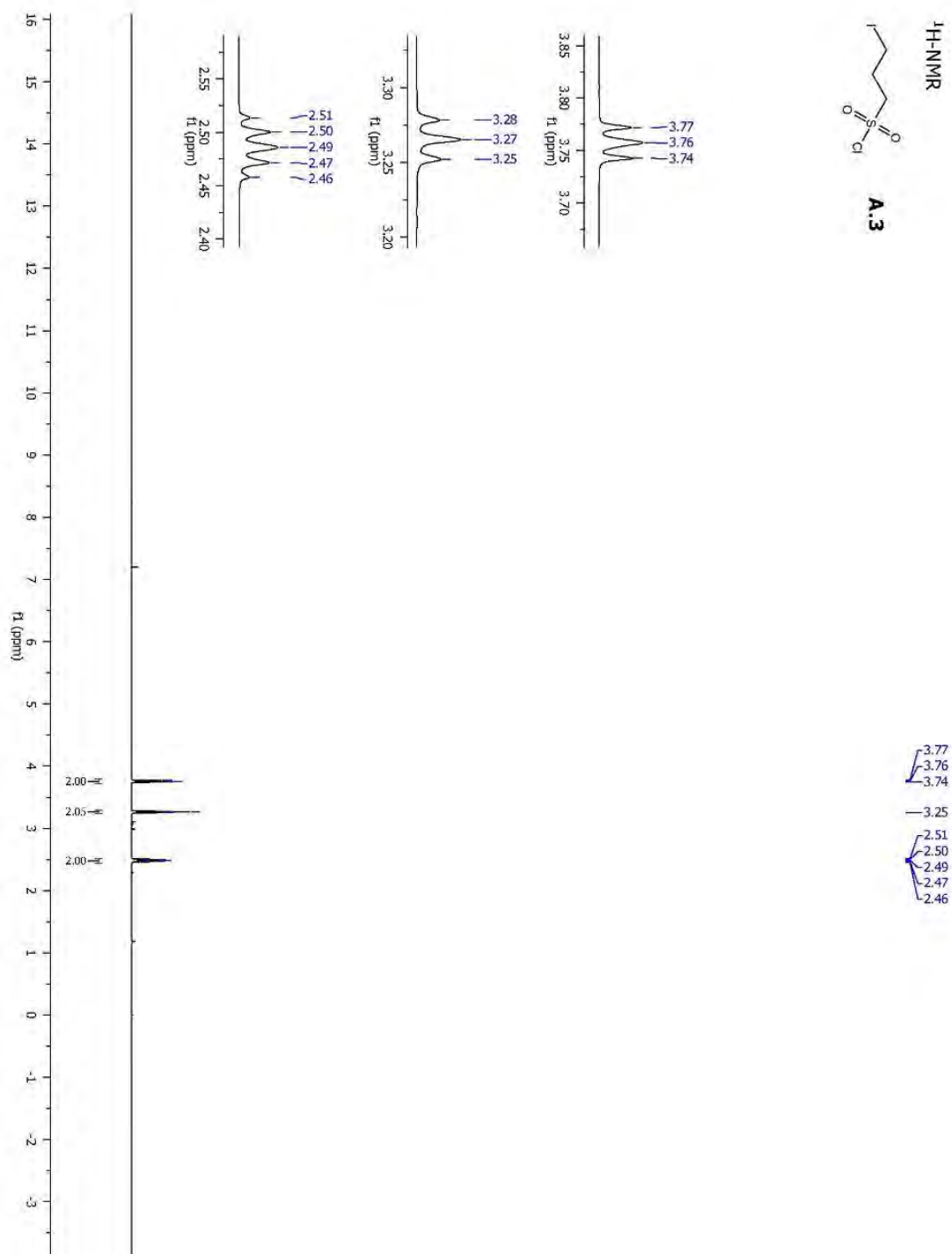
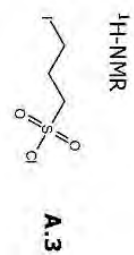
42.08

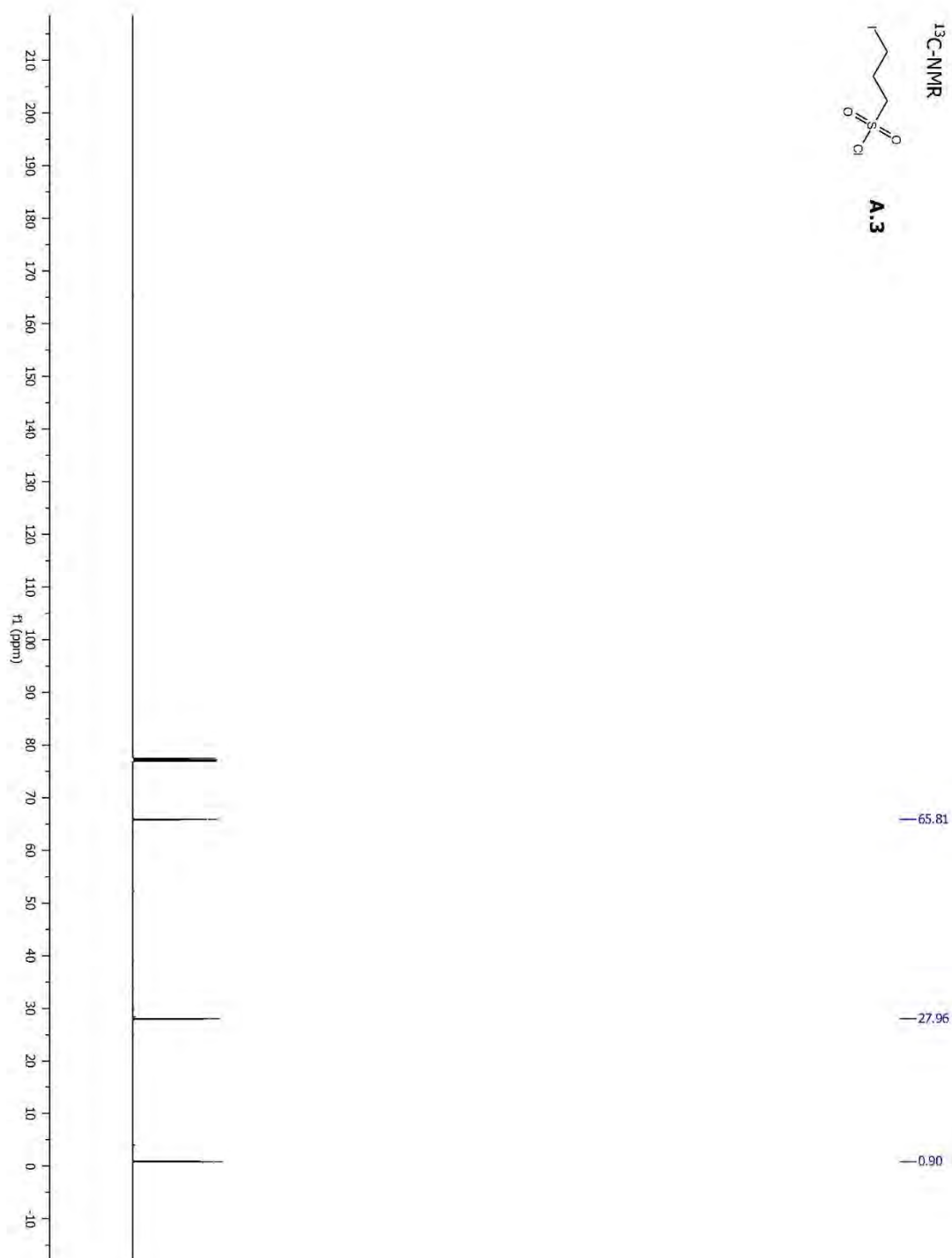
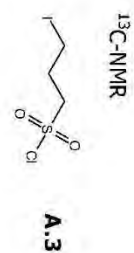
26.51
22.93

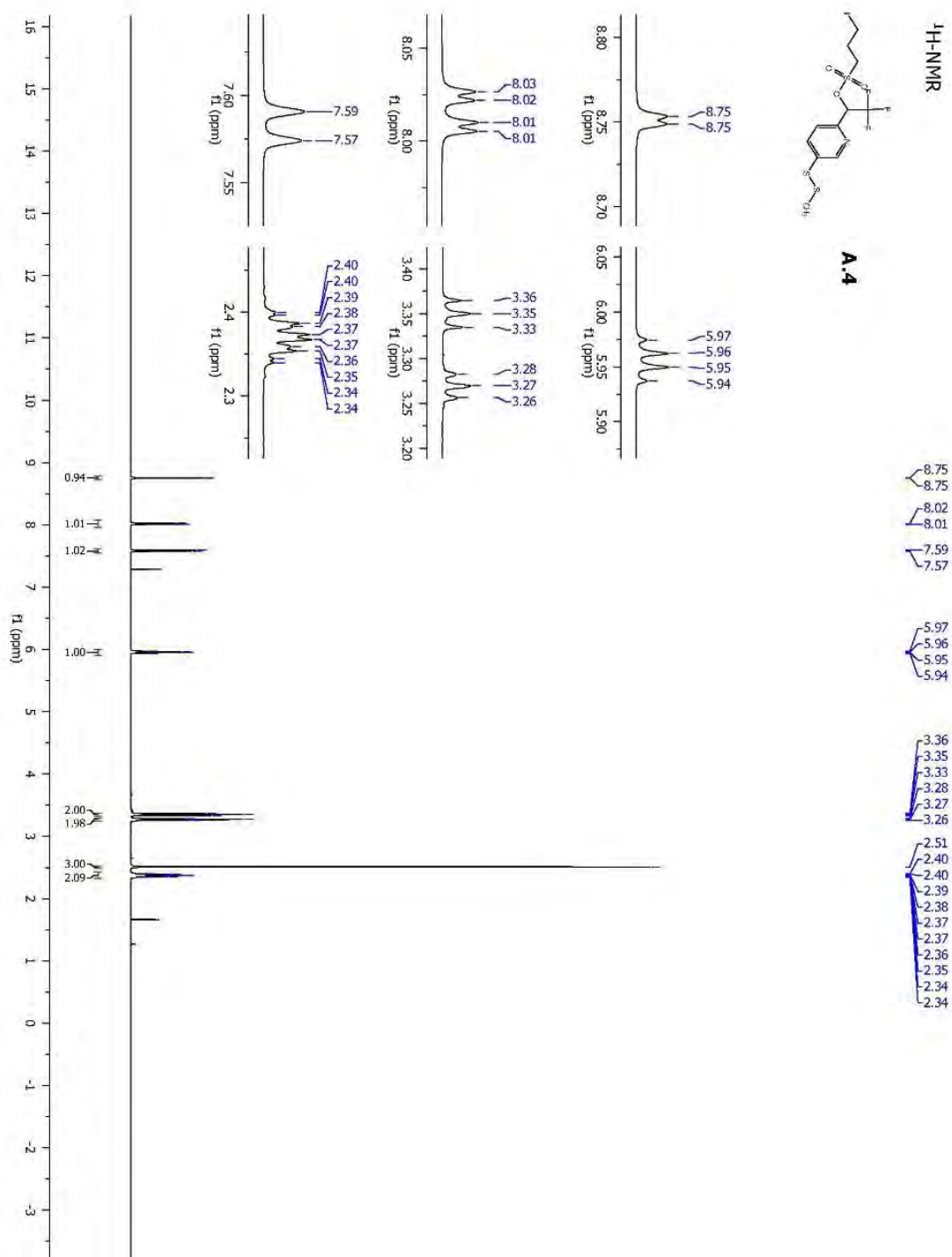


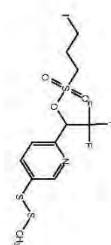




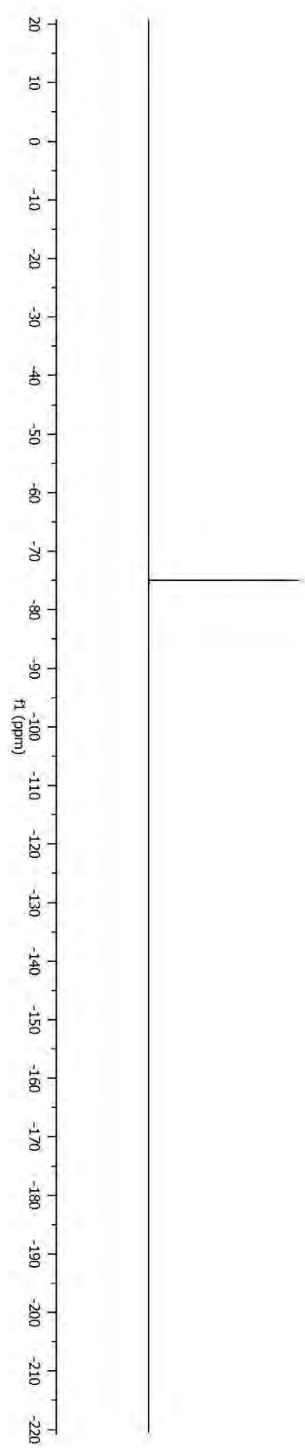
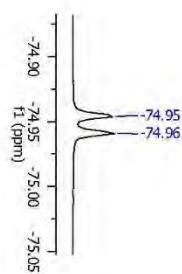


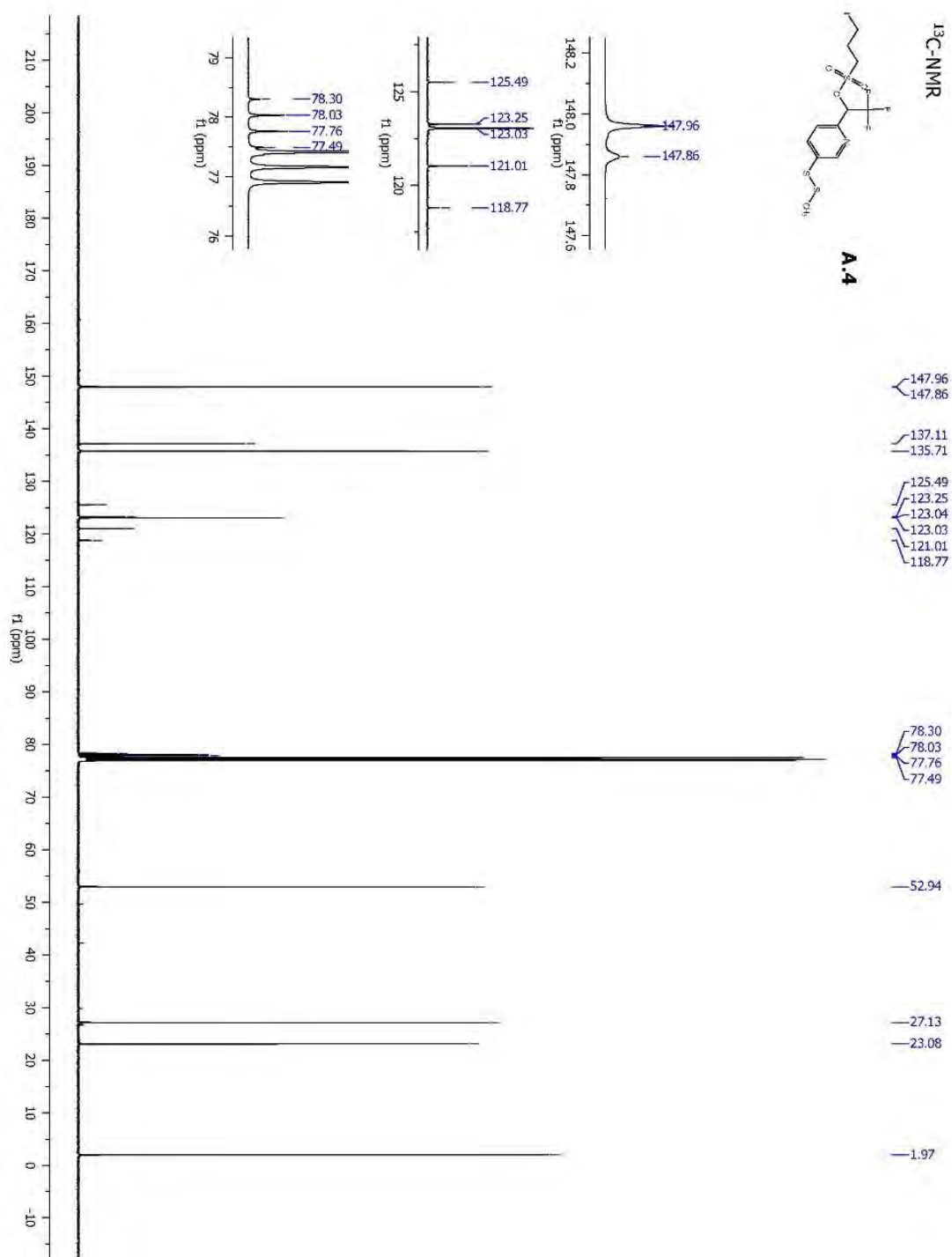


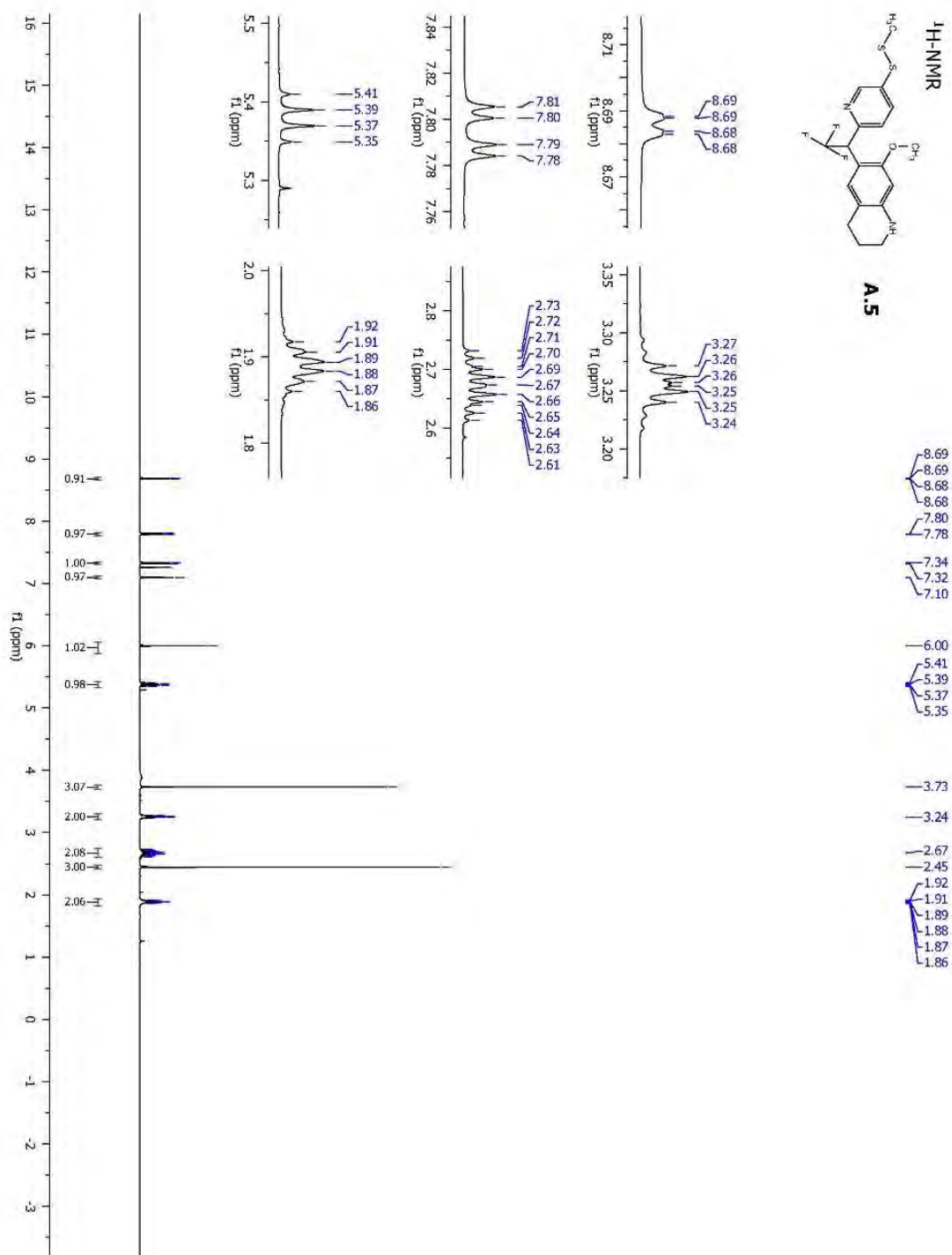


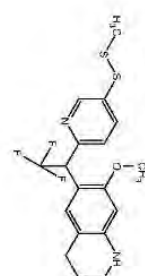
¹⁹F-NMR**A.4**

-74.95
-74.96



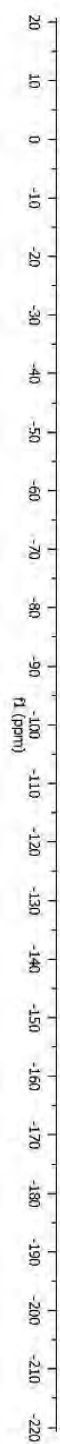
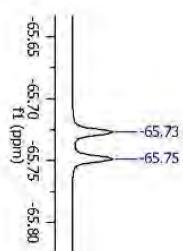


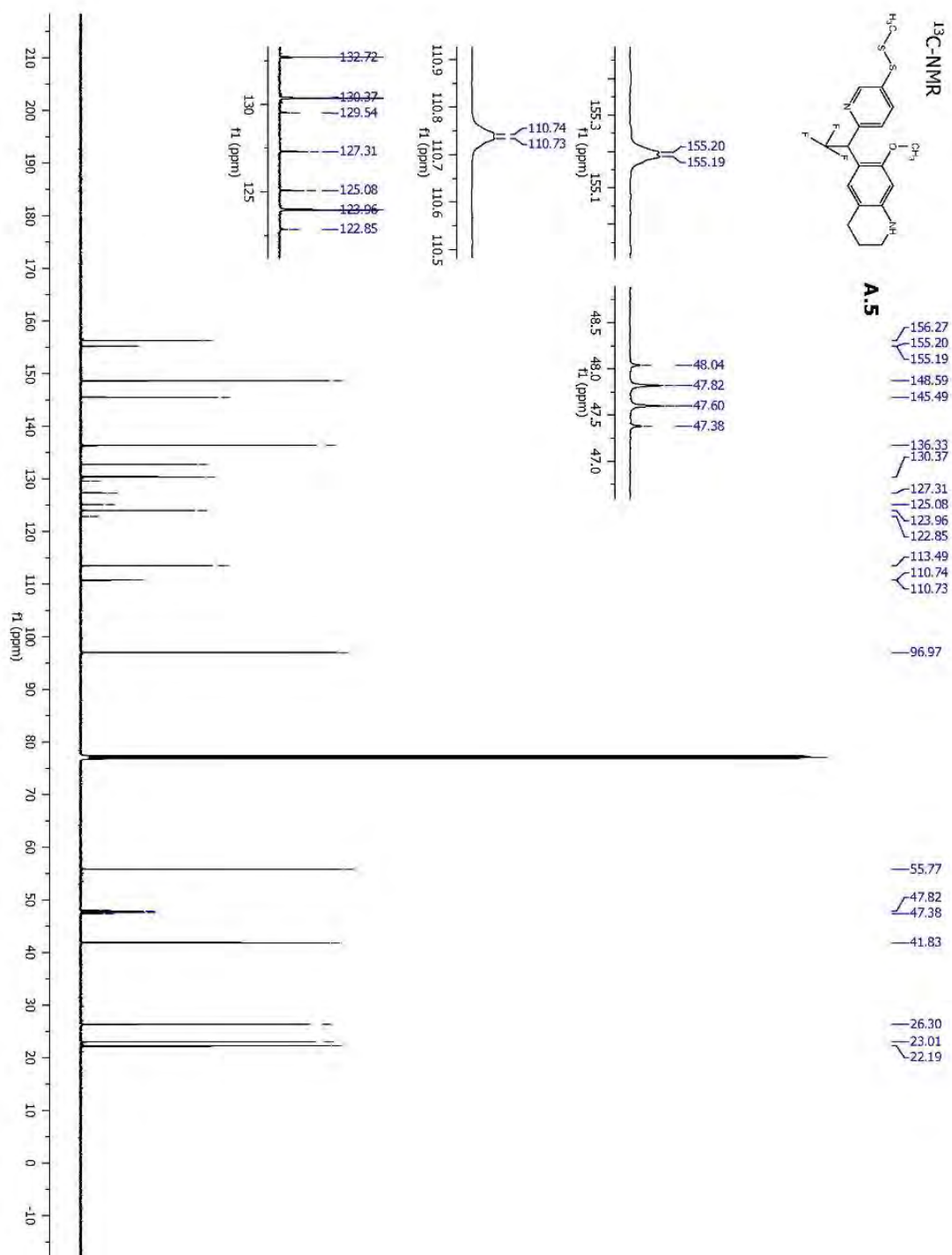


¹⁹F-NMR

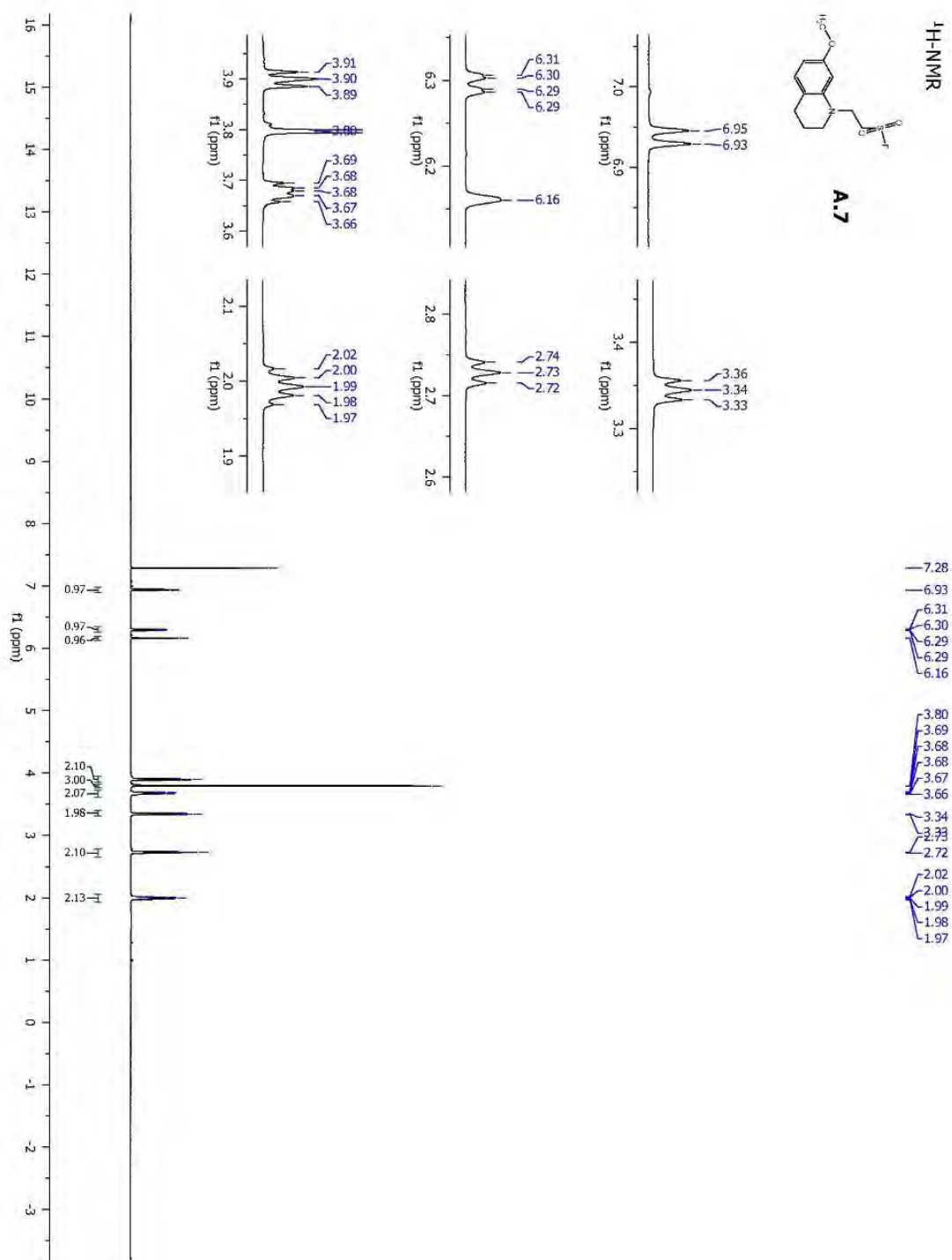
A.5

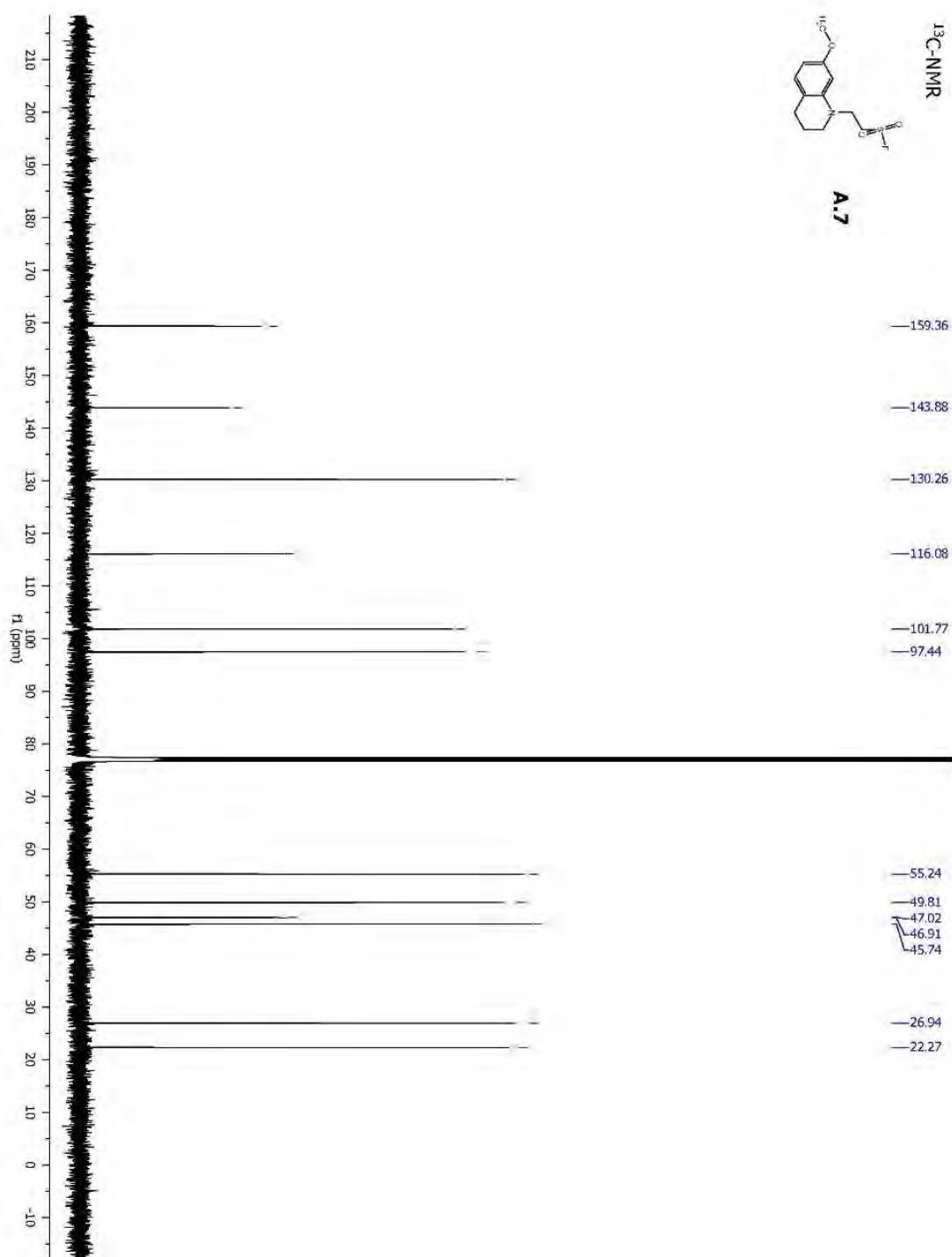
-65.73
-65.75

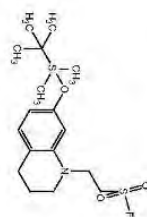
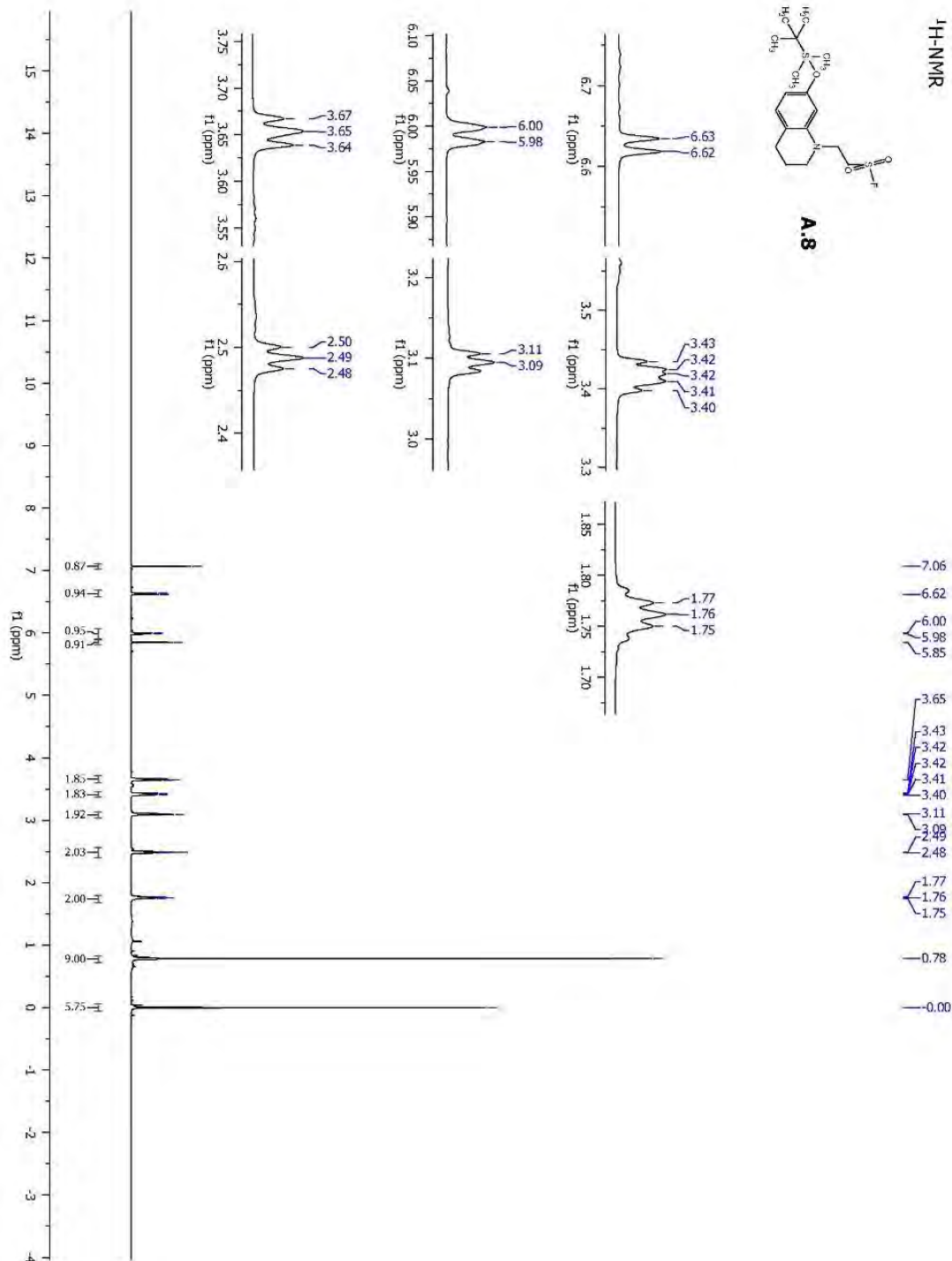


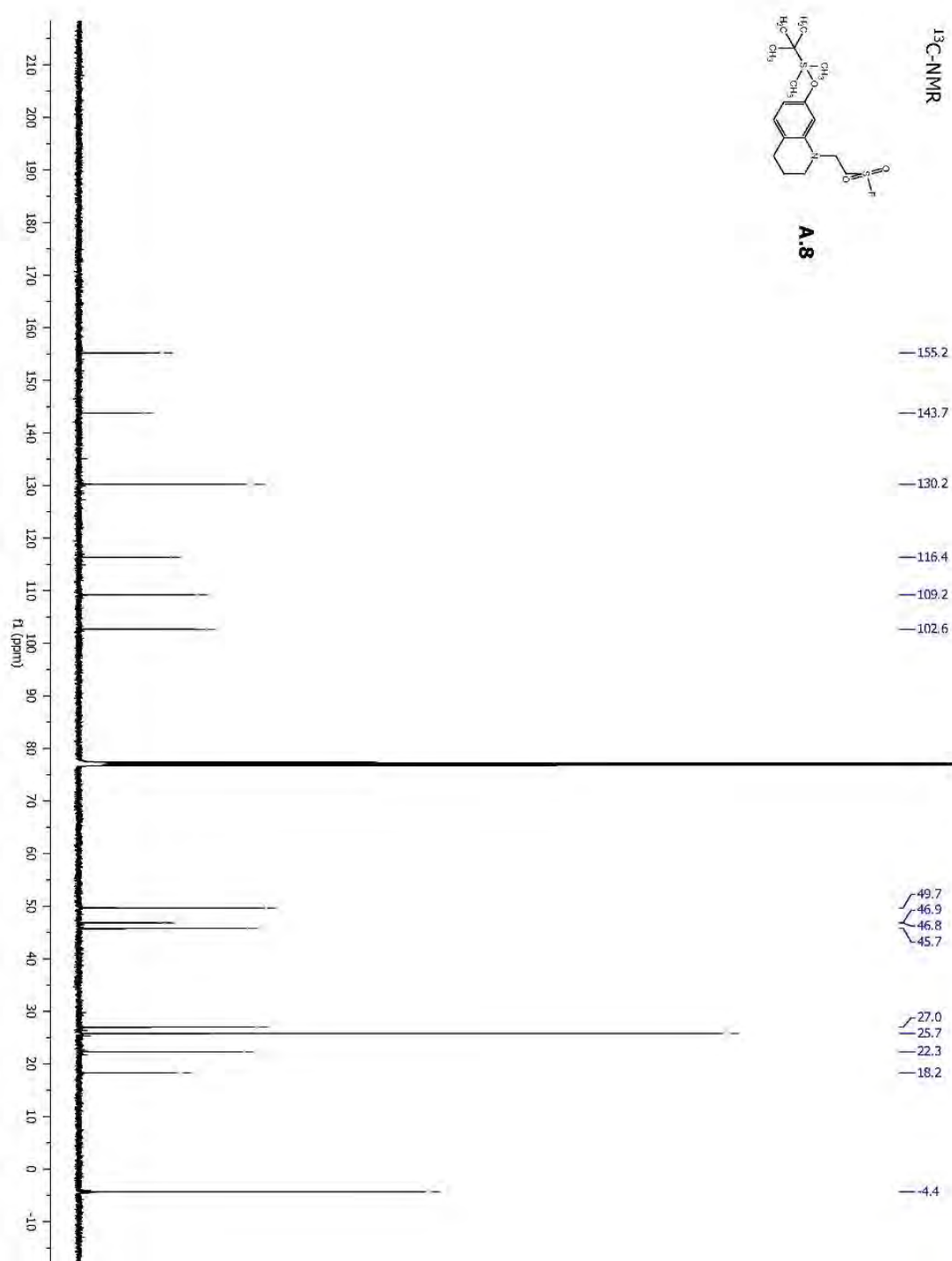


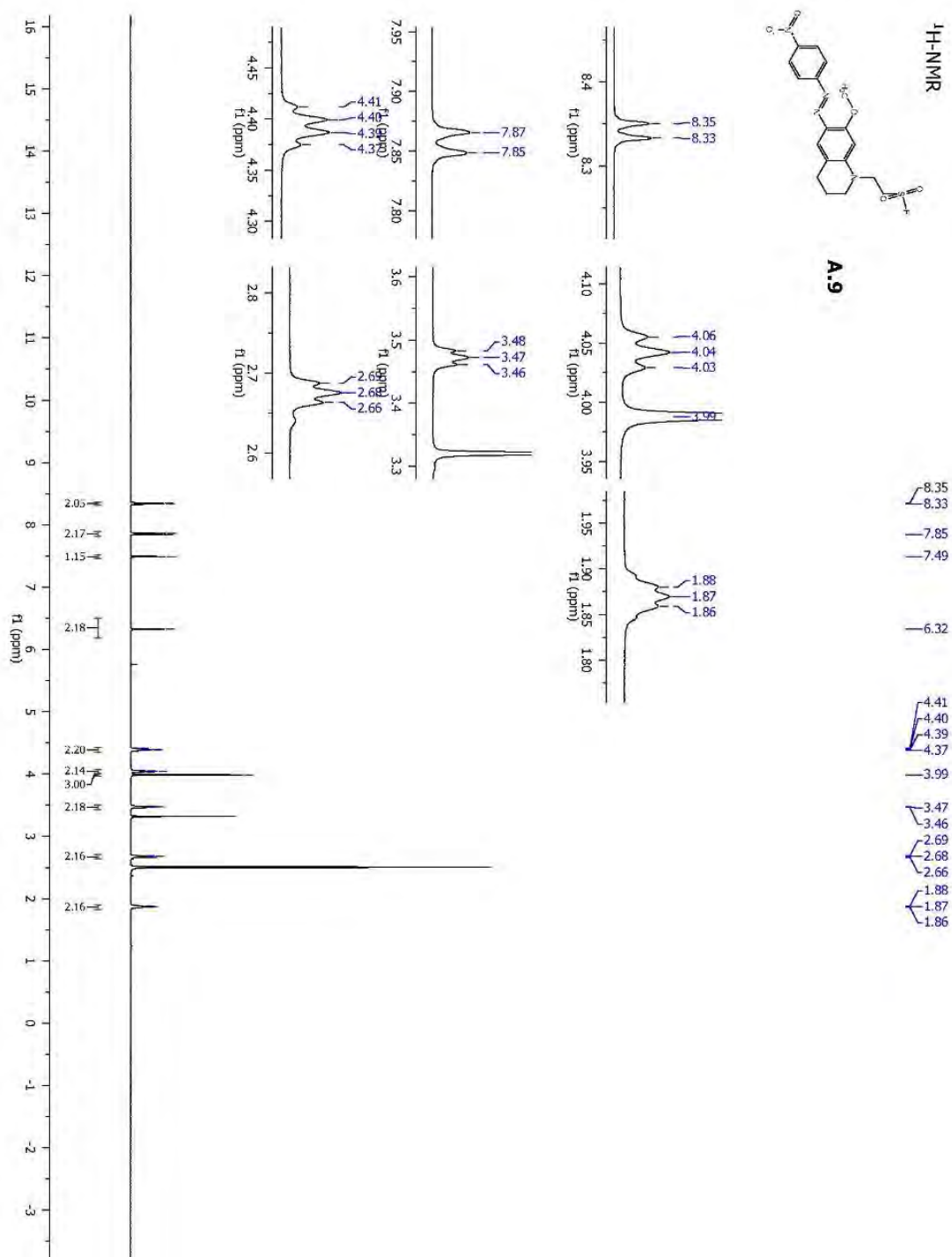
6

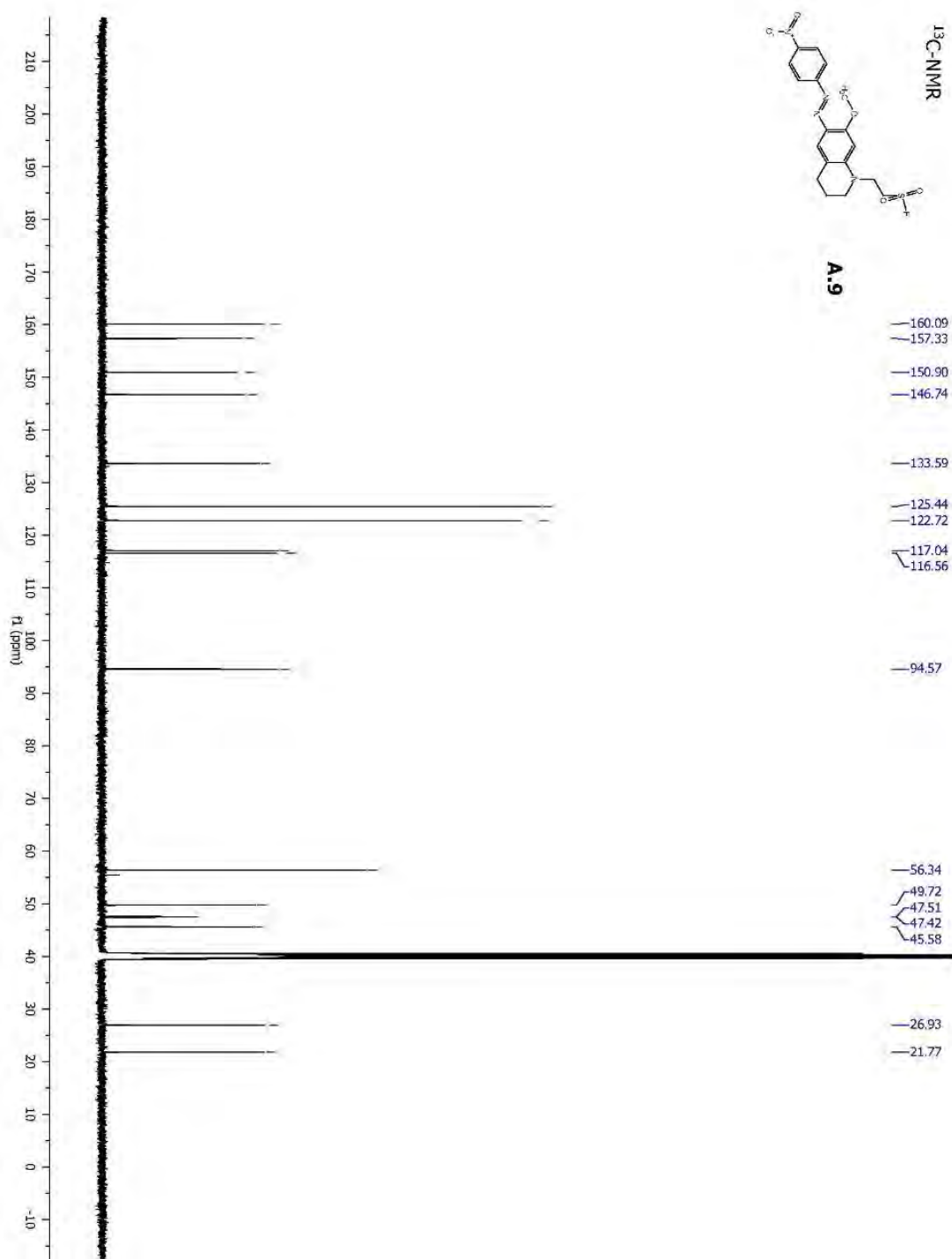


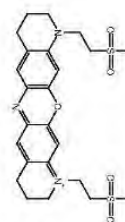
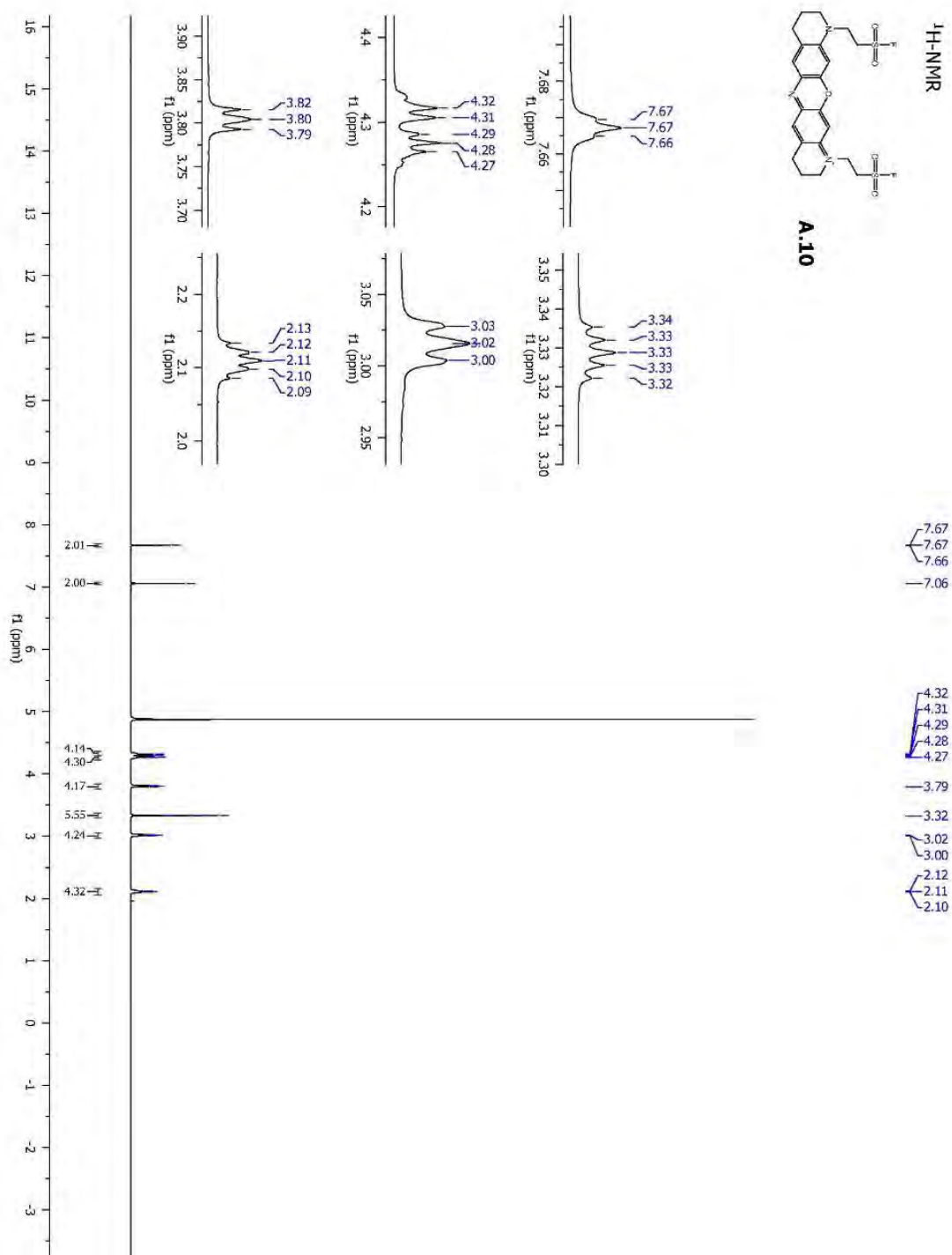


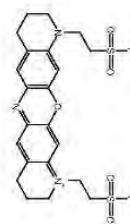
¹H-NMR**A.8**



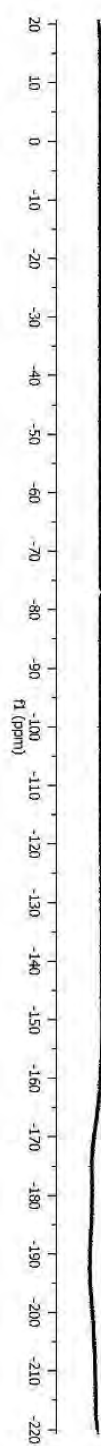
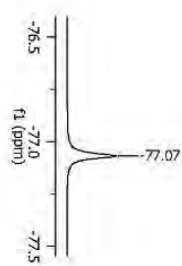


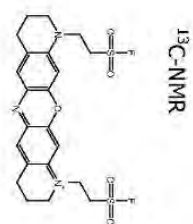
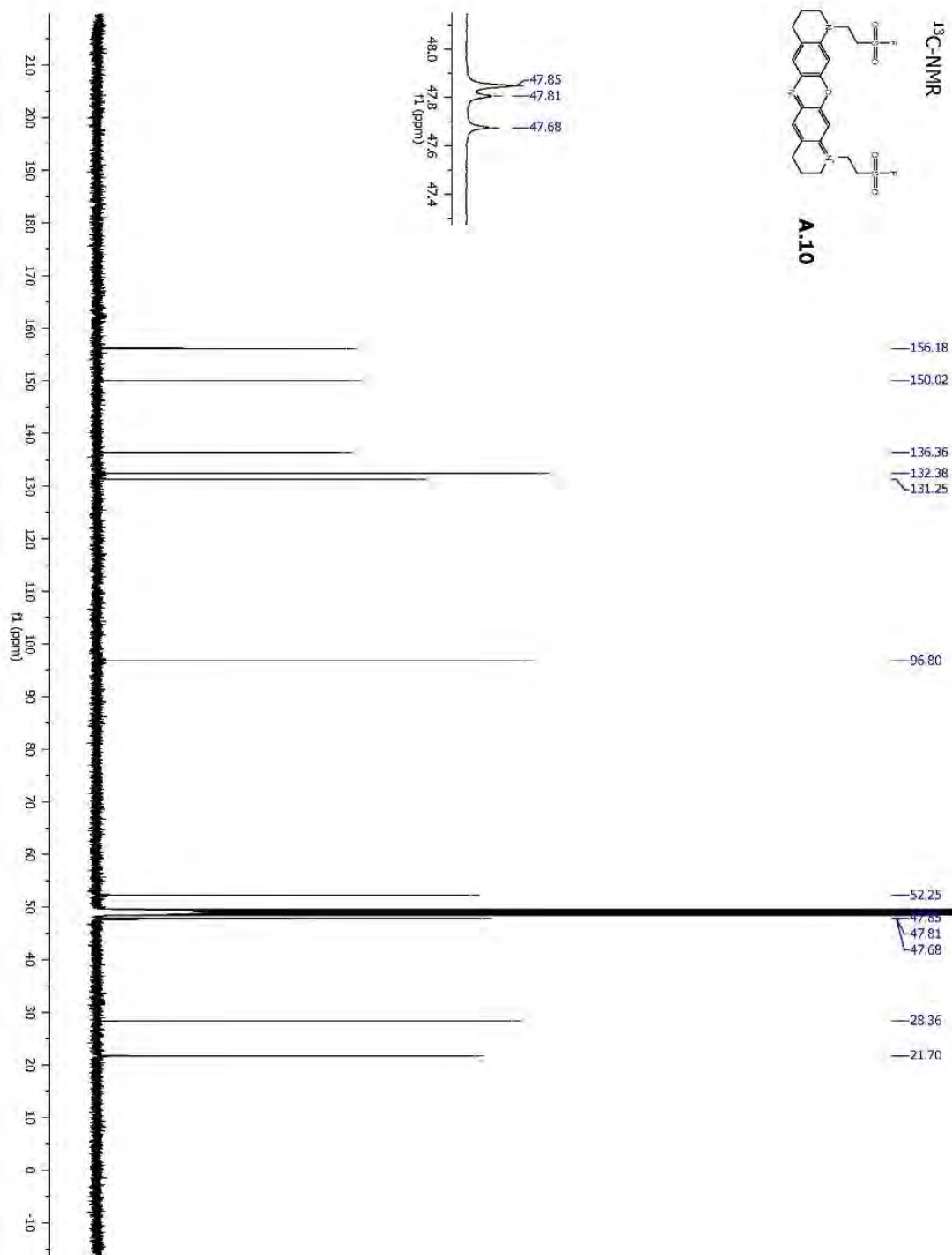


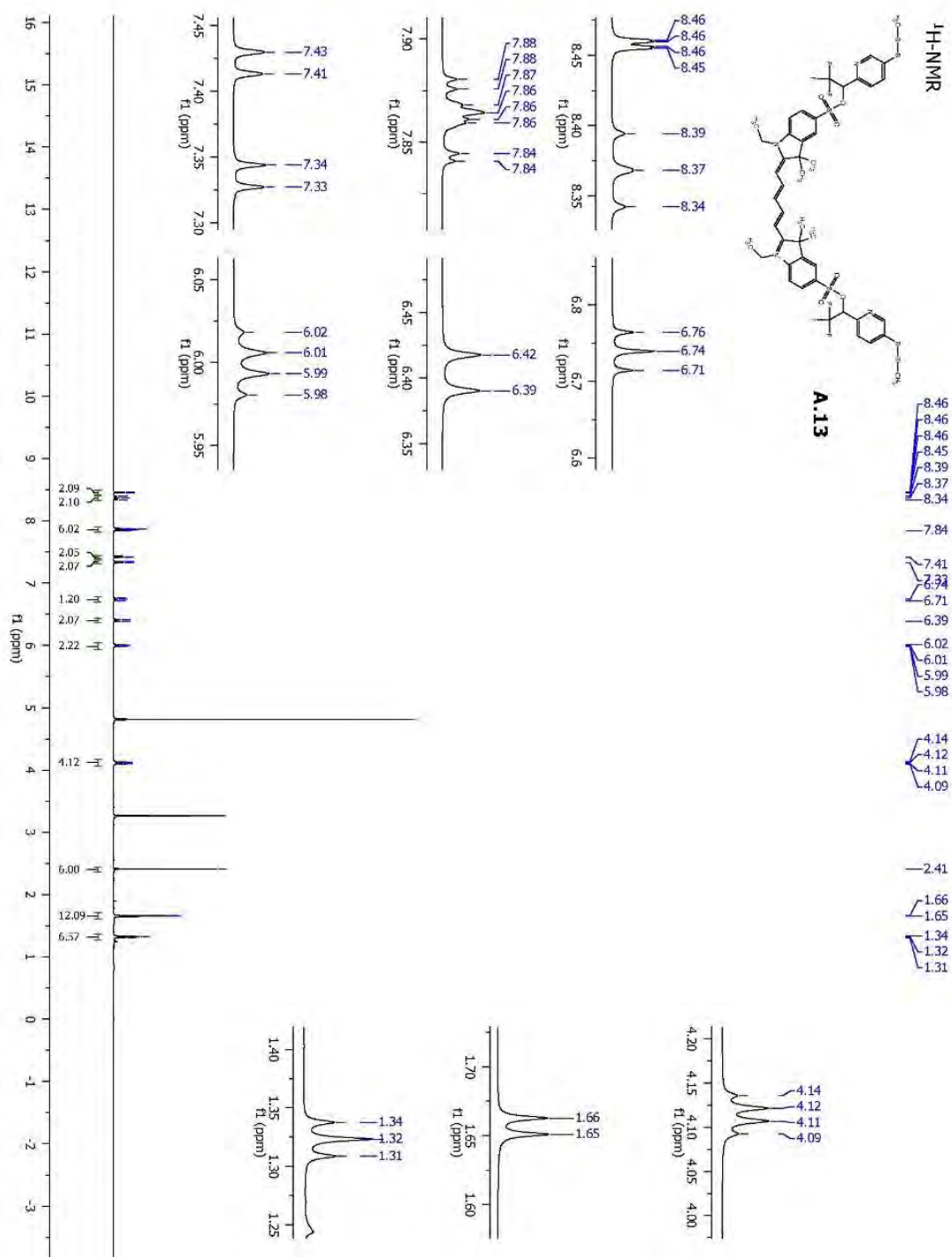
¹H-NMR**A.10**

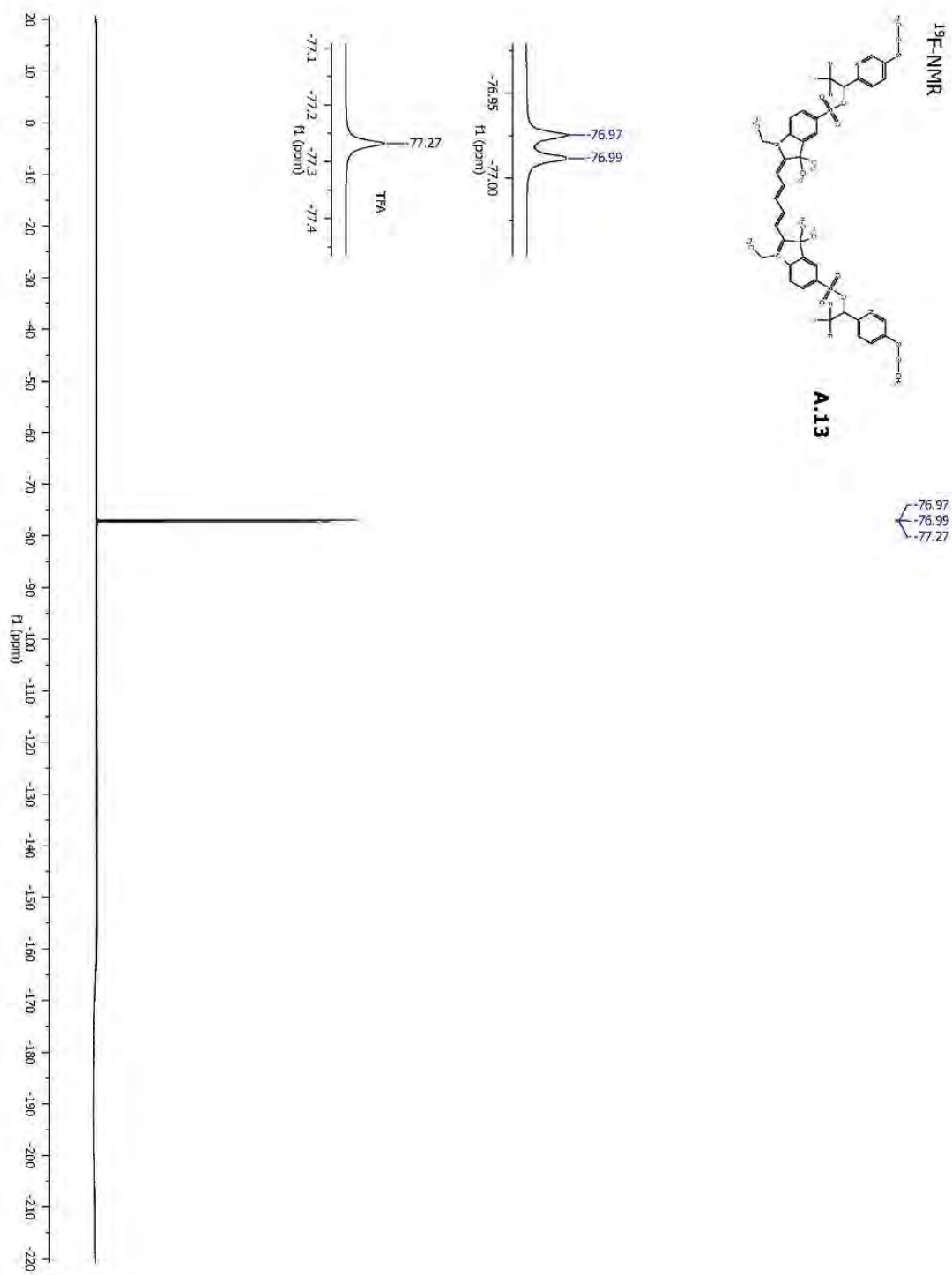
¹⁹F-NMR**A.10**

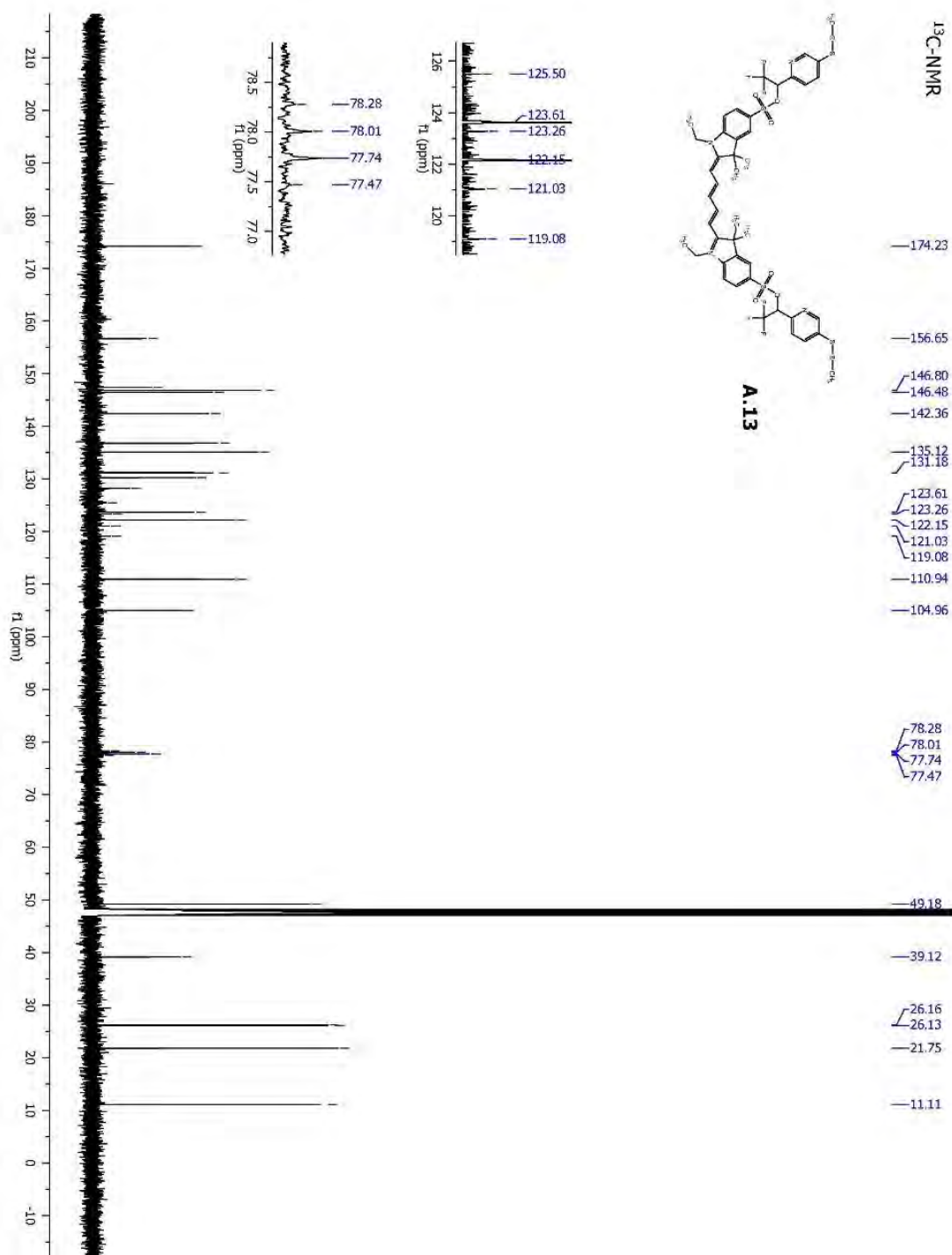
— -77.07

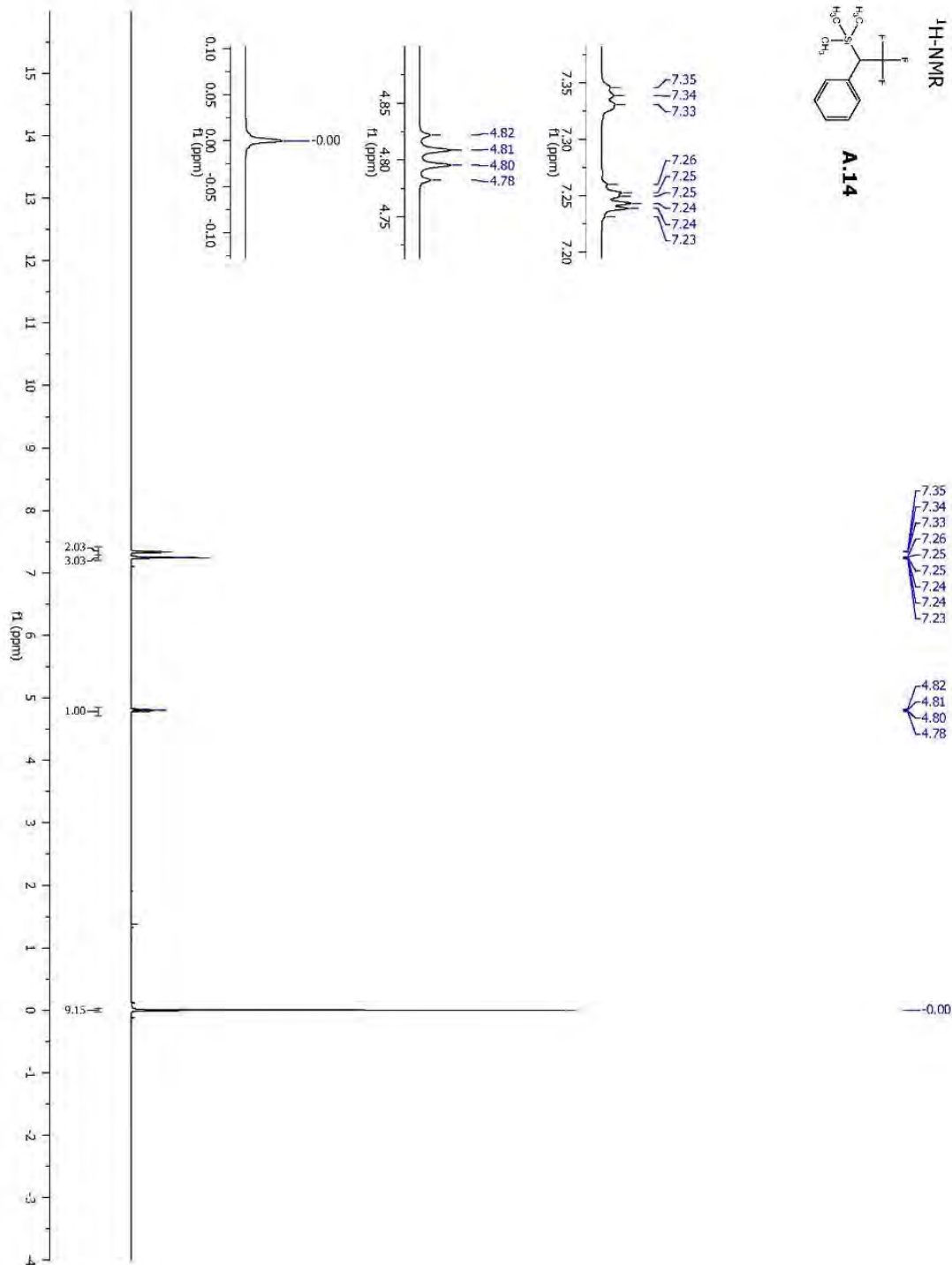
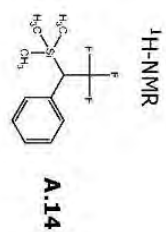


**A.10**



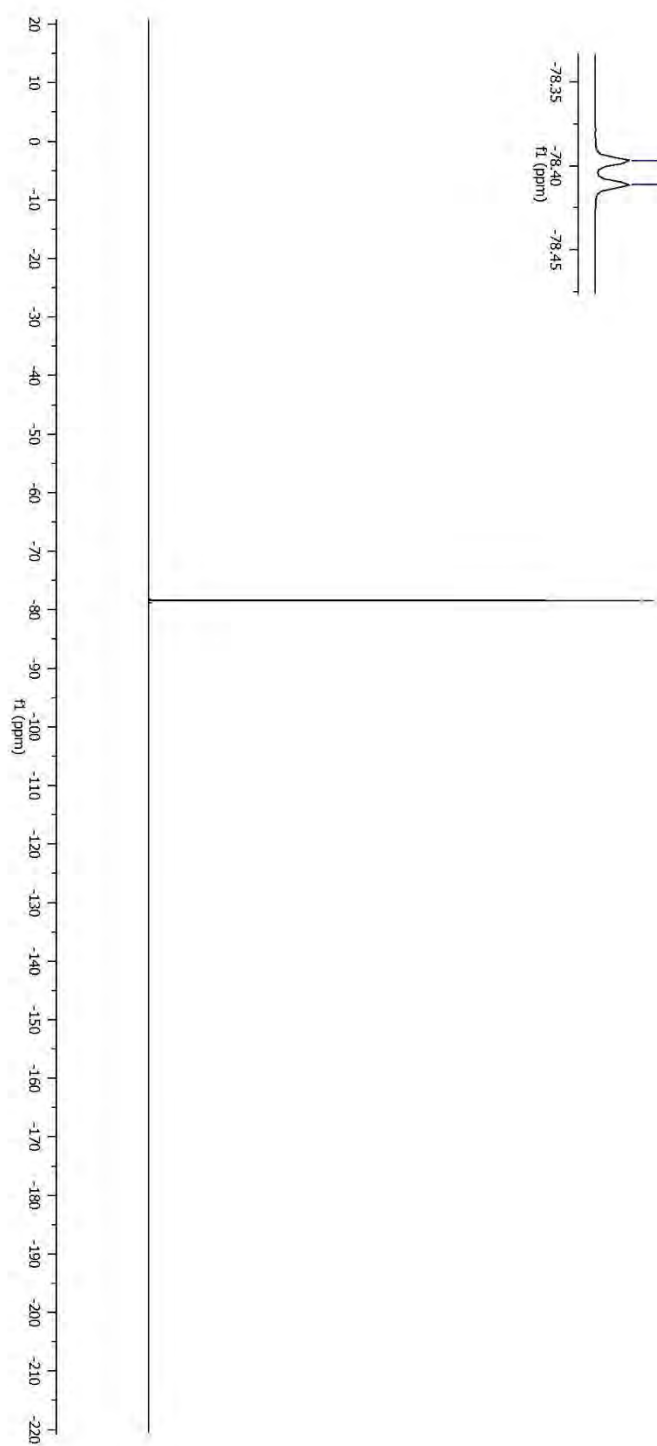
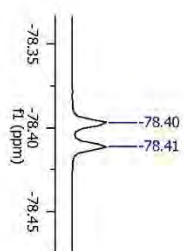


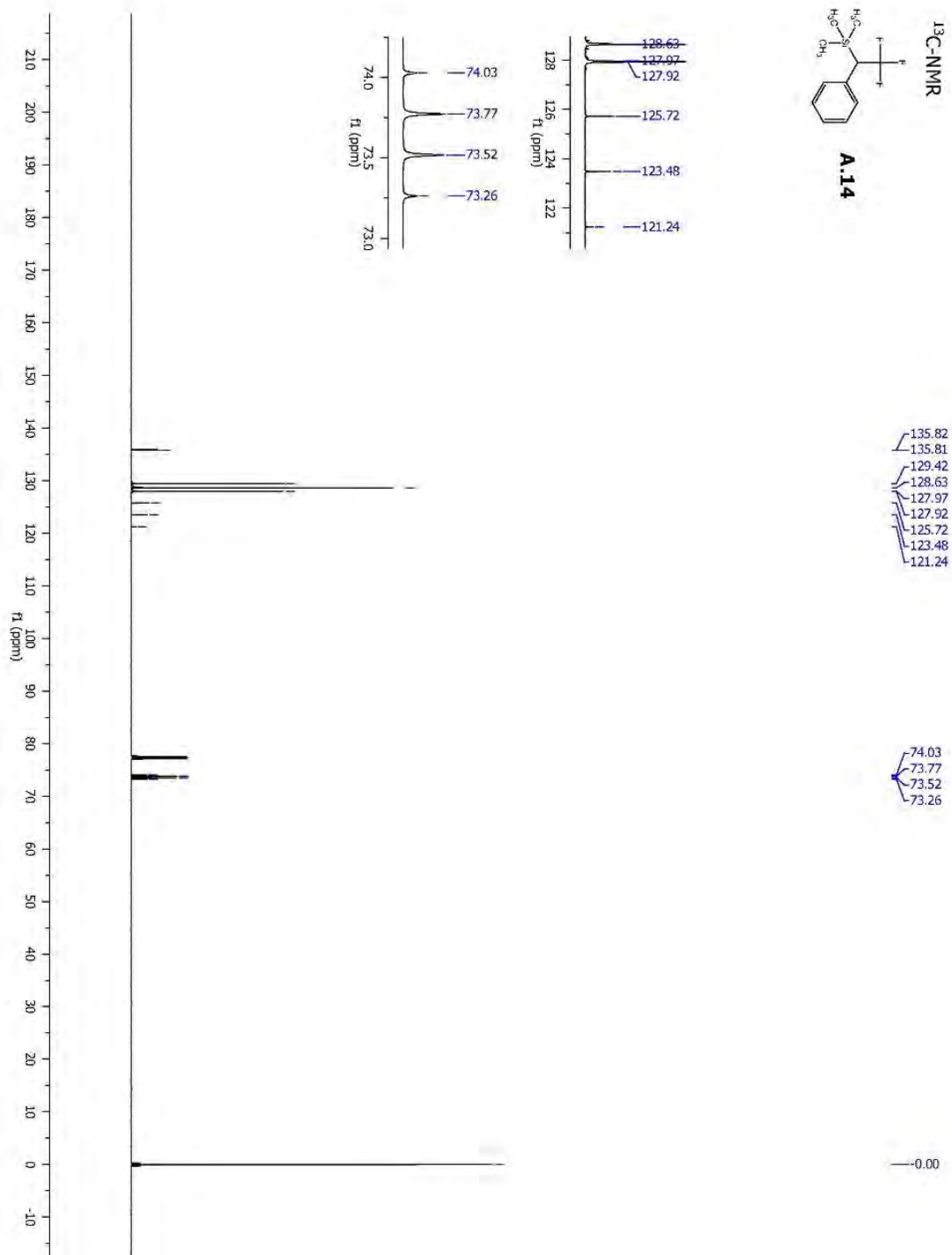
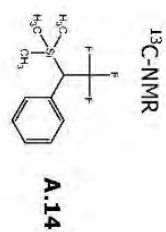




¹⁹F-NMR**A.14**

-78.40
-78.41





BIBLIOGRAPHY

- (1) Lichtman, J. W.; Conchello, J.-A. Fluorescence Microscopy. *Nat Meth* **2005**, 2 (12), 910–919.
- (2) Brouwer, A. M. Standards for Photoluminescence Quantum Yield Measurements in Solution (IUPAC Technical Report). *Pure Appl. Chem., PAC* **2011**, 83 (12), 2213–2228.
- (3) Lakowicz, J. R. *Principles of Fluorescence Spectroscopy*, 2nd ed.; Springer US, 1999.
- (4) Berezin, M. Y.; Achilefu, S. Fluorescence Lifetime Measurements and Biological Imaging. *Chemical Reviews* **2010**, 110 (5), 2641–2684.
- (5) Baptista, M. S.; Cadet, J.; Mascio, P. D.; Ghogare, A. A.; Greer, A.; Hamblin, M. R.; Lorente, C.; Nunez, S. C.; Ribeiro, M. S.; Thomas, A. H.; et al. Type I and Type II Photosensitized Oxidation Reactions: Guidelines and Mechanistic Pathways. *Photochemistry and Photobiology* **2017**, 93 (4), 912–919.
- (6) Zhang, J.; Jiang, C.; Figueiró Longo, J. P.; Azevedo, R. B.; Zhang, H.; Muehlmann, L. A. An Updated Overview on the Development of New Photosensitizers for Anticancer Photodynamic Therapy. *Acta Pharmaceutica Sinica B* **2018**, 8 (2), 137–146.
- (7) Kaschula, C. H.; Lang, D.; Parker, M. I. Live In-Cell Visualization of Proteins Using Super Resolution Imaging. **2012**.
- (8) Garland, M.; Yim, J. J.; Boggyo, M. A Bright Future for Precision Medicine: Advances in Fluorescent Chemical Probe Design and Their Clinical Application. *Cell Chemical Biology* **2016**, 23 (1), 122–136.
- (9) Koide, Y.; Urano, Y.; Hanaoka, K.; Terai, T.; Nagano, T. Development of an Si-Rhodamine-Based Far-Red to Near-Infrared Fluorescence Probe Selective for Hypochlorous Acid and Its Applications for Biological Imaging. *J. Am. Chem. Soc.* **2011**, 133 (15), 5680–5682.
- (10) Terai, T.; Nagano, T. Small-Molecule Fluorophores and Fluorescent Probes for Bioimaging. *Pflugers Arch - Eur J Physiol* **2013**, 465 (3), 347–359.
- (11) Zhang, L.; Bellve, K.; Fogarty, K.; Kobertz, W. R. Fluorescent Visualization of Cellular Proton Fluxes. *Cell Chemical Biology* **2016**, 23 (12), 1449–1457.

- (12) Bandara, H. M. D.; Hua, Z.; Zhang, M.; Pauff, S. M.; Miller, S. C.; Davie, E. A. C.; Kobertz, W. R. Palladium-Mediated Synthesis of a Near-Infrared Fluorescent K⁺ Sensor. *J. Org. Chem.* **2017**, *82* (15), 8199–8205.
- (13) Paredes, R. M.; Etzler, J. C.; Watts, L. T.; Lechleiter, J. D. Chemical Calcium Indicators. *Methods* **2008**, *46* (3), 143–151.
- (14) Mikhaylova, M.; Cloin, B. M. C.; Finan, K.; Berg, R. van den; Teeuw, J.; Kijanka, M. M.; Sokolowski, M.; Katrukha, E. A.; Maidorn, M.; Opazo, F.; et al. Resolving Bundled Microtubules Using Anti-Tubulin Nanobodies. *Nature Communications* **2015**, *6*, 7933.
- (15) MitoTracker Green FM - Special Packaging - Thermo Fisher Scientific
<https://www.thermofisher.com/order/catalog/product/M7514> (accessed Jun 20, 2018).
- (16) ER-Tracker Blue-White DPX, for live-cell imaging - Thermo Fisher Scientific
<https://www.thermofisher.com/order/catalog/product/E12353> (accessed Jun 20, 2018).
- (17) LysoTracker Red DND-99 - Special Packaging - Thermo Fisher Scientific
<https://www.thermofisher.com/order/catalog/product/L7528> (accessed Jun 20, 2018).
- (18) eBioscience DRAQ5 - Thermo Fisher Scientific
<https://www.thermofisher.com/order/catalog/product/65-0880-92> (accessed Jun 20, 2018).
- (19) Kilgore, J. A.; Dolman, N. J.; Davidson, M. W. A Review of Reagents for Fluorescence Microscopy of Cellular Compartments and Structures, Part II: Reagents for Non-Vesicular Organelles. *Current Protocols in Cytometry* **66** (1), 12.31.1-12.31.24.
- (20) Blacker, T. S.; Mann, Z. F.; Gale, J. E.; Ziegler, M.; Bain, A. J.; Szabadkai, G.; Duchon, M. R. Separating NADH and NADPH Fluorescence in Live Cells and Tissues Using FLIM. *Nature Communications* **2014**, *5*, 3936.
- (21) Zipfel, W. R.; Williams, R. M.; Christie, R.; Nikitin, A. Y.; Hyman, B. T.; Webb, W. W. Live Tissue Intrinsic Emission Microscopy Using Multiphoton-Excited Native Fluorescence and Second Harmonic Generation. *Proc Natl Acad Sci U S A* **2003**, *100* (12), 7075–7080.
- (22) Weissleder, R.; Ntziachristos, V. Shedding Light onto Live Molecular Targets. *Nature Medicine* **2003**, *9* (1), nm0103-123–123.

- (23) Godley, B. F.; Shamsi, F. A.; Liang, F.-Q.; Jarrett, S. G.; Davies, S.; Boulton, M. Blue Light Induces Mitochondrial DNA Damage and Free Radical Production in Epithelial Cells. *J. Biol. Chem.* **2005**, *280* (22), 21061–21066.
- (24) Dixit, R.; Cyr, R. Cell Damage and Reactive Oxygen Species Production Induced by Fluorescence Microscopy: Effect on Mitosis and Guidelines for Non-Invasive Fluorescence Microscopy. *The Plant Journal* **36** (2), 280–290.
- (25) Magidson, V.; Khodjakov, A. Circumventing Photodamage in Live-Cell Microscopy. *Methods Cell Biol* **2013**, *114*.
- (26) Wäldchen, S.; Lehmann, J.; Klein, T.; Linde, S. van de; Sauer, M. Light-Induced Cell Damage in Live-Cell Super-Resolution Microscopy. *Scientific Reports* **2015**, *5*, 15348.
- (27) Hong, G.; Antaris, A. L.; Dai, H. Near-Infrared Fluorophores for Biomedical Imaging. *Nature Biomedical Engineering* **2017**, *1* (1), 0010.
- (28) Ogawa, M.; Regino, C. A. S.; Choyke, P. L.; Kobayashi, H. In Vivo Target-Specific Activatable near-Infrared Optical Labeling of Humanized Monoclonal Antibodies. *Mol. Cancer Ther.* **2009**, *8* (1), 232–239.
- (29) Rurack, K.; Spieles, M. Fluorescence Quantum Yields of a Series of Red and Near-Infrared Dyes Emitting at 600–1000 Nm. *Anal. Chem.* **2011**, *83* (4), 1232–1242.
- (30) Würth, C.; Grabolle, M.; Pauli, J.; Spieles, M.; Resch-Genger, U. Relative and Absolute Determination of Fluorescence Quantum Yields of Transparent Samples. *Nature Protocols* **2013**, *8* (8), 1535–1550.
- (31) Luo, S.; Zhang, E.; Su, Y.; Cheng, T.; Shi, C. A Review of NIR Dyes in Cancer Targeting and Imaging. *Biomaterials* **2011**, *32* (29), 7127–7138.
- (32) Umezawa, K.; Citterio, D.; Suzuki, K. New Trends in Near-Infrared Fluorophores for Bioimaging. *Anal Sci* **2014**, *30* (3), 327–349.
- (33) Gibbs, S. L. Near Infrared Fluorescence for Image-Guided Surgery. *Quant Imaging Med Surg* **2012**, *2* (3), 177–187.
- (34) Waggoner. Cyanine dye labeling reagents: Sulfoindocyanine succinimidyl esters - Bioconjugate Chemistry (ACS Publications)
<https://pubs.acs.org/doi/abs/10.1021/bc00020a001> (accessed May 3, 2018).
- (35) Atchison, J.; Kamila, S.; Nesbitt, H.; Logan, K. A.; Nicholas, D. M.; Fowley, C.; Davis, J.; Callan, B.; McHale, A. P.; Callan, J. F. Iodinated Cyanine Dyes: A

New Class of Sensitisers for Use in NIR Activated Photodynamic Therapy (PDT). *Chemical Communications* **2017**, 53 (12), 2009–2012.

- (36) Santos, P. F.; Reis, L. V.; Almeida, P.; Oliveira, A. S.; Vieira Ferreira, L. F. Singlet Oxygen Generation Ability of Squarylium Cyanine Dyes. *Journal of Photochemistry and Photobiology A: Chemistry* **2003**, 160 (3), 159–161.
- (37) Marks, P.; Levine, M. Synthesis of a Near-Infrared Emitting Squaraine Dye in an Undergraduate Organic Laboratory. *J. Chem. Educ.* **2012**, 89 (9), 1186–1189.
- (38) Gassensmith, J. J.; Baumes, J. M.; Smith, B. D. Discovery and Early Development of Squaraine Rotaxanes. *Chem. Commun.* **2009**, 0 (42), 6329–6338.
- (39) Pansare, V. J.; Hejazi, S.; Faenza, W. J.; Prud'homme, R. K. Review of Long-Wavelength Optical and NIR Imaging Materials: Contrast Agents, Fluorophores, and Multifunctional Nano Carriers. *Chem. Mater.* **2012**, 24 (5), 812–827.
- (40) Arunkumar, E.; Forbes, C. C.; Noll, B. C.; Smith, B. D. Squaraine-Derived Rotaxanes: Sterically Protected Fluorescent Near-IR Dyes. *J. Am. Chem. Soc.* **2005**, 127 (10), 3288–3289.
- (41) Umezawa, K.; Citterio, D.; Suzuki, K. Water-Soluble NIR Fluorescent Probes Based on Squaraine and Their Application for Protein Labeling. *Anal Sci* **2008**, 24 (2), 213–217.
- (42) Loudet, A.; Burgess, K. BODIPY Dyes and Their Derivatives: Syntheses and Spectroscopic Properties. *Chem. Rev.* **2007**, 107 (11), 4891–4932.
- (43) Fan, G.; Yang, L.; Chen, Z. Water-Soluble BODIPY and Aza-BODIPY Dyes: Synthetic Progress and Applications. *Front. Chem. Sci. Eng.* **2014**, 8 (4), 405–417.
- (44) Li, L.; Han, J.; Nguyen, B.; Burgess, K. Syntheses and Spectral Properties of Functionalized, Water-Soluble BODIPY Derivatives. *J. Org. Chem.* **2008**, 73 (5), 1963–1970.
- (45) Kamkaew, A.; Burgess, K. Aza-BODIPY Dyes with Enhanced Hydrophilicity. *Chem. Commun.* **2015**, 51 (53), 10664–10667.
- (46) Panchuk-Voloshina, N.; Haugland, R. P.; Bishop-Stewart, J.; Bhalgat, M. K.; Millard, P. J.; Mao, F.; Leung, W.-Y.; Haugland, R. P. Alexa Dyes, a Series of New Fluorescent Dyes That Yield Exceptionally Bright, Photostable Conjugates. *J Histochem Cytochem.* **1999**, 47 (9), 1179–1188.

- (47) Grimm, J. B.; English, B. P.; Chen, J.; Slaughter, J. P.; Zhang, Z.; Revyakin, A.; Patel, R.; Macklin, J. J.; Normanno, D.; Singer, R. H.; et al. A General Method to Improve Fluorophores for Live-Cell and Single-Molecule Microscopy. *Nature Methods* **2015**, *12* (3), 244–250.
- (48) Rusha, L.; Miller, S. C. Design and Application of Esterase-Labile Sulfonate Protecting Groups. *Chem. Commun.* **2011**, *47* (7), 2038–2040.
- (49) Pauff, S. M.; Miller, S. C. Synthesis of Near-IR Fluorescent Oxazine Dyes with Esterase-Labile Sulfonate Esters. *Org. Lett.* **2011**, *13* (23), 6196–6199.
- (50) Huttunen, K. M.; Raunio, H.; Rautio, J. Prodrugs—from Serendipity to Rational Design. *Pharmacol Rev* **2011**, *63* (3), 750–771.
- (51) Rautio, J.; Kumpulainen, H.; Heimbach, T.; Oliyai, R.; Oh, D.; Järvinen, T.; Savolainen, J. Prodrugs: Design and Clinical Applications. *Nature Reviews Drug Discovery* **2008**, *7* (3), 255–270.
- (52) Miller, S. C. Profiling Sulfonate Ester Stability: Identification of Complementary Protecting Groups for Sulfonates. *J. Org. Chem.* **2010**, *75* (13), 4632–4635.
- (53) Fu, M.; Xiao, Y.; Qian, X.; Zhao, D.; Xu, Y. A Design Concept of Long-Wavelength Fluorescent Analogs of Rhodamine Dyes: Replacement of Oxygen with Silicon Atom. *Chem. Commun.* **2008**, *0* (15), 1780–1782.
- (54) Horváth, P.; Šebej, P.; Šolomek, T.; Klán, P. Small-Molecule Fluorophores with Large Stokes Shifts: 9-Iminopyronin Analogues as Clickable Tags. *J. Org. Chem.* **2015**, *80* (3), 1299–1311.
- (55) Grimm, J. B.; Brown, T. A.; Tkachuk, A. N.; Lavis, L. D. General Synthetic Method for Si-Fluoresceins and Si-Rhodamines. *ACS Cent. Sci.* **2017**, *3* (9), 975–985.
- (56) Grimm, J. B.; Klein, T.; Kopek, B. G.; Shtengel, G.; Hess, H. F.; Sauer, M.; Lavis, L. D. Synthesis of a Far-Red Photoactivatable Silicon-Containing Rhodamine for Super-Resolution Microscopy. *Angew. Chem. Int. Ed.* **2016**, *55* (5), 1723–1727.
- (57) Koide, Y.; Urano, Y.; Hanaoka, K.; Piao, W.; Kusakabe, M.; Saito, N.; Terai, T.; Okabe, T.; Nagano, T. Development of NIR Fluorescent Dyes Based on Si-Rhodamine for in Vivo Imaging. *J. Am. Chem. Soc.* **2012**, *134* (11), 5029–5031.
- (58) Ikeno Takayuki; Nagano Tetsuo; Hanaoka Kenjiro. Silicon-substituted Xanthene Dyes and Their Unique Photophysical Properties for Fluorescent Probes. *Chemistry – An Asian Journal* **2017**, *12* (13), 1435–1446.

- (59) Wang, T.; Zhao, Q.-J.; Hu, H.-G.; Yu, S.-C.; Liu, X.; Liu, L.; Wu, Q.-Y. Spirolactonized Si-Rhodamine: A Novel NIR Fluorophore Utilized as a Platform to Construct Si-Rhodamine-Based Probes. *Chem. Commun.* **2012**, 48 (70), 8781–8783.
- (60) Lukinavičius, G.; Umezawa, K.; Olivier, N.; Honigsmann, A.; Yang, G.; Plass, T.; Mueller, V.; Reymond, L.; Jr, I. R. C.; Luo, Z.-G.; et al. A Near-Infrared Fluorophore for Live-Cell Super-Resolution Microscopy of Cellular Proteins. *Nature Chemistry* **2013**, 5 (2), 132–139.
- (61) Butkevich, A. N.; Ta, H.; Ratz, M.; Stoldt, S.; Jakobs, S.; Belov, V. N.; Hell, S. W. Two-Color 810 Nm STED Nanoscopy of Living Cells with Endogenous SNAP-Tagged Fusion Proteins. *ACS Chem. Biol.* **2017**.
- (62) Koide, Y.; Urano, Y.; Hanaoka, K.; Terai, T.; Nagano, T. Evolution of Group 14 Rhodamines as Platforms for Near-Infrared Fluorescence Probes Utilizing Photoinduced Electron Transfer. *ACS Chem. Biol.* **2011**, 6 (6), 600–608.
- (63) Chai, X.; Cui, X.; Wang, B.; Yang, F.; Cai, Y.; Wu, Q.; Wang, T. Near-Infrared Phosphorus-Substituted Rhodamine with Emission Wavelength above 700 Nm for Bioimaging. *Chemistry – A European Journal* **21** (47), 16754–16758.
- (64) Liu, J.; Sun, Y.-Q.; Zhang, H.; Shi, H.; Shi, Y.; Guo, W. Sulfone-Rhodamines: A New Class of Near-Infrared Fluorescent Dyes for Bioimaging. *ACS Appl. Mater. Interfaces* **2016**, 8 (35), 22953–22962.
- (65) Choi, H. S.; Gibbs, S. L.; Lee, J. H.; Kim, S. H.; Ashitate, Y.; Liu, F.; Hyun, H.; Park, G.; Xie, Y.; Bae, S.; et al. Targeted Zwitterionic Near-Infrared Fluorophores for Improved Optical Imaging. *Nature Biotechnology* **2013**, 31 (2), 148–153.
- (66) Choi, A.; Miller, S. C. Reductively-Labile Sulfonate Ester Protecting Groups That Are Rapidly Cleaved by Physiological Glutathione. *Org. Biomol. Chem.* **2017**, 15 (6), 1346–1349.
- (67) Seki, H.; Kawaguchi, T.; Higuchi, T. Specificity of Esterases and Structure of Prodrug Esters: Reactivity of Various Acylated Acetaminophen Compounds and Acetylaminobenzoated Compounds. *Journal of Pharmaceutical Sciences* **1988**, 77 (10), 855–860.
- (68) Tian, L.; Yang, Y.; Wysocki, L. M.; Arnold, A. C.; Hu, A.; Ravichandran, B.; Sternson, S. M.; Looger, L. L.; Lavis, L. D. Selective Esterase–Ester Pair for Targeting Small Molecules with Cellular Specificity. *Proc Natl Acad Sci U S A* **2012**, 109 (13), 4756–4761.

- (69) Musicki, B.; Widlanski, T. S. Synthesis of Carbohydrate Sulfonates and Sulfonate Esters. *J. Org. Chem.* **1990**, *55* (14), 4231–4233.
- (70) Wuts, P. G. M.; Greene, T. W. *Greene's Protective Groups in Organic Synthesis*; John Wiley & Sons, 2006.
- (71) Hine, J.; Ghirardelli, R. Notes - The S_N - Reactivity of β -Fluorethyl Iodides. *J. Org. Chem.* **1958**, *23* (10), 1550–1552.
- (72) Pauff, S. M.; Miller, S. C. A Trifluoroacetic Acid-Labile Sulfonate Protecting Group and Its Use in the Synthesis of a near-IR Fluorophore. *J Org Chem* **2013**, *78* (2), 711–716.
- (73) Ottaviano, F. G.; Handy, D. E.; Loscalzo, J. Redox Regulation in the Extracellular Environment. *Circ. J.* **2008**, *72* (1), 1–16.
- (74) Maher, P. The Effects of Stress and Aging on Glutathione Metabolism. *Ageing Research Reviews* **2005**, *4* (2), 288–314.
- (75) Go, Y.-M.; Jones, D. P. Redox Compartmentalization in Eukaryotic Cells. *Biochimica et Biophysica Acta (BBA) - General Subjects* **2008**, *1780* (11), 1273–1290.
- (76) Jancova, P.; Anzenbacher, P.; Anzenbacherova, E. Phase II Drug Metabolizing Enzymes. *Biomed Pap Med Fac Univ Palacky Olomouc Czech Repub* **2010**, *154* (2), 103–116.
- (77) Senter, P. D.; Pearce, W. E.; Greenfield, R. S. Development of a Drug-Release Strategy Based on the Reductive Fragmentation of Benzyl Carbamate Disulfides. *J. Org. Chem.* **1990**, *55* (9), 2975–2978.
- (78) Itoh, T.; Fujikawa, K.; Kubo, M. P-Thioquinone Methides: Synthesis and Reaction. *J. Org. Chem.* **1996**, *61* (23), 8329–8331.
- (79) Vigalok, A.; Milstein, D. Metal-Stabilized Quinone and Thioquinone Methides. *J. Am. Chem. Soc.* **1997**, *119* (33), 7873–7874.
- (80) Newman, M. S.; Karnes, H. A. The Conversion of Phenols to Thiophenols via Dialkylthiocarbamates¹. *J. Org. Chem.* **1966**, *31* (12), 3980–3984.
- (81) Kwart, H.; Evans, E. R. The Vapor Phase Rearrangement of Thioncarbonates and Thioncarbarnates. *J. Org. Chem.* **1966**, *31* (2), 410–413.
- (82) Moseley, J. D.; Lenden, P. A High Temperature Investigation Using Microwave Synthesis for Electronically and Sterically Disfavoured Substrates of the Newman–Kwart Rearrangement. *Tetrahedron* **2007**, *63* (19), 4120–4125.

- (83) Moseley, J. D.; Sankey, R. F.; Tang, O. N.; Gilday, J. P. The Newman–Kwart Rearrangement Re-Evaluated by Microwave Synthesis. *Tetrahedron* **2006**, *62* (19), 4685–4689.
- (84) Itoh, T.; Mase, T. A General Palladium-Catalyzed Coupling of Aryl Bromides/Triflates and Thiols. *Org. Lett.* **2004**, *6* (24), 4587–4590.
- (85) Itoh, T.; Mase, T. Practical Thiol Surrogates and Protective Groups for Arylthiols for Suzuki–Miyaura Conditions. *J. Org. Chem.* **2006**, *71* (5), 2203–2206.
- (86) Toteva, M. M.; Richard, J. P. The Generation and Reactions of Quinone Methides. *Adv Phys Org Chem* **2011**, *45*, 39–91.
- (87) Thompson, D. C.; Thompson, J. A.; Sugumaran, M.; Moldéus, P. Biological and Toxicological Consequences of Quinone Methide Formation. *Chemico-Biological Interactions* **1993**, *86* (2), 129–162.
- (88) Chazotte, B. Mounting Live Cells onto Microscope Slides. *Cold Spring Harb Protoc* **2011**, *2011* (1), pdb.prot5554.
- (89) Choi, A.; Miller, S. C. Silicon Substitution in Oxazine Dyes Yields Near-Infrared Azasiline Fluorophores That Absorb and Emit beyond 700 Nm. *Org. Lett.* **2018**, *20* (15), 4482–4485.
- (90) Licha, K.; Riefke, B.; Ntziachristos, V.; Becker, A.; Chance, B.; Semmler, W. Hydrophilic Cyanine Dyes as Contrast Agents for Near-Infrared Tumor Imaging: Synthesis, Photophysical Properties and Spectroscopic In Vivo Characterization ¶. *Photochemistry and Photobiology* **72** (3), 392–398.
- (91) Alander, J. T.; Kaartinen, I.; Laakso, A.; Pätilä, T.; Spillmann, T.; Tuchin, V. V.; Venermo, M.; Välisuo, P. A Review of Indocyanine Green Fluorescent Imaging in Surgery <https://www.hindawi.com/journals/ijbi/2012/940585/> (accessed Jul 4, 2018).
- (92) Altman, R. B.; Terry, D. S.; Zhou, Z.; Zheng, Q.; Geggier, P.; Kolster, R. A.; Zhao, Y.; Javitch, J. A.; Warren, J. D.; Blanchard, S. C. Cyanine Fluorophore Derivatives with Enhanced Photostability. *Nature Methods* **2012**, *9* (1), 68–71.
- (93) Mujumdar, R. B.; Ernst, L. A.; Mujumdar, S. R.; Lewis, C. J.; Waggoner, A. S. Cyanine Dye Labeling Reagents: Sulfoindocyanine Succinimidyl Esters. *Bioconjugate Chem.* **1993**, *4* (2), 105–111.
- (94) Anzalone, A. V.; Wang, T. Y.; Chen, Z.; Cornish, V. W. A Common Diaryl Ether Intermediate for the Gram-Scale Assembly of Oxazine and Xanthene Fluorophores. *Angew Chem Int Ed Engl* **2013**, *52* (2).

- (95) Anzalone, A. V.; Chen, Z.; Cornish, V. W. Synthesis of Photoactivatable Azido-Acyl Caged Oxazine Fluorophores for Live-Cell Imaging. *Chem. Commun.* **2016**, 52 (60), 9442–9445.
- (96) Hintersteiner, M.; Enz, A.; Frey, P.; Jaton, A.-L.; Kinzy, W.; Kneuer, R.; Neumann, U.; Rudin, M.; Staufienbiel, M.; Stoeckli, M.; et al. *In Vivo* Detection of Amyloid- β Deposits by near-Infrared Imaging Using an Oxazine-Derivative Probe. *Nature Biotechnology* **2005**, 23 (5), 577–583.
- (97) Suzuki, R.; Tada, R.; Hosoda, T.; Miura, Y.; Yoshioka, N. Synthesis of Ester-Substituted Dihydroacridine Derivatives and Their Spectroscopic Properties. *New J. Chem.* **2016**, 40 (3), 2920–2926.
- (98) Sun, J. W.; Baek, J. Y.; Kim, K.-H.; Moon, C.-K.; Lee, J.-H.; Kwon, S.-K.; Kim, Y.-H.; Kim, J.-J. Thermally Activated Delayed Fluorescence from Azasiline Based Intramolecular Charge-Transfer Emitter (DTPDDA) and a Highly Efficient Blue Light Emitting Diode. *Chem. Mater.* **2015**, 27 (19), 6675–6681.
- (99) Koide, Y.; Urano, Y.; Hanaoka, K.; Piao, W.; Kusakabe, M.; Saito, N.; Terai, T.; Okabe, T.; Nagano, T. Development of NIR Fluorescent Dyes Based on Si–Rhodamine for in Vivo Imaging. *J. Am. Chem. Soc.* **2012**, 134 (11), 5029–5031.
- (100) Zhang, X.; Yu, H.; Xiao, Y. Replacing Phenyl Ring with Thiophene: An Approach to Longer Wavelength Aza-Dipyrromethene Boron Difluoride (Aza-BODIPY) Dyes. *J. Org. Chem.* **2012**, 77 (1), 669–673.
- (101) Basheer, M. C.; Santhosh, U.; Alex, S.; Thomas, K. G.; Suresh, C. H.; Das, S. Design and Synthesis of Squaraine Based near Infrared Fluorescent Probes. *Tetrahedron* **2007**, 63 (7), 1617–1623.
- (102) Perry, S. W.; Norman, J. P.; Barbieri, J.; Brown, E. B.; Gelbard, H. A. Mitochondrial Membrane Potential Probes and the Proton Gradient: A Practical Usage Guide. *BioTechniques* **2011**, 50 (2), 98–115.
- (103) Hood, R. D.; Jones, C. L.; Ranganathan, S. Comparative Developmental Toxicity of Cationic and Neutral Rhodamines in Mice. *Teratology* **1989**, 40 (2), 143–150.
- (104) Ranganathan, S.; Hood, R. D. Effects of in Vivo and in Vitro Exposure to Rhodamine Dyes on Mitochondrial Function of Mouse Embryos. *Teratog., Carcinog. Mutagen.* **1989**, 9 (1), 29–37.
- (105) Vennerstrom, J. L.; Makler, M. T.; Angerhofer, C. K.; Williams, J. A. Antimalarial Dyes Revisited: Xanthenes, Azines, Oxazines, and Thiazines. *Antimicrobial Agents and Chemotherapy* **1995**, 39 (12), 2671–2677.

- (106) Bunting, J. R. Influx and Efflux Kinetics of Cationic Dye Binding to Respiring Mitochondria. *Biophysical Chemistry* **1992**, 42 (2), 163–175.
- (107) Jeannot, V.; Salmon, J.-M.; Deumié, M.; Viallet, P. Intracellular Accumulation of Rhodamine 110 in Single Living Cells. *J Histochem Cytochem.* **1997**, 45 (3), 403–412.
- (108) Johnson, L. V.; Walsh, M. L.; Bockus, B. J.; Chen, L. B. Monitoring of Relative Mitochondrial Membrane Potential in Living Cells by Fluorescence Microscopy. *The Journal of Cell Biology* **1981**, 88 (3), 526–535.
- (109) Zhu, H.; Fan, J.; Du, J.; Peng, X. Fluorescent Probes for Sensing and Imaging within Specific Cellular Organelles. *Acc. Chem. Res.* **2016**, 49 (10), 2115–2126.
- (110) Chudakov, D. M.; Matz, M. V.; Lukyanov, S.; Lukyanov, K. A. Fluorescent Proteins and Their Applications in Imaging Living Cells and Tissues. *Physiological Reviews* **2010**, 90 (3), 1103–1163.
- (111) Resch-Genger, U.; Grabolle, M.; Cavaliere-Jaricot, S.; Nitschke, R.; Nann, T. Quantum Dots versus Organic Dyes as Fluorescent Labels. *Nature Methods* **2008**, 5 (9), 763–775.
- (112) Caddick, S.; Wilden, J. D.; Bush, H. D.; Wadman, S. N.; Judd, D. B. A New Route to Sulfonamides via Intermolecular Radical Addition to Pentafluorophenyl Vinylsulfonate and Subsequent Aminolysis. *Org. Lett.* **2002**, 4 (15), 2549–2551.
- (113) Marcotullio, M. C.; Campagna, V.; Sternativo, S.; Costantino, F.; Curini, M. A New, Simple Synthesis of N-Tosyl Pyrrolidines and Piperidines. *Synthesis* **2006**, No. 16, 2760–2766.
- (114) Kim, J.-G.; Jang, D. O. Mild and Efficient Indium Metal Catalyzed Synthesis of Sulfonamides and Sulfonic Esters. *Synlett* **2007**, No. 16, 2501–2504.
- (115) Hermanson, G. T. Chapter 3 - The Reactions of Bioconjugation. In *Bioconjugate Techniques (Third Edition)*; Hermanson, G. T., Ed.; Academic Press: Boston, 2013; pp 229–258.
- (116) Klayman, D. L.; White, J. D.; Sweeney, T. R. Unsymmetrical Disulfides from an Amino Bunte Salt. *J. Org. Chem.* **1964**, 29 (12), 3737–3738.
- (117) Swan, J. M. Thiols, Disulphides and Thiosulphates: Some New Reactions and Possibilities in Peptide and Protein Chemistry. *Nature* **1957**, 180 (4587), 643–645.

- (118) Distler, H. The Chemistry of Bunte Salts. *Angewandte Chemie International Edition in English* **1967**, 6 (6), 544–553.
- (119) Reeves, J. T.; Camara, K.; Han, Z. S.; Xu, Y.; Lee, H.; Busacca, C. A.; Senanayake, C. H. The Reaction of Grignard Reagents with Bunte Salts: A Thiol-Free Synthesis of Sulfides. *Org. Lett.* **2014**, 16 (4), 1196–1199.
- (120) Corey, J. Y.; Corey, E. R.; Chang, V. H. T.; Hauser, M. A.; Leiber, M. A.; Reinsel, T. E.; Riva, M. E. Reactions of Fluoride Ion Sources with Haloalkyl Derivatives of Phenazasilines and Phenoxasilins. *Organometallics* **1984**, 3 (7), 1051–1060.
- (121) Sun, W.-C.; Gee, K. R.; Klaubert, D. H.; Haugland, R. P. Synthesis of Fluorinated Fluoresceins. *J. Org. Chem.* **1997**, 62 (19), 6469–6475.
- (122) Paufl, S. Advancements in the Synthesis and Application of Near-Infrared Imaging Reagents: A Dissertation. *GSBS Dissertations and Theses* **2015**.
- (123) Sharma, D. K.; Adams, S. T.; Liebmann, K. L.; Miller, S. C. Rapid Access to a Broad Range of 6'-Substituted Firefly Luciferin Analogues Reveals Surprising Emitters and Inhibitors. *Org. Lett.* **2017**, 19 (21), 5836–5839.
- (124) Fors, B. P.; Watson, D. A.; Biscoe, M. R.; Buchwald, S. L. A Highly Active Catalyst for Pd-Catalyzed Amination Reactions: Cross-Coupling Reactions Using Aryl Mesylates and the Highly Selective Monoarylation of Primary Amines Using Aryl Chlorides. *J. Am. Chem. Soc.* **2008**, 130 (41), 13552–13554.
- (125) Los, G. V.; Encell, L. P.; McDougall, M. G.; Hartzell, D. D.; Karassina, N.; Zimprich, C.; Wood, M. G.; Learish, R.; Ohana, R. F.; Urh, M.; et al. HaloTag: A Novel Protein Labeling Technology for Cell Imaging and Protein Analysis. *ACS Chem. Biol.* **2008**, 3 (6), 373–382.
- (126) Nikić, I.; Kang, J. H.; Girona, G. E.; Aramburu, I. V.; Lemke, E. A. Labeling Proteins on Live Mammalian Cells Using Click Chemistry. *Nature Protocols* **2015**, 10 (5), 780–791.
- (127) Grimm, J. B.; Brown, T. A.; English, B. P.; Lionnet, T.; Lavis, L. D. Synthesis of Janelia Fluor HaloTag and SNAP-Tag Ligands and Their Use in Cellular Imaging Experiments. *Methods Mol. Biol.* **2017**, 1663, 179–188.
- (128) Xie, M.; Widlanski, T. S. A New Protecting Group for the Synthesis of Complex Sulfonates. *Tetrahedron Letters* **1996**, 37 (26), 4443–4446.
- (129) Murphy, M. P. Selective Targeting of Bioactive Compounds to Mitochondria. *Trends in Biotechnology* **1997**, 15 (8), 326–330.

- (130) Turksoy, A.; Yildiz, D.; Akkaya, E. U. Photosensitization and Controlled Photosensitization with BODIPY Dyes. *Coordination Chemistry Reviews* **2017**.
- (131) Dong, J.; Krasnova, L.; Finn, M. G.; Sharpless, K. B. Sulfur(VI) Fluoride Exchange (SuFEx): Another Good Reaction for Click Chemistry. *Angewandte Chemie International Edition* **53** (36), 9430–9448.
- (132) King, J. F. Return of Sulfenes. *Acc. Chem. Res.* **1975**, *8* (1), 10–17.
- (133) Sun, W.; Guo, S.; Hu, C.; Fan, J.; Peng, X. Recent Development of Chemosensors Based on Cyanine Platforms. *Chem. Rev.* **2016**, *116* (14), 7768–7817.
- (134) CDC - Onchocerciasis - Epidemiology & Risk Factors
<https://www.cdc.gov/parasites/onchocerciasis/epi.html> (accessed Jul 26, 2018).
- (135) Page, A. P.; Stepek, G.; Winter, A. D.; Pertab, D. Enzymology of the Nematode Cuticle: A Potential Drug Target? *Int J Parasitol Drugs Drug Resist* **2014**, *4* (2), 133–141.
- (136) Politz, S. M.; Philipp, M. *Caenorhabditis Elegans* as a Model for Parasitic Nematodes: A Focus on the Cuticle. *Parasitology Today* **1992**, *8* (1), 6–12.
- (137) Bürglin, T. R.; Lobos, E.; Blaxter, M. L. *Caenorhabditis Elegans* as a Model for Parasitic Nematodes. *International Journal for Parasitology* **1998**, *28* (3), 395–411.
- (138) Favre, R.; Cermola, M.; Nunes, C. P.; Hermann, R.; Müller, M.; Bazzicalupo, P. Immuno-Cross-Reactivity of CUT-1 and Cuticlin Epitopes Between *Ascaris Lumbricoides*, *Caenorhabditis Elegans*, and *Heterorhabditis*. *Journal of Structural Biology* **1998**, *123* (1), 1–7.
- (139) Sutphin, G. L.; Kaeberlein, M. Measuring *Caenorhabditis Elegans* Life Span on Solid Media. *J Vis Exp* **2009**, No. 27.
- (140) Zhang, null; Chung, null; Oldenburg, null. A Simple Statistical Parameter for Use in Evaluation and Validation of High Throughput Screening Assays. *J Biomol Screen* **1999**, *4* (2), 67–73.
- (141) Duerr, J. Immunohistochemistry. *WormBook* **2006**.
- (142) Rothman, J. H.; Singson, A. *Caenorhabditis Elegans: Cell Biology and Physiology*; Academic Press, 2012.
- (143) Solis, G. M.; Petrascheck, M. Measuring *Caenorhabditis Elegans* Life Span in 96 Well Microtiter Plates. *J Vis Exp* **2011**, No. 49.